UNIVERSITY OF NEWCASTLE UPON TYNE

NEWCASTLE UNIVERSITY LIBRARY

M5 084 09896 6 NR

THE DYNAMICS OF RIGID AND FLEXIBLE FOUR-BAR LINKAGE MECHANISMS

BY

M. R. SMITH B.Sc.

A Thesis submitted for the

Degree of Doctor of Philosophy in the

Faculty of Applied Science,

University of Newcastle upon Tyne

May 1972

Acknowledgements

The author wishes to express his twofold gratitude to Professor L. Maunder. Firstly for his continuing encouragement and guidance throughout the course of the work described herein and secondly for making available the numerous facilities of the Department of Mechanical Engineering especially in relation to the experimental work. In this context the assistance of Messrs P.Elliott, R.Batey., T.B.Smith, and W.H.B.Young is gratefully acknowledged. Their help in overcoming the many practical problems involved was invaluable. For the construction of the experimental apparatus I am indebted to Messrs T.B.Smith, A. Jamieson and D.Robinson and for assistance with associated electrical equipment to Messrs W.H.B.Young and G. Winskill.

In connection with various aspects of the theoretical and design work I express deep gratitude to my colleagues Mr. A.A.Fogarasy and Dr. K. Hamer and to Dr. A.D.S.Barr of Edinburgh University who gave generously of their time in numerous discussions.

Finally I acknowledge the financial support of the Science Research Council in the shape of Grant No. B/SR/1818 under which this work was commenced.

CONTENTS

LIST OF FIGURES

Fig. 26 ACCELERATION COMPONENTS IN DEFLECTED COUPLER

27(a) COMPONENTS OF COUPLER END-FORCE (2,1,2,2)

27(b) " " " " " (4,1,4,4)

27(c) " " " " " (5,1,5,2)

27(d) " " " " " (10,1,10,4)

27(e) " " " " " (54,0.4,54,3)

28 SOLUTION OF HILL'S EQUATION : Effect of Step-length

29 " " " " : " " "

30 " " " " : Comparison of two methods

31 " " " " : Amplitudes of First Three Modes

32 FORCING FUNCTIONS IN EQUATION (6.14)

33 STABLE AND UNSTABLE SOLUTIONS OF EQUATION (6.15)

34 STABILITY CHART

35 STABILITY CHART : Effect of Change of Dimensions

36 STABILITY CHART : First Unstable Region (2,1,2,2)

37 STABILITY CHART : Effect of Increasing Damping Coefficient

38 CHARACTERISTIC STABILITY SPACE

39 GENERAL VIEW OF APPARATUS

40 MOUNTING OF DRIVE MOTOR

41 DETAILS OF EXPERIMENTAL LINKAGE (ASSEMBLED)

42 COUPLER AND FOLLOWER COMPONENTS

43 CIRCUITRY

44 MEASUREMENT OF COUPLER STIFFNESS

45 CALIBRATION OF VIBRATIONAL AMPLITUDE

46 CALIBRATION CURVES

47 COMPARISON OF THEORETICAL AND EXPERIMENTAL WAVE-FORMS ($\omega_2 = \Omega/8$)

48 " " " " ($\omega_2 = \Omega/5$)

49 " " " " ($\omega_2 = \Omega/3$)

50 " " " " ($\omega_2 = \Omega/4$)

51 " " " " ($\omega_2 = \Omega/4.7$)

Fig. 52 FREQUENCY RESPONSE (5,1,5,2), 3/64 in, I_{MIN}

53 " " (10,1,10,4), 1/32 in, I = 0.00783

54 CHANGE OF MODE SHAPE THROUGH RESONANCE

55 EFFECT OF FOLLOWER INERTIA UPON COUPLER VIBRATION

56 FREQUENCY RESPONSE (5,1,5,2), 1/32 in, I = 0.0069

57 " " " " I = 0.0079

58 " " " " I = 0.0109

59 " " " " I = 0.0130

60 " " " " I = 0.0149

61 " " " " I_{MAX}

62 " " (10,1,10,4) " I_{MIN}

63 " " " " "

64 VIBRATION OF PERIOD 4π

65 FREQUENCY RESPONSE (10,1,10,4), 1/32 in, I = 0.0079

66 " " " " I_{MIN} , SPEED DECREASING

67 " " " " " " "

68 " " " " I = 0.0079 " "

69 NON-LINEAR RESONANCE AT $\Omega/2$ and INSTABILITY AT $2\Omega/3$

70 NON-LINEAR RESONANCE (5,1,5,2), 1/16 in, I_{MIN} , SPEED INCREASING

71 " " " " " , SPEED DECREASING

72 DAMPED FREE VIBRATION, 1/16 in, COUPLER

73 " " " 3/64 in. COUPLER

74 FREQUENCY RESPONSE (5,1,5,2), 3/64 in, I_{MIN}

75 " " " " "

76 " " " " I = 0.0109

77 NON-LINEAR RESPONSE " " I_{MIN}

78 " " " " " , SPEED DECREASING

79 FREQUENCY RESPONSE " 1/16 in, I_{MIN}

80 " " " " "

81 ONSET OF INSTABILITY " 1/32 "

82 STABILITY CHART " "

83 " " " 3/64 in.

84 " " " 1/16 in.

Fig. 85 STABILITY CHART (10,1,10,4) 1/32 in. COUPLER

86 " " " 3/64 in. "

87 " " " 1/16 in. "

88 ONSET OF INSTABILITY. FRAMES FROM HIGH-SPEED FILM

89 " " " " " " " "

Note: Wherever possible figures follow the page on which they are first referred to.

CHAPTER 1

INTRODUCTION

The work described in this thesis was carried out in the Department of Mechanical Engineering of the University of Newcastle upon Tyne. The programme of work was undertaken with the aim of adding to the current knowledge of mechanism dynamics with particular reference to the four-bar linkage since, at the time the work was commenced, there was a marked paucity of published work on the topic in this country.

Part I of the thesis contains a brief but necessary presentation of the kinematics of plan ar linkage mechanisms. Although the principles involved have been well known for the past century (1-5), the equations developed herein are presented in a form particularly appropriate for use with digital computers, the recent rapid development of which has made the study of mechanism kinematics a much simpler task than hitherto. The methods employed here in obtaining illustrative results can be simply adapted for application to mechanisms considerably more complex than the four-bar chain. Fourier analysis of the motions of the links in such mechanisms is also considered, a simple numerical integration procedure being used for the calculation of coefficients rather than the analytical method developed by Freudenstein (25) which is considerably more complicated and of a more theoretical interest.

The kinematic effects of the presence of a finite clearance in the pin-joints of the four-bar linkage are examined and the importance of the effect of transmission angle magnitude upon the amplitude of the possible free motion of the out-put link is illustrated theoretically and with sample numerical results. The considerably more complex subject of the dynamic effects of clearance is not considered here.

In Part II the dynamics of planar linkage mechanisms is examined using the formulae derived in Part I to evaluate pin-forces developed due to the inertia of the links themselves. The equations may be simply adapted to include the

effects of external loading and are again in a form suited to digital computing. An important extension of this part of the work is in the modification of the equations to include the effects of balancing, either partial or total. It is shown that in general there is an optimum balancing condition for each of the individual links by which, even in the totally balanced condition when the net force will be zero, the increase in individual pin-forces and torque exerted upon the frame may be kept to a minimum.

The work covered in Parts I and II, which has been published in abbreviated form in the Journal of Mechanical Engineering Science (16), deals mainly with "ideal" mechanisms, viz. mechanisms in which the effects of friction and clearance in bearings and elasticity of individual links are ignored. Parts III and IV on the other hand are concerned with the dynamics of mechanisms with elastic links, in particular the crank and rocker type linkage with an elastic coupler or connecting link. In Part III the equation of motion is derived and, subject to certain linearizing assumptions, is found to be a special type of Hill's equation. An account of this work has been published in the Journal of Mechanical Engineering Science (35). A perturbation method of analysis is applied to the equation of motion in order to determine the stability criteria of the system in terms of the Fourier coefficients of the periodic functions in the equation, which are kinematic functions of the linkage, and other parameters which are kinematic and dynamic functions of the links themselves. It is found that the equation of motion may be simplified under certain conditions which allow a more thorough examination of the stability criteria. Furthermore, the analysis of the full equation requires a modification to the familiar perturbation technique in order to allow the stability criteria to be found. Descriptions of this modified method have been published in the Journal of Applied Mechanics (30) and the Proceedings of the 3rd World Congress for the Theory of Machines and Mechanisms (29).

Part IV deals with the experimental investigations carried out in association with the theoretical work of Part III. Vibrations generated in a number of experimental mechanisms are compared with theoretical wave-forms obtained from

digital computer solutions of the equation of motion. Good agreement is obtained between experiment and two computed solutions obtained by quite different methods. The speeds at which the motion becomes unstable in these mechanisms are also compared with the theoretically predicted speeds.

PART I

KINEMATICS

CHAPTER 2

KINEMATICS OF LINKAGE MECHANISMS

2.1 Historical

The study of the kinematics of mechanisms may be considered to have begun with the work of Willis[1] and Reuleux[2] in the latter half of the nineteenth century. An extensive literature has been produced since then which covers a wide range of geometrical and algebraic techniques applied to the analysis of mechanisms of all types, both planar and spatial [6,7]. The present discussion will be restricted to an examination of the kinematic properties of the planar four bar linkage and a limited number of closely associated mechanisms.

The planar four bar linkage is the basic mechanism of all higher classes of linkage mechanisms and consequently a study of the kinematic properties forms the basis for all subsequent work. Since the first descriptive work of the nineteenth century, many slightly different but essentially similar methods have been proposed to deal with the problem. Blokh[8] has been credited with the first use of complex number methods in connection with synthesis of mechanisms but the method is equally suited to analytical work and has been widely adopted. It will be used also in this work.

2.2 Position

2.2.1 Crank - Rocker and Double Rocker Configurations

Fig. 1 shows a four bar linkage ABCD in which AD is the fixed link, or frame of length ℓ_1, AB the crank or input link of length ℓ_2, BC the coupler or connecting link of length ℓ_3 and CD the follower or output link of length ℓ_4.

The orientations θ_i of the three movable links are measured with respect to the fixed link and are considered positive in the anticlockwise sense as shown.

This notation is becoming generally accepted internationally and will be used throughout this work.

In order to develop equations which will enable the output angle θ_4 to be evaluated in terms of the input angle θ_2, we consider the mechanism as a vector polygon composed of two pairs of vectors as shown in Fig. 2.

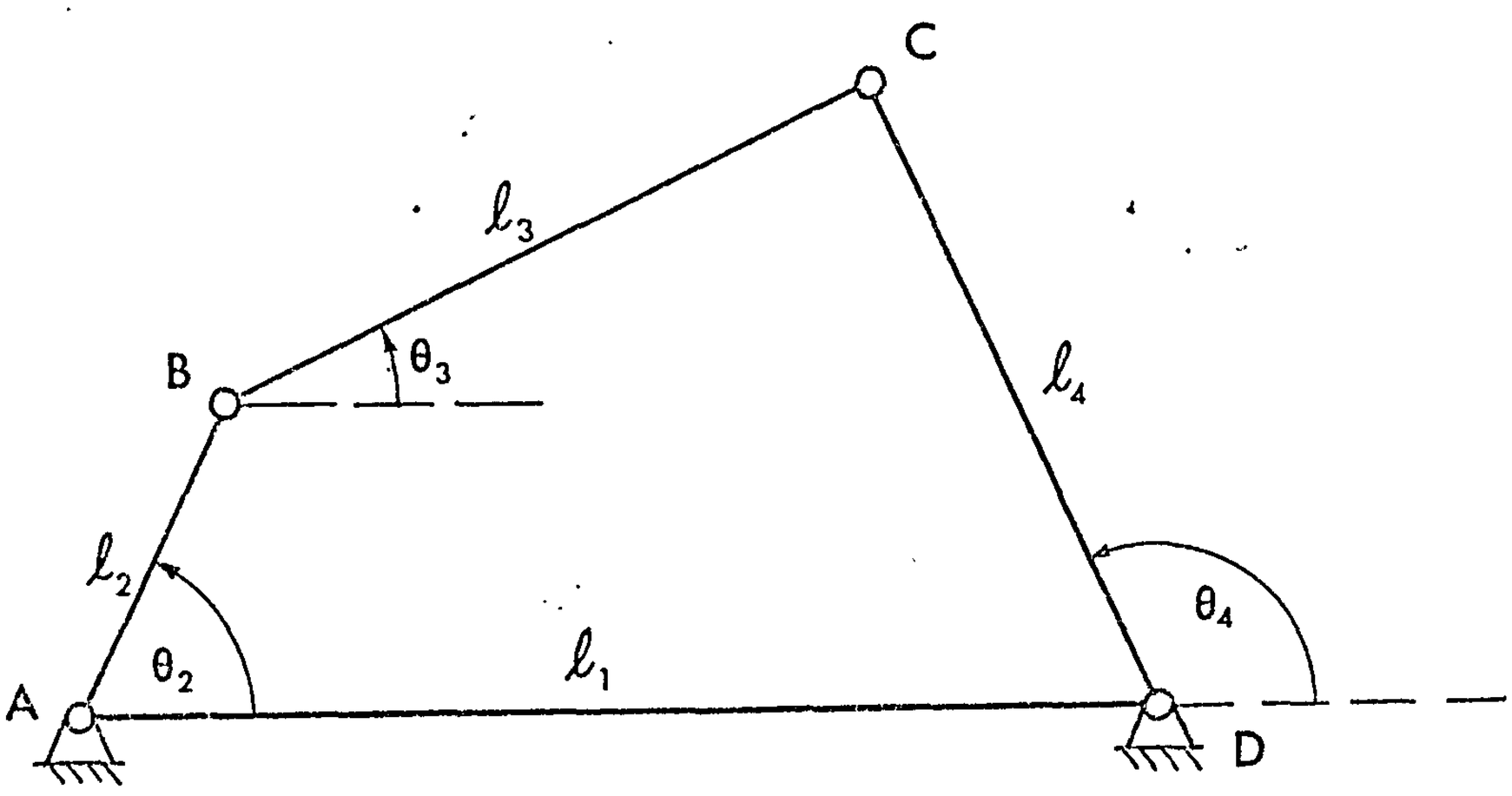

FIG. 1. FOUR-BAR LINKAGE : Notation

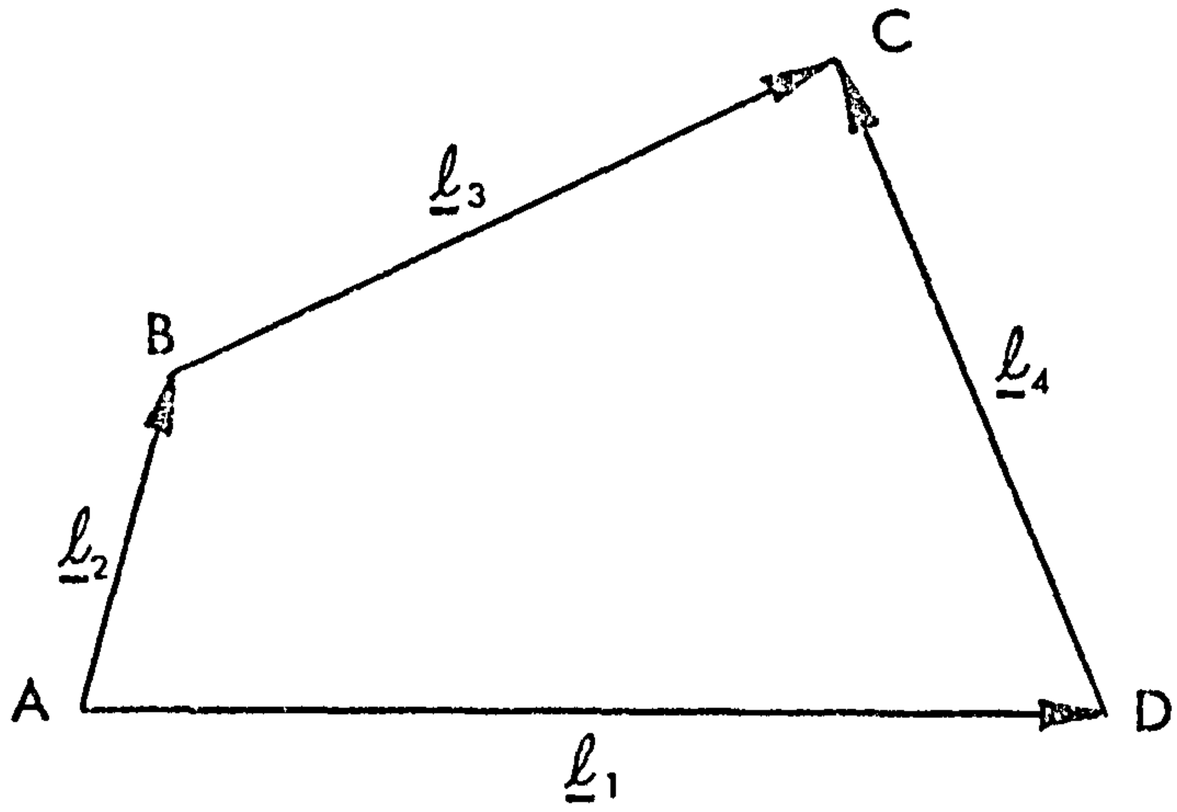

FIG.2. FOUR-BAR LINKAGE : Vector Representation

$$\underline{AB} + \underline{BC} = \underline{AC} + \underline{DC}$$

or, in terms of the vector lengths

$$\underline{\ell_2} + \underline{\ell_3} = \underline{\ell_1} + \underline{\ell_4} \qquad (2.1)$$

The angular orientations of the vectors are introduced by considering the horizontal and vertical projections of the polygon. Details of the resultant calculations are given in Appendix 1. We quote here the required expression for the output angle.

$$\cos\theta_4 = \frac{-AB}{D^2} \pm \sqrt{\left(\frac{AB}{D^2}\right)^2 - \frac{B^2 - C^2}{D^2}} \qquad (2.2)$$

where $A = 2\ell_4(\ell_2\cos\theta_2 - \ell_1)$

$B = \ell_3^2 - \ell_1^2 - \ell_2^2 - \ell_4^2 + 2\ell_1\ell_2\cos\theta_2$

$C = 2\ell_2\ell_4\sin\theta_2$

and $D = A^2 + C^2$

This equation enables the cosine of the output angle θ_4 to be determined in terms of the input angle θ_2. The corresponding sine value may be obtained directly from the cosine or from the equation (see Appendix 1),

$$A\cos\theta_4 + B + C\sin\theta_4 = 0 \qquad (2.3)$$

As will be seen below, the formulae for angular velocity and acceleration contain trigonometric functions of the angles θ_i rather than the angles themselves. It is therefore appropriate to work in terms of these functions, especially when using digital computer techniques.

Having obtained the required functions of θ_4, it remains solely to determine in which quadrant the angle occurs. However the possibility of two values for the cosine necessitates a consideration of the geometry of the linkage itself. Fig. 3 shows the two possible orientations of the mechanism for a fixed crank position.

For the mechanism ABCD, θ_4 must lie in the first or second quadrant whereas for the mechanism ABC'D, θ'_4 will be in the third or fourth quadrant.

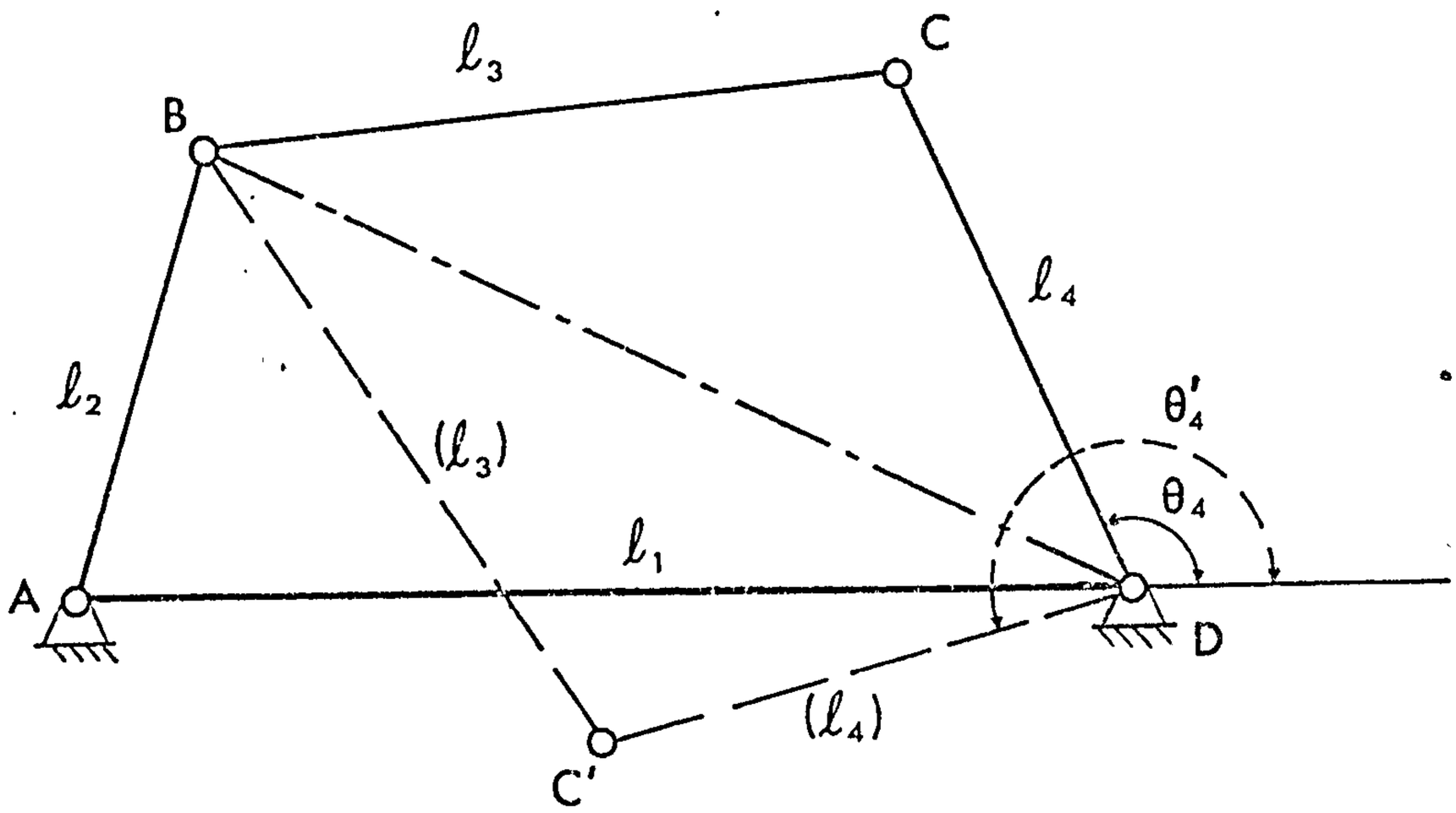

FIG.3. FOUR-BAR LINKAGE: Two Possible Orientations of links.

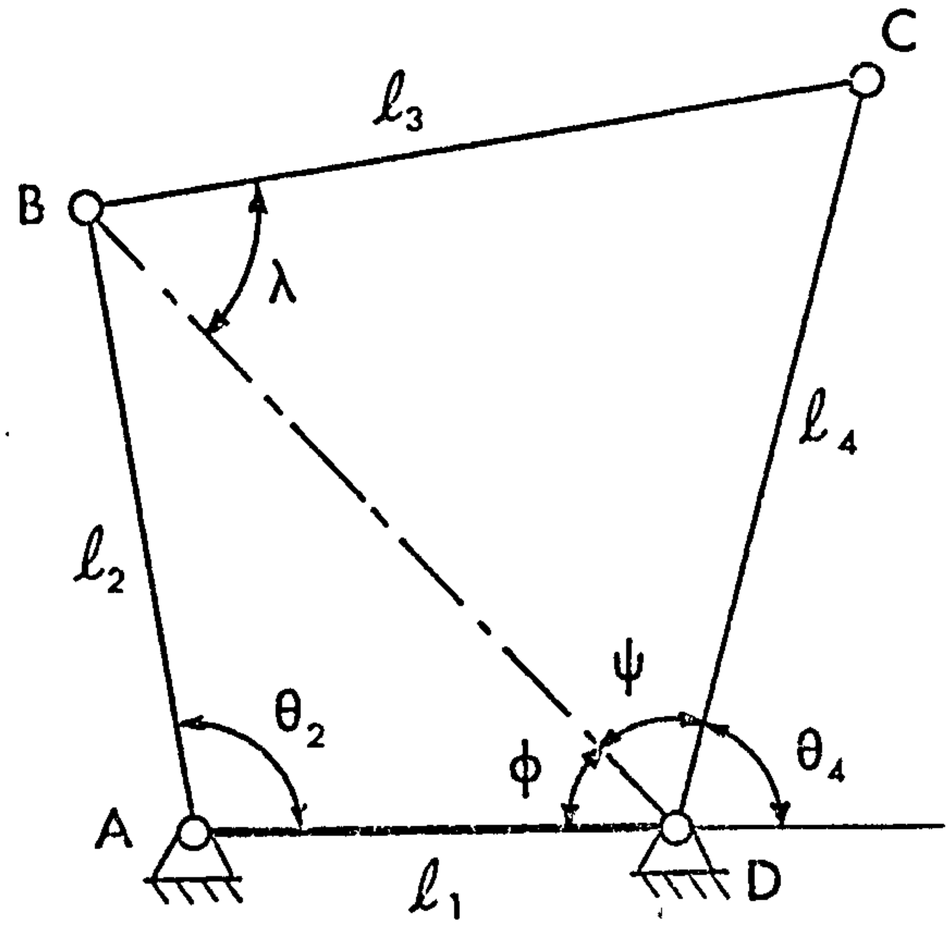

FIG.4. FOUR-BAR LINKAGE : Drag link Notation

A further examination of equation (2.2) shows that the first term on the right hand side is equivalent to - cos $\widehat{ADB}$. cos $\widehat{BDC}$ while the second term is equivalent to sin $\widehat{ADB}$. sin $\widehat{BDC}$.

Hence equation (2.2) may be written

$$\cos \theta_4 = - \cos (\widehat{ADB} \pm \widehat{BDC}) \qquad (2.4)$$

and we see the significance of the two values of θ_4 reflected in the geometry of the mechanism (fig.3). The angle ($\widehat{ADB}$ + $\widehat{BDC}$) = $\widehat{ADC}$ = (π - θ_4) gives the upper or 'open' position of ℓ_4 whereas the alternative value ($\widehat{ADB}$ - $\widehat{BDC}$) = $\widehat{ADC'}$ = (θ'_4 - π) gives the lower or 'crossed' position of ℓ_4.

Having determined θ_4 from equation (2.2), it is possible to evaluate θ_3 if required either from an analogous equation resulting from the elimination of θ_4 or as described in Appendix 1.

2.2.2 Drag Link Configurations

The foregoing suggests a possible alternative method of obtaining the correct value of the angle θ_4 in mechanisms such as the drag link in which the output link rotates completely about its fixed pivot with the consequence that θ_4 may lie in any of the four quadrants. The ability to determine simply the sign of the trigonometric function is of importance in programme writing for digital computer work where equations such as (2.2) are used.

Fig. 4 shows a drag link mechanism with angles θ_i defined as before but with additional angles ϕ, ψ, λ defined as shown. The first of these is defined immediately by

$$\sin \phi = \frac{\ell_2}{BD} \sin \theta_2$$

$$\cos \phi = \pm \sqrt{1 - \sin^2 \phi}$$

When $\phi > 90^0$, the negative value is given to the cosine and this occurs when

$$\ell_2 \cos \theta_2 > \ell_1$$

The remaining two angles are defined by the cosine rule applied to triangle BCD as follows,

$$\cos \lambda = \frac{\ell_3^2 - \ell_4^2 + BD^2}{2\ell_3 \cdot BD}$$

$$\cos \psi = \frac{\ell_4^2 - \ell_3^2 + BD^2}{2\ell_4 \cdot BD}$$

The corresponding sines are always positive since both λ and ψ are always less than 180^0.

Finally, θ_3 and θ_4 are defined by the equations

$$\begin{aligned}
\sin \theta_3 &= \sin (\lambda - \phi) = \sin \lambda \cos \phi - \cos \lambda \sin \phi \\
\cos \theta_3 &= \cos (\lambda - \phi) = \cos \lambda \cos \phi + \sin \lambda \sin \phi \\
\\
\sin \theta_4 &= \sin (\phi + \psi) = \sin \phi \cos \psi + \cos \phi \sin \psi \\
\cos \theta_4 &= -\cos (\phi + \psi) = -\cos \phi \cos \psi + \sin \phi \sin \psi
\end{aligned}$$

This method enables a simpler programming of the drag link kinematics to be achieved and reduces the probability of the use of incorrect sine or cosine values.

2.3 Angular Velocities

The angular velocities of the coupler and follower may be determined from differentiation of equation (2.2). This however causes considerable unnecessary complication in the calculations and a more convenient method is to consider the vector equation (2.1).

Using the vector notation $\underline{\ell}_i = \ell_i e^{i\theta_i}$ and differentiating we have

$$i\omega_2 \underline{\ell}_2 + i\omega_3 \underline{\ell}_3 - i\omega_4 \underline{\ell}_4 = 0 \qquad (2.5)$$

Again considering horizontal and vertical components, we obtain two equations

$$\left.\begin{aligned}
\ell_2 \omega_2 \cos \theta_2 + \ell_3 \omega_3 \cos \theta_3 - \ell_4 \omega_4 \cos \theta_4 &= 0 \\
\ell_2 \omega_2 \sin \theta_2 + \ell_3 \omega_3 \sin \theta_3 - \ell_4 \omega_4 \sin \theta_4 &= 0
\end{aligned}\right\} \qquad (2.6)$$

which may be solved simultaneously for ω_3 and ω_4.

$$\left.\begin{aligned}
\omega_3 &= -\omega_2 \frac{\ell_2 \sin (\theta_2 - \theta_4)}{\ell_3 \sin (\theta_3 - \theta_4)} \\
\omega_4 &= -\omega_2 \frac{\ell_2 \sin (\theta_2 - \theta_3)}{\ell_4 \sin (\theta_3 - \theta_4)}
\end{aligned}\right\} \qquad (2.7)$$

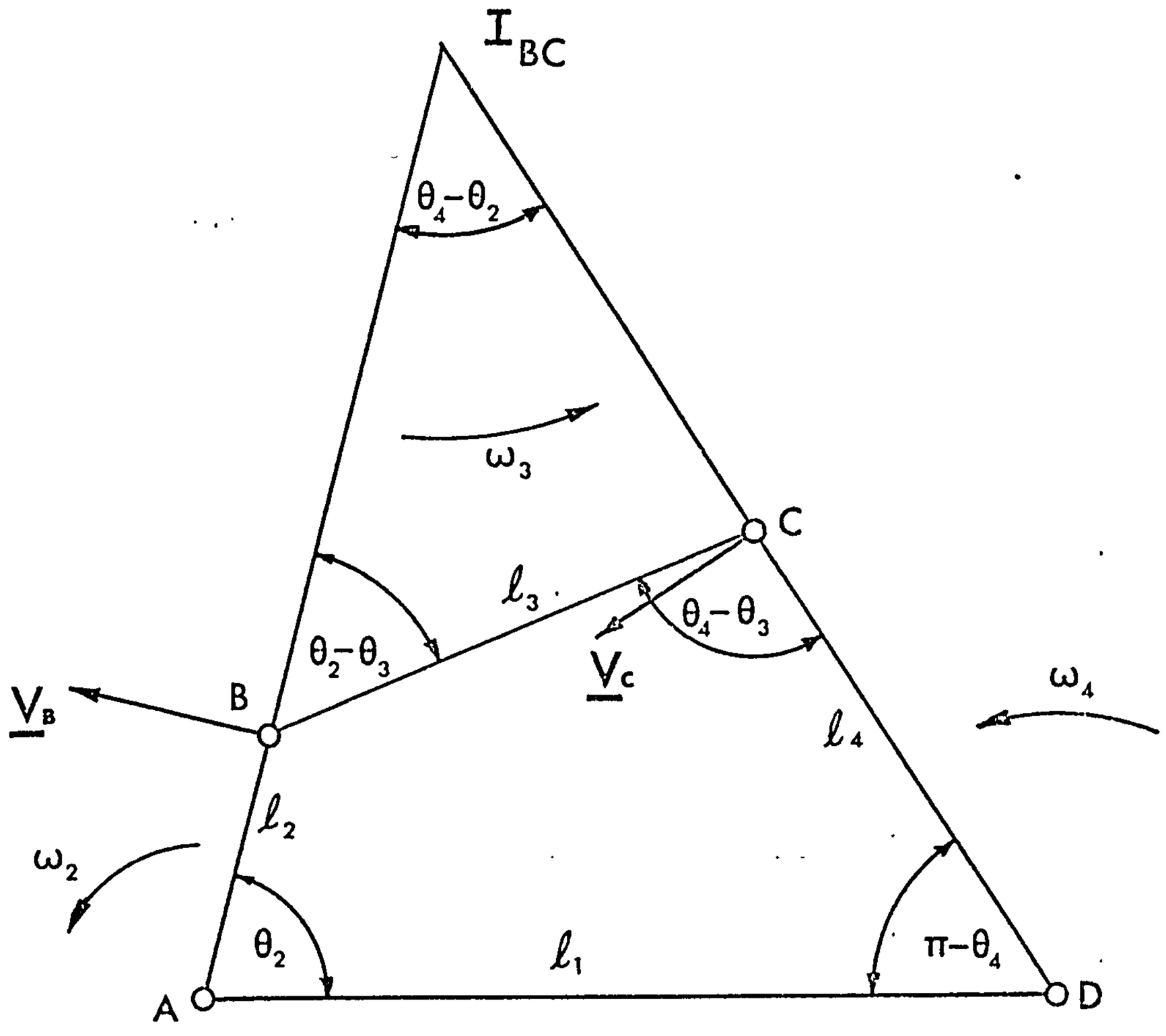

$$V_B = \ell_2 \omega_2 = -B I_{BC} \cdot \omega_3$$

$$\omega_3 = -\frac{\ell_2 \omega_2}{B I_{BC}}$$

$$\& \quad \frac{B I_{BC}}{\sin(\pi+\theta_3-\theta_4)} = \frac{\ell_3}{\sin(\theta_4-\theta_2)}$$

$$\therefore \quad \omega_3 = -\omega_2 \frac{\ell_2 \sin(\theta_2-\theta_4)}{\ell_3 \sin(\theta_3-\theta_4)}$$

FIG.5. FOUR-BAR LINKAGE : Geometric Properties

These simple relationships may also be obtained conveniently from a consideration of the geometry of the linkage as shown in Fig. 5.

2.4 Angular Accelerations

Again differentiating equation (2.5) we obtain the equation of the acceleration vector polygon:

$$(i\alpha_2 - \omega_2^2)\underline{\ell}_2 + (i\alpha_3 - \omega_3^2)\underline{\ell}_3 - (i\alpha_4 - \omega_4^2)\underline{\ell}_4 = 0 \qquad (2.8)$$

The horizontal and vertical components of which are

$$-\ell_2(\alpha_2 \sin\theta_2 + \omega_2^2 \cos\theta_2) - \ell_3(\alpha_3 \sin\theta_3 + \omega_3^2 \cos\theta_3) + \ell_4(\alpha_4 \sin\theta_4 + \omega_4^2 \cos\theta_4) = 0$$

$$+\ell_2(\alpha_2 \cos\theta_2 - \omega_2^2 \sin\theta_2) + \ell_3(\alpha_3 \cos\theta_3 - \omega_3^2 \sin\theta_3) - \ell_4(\alpha_4 \cos\theta_4 - \omega_4^2 \sin\theta_4) = 0 \qquad (2.9)$$

Solving equations (2.9) for α_3, α_4 yields

$$\alpha_3 = \left(\frac{\omega_3}{\omega_2}\right)\alpha_2 - \left\{\frac{\omega_2^2 \ell_2 \cos(\theta_2 - \theta_4) + \omega_3^2 \ell_3 \cos(\theta_3 - \theta_4) - \omega_4^2 \ell_4}{\ell_3 \sin(\theta_3 - \theta_4)}\right\} \qquad (2.10)$$

$$\alpha_4 = \left(\frac{\omega_4}{\omega_2}\right)\alpha_2 - \left\{\frac{\omega_2^2 \ell_2 \cos(\theta_2 - \theta_3) - \omega_4^2 \ell_4 \cos(\theta_3 - \theta_4) + \omega_3^2 \ell_3}{\ell_4 \sin(\theta_3 - \theta_4)}\right\}$$

2.5 Digital Computation

The equations developed in the foregoing sections are in a form which is particularly suitable for application to digital computation. Since the angular positions, velocity and acceleration of the links are determined in terms of the sines and cosines of the angles, the latter quantities may be used as the basic variables in an algorithm. Such terms as $\sin(\theta_3 - \theta_4)$ for instance are evaluated from the simple relationship

$$\sin(\theta_3 - \theta_4) = \sin\theta_3 \cos\theta_4 - \cos\theta_3 \sin\theta_4$$

A simple programme based on this approach and which evaluates positions, velocities and accelerations for a crank and rocker type of four bar linkage is shown in Appendix 2. (This programme forms the core of a larger programme used by the Engineering Sciences Data Unit Kinematics Committee of which the author is a member. The programme will be used to produce data for a Design Memorandum on Analysis and Synthesis of Four Bar linkage Mechanisms).

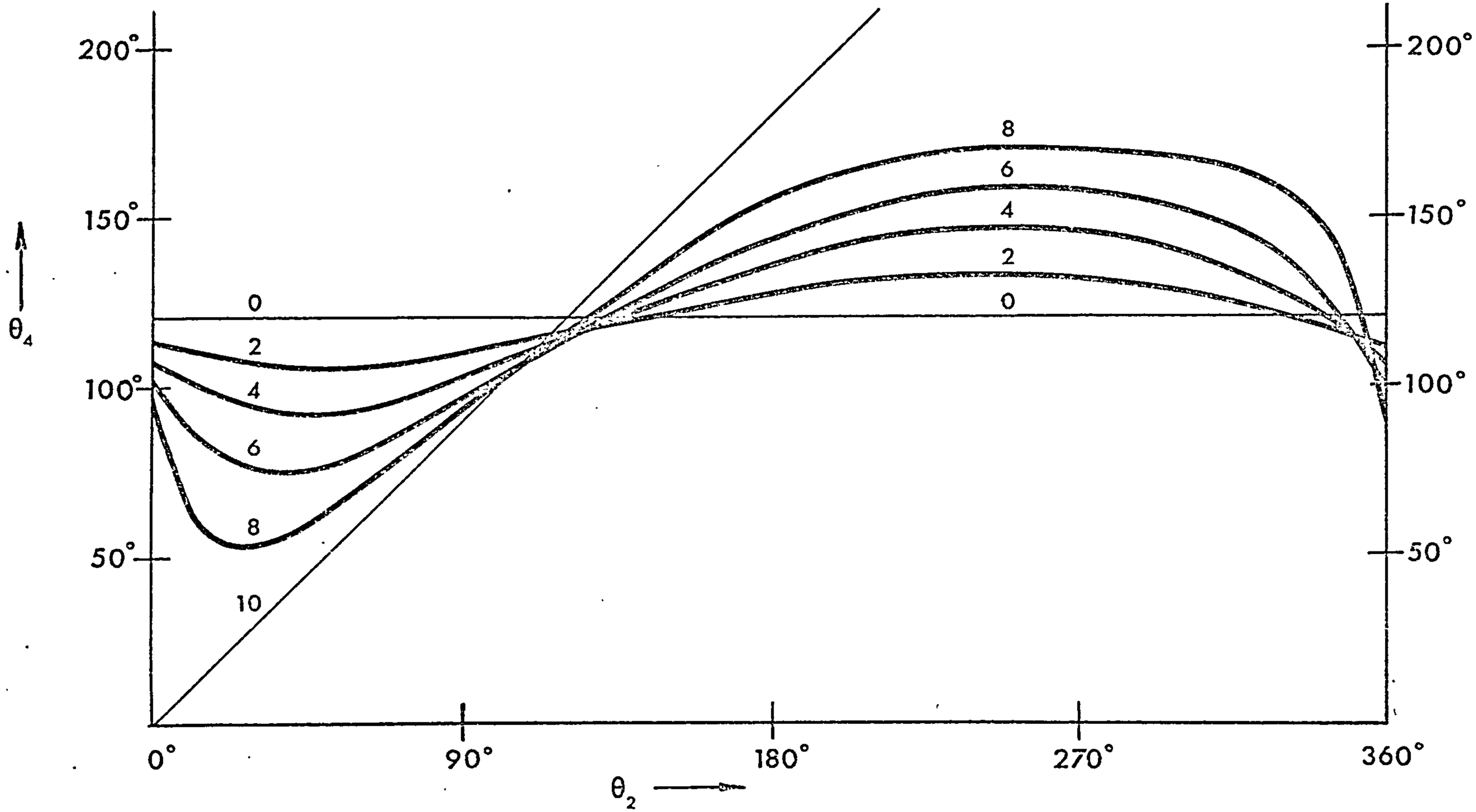

FIG. 6(a) OUTPUT ANGLE vs. INPUT ANGLE

($\ell_1 = \ell_3 = \ell_4 = 10$; Value of ℓ_2 as shown)

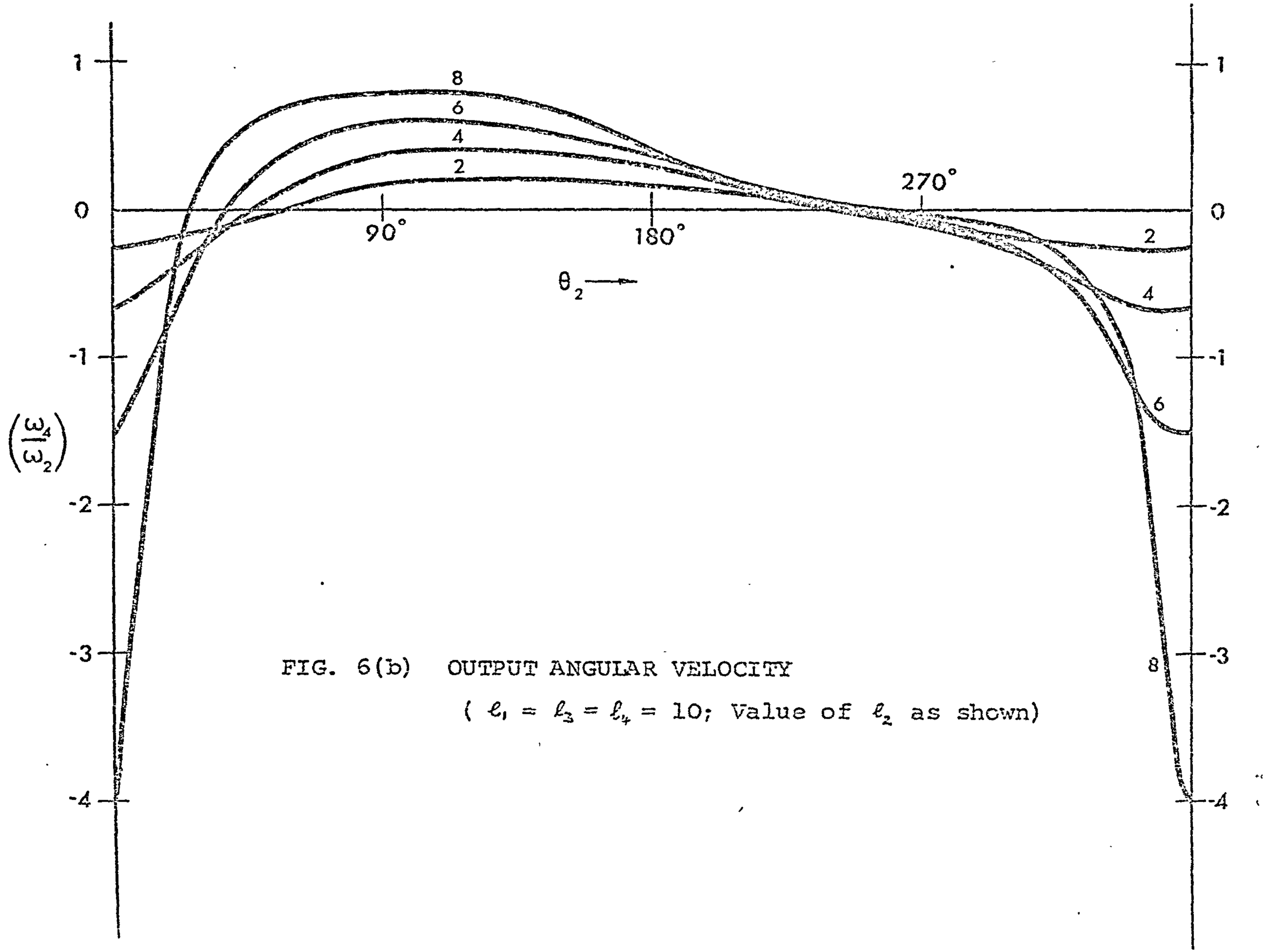

FIG. 6(b) OUTPUT ANGULAR VELOCITY

($\ell_1 = \ell_3 = \ell_4 = 10$; Value of ℓ_2 as shown)

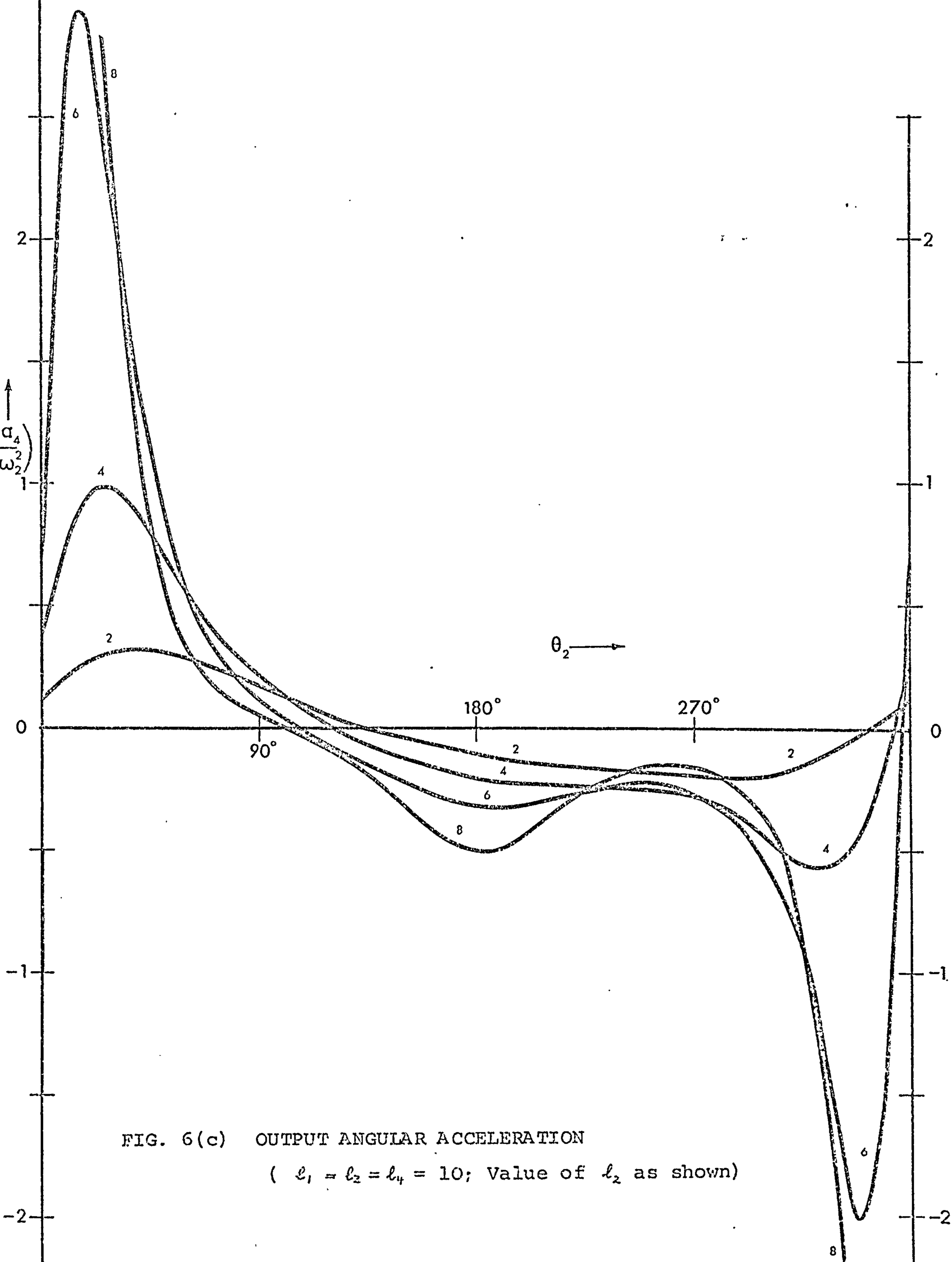

FIG. 6(c) OUTPUT ANGULAR ACCELERATION

($\ell_1 = \ell_2 = \ell_4 = 10$; Value of ℓ_2 as shown)

With such a programme available, it is instructive to investigate how the Kinematic properties of the four bar linkage vary with change of linkage dimensions. Figs. 6 (a,b,c,) show respectively position, angular velocity and acceleration of the follower of a crank and rocker mechanism with constant unit i/p speed for a range of crank lengths while the remaining three link lengths are constant and equal to each other. As the crank length $\ell_2 \rightarrow 0$, the mechanism attains the form of an equilateral triangle in which $\theta_4 = 120^\circ$ and velocity and acceleration approach zero. At the other end of the range, as ℓ_2 approaches the value of ℓ_1 ($= \ell_3 = \ell_4$) the mechanism becomes a parallel motion device in which $\theta_4 = \theta_2$, $\omega_4 = \omega_2$ and $\alpha_4 = \alpha_2$. In the case of constant input motion, $\alpha_4 = \alpha_2 = 0$.

The θ_4 curve for the parallel motion mechanism appears as a saw-tooth form suggesting a discontinuity at $\theta_2 = 0$. This is a natural consequence of the method of showing output angle as a function of input angle, the physical motion being constant rotation. (It is worthy of note here perhaps that in such mechanisms, dynamic effects are most important and it is usual to employ subsidiary mechanisms or other devices to overcome the problem of jamming or sudden reversals at dead-centre positions).

2.6 Fourier Analysis

Freudenstein[25] has described an analytical method for the harmonic analysis of four bar linkage motions. In particular, the output motion is often of interest and Freudenstein's paper deals with the problem of obtaining an expression for the output angle in terms of harmonics of the input angle. The method involves considerable calculation which in the majority of cases would require the assistance of a digital computer. A more direct method would therefore seem to present itself; that of calculating directly the Fourier coefficients of the output angle θ_4 when expressed as a periodic function of input angle θ_2. Appendix 3 lists a simple integration procedure, using Simpson's rule to evaluate any number of such coefficients to any prescribed accuracy. The method works well and a selection of typical results is shown in Fig. 7 where sine and cosine coefficients are compared over a range of mechanism dimensions. As may be seen,

$$\theta_4 = \sum_{n=0}^{\infty} \{a_n \cos n\theta_2 + b_n \sin n\theta_2\}$$

a_0 not shown

a_n

b_n

$\left(\ell_1 = \ell_3 = \ell_4 = 10\right)$

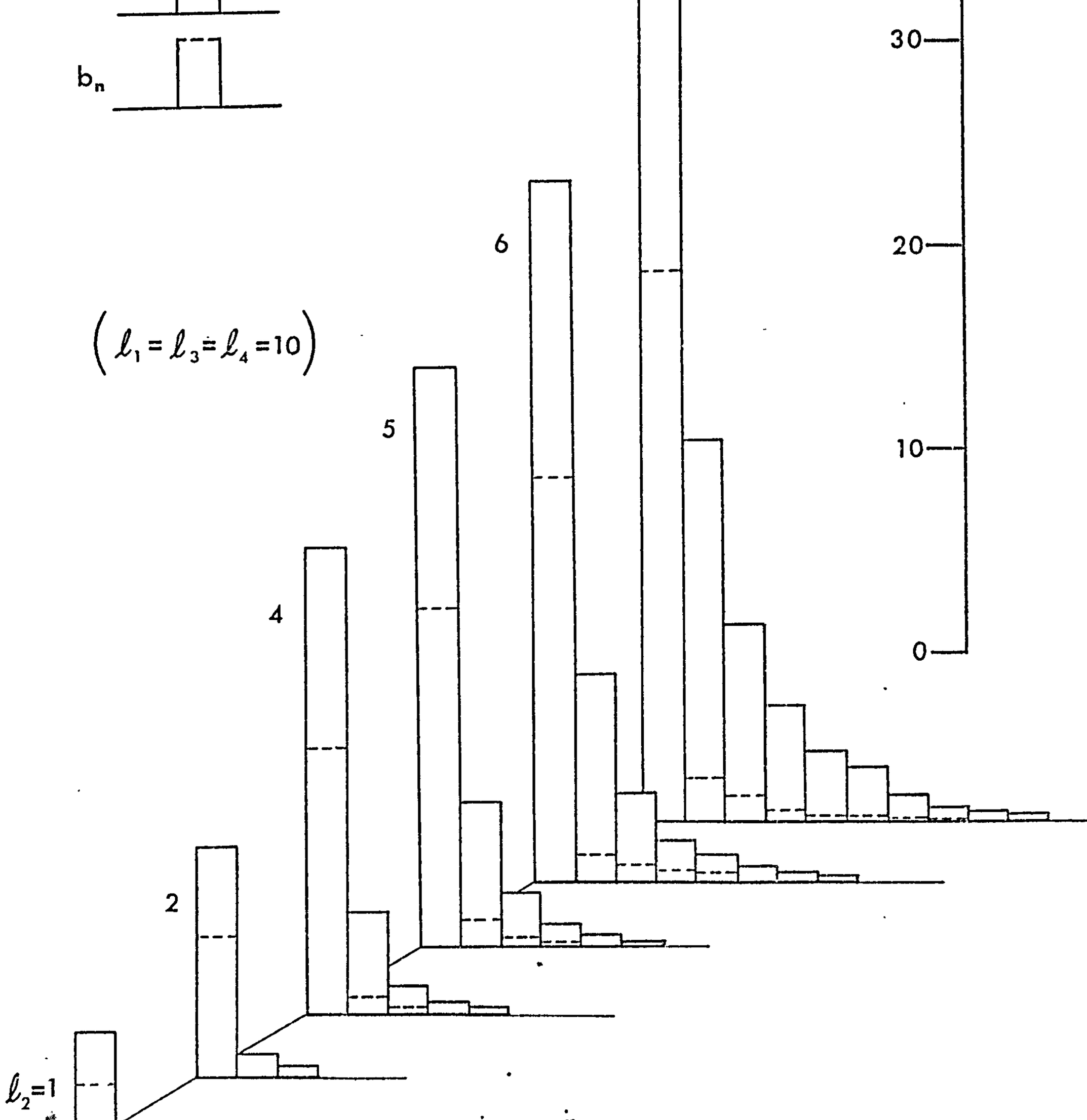

FIG.7. FOURIER COMPONENTS of OUTPUT MOTION

for small values of ℓ_2, only the first sine and cosine coefficients are significant. As ℓ_2 increases however, more of the coefficients become important but of the sine terms only the first increases noticably. The cosine terms become larger and are always greater than the corresponding sine terms.

The coefficients shown in Fig. 7 refer to θ_4 as a function of θ_2. The procedure given in Appendix 3 may be used for any periodic function and, as will be seen below, this becomes important in the dynamic analysis of mechanisms when the Fourier coefficients of periodic forces must be determined.

CHAPTER 3

KINEMATIC EFFECTS OF CLEARANCE

The kinematic effects of clearances present at the pin joints upon the output motion of a linkage mechanism are much more easily determined than are the dynamic effects. However, they have apparently been given little attention and there are few references on the subject. It may be useful therefore to examine such effects of a clearance at one of the pin joints of the coupler in a four bar linkage.

Fig. 8 shows schematically such a linkage ABCD in which there is present a clearance c at the coupler-follower joint C (the magnitude of the clearance is exaggerated for clarity). For a given crank angle θ_2, the nominal positions of the coupler BC and follower CD will be as shown (i.e. with zero clearance). However in the presence of some finite clearance c, the coupler and follower may take up any positions between the two extremes BC'D and BC"D.

To investigate how the range of possible values of output angle θ_4 varies with crank angle and linkage geometry, we consider the triangles BCD, BC'D and BC"D. Using the cosine rule we have :

$$BC^2 = BD^2 + CD^2 - 2BD.\ CD\ \cos\phi$$

$$BC'^2 = BD^2 + C'D^2 - 2BD.C'D\ \cos\phi'$$

$$BC''^2 = BD^2 + C''D^2 - 2BD.C''D\ \cos\phi''$$

Now $CD = C'D = C''D = \ell_4$

$$BC = \ell_3$$

$$BC' = \ell_3 + \frac{c}{2}$$

$$BC'' = \ell_3 - \frac{c}{2}$$

Hence $$\ell_3^2 = BD^2 + \ell_4^2 - 2BD.\ell_4\cos\phi$$

$$(\ell_3 + \frac{c}{2})^2 = BD^2 + \ell_4^2 - 2BD.\ell_4\cos\phi'$$

and $$(\ell_3 - \frac{c}{2})^2 = BD^2 + \ell_4^2 - 2BD.\ell_4\cos\phi''$$

$$\therefore\quad (\ell_3 + \frac{c}{2})^2 - \ell_3^2 = 2BD.\ell_4(\cos\phi - \cos\phi')$$

$$\cos\phi - \cos\phi' = \frac{\ell_3 c + \frac{c^2}{4}}{2BD.\ell_4} \qquad (3.1)$$

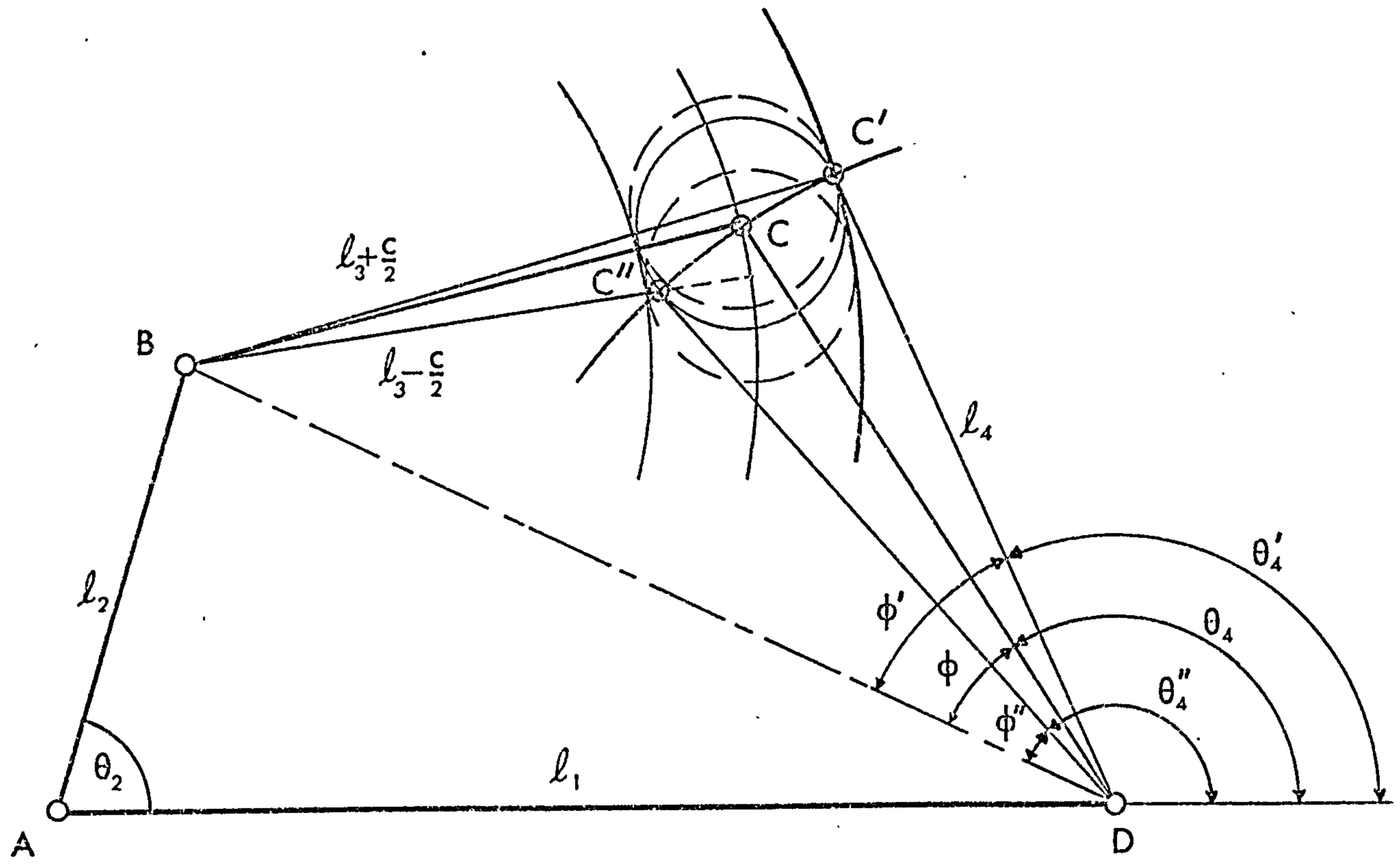

FIG.8. KINEMATIC EFFECTS OF CLEARANCE IN COUPLER-FOLLOWER JOINT.

Similarly

$$\cos \phi'' - \cos \phi = \frac{\ell_3 c - \frac{c^2}{4}}{2BD.\ \ell_4} \qquad (3.2)$$

Writing $\phi' = \phi + \delta\phi'$

and $\phi'' = \phi - \delta\phi''$

we have (for small $\delta\phi$)

$$\cos \phi' \doteq \cos \phi - \delta\phi' \sin \phi$$

$$\cos \phi'' \doteq \cos \phi + \delta\phi'' \sin \phi$$

whence we obtain

$$\delta\phi' = \frac{\ell_3 c + \frac{c^2}{4}}{2BD\,\ell_4 \sin \phi}$$

$$\delta\phi'' = \frac{\ell_3 c - \frac{c^2}{4}}{2BD\,\ell_4 \sin \phi}$$

$$\text{or} \quad \delta\phi = (\delta\phi' + \delta\phi'') = \frac{\ell_3 c}{BD\,\ell_4 \sin \phi} \qquad (3.3)$$

This equation defines the maximum angular movement of the follower for small clearance (second order terms in $\delta\phi$ having been ignored). The exact equations (3.1) and (3.2) must be used if the clearances are large or when the geometry of the linkage is such that comparatively large movements are possible. When the angle ϕ becomes very small, the approximate equation (3.3) yields increasingly large values for $\delta\phi$ indicating that the exact equation must be used. Consider the case in which $\phi = 0^o$ (in a practical mechanism this would be an extreme point in a double rocker configuration Fig. 9(a)). We now have

$$\cos \phi - \cos \phi' = \frac{\ell_3 c + \frac{c^2}{4}}{2BD.\ \ell_4}$$

and $\cos \phi = 1$

$BD = (\ell_3 + \ell_4)$

Hence $\cos \phi' = 1 - \frac{\ell_3 c + \frac{c^2}{4}}{2\ell_4 (\ell_3 + \ell_4)}$

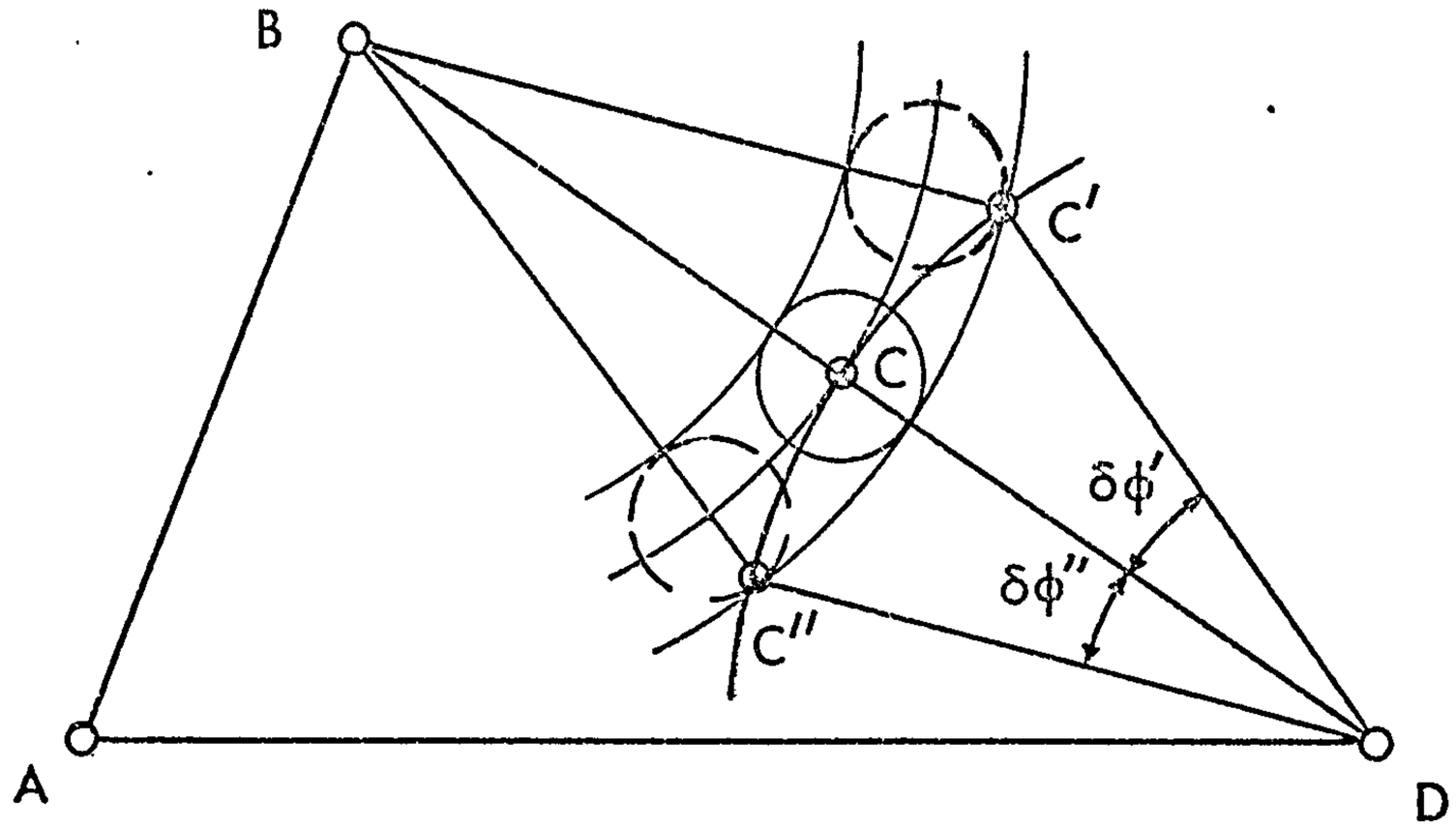

FIG. 9(a) KINEMATIC EFFECTS OF CLEARANCE
(Extreme Position $\phi = 0^{o}$)

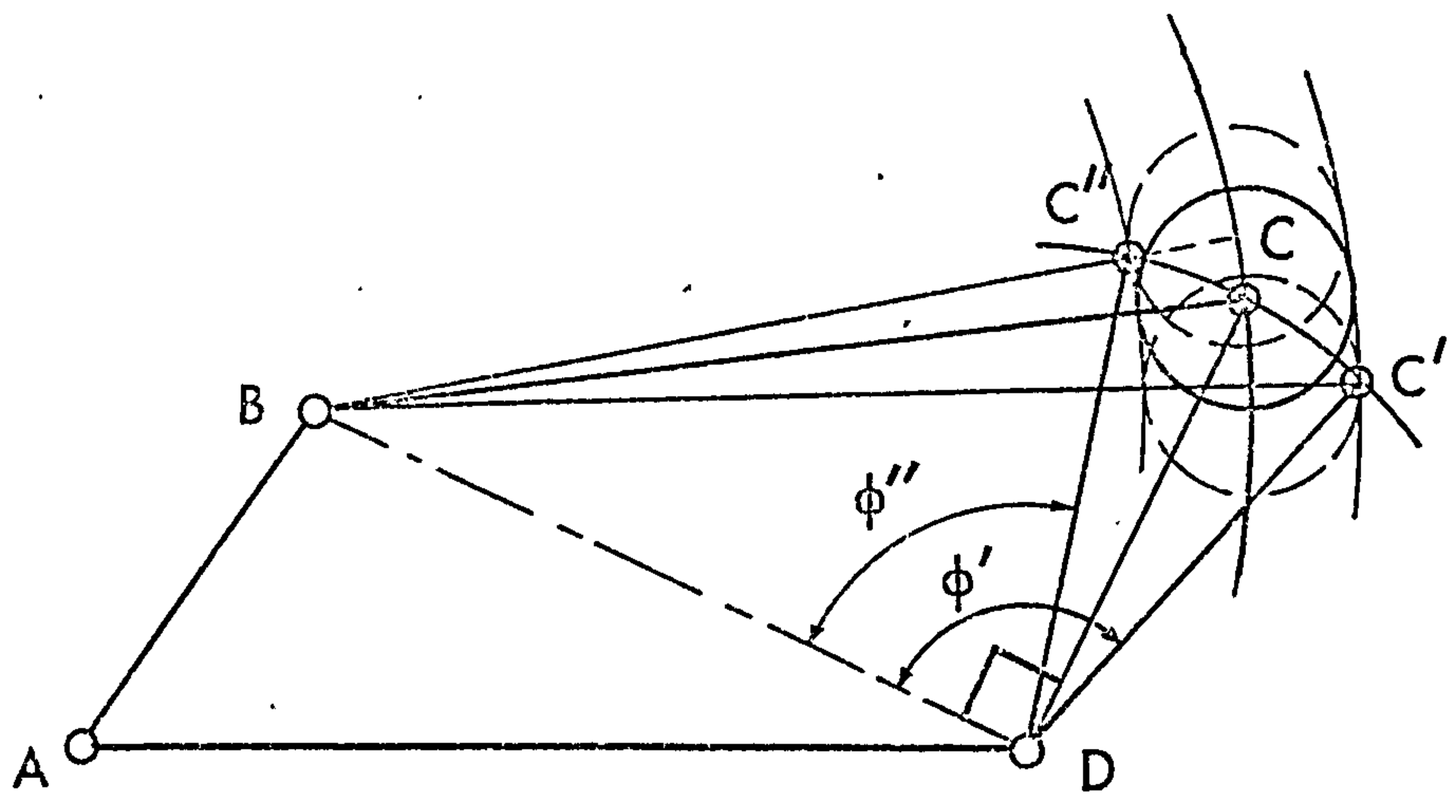

FIG.9.(b) KINEMATIC EFFECTS OF CLEARANCE
(Extreme Position $\phi = 90^{o}$)

The value of cos ϕ'' will be similar in this case.

The other limiting case is that for which $\phi = 90^{\circ}$ (see Fig. 9(b)).

The exact equation now yields immediately

$$\cos \phi' = - \frac{\ell_3 c + c^2/4}{2BD.\ \ell_4} \qquad \text{with} \quad BD^2 = \ell_3^2 - \ell_4^2$$

$$= \cos \left(\frac{\pi}{2} + \delta\phi' \right) \qquad = - \sin \delta\phi'$$

The approximate equation gives a similar result;

$$\delta\phi' \simeq \sin \delta\phi' = \frac{\ell_3 c + c^2/4}{2BD.\ \ell_4}$$

Considering again the general approximate equation, we see that the magnitude of the possible angular movement depends not only upon the amount of clearance present, but also upon the geometry of the linkage. Applying the sine rule to triangle BCD we have

$$\frac{BD}{\sin \mu} = \frac{\ell_3}{\sin \phi} \qquad \text{where} \quad \mu = \text{transmission angle } \widehat{BCD}$$

Therefore $$\delta\phi' = \frac{c}{\ell_4} \frac{}{\sin \mu}$$

This equation shows clearly the dependence of $\delta\phi'$ upon the linkage geometry. As the transmission angle μ approaches 90°, $\delta\phi'$ obtains its minimum value for any fixed c and ℓ_4.

Fig. 10 shows the variation of $\delta\phi'$ with crank angle θ_2 for a mechanism of dimensions $\ell_1 = \ell_3 = \ell_4 = 10$, $\ell_2 = 8$, for a number of values of the clearance c.

The maximum value of $\delta\phi'$ occurs at $\theta_2 = 0^{\circ}$ corresponding to the minimum value of transmission angle μ. There may also be a local maximum value at $\theta_2 = 180^{\circ}$ corresponding to the other extreme value of μ. In general these extreme values of μ will be respectively $< 90^{\circ}$ and $> 90^{\circ}$ so that the maximum value of sin μ will lie between those giving a minimum value of $\delta\phi'$. There is however, a range of mechanisms in which the transmission angle is always $< 90^{\circ}$.

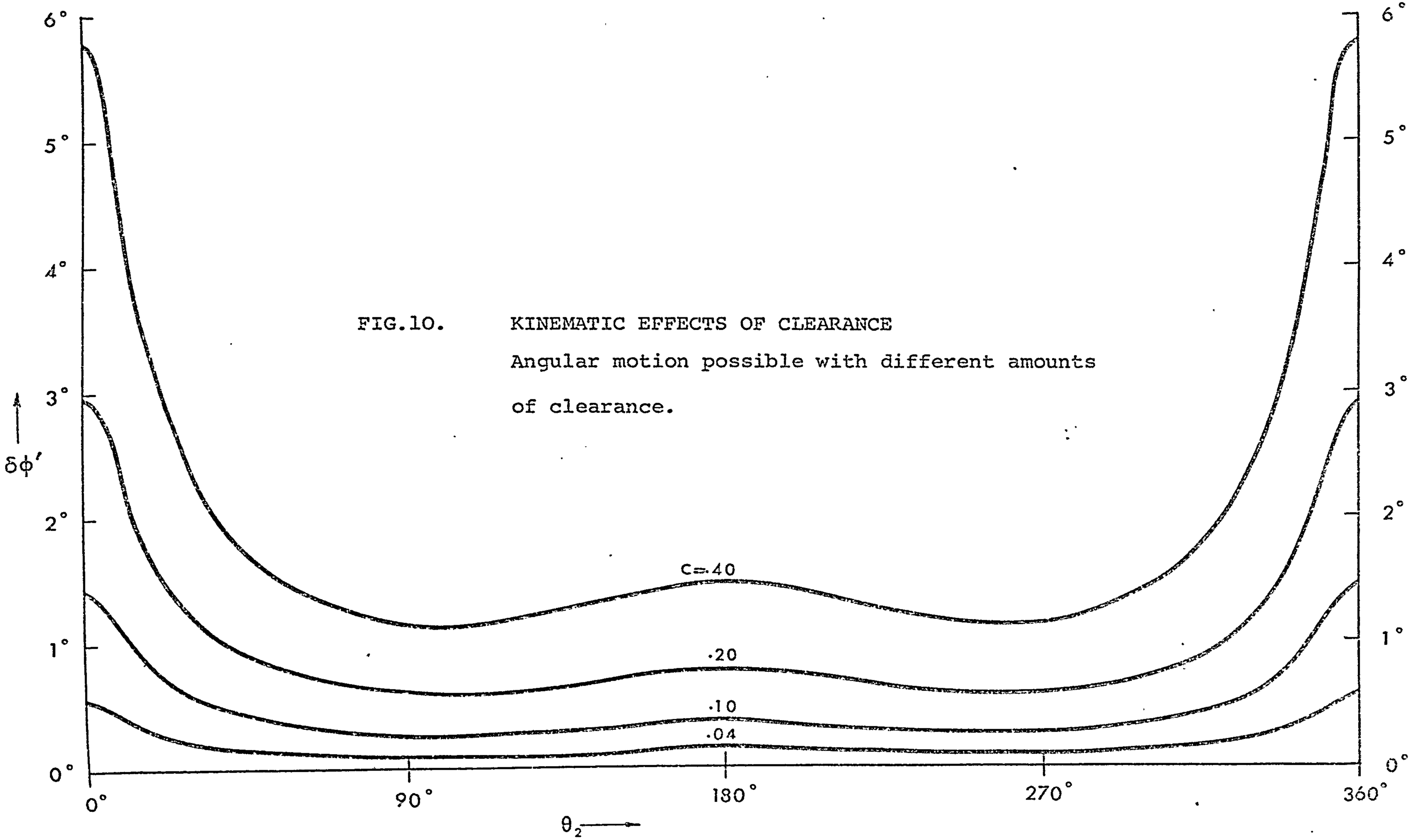

FIG.10. KINEMATIC EFFECTS OF CLEARANCE

Angular motion possible with different amounts of clearance.

From the Figure below, μ is always $< 90^{\circ}$ if

$$(\ell_1 + \ell_2)^2 < \ell_3^2 + \ell_4^2$$

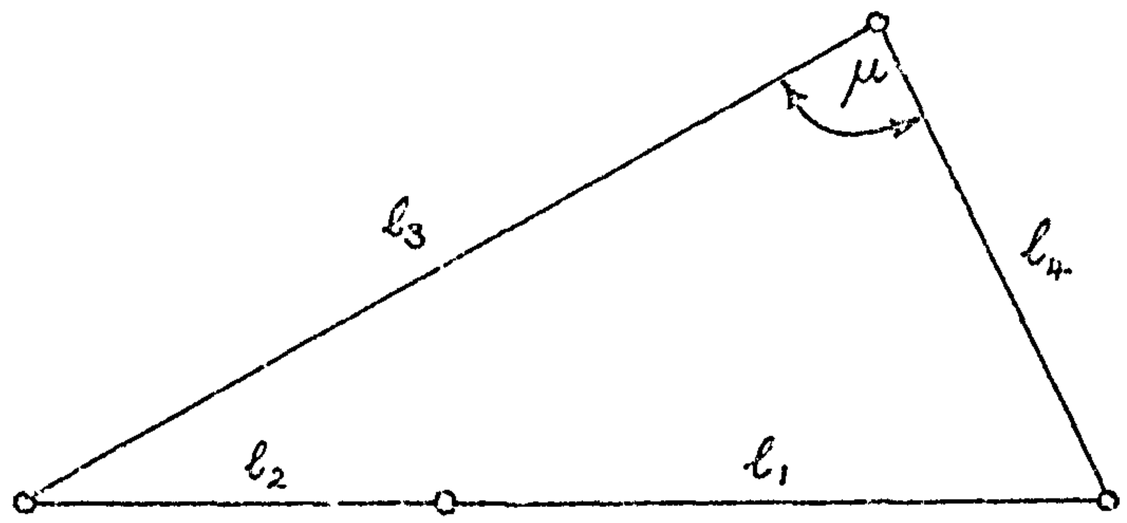

In such cases the minimum value of $\delta\phi'$ will occur at $\theta_2 = 180^{\circ}$..

It may be pointed out that kinematically, it is of no consequence whether the clearance is present at the crank-coupler joint or the coupler-follower joint. The range of free motion of the follower link will be the same in both cases. Dynamically, however the inertia of the coupler will be important and must be taken into account. Kobrinskii[31] has examined vibro-impact systems in general, considering also the effect of springs added to the systems. Wilson[34] has examined the dynamic effects of a clearance between slider and guide in a slider-crank mechanism with reference to the change in impact behaviour of the slides when geometric and dynamic parameters are varied. The more complicated situation of a clearance in the crank and rocker mechanism discussed in this chapter appears not to have been investigated dynamically so far as the author is aware.

PART II

DYNAMICS

CHAPTER 4

DYNAMICS OF PLANAR MECHANISMS

4.1 Introduction

The forces developed in a linkage mechanism during its operation will in general be functions of the link dimensions and any externally applied load. In the absence of such external loads, the forces will be due solely to the inertia of the links themselves and, in the case of a constant rotary input, the inertia of the coupler and follower links only. In this chapter, equations are derived for the pin-forces and shaking moment produced in a four bar linkage with zero external load. Illustrative results are calculated for the case of crank-rocker mechanisms operating at constant input speed.

4.2 Inertia Forces

Fig. 11 shows the freebody diagram of a four bar linkage ABCD in which the moving links AB, BC, CD are considered to be uniform bars of mass M_2, M_3, M_4 respectively and corresponding inertias I_{2A}, I_{3B}, I_{4D} about axes perpendicular to the plane of the mechanism through points A, B and D. The crank AB is driven anticlockwise at angular velocity ω_2 by an applied torque T. In the absence of any external load, the forces developed at the pins will be due entirely to the inertia of the mechanism. The components of the pin-forces in the horizontal and vertical directions are defined as shown (e.g. X_{23} is the horizontal component of the force exerted by link 2 upon link 3). As a consequence of this definition of the pin forces, $X_{ij} = - X_{ji}$ for i, j = 1, 2, 3, 4. The centres of gravity of the moving links G_2, G_3, G_4 are located at distances r_2 from A, r_3 from B and r_4 from D as shown and have acceleration components (a_{2x}, a_{2y}), (a_{3x}, a_{3y}) and (a_{4x}, a_{4y}) respectively which are defined by the following equations

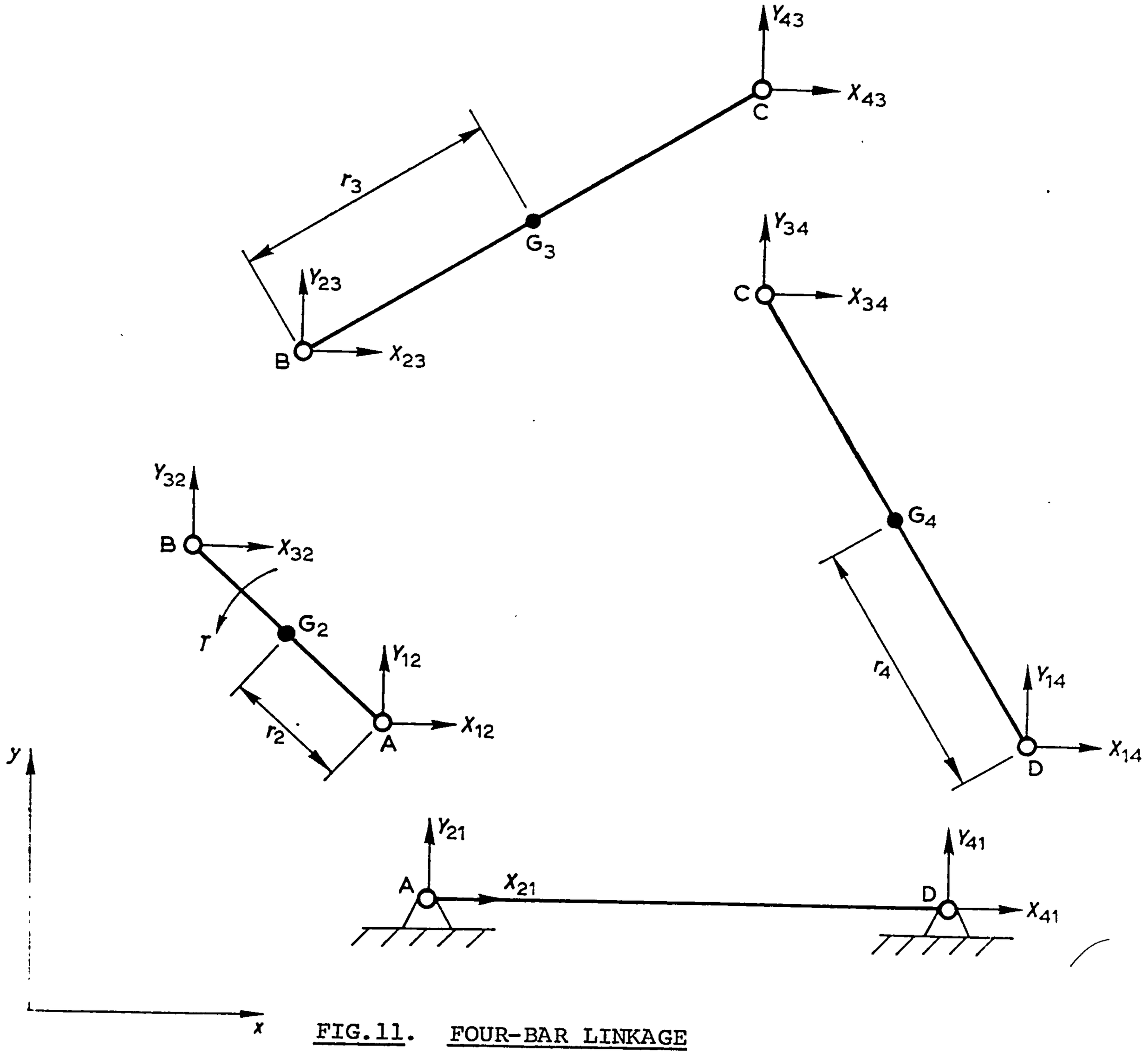

FIG.11. FOUR-BAR LINKAGE
Free Body Diagram

$$a_{2x} = -r_2(\omega_2^2 \cos\theta_2 + \alpha_2 \sin\theta_2)$$

$$a_{2y} = -r_2(\omega_2^2 \sin\theta_2 - \alpha_2 \cos\theta_2) \qquad (4.1)$$

$$a_{3x} = -\ell_2(\omega_2^2 \cos\theta_2 + \alpha_2 \sin\theta_2) - r_3(\omega_3^2 \cos\theta_3 + \alpha_3 \sin\theta_3)$$

$$= \frac{\ell_2}{r_2} a_{2x} - r_3(\omega_3^2 \cos\theta_3 + \alpha_3 \sin\theta_3) \qquad (4.2)$$

$$a_{3y} = -\ell_2(\omega_2^2 \sin\theta_2 - \alpha_2 \cos\theta_2) - r_3(\omega_3^2 \sin\theta_3 - \alpha_3 \cos\theta_3)$$

$$= \frac{\ell_2}{r_2} a_{2y} - r_3(\omega_3^2 \sin\theta_3 - \alpha_3 \cos\theta_2)$$

$$a_{4x} = -r_4(\omega_4^2 \cos\theta_4 + \alpha_4 \sin\theta_4) \qquad (4.3)$$

$$a_{4y} = -r_4(\omega_4^2 \sin\theta_4 - \alpha_4 \cos\theta_4)$$

In order to obtain expressions for the pin forces and driving torque, the equations of motion of all links must be solved simultaneously. Taking each link in turn, the equations are :-

link AB:
$$X_{12} - X_{23} = M_2 a_{2x}$$

$$Y_{12} - Y_{23} = M_2 a_{2y} \qquad (4.4)$$

$$T + X_{23}\ell_2 \sin\theta_2 - Y_{23}\ell_2 \cos\theta_2 = I_{2A}\alpha_2$$

link BC:
$$X_{23} - X_{34} = M_3 a_{3x}$$

$$Y_{23} - Y_{34} = M_3 a_{3y} \qquad (4.5)$$

$$X_{23} r_3 \sin\theta_3 - Y_{23} r_3 \cos\theta_3 + X_{34}(\ell_3 - r_3)\sin\theta_3 - Y_{34}(\ell_3 - r_3)\cos\theta_3$$

$$= (I_{3B} - M_3 r_3^2)\alpha_3$$

link CD: $X_{34} - X_{41} = M_4 \alpha_{4x}$

$$Y_{34} - Y_{41} = M_4 \alpha_{4y} \tag{4.6}$$

$$- X_{34} \ell_4 \sin\theta_4 + Y_{34} \ell_4 \cos\theta_4 = I_{4D} \alpha_4$$

These equations may conveniently be put in matrix form and solved by inversion, but in view of the simplicity of most of the equations, it is a comparatively simple task to solve them analytically with the following results:

$$X_{34} = \frac{\{I_{3B}\alpha_3 \ell_4 \cos\theta_4 + I_{4D}\alpha_4 \ell_3 \cos\theta_3 - m_3 r_3 \ell_2 \ell_4 \cos\theta_4 [\omega_2^2 \sin(\theta_2-\theta_3) - \alpha_2 \cos(\theta_2-\theta_3)]\}}{\ell_3 \ell_4 \sin(\theta_3-\theta_4)}$$

(4.7)

$$Y_{34} = \frac{\{I_{3B}\alpha_3 \ell_4 \sin\theta_4 + I_{4D}\alpha_4 \ell_3 \sin\theta_3 - m_3 r_3 \ell_2 \ell_4 \sin\theta_4 [\omega_2^2 \sin(\theta_2-\theta_3) - \alpha_2 \cos(\theta_2-\theta_3)]\}}{\ell_3 \ell_4 \sin(\theta_3-\theta_4)}$$

$$X_{23} = -m_3(\ell_2\omega_2^2 \cos\theta_2 + \ell_2\alpha_2 \sin\theta_2 + r_3\omega_3^2 \cos\theta_3 + r_3\alpha_3 \sin\theta_3) + X_{34}$$

(4.8)

$$Y_{23} = -m_3(\ell_2\omega_2^2 \sin\theta_2 - \ell_2\alpha_2 \cos\theta_2 + r_3\omega_3^2 \sin\theta_3 - r_3\alpha_3 \cos\theta_3) + Y_{34}$$

$$\left.\begin{aligned} X_{12} &= -m_2\left(r_2\omega_2^2\cos\theta_2 + r_2\alpha_2\sin\theta_2\right) + X_{23} \\ Y_{12} &= -m_2\left(r_2\omega_2^2\sin\theta_2 - r_2\alpha_2\cos\theta_2\right) + Y_{23} \end{aligned}\right\} \quad (4.9)$$

$$\left.\begin{aligned} X_{41} &= m_4\left(r_4\omega_4^2\cos\theta_4 + r_4\alpha_4\sin\theta_4\right) + X_{34} \\ Y_{41} &= m_4\left(r_4\omega_4^2\sin\theta_4 - r_4\alpha_4\cos\theta_4\right) + Y_{34} \end{aligned}\right\} \quad (4.10)$$

$$T = I_{2A}\alpha_2 + Y_{23}\ell_2\cos\theta_2 - X_{23}\ell_2\sin\theta_2 . \quad (4.11)$$

The force exerted on the frame due to the motion of the links will be simply the sum of the inertia forces:

$$X_{Frame} = X_{41} - X_{12} = -(M_2 a_{2x} + M_3 a_{3x} + M_4 a_{4x})$$

$$Y_{Frame} = Y_{41} - Y_{12} = -(M_2 a_{2y} + M_3 a_{3y} + M_4 a_{4y}) \qquad (4.12)$$

In addition there will be a shaking moment on the frame which may conveniently be taken about the crank pivot A

$$M_{Frame} = Y_{41} \ell_1 \qquad (4.13)$$

Equations (4.7) - (4.11) and (4.12), (4.13) give a completely general inertia force analysis for the four bar linkage which may conveniently be examined in detail with the aid of a digital computer. In the majority of cases, the crank is considered to rotate with constant velocity so that the equations are simplified slightly by the omission of terms in α_2. Equations (4.7) - (4.11) then resemble those given by Talbourdet[9] who produced results showing the effect of changing the material from which the links are made.

In the case when the crank rotates at a constant rate, all pin forces and torques will be periodic functions of time or crank angle ($\theta_2 = \omega_2 t$). A useful method of showing the variations of such forces with crank position is the polar diagram. Figs. 12 - 16 show a typical set of pin forces for a crank and rocker mechanism of the following proportions

$\ell_1 = \ell_3 = \ell_4 = 12"$; $\ell_2 = 6"$

$W_3 = W_4 = 1$ lbf ; $W_2 = 0.5$ lbf

$I_{3B} = I_{4D} = 0.125$ lbf in sec^2 ; Crank speed $\omega_2 = 10$ rad/s.

The convention used in Figs. 12 - 16 and similar figures is that values of X_{ij} and Y_{ij} are plotted simultaneously thus showing the value of F_{ij} in magnitude and direction for a particular value of the crank angle θ_2. A radial vector drawn from the origin to a point labelled 0^o for example, will represent the pin force in magnitude and direction when the value of θ_2 is 0^o.

FIG.12. FOUR-BAR LINKAGE. Pin Forces FIG.13.

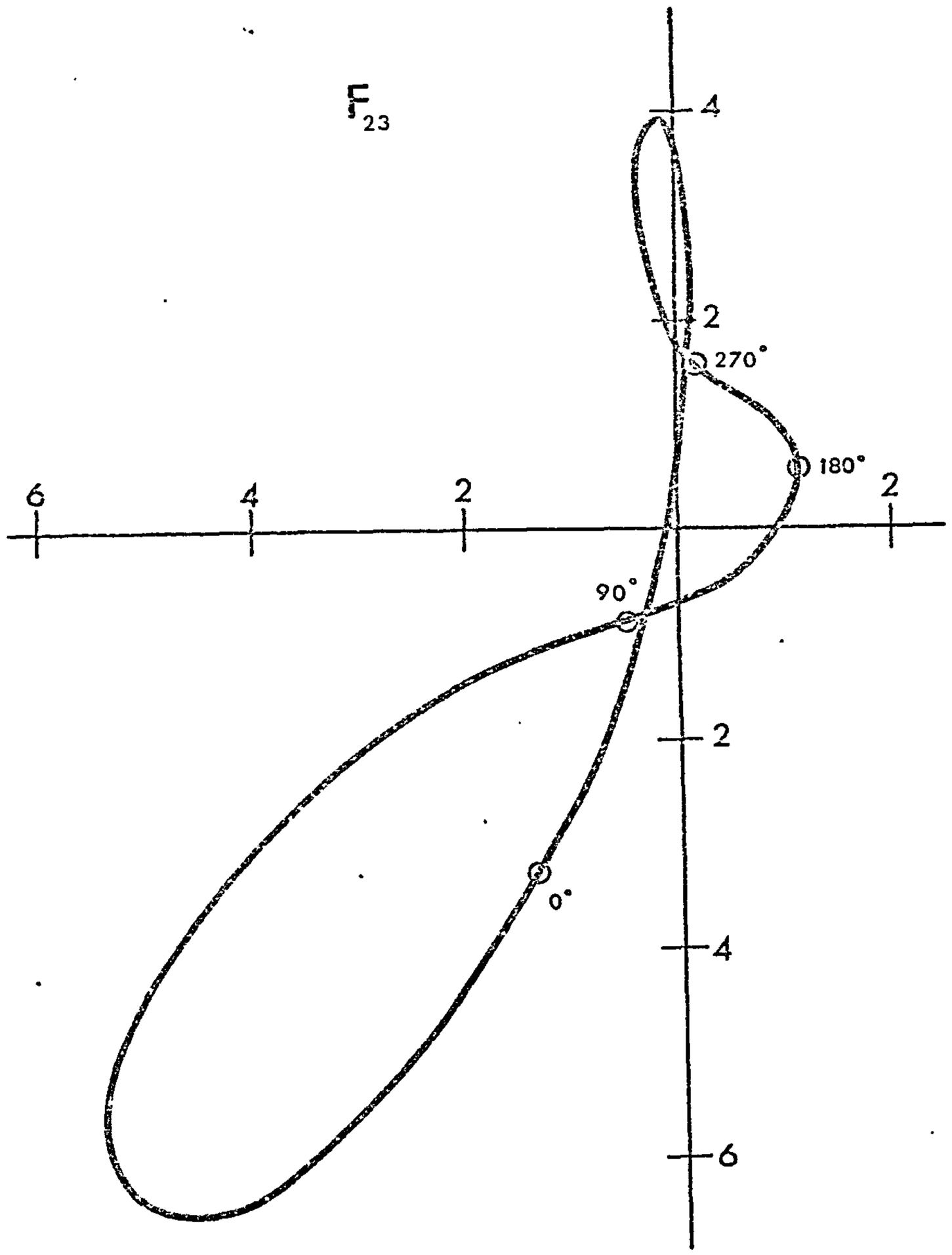

(lbf)

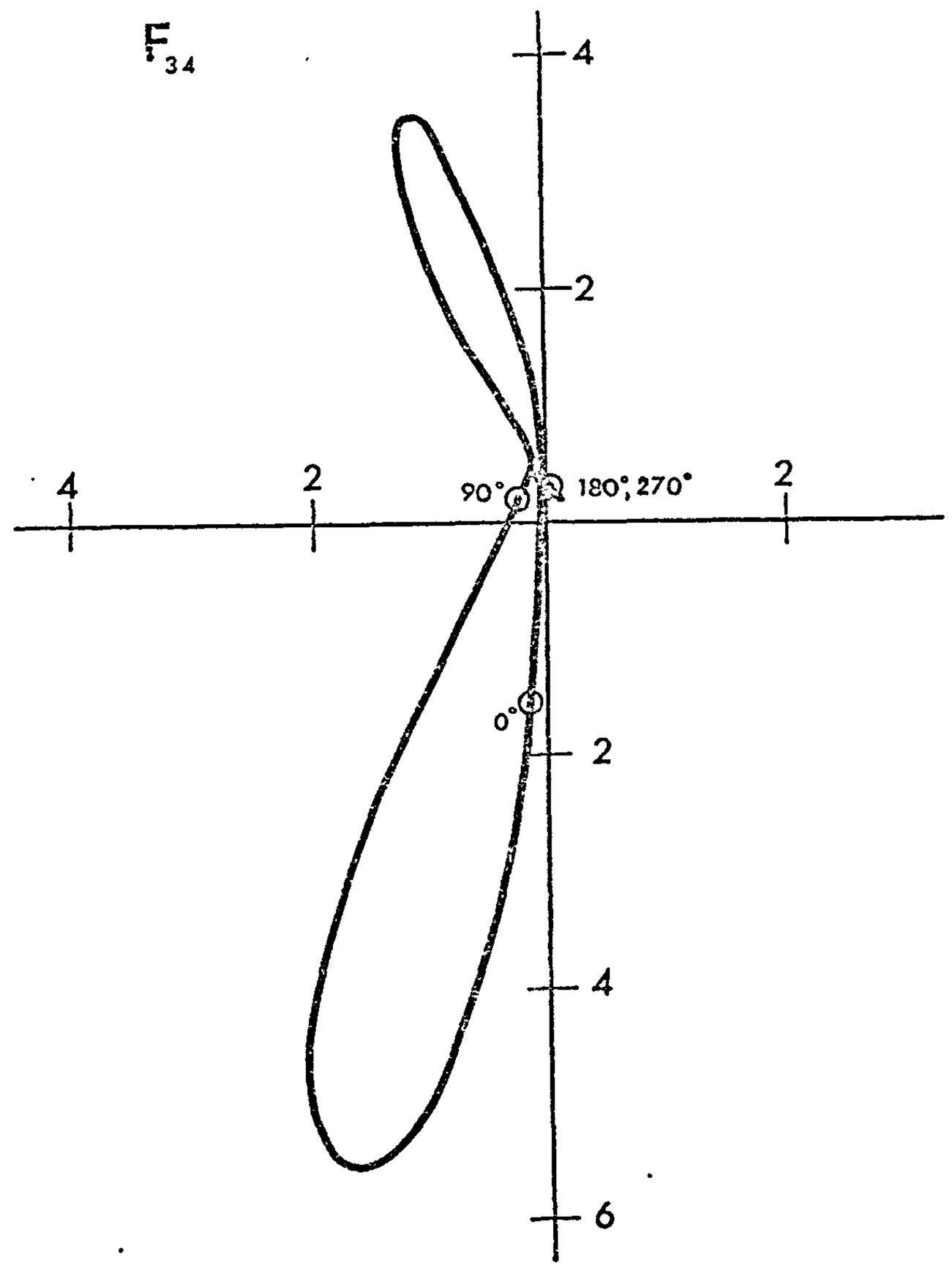

FIG.14. FOUR-BAR LINKAGE. PIN FORCES

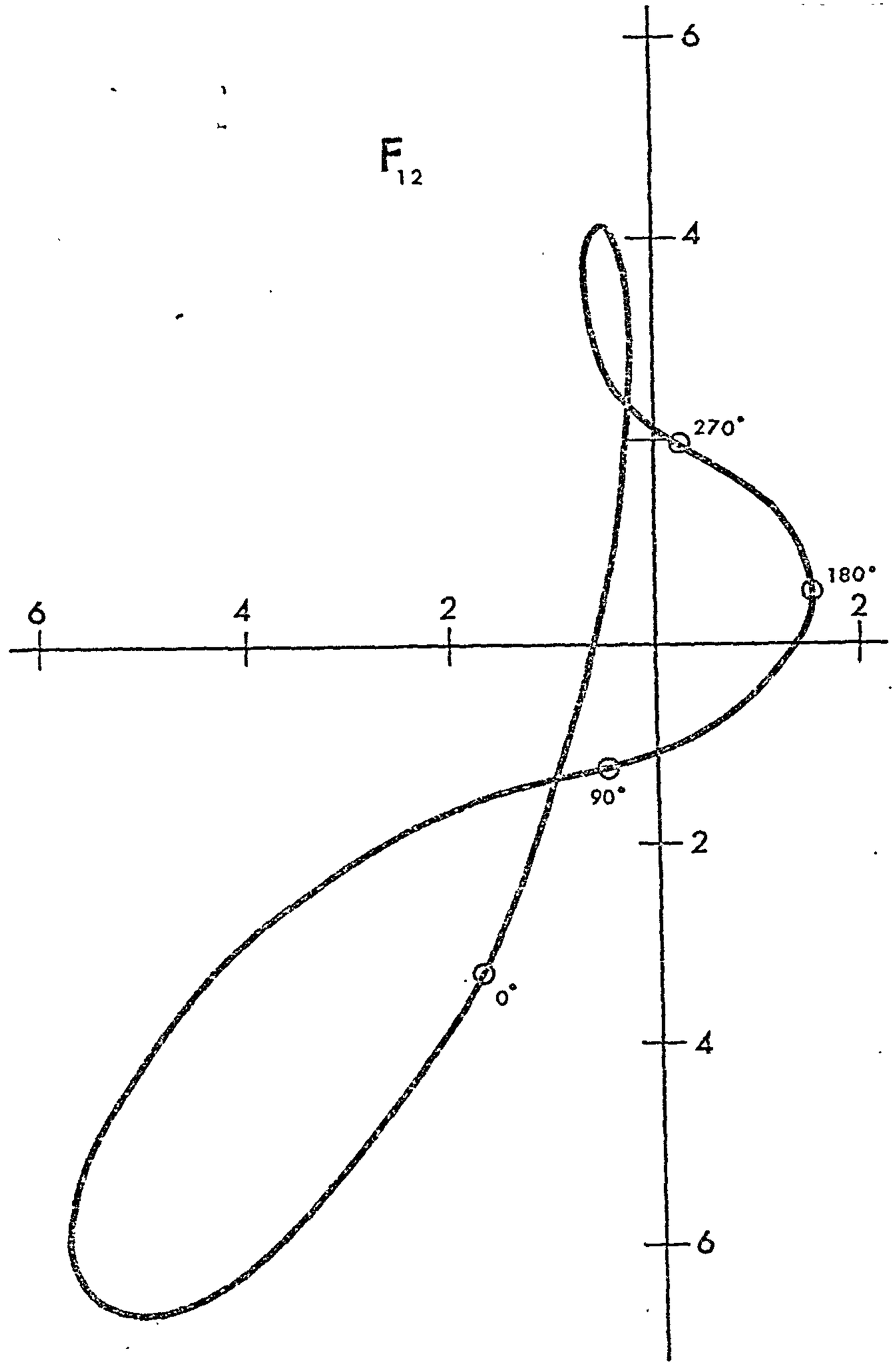

FIG.15.

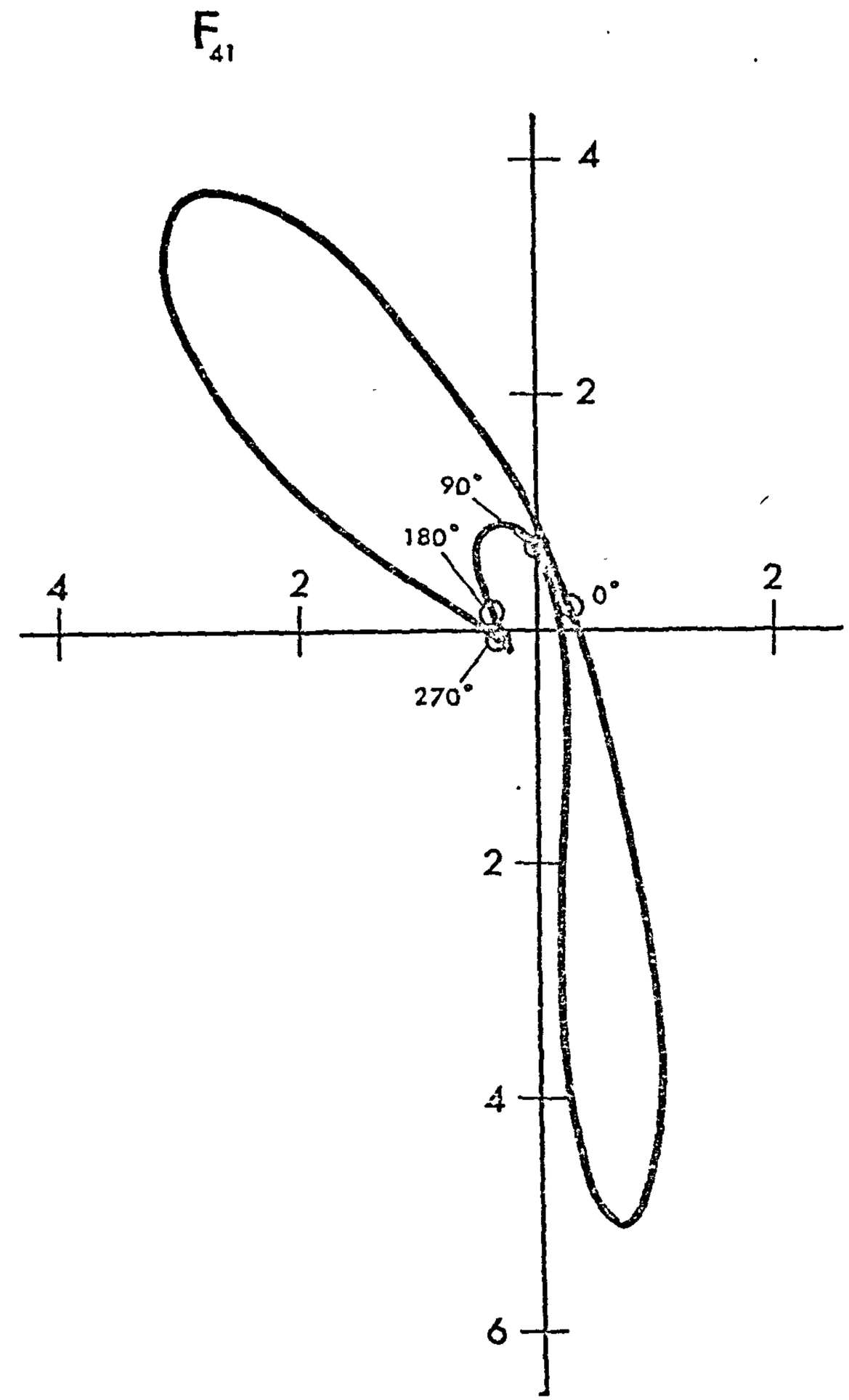

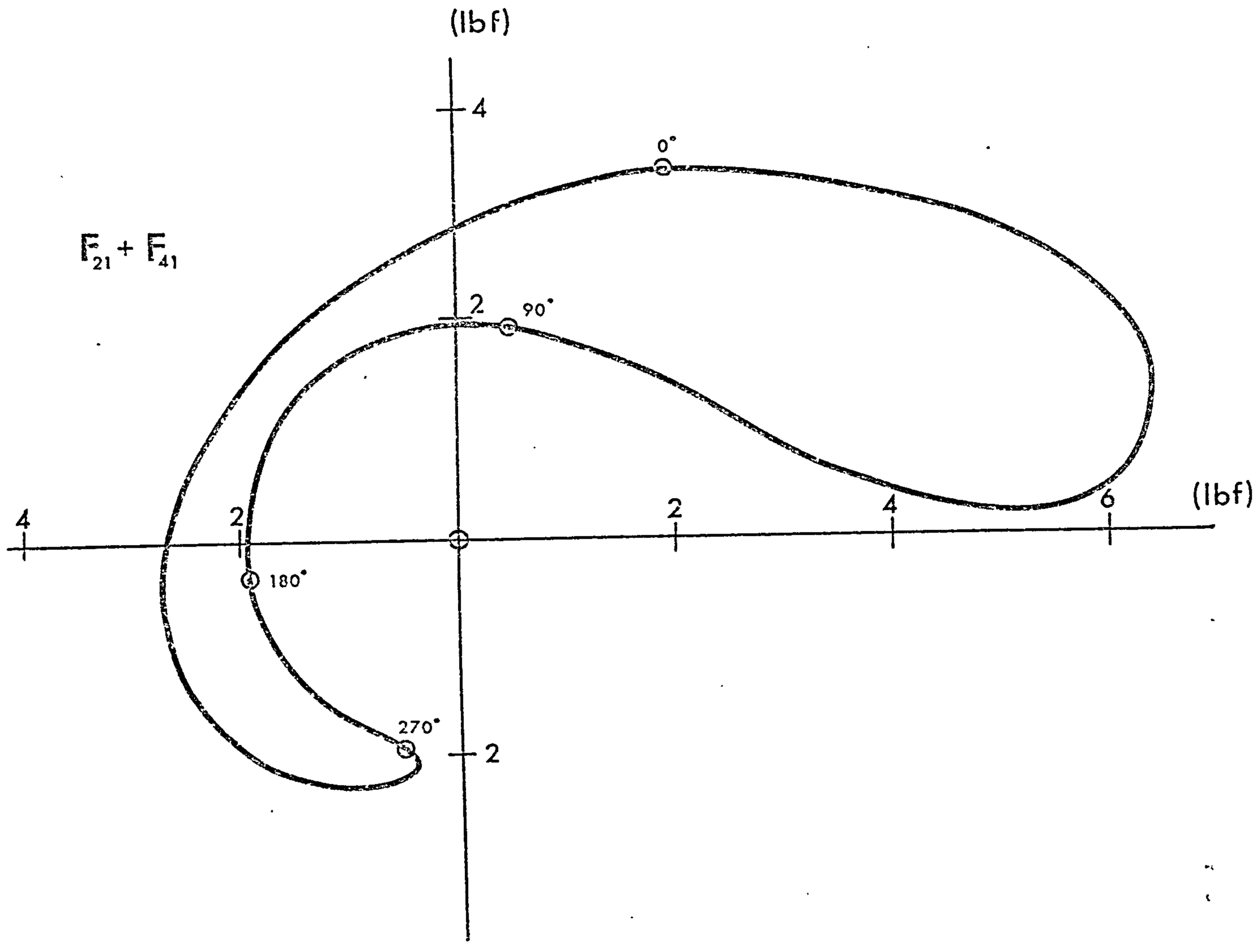

FIG.16. FOUR-BAR LINKAGE. Force on Frame

As a consequence of the kinematics of the linkage, the maxima of the forces occur in the region of $\theta_2 = 0^o$ where maximum accelerations occur together with minimum transmission angle. It has already been seen that maximum values of acceleration increase rapidly as the crank length if increased with respect to the other links. The corresponding increase in pin forces is shown in Figs. 17 - 19. The relevant mechanism dimensions are shown as the figures as (ℓ_1, ℓ_2, ℓ_3, ℓ_4) which is a useful convention to adopt as a brief and easily understood method of indicating the link lengths of any four bar linkage.

All results quoted here as examples are concerned only with inertia forces. It is a simple matter to include the effects of additional external loads acting on the mechanism by adding appropriate terms to the pin-force equations.

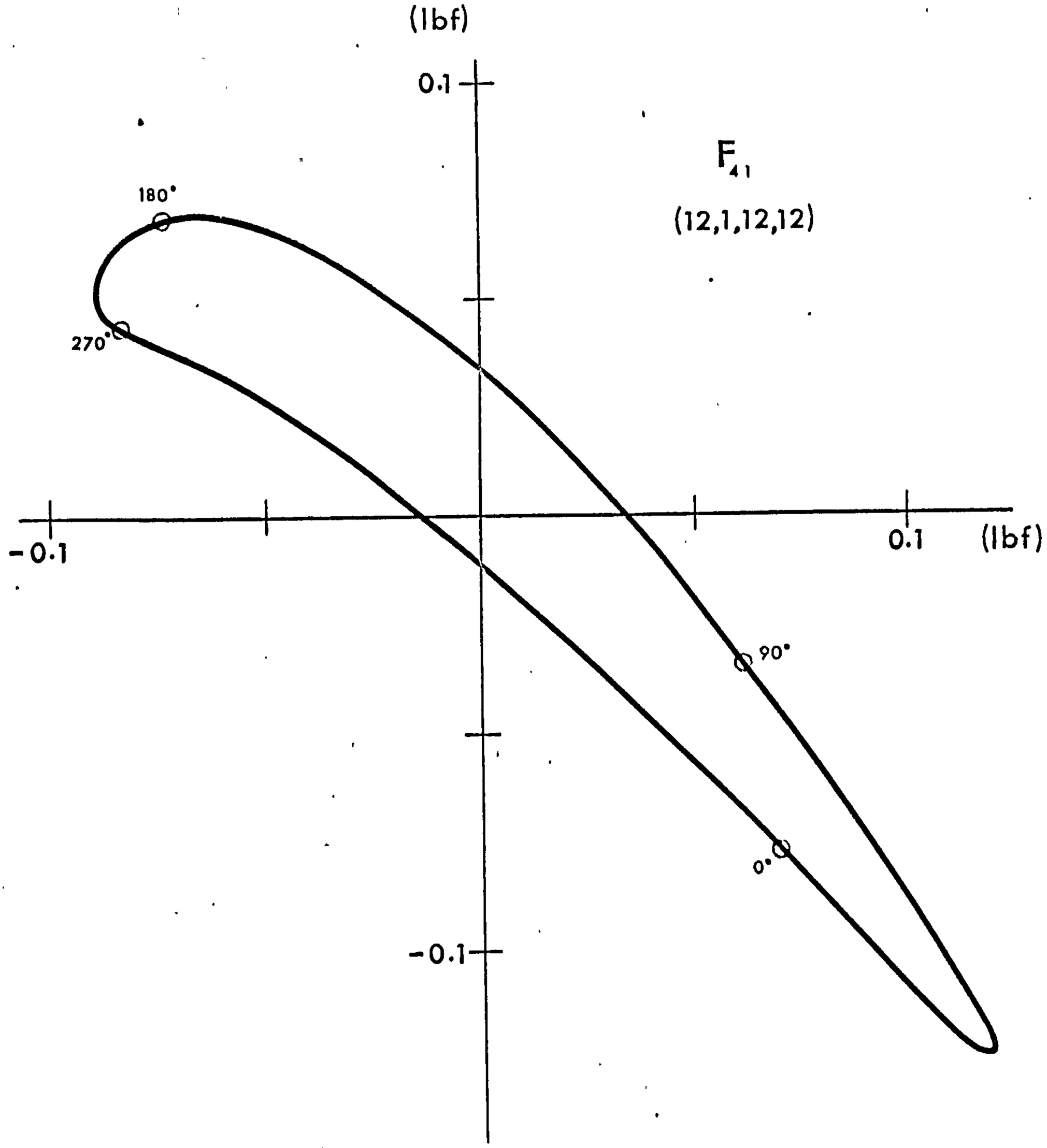

FIG. 17. FOLLOWER-FRAME FORCE: Effect of Change of Dimensions.

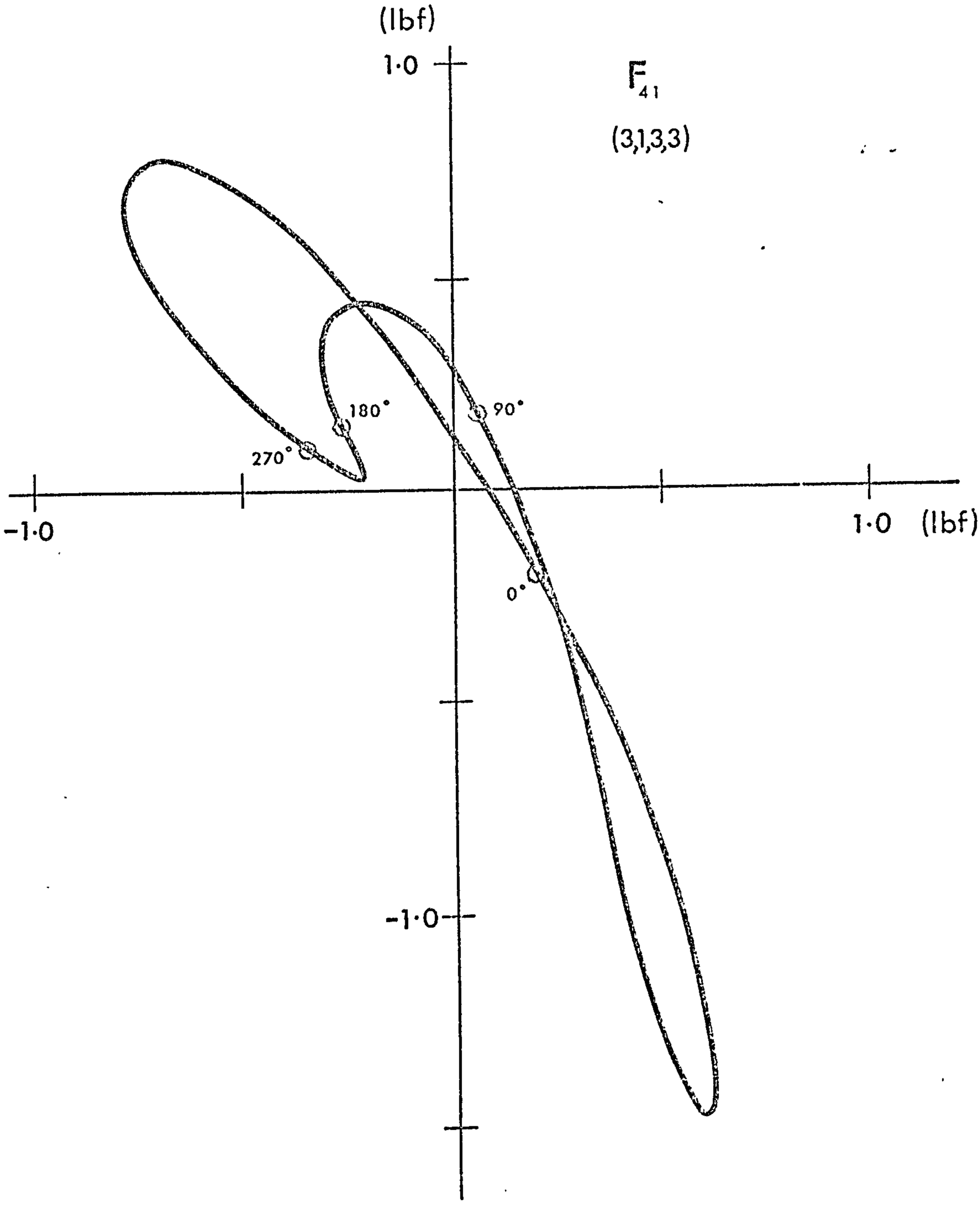

FIG. 18. FOLLOWER-FRAME FORCE: Effect of Change of Dimensions.

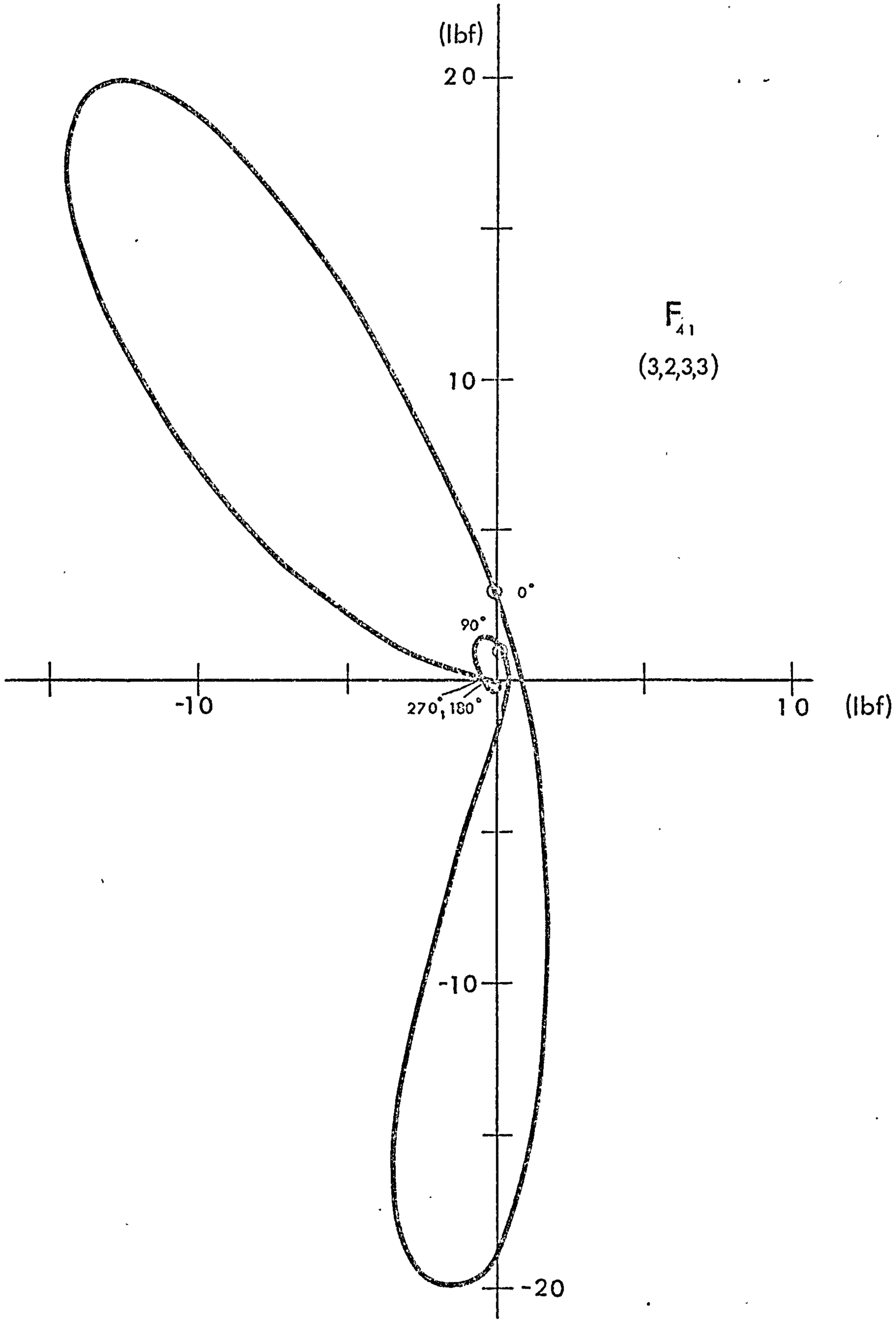

FIG. 19. FOLLOWER-FRAME FORCE: Effect of Change of Dimensions.

CHAPTER 5

BALANCING

The previous chapter has dealt with the forces produced in a mechanism as a consequence of the inertia of the moving links. Although it is common practice to assume such links to be uniform rods, they may in fact take a variety of forms and in many instances the links with fixed pivots will be balanced, either partially or totally. The equations (4.7) - (4.11) will not be affected by this however except for the necessary adjustments to the values of I_i and $\mathcal{A}_i$, the latter of which may sometimes be zero.

In general, the balancing of a link about any axis is achieved by the addition of counterweights to that link with a resultant increase in the moment of inertia about that axis. A direct consequence of this is that although the <u>total</u> force (on the frame) may be reduced to zero by balancing, there will be adverse effects upon the individual pin forces in the mechanism and upon the torque developed. To achieve an optimum condition of balance in any mechanism therefore, a number of important factors must be borne in mind. Figs. 20 (a-d) show a number of ways in which balance may be obtained in the four bar linkage. Fig. 20 (a) shows the unbalanced linkage, Fig. 20 (b) the partially balanced case in which crank and follower only are balanced about their fixed pivots, while Figs. 20 (c), (d) show two completely balanced mechanisms. The first of these contains a coupler which is balanced at the crank pin and a crank which is balanced so that the <u>combined</u> centre of mass of coupler and crank is located at the fixed pivot A. The follower is balanced on the fixed pivot D as in case (b). The second fully balanced linkage, Fig. 20 (d), contains only two counterweights each of which balances the link to which it is attached and in addition a proportion of the coupler which is considered to be replaced by its approximately equivalent system of two concentrated masses at B and C. If the centre of mass of these two is coincident with that of the coupler, and their total mass is the same as that of the coupler, then the inertia <u>forces</u> generated by the equivalent system will be similar to the original coupler and the whole mechanism may be balanced as

FIG.20. UNBALANCED, PARTIALLY BALANCED AND FULLY BALANCED LINKAGE CONFIGURATIONS.

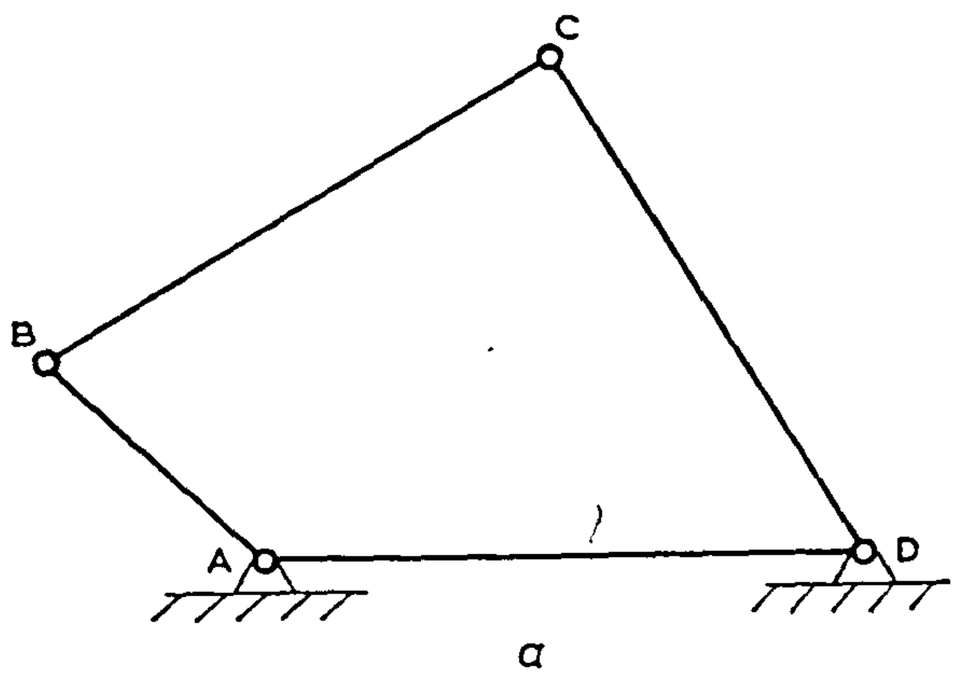

a

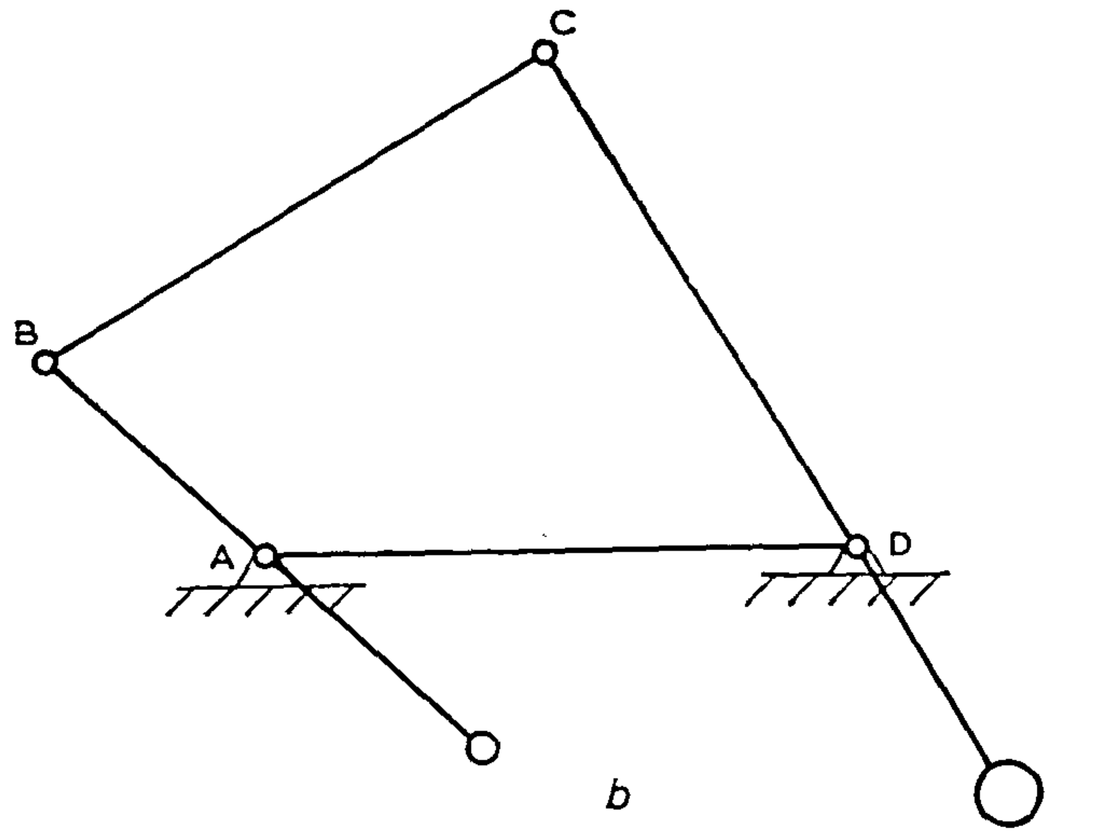

b

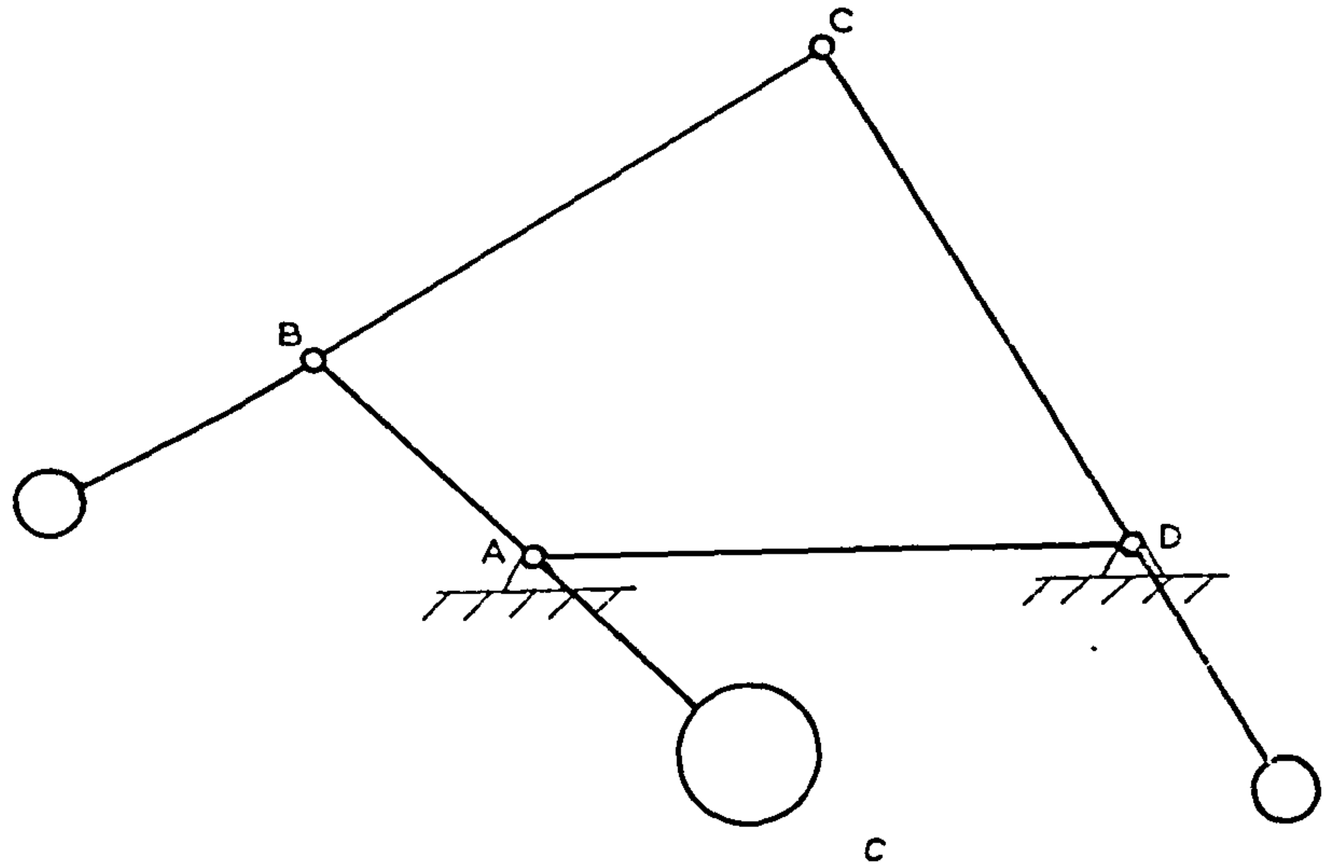

c

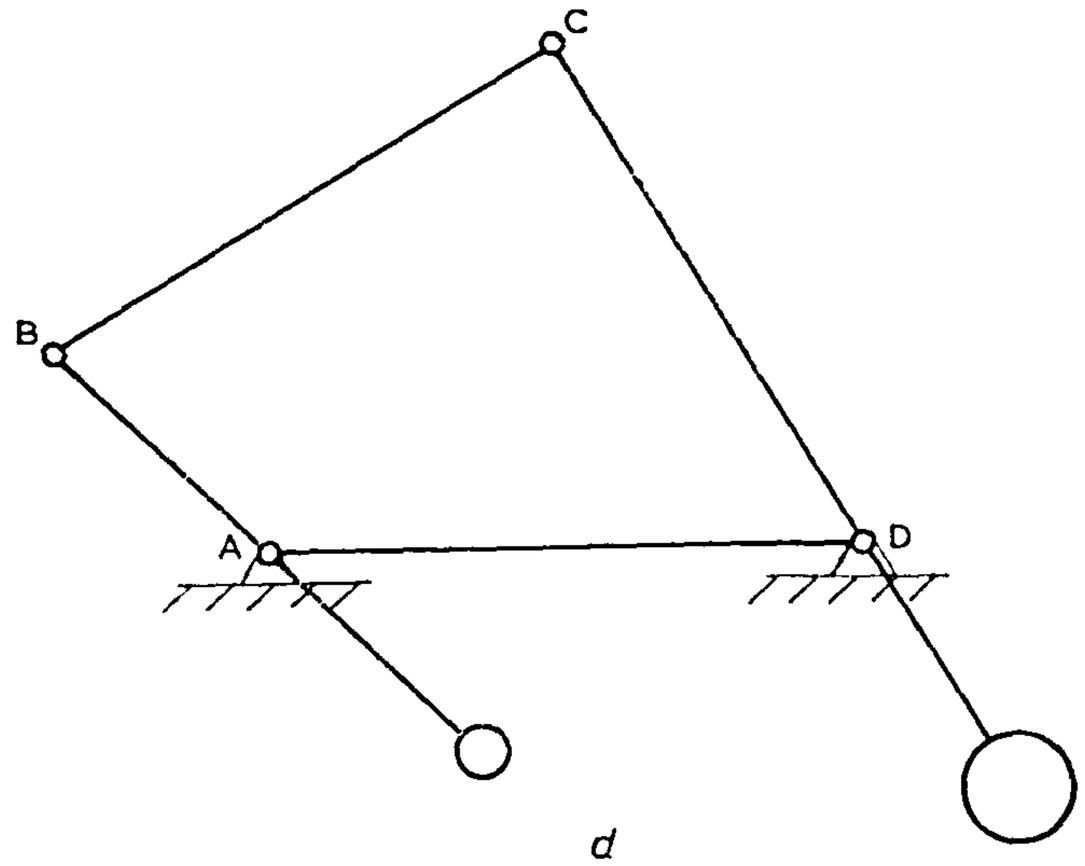

d

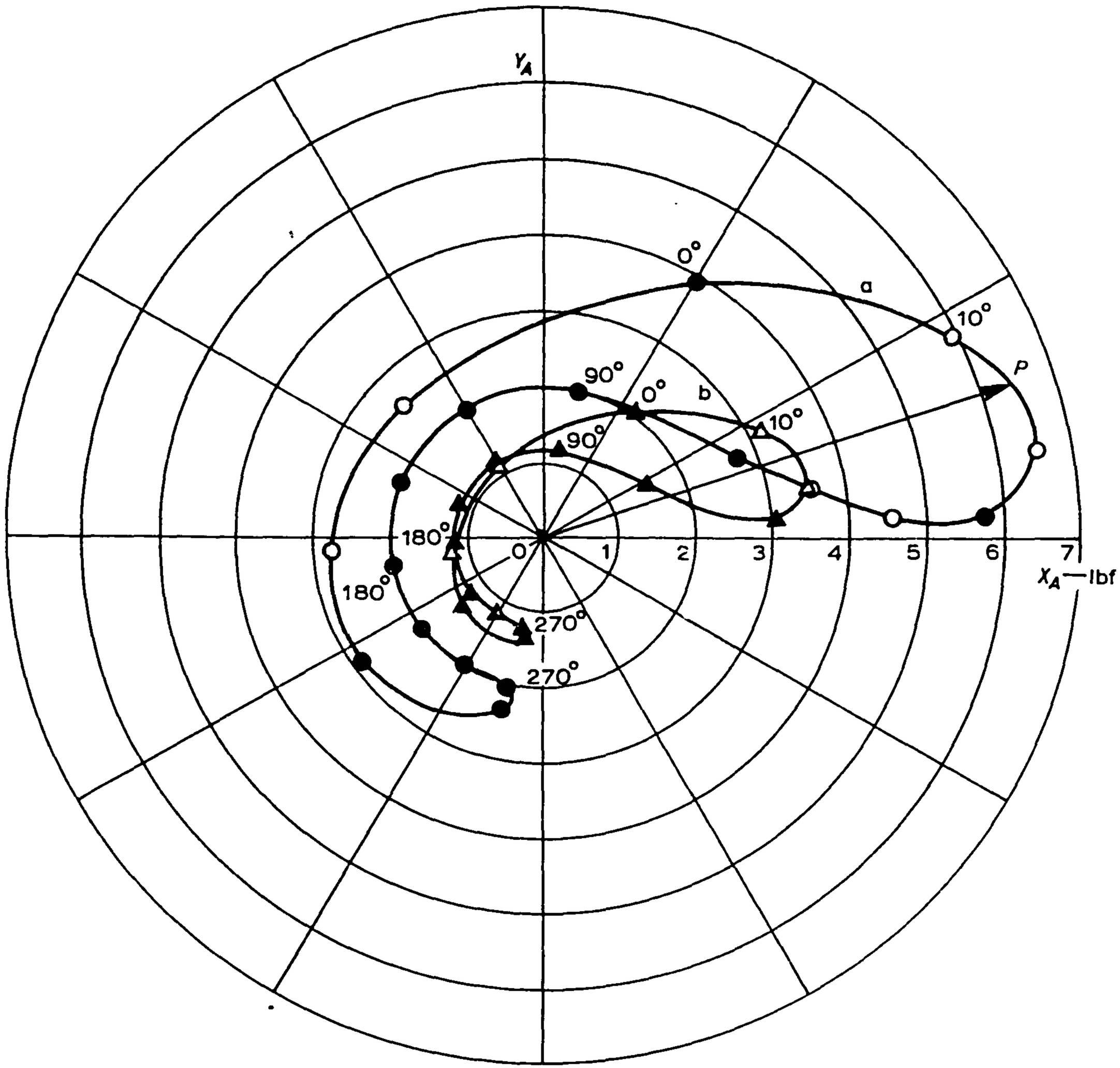

(a) Unbalanced linkage:

○ θ_2 marked at 10 intervals. ● θ_2 marked at 30 intervals.

(b) Partially balanced linkage:

△ θ_2 marked at 10 intervals. ▲ θ_2 marked at 30 intervals.

FIG. 21. FORCE ON FRAME
Effect of Balancing

FIG.22. TORQUE ON FRAME

Effect of Balancing.

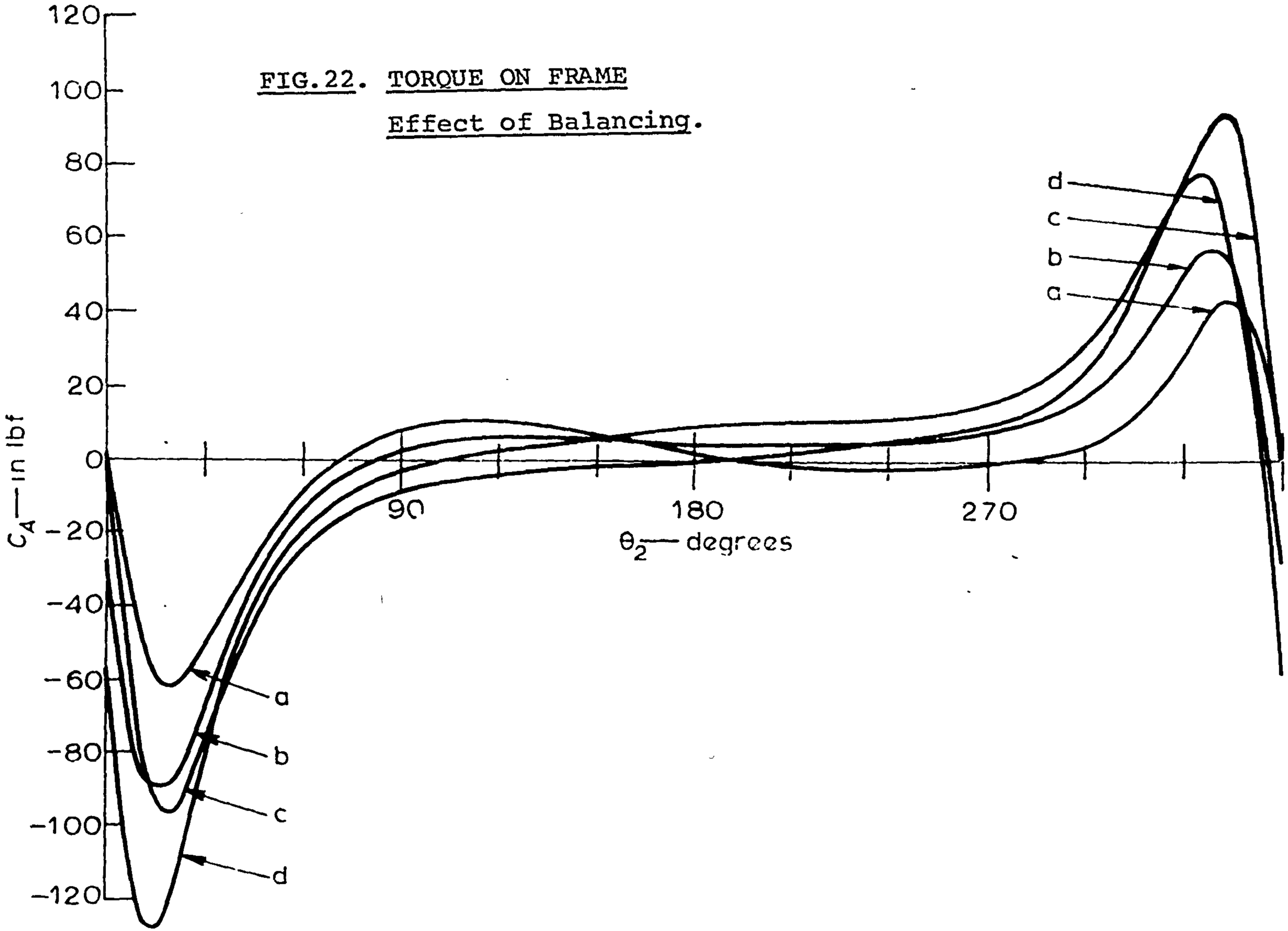

(a) Unbalanced linkage.
(b) Partially balanced linkage.
(c) Fully balanced linkage (3 counterweights).
(d) Fully balanced linkage (2 counterweights).

shown. However, the moment of inertia of the equivalent system will differ from that of the coupler so that individual pin forces and the resultant torque on the frame may be increased.

Fig. 21 shows a comparison of the forces exerted upon the frame by the mechanisms shown in Fig. 20 (a), (b). Even partial balance is seen to reduce the maximum value by approximately 50%. Fig. 22 shows the torque on the frame produced by the four cases in Fig. 20 (a) - (d). The partially balanced case causes a 50% increase in the maxima of the balanced case whereas the corresponding increase caused by the fully balanced examples is nearer 100%. In each case, the mechanism data were as given for Figs. 12 - 16. Counterweights were assumed to be located 6 in. from the relevant pin joints.

The magnitude of the increase in the moment of inertia of any link as a consequence of the addition of a counterweight will be governed by the point of location of that counterweight as may be seen from the following simplified example.

Consider a thin uniform rod of length L, mass M, pivoted about one end and carrying a cylindrical counterweight of mass M_c, radius r_c, centred at distance ℓ from the pivot. The counterweight thickness is h, material density ρ and the extension of the rod is of similar X-section to that of the rod itself.

If the system is pivoted at its centre of gravity G, then the total moment of inertia is given by the following expression where the thickness of the rod itself has been ignored;

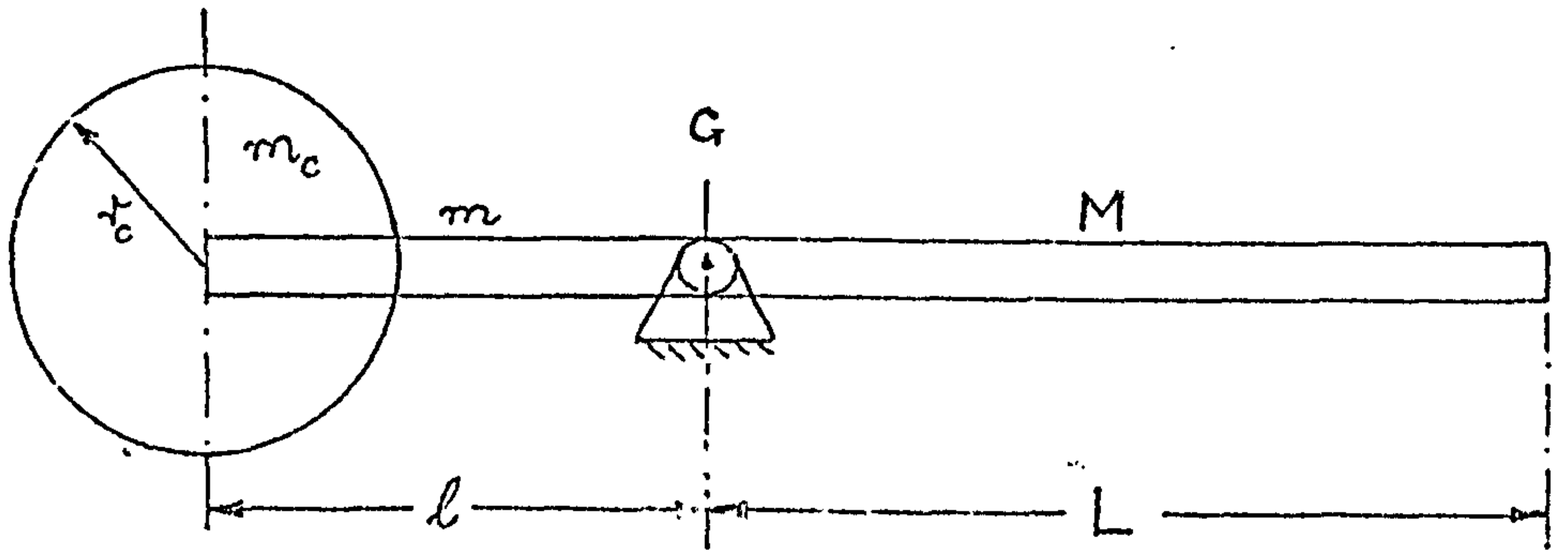

$$I_G = \tfrac{1}{3}ML^2 + \tfrac{1}{3}ml^2 + (\tfrac{1}{2}m_c r_c^2 + m_c \ell^2)$$

where $\frac{m}{M} = \frac{\ell}{L}$, $\frac{ML}{2} = \frac{m\ell}{2} + m_c \ell$ and $m_c = \pi r_c^2 h \rho$

Writing I_G in terms of the non-dimensionalised off-set $\ell/L = \gamma$, we have

$$I_G = \tfrac{1}{3}ML^2 + \tfrac{1}{3}M(\frac{\ell}{L})^3 L^2 + \frac{M^2}{8\pi h\rho}(\frac{L}{\ell} - \frac{\ell}{L})^2 + \frac{ML^2}{2}(\frac{\ell}{L} - (\frac{\ell}{L})^3)$$

$$= \tfrac{1}{3}ML^2(1 + \gamma^3) + \frac{M^2}{8\pi h\rho}(\frac{1}{\gamma} - \gamma)^2 + \frac{ML^2}{2}(\gamma - \gamma^3)$$

Differentiating this expression with respect to γ and setting the result equal to zero yields an equation which is satisfied by the value of γ which corresponds to the extreme value or values for I_G.

$$\frac{\partial I_G}{\partial \gamma} = \frac{ML^2}{2}(1 - \gamma^2) + \frac{M^2}{4\pi h\rho}(\gamma - \frac{1}{\gamma^3}) = 0$$

Re-arranging this gives

$$(1 - \gamma^2) + \frac{M}{2\pi h\rho L^2} \cdot (\gamma - \frac{1}{\gamma^3}) = 0$$

and, with $K = \frac{M}{2\pi L^2 h\rho}$

$$\gamma^5 - K\gamma^4 - \gamma^3 + K = 0$$

This equation may be re-arranged and simplified as follows

$$K = \frac{(1 - \gamma^2)}{(\frac{1}{\gamma^3} - \gamma)} = \frac{\gamma^3(1 - \gamma^2)}{(1 - \gamma^4)} = \frac{\gamma^3}{(1 + \gamma^2)}$$

Extreme values of I_G will therefore occur when the value of K coincides with $\gamma^3/(1 + \gamma^2)$ Fig. 23 (a) shows this function of γ the value of which ranges from 0 to 0.5 . The value of K must hence lie between these two values for an extreme value of I_G to exist. If, for example the counter-

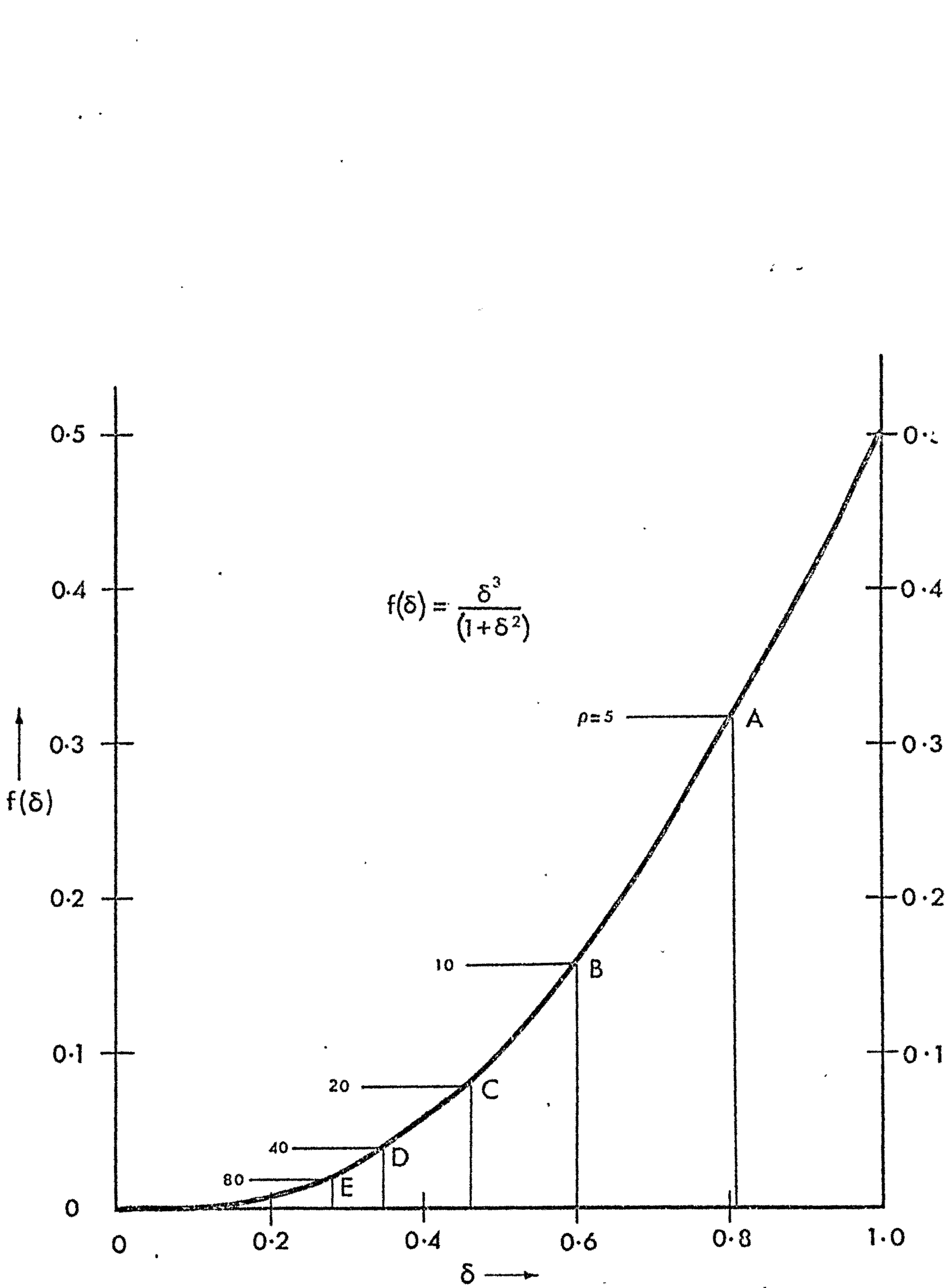

FIG.23 (a) LOCATION OF COUNTERWEIGHT TO ACHIEVE MINIMUM INERTIA IN A BALANCED LINK

weight density ρ is low so that the value of K exceeds 0.5 , the theoretical extreme value of I_G will not lie within the physically possible range of δ . Increasing ρ will decrease the corresponding value of K and give minimum values of I_G for $0 < \delta < 1$.

Figs. 23 (b, c) show the moment of inertia of a balanced link for a range of values of counterweight density and for $0 < \delta \leq 1$. . For low density values, the minimum inertia occurs at $\delta = 1.0$ corresponding to a link of length 2L pivoted at its centre point. The counterweight in this case is of zero radius. For increased values of density, the minimum inertia values occur within the range $0 < \delta < 1$, the corresponding points being marked on Fig. 23 (a) lettered A,B.C,D,E. Arbitrary values of the various parameters were chosen as follows: M = 1; L = 1; h = 0.1; ρ = 5, 10, 20, 40, 80. These serve adequately to demonstrate the variations of I_G with δ and ρ .

The effect of the location of the counterweight in the balanced mechanism shown in Fig. 20 (d) is shown in Fig. 23 (d). The crank-coupler force F_{23} for the unbalanced case is compared with three balanced cases in which the two counterweights are located 1 in, 3 in. and 6 in.from the fixed pivots A and D. As may be seen, the addition of the counterweights brings about an increase in the pin force but by correct choice of the off-set distance (in this case approximately 3 in.) the increase can be kept much lower than an arbitrarily chosen value.

The majority of the work described in Chapters 4 and 5 has been published in the Journal of Mechanical Engineering Science[10].

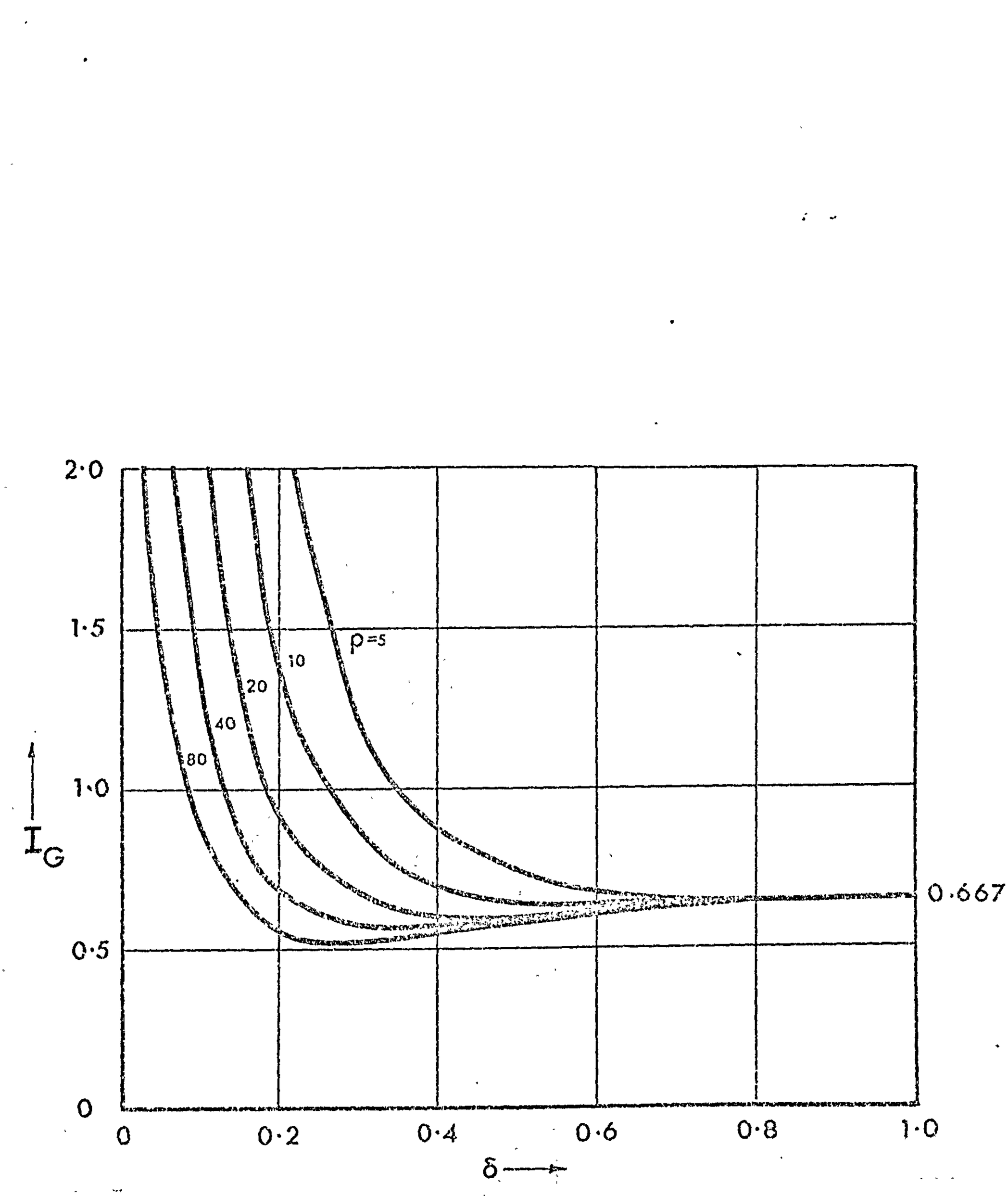

FIG.23(b) MOMENT OF INERTIA OF A BALANCED LINK

Effect of Density and Position of Counterweight.

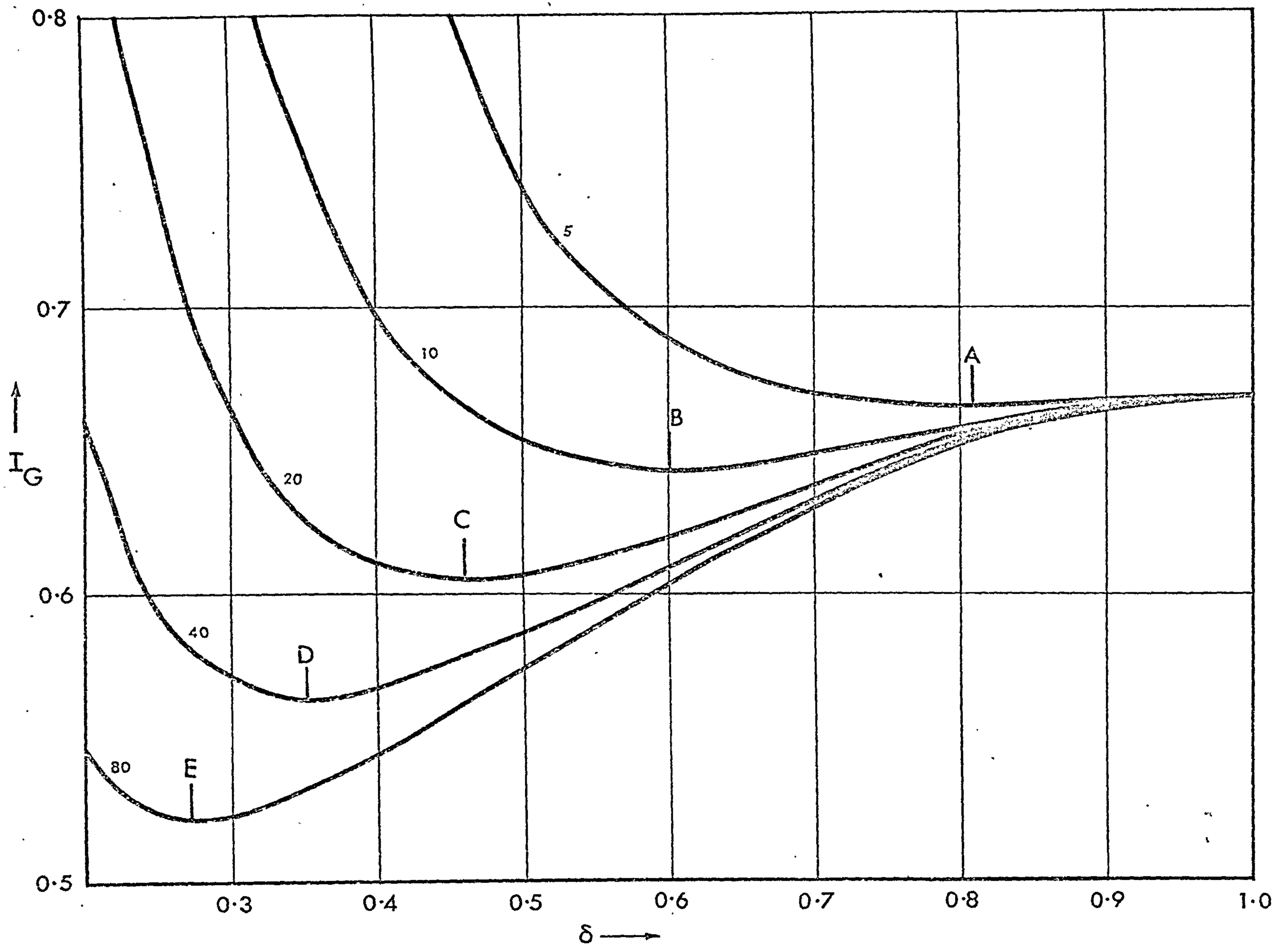

FIG.23(c) LOCATION OF MINIMUM VALUES OF INERTIA

Effect of Density of Counterweight

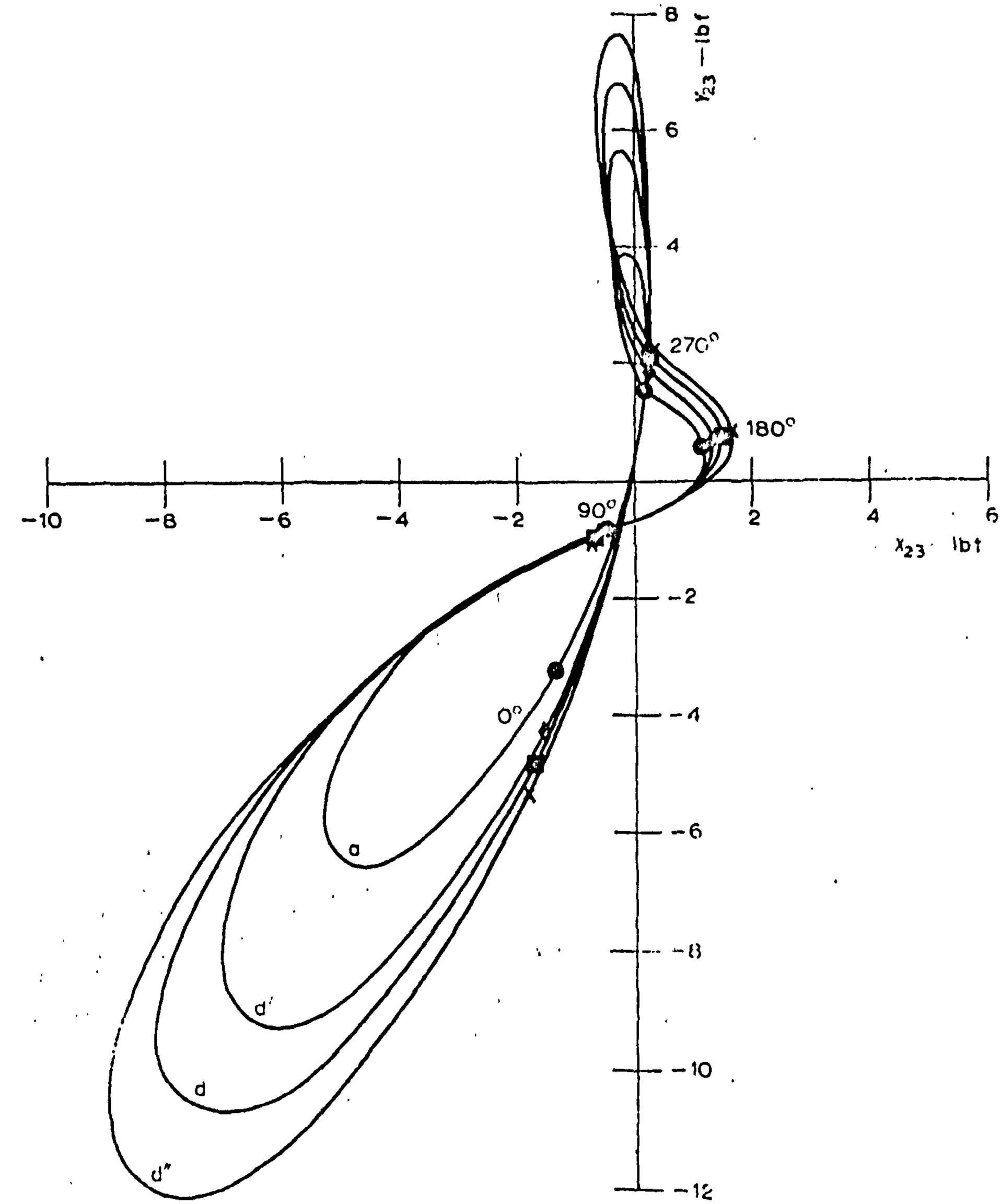

FIG.23(d) CRANK PIN FORCE : EFFECT OF COUNTERWEIGHT OFFSET

(a) Unbalanced linkage (FIG.20(a))

(d) Balanced linkage (FIG.20(d)) Offset = 6 in.

(d') Balanced linkage (FIG.20(d)) Offset = 3 in.

(d") Balanced linkage (FIG.20(d)) Offset = 1 in.

PART III

ELASTICITY and STABILITY

CHAPTER 6

EFFECTS OF ELASTICITY

6.1 Modes of Vibration

The preceding chapters have dealt with the kinematics and dynamics of ideal mechanisms in so far as the links have been assumed to be rigid. In practice, however, the elasticities of the individual links will have modifying effects upon both the kinematics and dynamics of the mechanism, the magnitudes of the effects depending to a large extent upon the way the links deflect. In Fig. 24 for example, the input motion is transmitted to the crank AB by means of the shaft O_1A and output motion is taken from shaft O_2D attached to link CD. In general, there will be torsional bending in both shafts in addition to bending in the links AB and CD in the plane of the mechanism. The non-symmetrical pin joints at B and C will impose torques upon all three moving links producing bending in the plane perpendicular to that of the mechanism in addition to about the longitudinal axes of the links. The gross motion of the coupler BC will cause transverse vibration in the plane of the mechanism and end-loads will add to this the possibility of out-of-plane vibrations.

There are then, many different possible modes of vibration which may occur and the mechanism is a multiple degree of freedom system in the general case. Houben[11] has examined such a four bar linkage and has developed the coupled equations of motion for in-plane bending, out-of-plane bending and torsion of the three moving links. The equations are then simplified and their stability examined by analogue computer methods.

The complexity of the completely general case is such that it is usual to consider only single modes of vibration and a number of these have been investigated. Gayfer and Mills[12] and Mahalingham[13] have examined the vibrations of a stationary four bar linkage in which the crank and follower are the flexible elements. The problem is akin to that of a portal frame of variable geometry and with a number of different end-conditions.

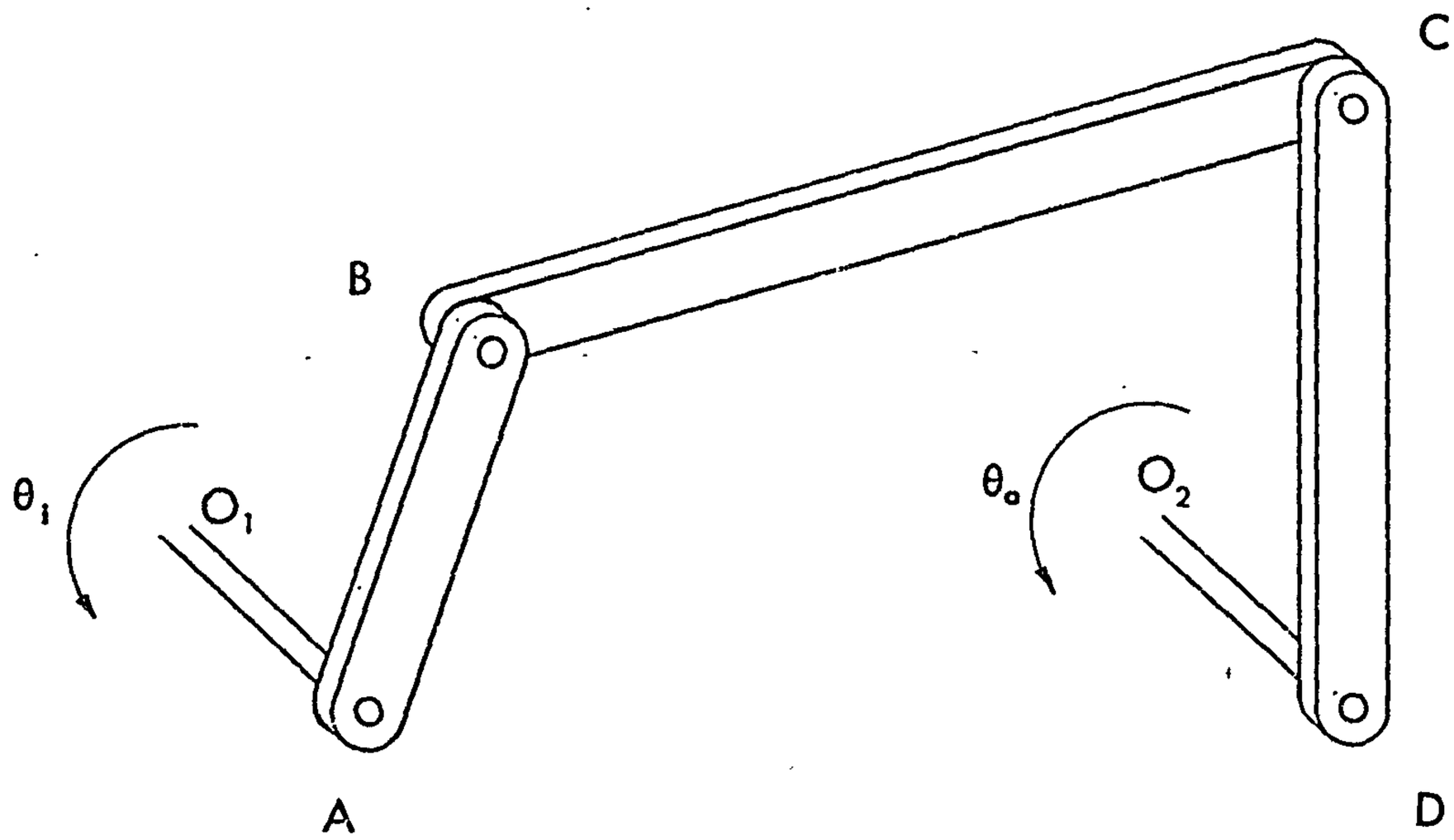

FIG.24. FOUR-BAR LINKAGE WITH ELASTIC COMPONENTS

A number of more realistic and considerably more complex dynamic problems has been examined, most notably by Meyer zur Capellen[14] and Houben[15] who have carried out extensive investigations into the nature of longitudinal and transverse vibrations of the elements of various linkage mechanisms. Neubauer, Cohen and Hall[16] have investigated the transverse vibrations of the connecting rod in a crank and slider mechanism and more recent work has been reported by Viscomi[17]. Both of these latter references however are entirely theoretical in so far as only computed solutions are discussed.

Meyer zur Capellen and Houben have also investigated the longitudinal vibrations of linkage elements[15] and the torsional vibrations of input and output shafts[18].

Two more general but excellent "standard works" are those of Kobrinskii[31] and Bolotin[32], both of which contain extensive bibliographies.

6.2 Transverse Vibrations of Links

6.2.1 Transverse Coupler Vibrations

As mentioned above, it is usually necessary to restrict attention to one particular mode of vibration in order to be able to achieve some meaningful results from an analysis of the problem. The present investigation will be concerned mainly with the transverse vibrations of the coupler in a crank and rocker mechanism in which both crank and follower are considered rigid. This condition is frequently met in practice where the crank usually forms part of a relatively large and rigid drive shaft and the follower may form part of a subsidiary mechanism and therefore have larger overall proportions than those of the transmission link.

We shall examine initially vibrations in the plane of the mechanism.

6.2.2 Equation of Motion

Fig. 25 shows a four bar linkage ABCD with flexible coupler BC in which bending may occur in the plane of the mechanism. The rigid crank AB is considered to rotate at constant angular velocity ω_2 and the rigid follower CD has inertia I_4 about an axis through D. The coupler has stiffness (EI), mass per unit length μ, and inertia I_3 about the crank pin B.

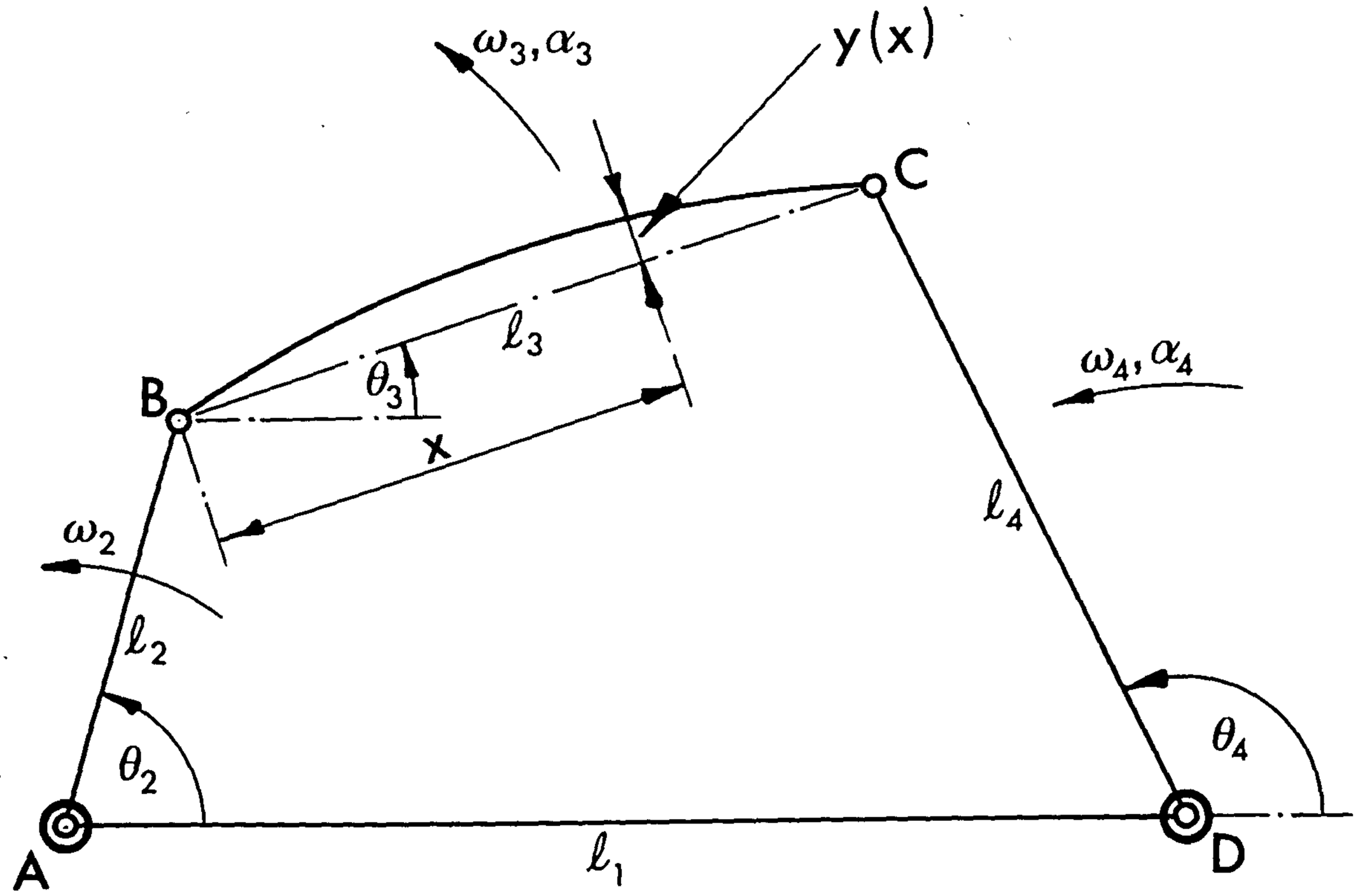

FIG.25. FOUR-BAR LINKAGE WITH FLEXIBLE COUPLER.

To obtain the equation of motion of the flexible coupler with respect to its undeflected position BC, we consider the general deflected form of the link as shown in Fig. 26. If the deflection of an element of the coupler situated a distance x from B is $y(x)$, then the acceleration components of that element are

$$a_x = - \ell_2 \omega_2^2 \cos(\theta_2 - \theta_3) - y(x)\alpha_3 - x\omega_3^2 - 2\dot{y}(x)\omega_3$$

$$a_y = - \ell_2 \omega_2^2 \sin(\theta_2 - \theta_3) - y(x)\omega_3^2 + x\alpha_3 + \ddot{y}(x)$$

where the axes O'xy have origin at the crank pin B and move with the coupler, the x direction being defined as the undeflected coupler centre line BC.

Considering only small oscillations of the beam and ignoring second order effects such as change in the x co-ordinate due to deflection y, we may obtain the moment equation for the element at distance x from the crank pin from linear beam theory as follows

$$EI\frac{\partial^2 y}{\partial x^2} = F_y(\ell_3 - x) + F_x y - \int_x^{\ell_3} f_y(\xi)(\xi - x)\,d\xi - \int_x^{\ell_3} \{y(x) - y(\xi)\} f_x(\xi)\,d\xi \qquad (6.1)$$

where $x \leq \xi \leq \ell_3$. F_x, F_y are the components of the pin force at C in the x and y directions respectively and f_x, f_y are the inertia forces defined by

$$\left.\begin{aligned} f_x(\xi) &= -\mu a_x(\xi) = \mu\left\{\ell_2\omega_2^2\cos(\theta_2-\theta_3) + y(\xi)\alpha_3 + \{\omega_3^2 + 2\dot{y}(\xi)\omega_3\}\right. \\ f_y(\xi) &= -\mu a_y(\xi) = \mu\left\{\ell_2\omega_2^2\sin(\theta_2-\theta_3) + y(\xi)\omega_3^2 - \{\alpha_3 - \ddot{y}(\xi)\}\right. \end{aligned}\right\} \qquad (6.2)$$

In order to obtain the equation of motion in the usual form, we must differentiate equation (6.1) twice with respect to the variable x. This involves the differentiation of two integrals which is accomplished by use of the following well known formula:-

$$\frac{d}{dx}\int_\phi^\psi f(x,s)\,ds = \int_\phi^\psi \frac{\partial f}{\partial x}\,ds + f(x,\psi)\frac{d\psi}{dx} - f(x,\phi)\frac{d\phi}{dx}$$

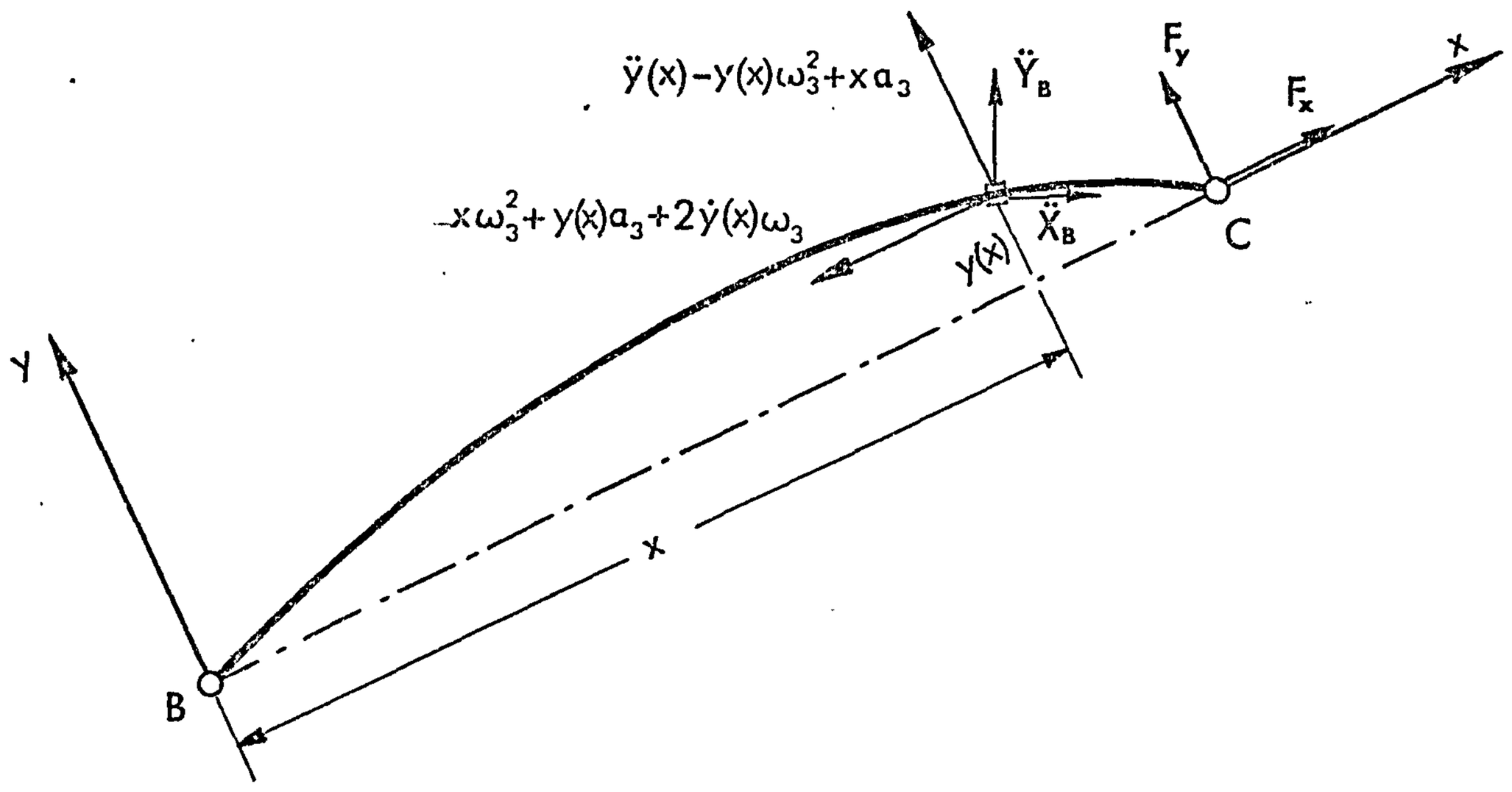

FIG.26. ACCELERATION COMPONENTS IN DEFLECTED COUPLER

Applying this to the first integral in equation (6.1) yields

$$\frac{\partial}{\partial x}\int_x^{\ell_3} f_y(\xi)(\xi - x)\, d\xi = \int_x^{\ell_3} f_y(\xi).(-1)\, d\xi$$

$$\frac{\partial}{\partial x}\int_x^{\ell_3} -f_y(\xi)\, d\xi = -f_y(\ell_3).0 + f_y(x).1 = f_y(x)$$

and to the second

$$\frac{\partial}{\partial x}\int_x^{\ell_3} \{y(x) - y(\xi)\}.f_x(\xi)\, d\xi = \int_x^{\ell_3} \frac{\partial y(x)}{\partial x} f_x(\xi)\, d\xi$$

$$\frac{\partial}{\partial x}\int_x^{\ell_3} \frac{\partial y(x)}{\partial x}.f_x(\xi)\, d\xi = \int_x^{\ell_3} \frac{\partial^2 y(x)}{\partial x^2}.f_x(\xi)\, d\xi - \frac{\partial y(x)}{\partial x}.f_x(x)$$

$$= \frac{\partial^2 y(x)}{\partial x^2}\int_x^{\ell_3} f_x(\xi)\, d\xi - \frac{\partial y(x)}{\partial x}.f_x(x)$$

The equation of motion may now be written as

$$EI\frac{\partial^4 y}{\partial x^4} = F_x\frac{\partial^2 y}{\partial x^2} + f_y(x) + \frac{\partial^2 y}{\partial x^2}\int_x^{\ell_3} f_x(\xi)\, d\xi - \frac{\partial y}{\partial x}.f_x(x) \qquad (6.3)$$

Evaluating the integral, we obtain

$$\int_x^{\ell_3} f_x(\xi)\, d\xi = \mu\left\{\ell_2(\ell_2 - x)\omega_2^2\cos(\theta_2 - \theta_3) + \alpha_3\int_x^{\ell_3} y(\xi)\, d\xi + \tfrac{1}{2}(\ell_3^2 - x^2)\omega_3^2 + 2\omega_3\int_x^{\ell_3}\dot{y}(\xi)\, d\xi\right\} \qquad (6.4)$$

and writing the inertia terms in full, the following form of the equation of motion is obtained

$$EI\frac{\partial^4 y}{\partial x^4} = \frac{\partial^2}{\partial x^2}\left\{F_x + \mu\left(\ell_2(\ell_2 - x)\omega_2^2\cos(\theta_2 - \theta_3) + \alpha_3\int_x^{\ell_3} y(\xi)\, d\xi + \tfrac{1}{2}(\ell_3^2 - x^2)\omega_3^2 + 2\omega_3\int_x^{\ell_3}\dot{y}(\xi)\, d\xi\right)\right\}$$

$$- \frac{\partial}{\partial x}\left\{\mu\left(\ell_2\omega_2^2\cos(\theta_2 - \theta_3) + y\alpha_3 + x\omega_3^2 + 2\omega_3\dot{y}\right)\right\} \qquad (6.5)$$

$$+ \mu\left(\ell_2\omega_2^2\sin(\theta_2 - \theta_3) + y\omega_3^2 - x\alpha_3 - \ddot{y}\right\}$$

This is the full form of the equation of motion which is seen to be a fourth order integro-differential equation with periodic coefficients. In order to be able to examine this equation further, it is necessary to make certain approximations, the first of which is to ignore second order terms in y. Since we are considering only small oscillations, we eliminate the second and fourth terms in the coefficients of $\frac{\partial_y^2}{\partial_x^2}$ and $\frac{\partial_y}{\partial_x}$ with the result that the equation may now be written in the following form, after some re-arrangement,

$$\frac{\partial^2 y}{\partial t^2} + \frac{EI}{\mu}\frac{\partial^4 y}{\partial x^4} - \frac{\partial^2 y}{\partial x^2}\left\{\frac{Fx}{\mu} + \ell_2(\ell_3 - x)\omega_2^2\cos(\theta_2-\theta_3) + \tfrac{1}{2}(\ell_3^2 - x^2)\omega_3^2\right\} \qquad (6.6)$$

$$+ \frac{\partial y}{\partial x}\left\{\ell_2\omega_2^2\cos(\theta_2-\theta_3) + x\omega_3^2\right\} - y\omega_3^2 = \ell_2\omega_2^2\sin(\theta_2-\theta_3) - x\alpha_3$$

This equation agrees with that obtained by Houben[11,19] with the exception of terms included by Houben to take account of the flexibility of the crank. Meyer zur Capellen[32] also obtains an equation essentially of the above form but gives little help with the solution apart from a brief description of Fourier series methods and makes no mention of instability. Houben[11] on the other hand employs the Galerkin technique to simplify the equation which reduces to a series of coupled 2nd order equations. Then, choosing to examine a linkage of extreme proportions, he examines the first two coupled equations and shows that not only may the coupling terms be ignored, but also that the periodic terms may be approximated to simple harmonic functions. The problem is thus reduced to the examination of two Mathieu equations which is accomplished by analogue computer methods and some experimental verification of the stability boundaries and regions of resonance and instability.

A similar but slightly less complex problem of the transverse vibrations of the connecting-rod of a crank and slider mechanism has been examined by Neubauer, Cohen and Hall[16]. The equation of motion which they obtain is essentially of the same form as equation (6.6). Linearizing assumptions are made including the reduction of the periodic term to a single cosine. This simplified

fourth order equation and a reduced second order equation (see below) are examined by digital computer techniques and the resulting solutions compared. As in Meyer zur Capellen's paper[32], no explicit mention is made of instability in the system, attention being concentrated on the accuracy of the computing methods used.

A recent paper by Viscomi and Ayre[17] reports further and more detailed work on the crank and slider in which the first two modes of vibration are examined. The solutions (obtained by analogue and digital computer) of the linearized and non-linearized equations are compared.

Seevers and Yang[20] also choose the crank and slider for a detailed study by analogue computer of the stability of vibrations of the connecting rod. Stability charts are shown in which instability is assumed to be present when the computed amplitude exceeds a predetermined value.

In the present investigation of the equation of motion, we will follow the usual method employed by Houben and assume a solution of the form

$$y(x,t) = \sum_{n=1}^{\infty} Y_n(t) \cdot \sin\left(\frac{n\pi x}{\ell_3}\right) \qquad (6.7)$$

which satisfies the boundary conditions $y(0,t) = y(\ell_3,t) = 0$, and $\ddot{y}(0,t) = \ddot{y}(\ell_3,t) = 0$.

Substitution of this into equation (6.6) leads to a second order differential equation in $Y_n(t)$ as follows.

Equation (4.6) becomes

$$\sum_{n=1}^{\infty} \ddot{Y}_n \sin\left(\frac{n\pi x}{\ell_3}\right) + \frac{EI}{\mu} \sum_{n=1}^{\infty} \left(\frac{n\pi}{\ell_3}\right)^4 Y_n \sin\left(\frac{n\pi x}{\ell_3}\right) + f_1(x,t) \sum_{n=1}^{\infty} \left(\frac{n\pi}{\ell_3}\right)^2 Y_n \sin\left(\frac{n\pi x}{\ell_3}\right)$$
$$+ f_2(x,t) \sum_{n=1}^{\infty} \left(\frac{n\pi}{\ell_3}\right) Y_n \cos\left(\frac{n\pi x}{\ell_3}\right) - \omega_3^2 \sum_{n=1}^{\infty} Y_n \sin\left(\frac{n\pi x}{\ell_3}\right) = f_3(x,t) \qquad (6.8)$$

where

$$\left.\begin{aligned} f_1(x,t) &= \frac{F_x}{\mu} + \ell_2(\ell_3 - x)\omega_2^2 \cos(\theta_2 - \theta_3) + \tfrac{1}{2}(\ell_3^2 - x^2)\omega_3^2 \\ f_2(x,t) &= \ell_2 \omega_2^2 \cos(\theta_2 - \theta_3) + x\omega_3^2 \\ f_3(x,t) &= \ell_2 \omega_2^2 \sin(\theta_2 - \theta_3) - x\alpha_3 \end{aligned}\right\} \qquad (6.9)$$

This equation may be simplified by multiplying throughout by $\sin\left(\frac{n\pi}{\ell_3}x\right)$ and integrating over the length of the coupler, taking into account the orthogonality relationships.

$$\int_0^{\ell_3} \sin\left(\frac{n\pi x}{\ell_3}\right)\sin\left(\frac{m\pi x}{\ell_3}\right)dx = \left\{\begin{array}{ll} 0 & \text{if } n \neq m \\ \frac{\ell_3}{2} & \text{if } n = m \end{array}\right\}. \qquad (6.10)$$

Considering each term of equation (6.8) in turn we have

$$\int_0^{\ell_3} \sin\left(\frac{m\pi x}{\ell_3}\right)\left(\sum_{n=1}^{\infty} \ddot{Y}_n \sin\left(\frac{n\pi x}{\ell_3}\right)\right) dx = \frac{\ell_3}{2}\,\ddot{Y}_m$$

$$\int_0^{\ell_3} \sin\left(\frac{m\pi x}{\ell_3}\right)\left(\sum_{n=1}^{\infty} \left(\frac{n\pi}{\ell_3}\right)^4 Y_n \sin\left(\frac{n\pi x}{\ell_3}\right)\right) dx = \frac{\ell_3}{2}\left(\frac{n\pi}{\ell_3}\right)^4 Y_m$$

$$\int_0^{\ell_3} f_1(x,t)\sin\left(\frac{m\pi x}{\ell_3}\right)\left(\sum_{n=1}^{\infty} \left(\frac{n\pi}{\ell_3}\right)^2 Y_n \sin\left(\frac{n\pi x}{\ell_3}\right)\right) dx = \frac{\ell_3}{2}\cdot\left(\frac{n\pi}{\ell_3}\right)^2\left(\frac{F_{ia}}{\mu}\right) Y_m$$

$$\int_0^{\ell_3} f_2(x,t)\sin\left(\frac{m\pi x}{\ell_3}\right)\left(\sum_{n=1}^{\infty} \left(\frac{n\pi}{\ell_3}\right) Y_n \cos\left(\frac{n\pi x}{\ell_3}\right)\right) dx = 0$$

$$\int_0^{\ell_3} \sin\left(\frac{m\pi x}{\ell_3}\right)\left(\sum_{n=1}^{\infty} Y_n \sin\left(\frac{n\pi x}{\ell_3}\right)\right) dx = \frac{\ell_3}{2}\cdot Y_m$$

The right hand side yields

$$\int_0^{\ell_3} f_3(x,t)\cdot \sin\left(\frac{m\pi x}{\ell_3}\right) dx = \left[\frac{-\ell_3}{m\pi} f_{r_3}(x,t)\cos\left(\frac{m\pi x}{\ell_3}\right)\right]_0^{\ell_3} - \int_0^{\ell_3} \frac{\alpha_3 \ell_3}{m\pi}\cos\left(\frac{m\pi x}{\ell_3}\right) dx$$

$$= -\frac{\ell_3}{m\pi}\left\{f_3(\ell_3,t)\cos m\pi - f(0,t)\right\} - \frac{\alpha_3\ell_3}{m\pi}\left[\frac{\ell_3}{m\pi}\sin\left(\frac{m\pi x}{\ell_3}\right)\right]_0^{\ell_3}$$

$$= -\frac{\ell_3}{m\pi}\left\{\pm \ell_2\omega_2^2\sin(\theta_2-\theta_3) \mp \ell_3\alpha_3 - \ell_2\omega_2^2\sin(\theta_2-\theta_3)\right\}$$

$$\begin{cases} = \dfrac{\ell_3}{m\pi}\left\{\ell_3\alpha_3\right\} & \text{when } m \text{ is even,} \\ = \dfrac{\ell_3}{m\pi}\left\{2\ell_2\omega_2^2\sin(\theta_2-\theta_3) - \ell_3\alpha_3\right\} & \text{when } m \text{ is odd.} \end{cases}$$

Substituting the values of all of these integrals into the equation and multiplying throughout by $2/\ell_3$ yields the final form of the equation

$$\ddot{Y}_m + Y_m\left\{\frac{EI}{\mu}\left(\frac{m\pi}{\ell_3}\right)^4 - \omega_3^2 + \frac{F_x}{\mu}\left(\frac{m\pi}{\ell_3}\right)^2\right\} \begin{cases} = \dfrac{2}{m\pi}\left\{2\ell_2\omega_2^2\sin(\theta_2-\theta_3) - \ell_3\alpha_3\right\} & (m \text{ odd}) \\ = \dfrac{2\ell_3\alpha_3}{m\pi} & (m \text{ even}). \end{cases} \tag{6.11}$$

which is effectively a set of equations in Y_m, the amplitude of the m th mode of vibration of the coupler. It can be seen that the first term in the coefficient of Y_m represents the natural frequency of vibration of the m th mode and for a stationary linkage, the equation reduces to the familiar beam equation

$$\ddot{Y}_m + \frac{EI}{\mu}\left(\frac{m\pi}{\ell_3}\right)^4 Y_m = 0 \tag{6.12}$$

$$\text{or} \quad \ddot{Y}_m + \Omega_m^2 Y_m = 0 \tag{6.13}$$

The coefficient of Y_m in equation (6.11) may now be written as

$$\frac{EI}{\mu} \cdot \left(\frac{m\pi}{\ell_3}\right)^4 \left\{1 - \left(\frac{\omega_3}{\Omega_m}\right)^2 + \frac{F_x}{F_{E_m}}\right\}$$

where $F_{E_m} = \frac{EIm^2\pi^2}{\ell_3^2}$ the m th Euler critical buckling load for the beam. We now see that the "effective" natural frequency of the coupler is equal to the undisturbed natural frequency plus two periodic terms, one arising from the angular velocity of the coupler itself and the other from the end-load F_x which is due to the inertia of the links.

Although in the majority of practical examples of mechanisms, ω_3 will be much smaller than the natural frequency Ω_m and the end-load F_x will be smaller than the critical Euler load F_E, these terms can not be neglected at this stage. It has been shown[21] that unstable vibration may occur in a rod subjected to a varying end load whose amplitude is considerably smaller than that of the first critical load while it is also possible to obtain stable vibrations in the presence of considerably larger end loads. The determination of the conditions under which such vibrations are stable or unstable is a problem of considerable complexity and one which has been given a great deal of attention. However, before considering the stability problem, we will examine some of the features of equation (6.11).

It is usual, when examining equations of the type (6.11) to assume tacitly that modes of vibration higher than the first may be ignored in comparison with the first. A few workers (e.g. Viscomi[17] and Neubauer et al[16]) show evidence to substantiate the assumption and it will be shown here too that the second and third mode amplitudes are usually two or three orders of magnitude smaller than that of the first. This is to be expected from a brief examination of equation (6.11). The natural frequencies are proportional to the fourth power of m and the Euler loads F_{E_m} to the second. Consequently the angular velocity term $(\omega_3/\Omega_m)^2$ for the second mode will be 16 times smaller and the end load term (F_x/F_{E_m}) four times smaller than the corresponding terms for the

first mode. For the higher modes therefore, the form of the equation of motion approaches that of equation (6.12) with the addition of a right hand side which is inversely proportional to the mode order n. Hence the forcing terms reduce in amplitude with increasing mode order giving correspondingly reduced responses.

The form of the right hand side of equation (6.11) depends upon whether the mode is odd or even and is associated with the transverse acceleration of the coupler.

We now see that equation (6.11) contains a number of periodic terms which are all determined uniquely by the dimensions of the mechanism. In general it will be difficult to predict or estimate the form of these periodic terms and only in certain particular cases will it be possible to ignore some of these or use simplifying approximations such as replacement by harmonic functions.

We now examine in more detail, the nature of the periodic terms in equation (6.11). The angular velocity of the coupler ω_3 is a known function of the geometry of the linkage and is determined uniquely for a mechanism of known link lengths. The coupler end-force F_x which we consider to be entirely due to the inertia of the mechanism links is however less easily determined. In chapter 4, the pin forces of the four bar linkage were evaluated with respect to fixed axes. We may now consider the force at the coupler-follower joint and resolve it into components parallel and perpendicular to the coupler. These components will be the F_x and F_y of equation (6.1). From Chapter 4 we have, as the horizontal and vertical components (fixed axes) of the coupler/follower force,

$$X_{43} = -\frac{\left\{ I_3 \alpha_3 \ell_4 \cos\theta_4 + I_4 \alpha_4 \ell_3 \cos\theta_3 - m_3 r_3 \ell_2 \ell_4 \cos\theta_4 \left[\omega_2^2 \sin(\theta_2 - \theta_3)\right]\right\}}{\ell_3 \ell_4 \sin(\theta_3 - \theta_4)}$$

$$Y_{43} = -\frac{\left\{ I_3 \alpha_3 \ell_4 \sin\theta_4 + I_4 \alpha_4 \ell_3 \sin\theta_3 - m_3 r_3 \ell_2 \ell_4 \sin\theta_4 \left[\omega_2^2 \sin(\theta_2 - \theta_3)\right]\right\}}{\ell_3 \ell_4 \sin(\theta_3 - \theta_4)}$$

Transforming now to the system of co-ordinates O'xy with origin at the crank pin B and moving with the coupler such that the angular separation between OXY and O'xy is θ_3, we obtain the components F_x and F_y as

$$F_x = \frac{-\{I_3\alpha_3 \ell_4 \cos(\theta_3-\theta_4) + I_4\alpha_4 \ell_3 - m_3 r_3 \ell_2 \ell_4 \cos(\theta_3-\theta_4)[\omega_2^2 \sin(\theta_2-\theta_3)]\}}{\ell_3 \ell_4 \sin(\theta_3-\theta_4)}$$

$$F_y = \frac{-\{I_3\alpha_3 - m_3 r_3 \ell_2 \omega_2^2 \sin(\theta_2-\theta_3)\}}{\ell_3}$$

We see from this transformation that F_y is independent of the follower inertia and that F_x is dependent upon the inertias of coupler and follower and the location of the coupler centre of mass. Re-writing F_x as follows

$$F_x = \frac{-\{I_3\alpha_3 - m_3 r_3 \ell_2 \omega_2^2 \sin(\theta_2-\theta_3)\}\ell_4 \cos(\theta_3-\theta_4) - I_4\alpha_4 \ell_3}{\ell_3 \ell_4 \sin(\theta_3-\theta_4)} \qquad (6.14)$$

the contributions from coupler and follower are seen more easily. For mechanisms with good transmission characteristics in which $(\theta_3 - \theta_4) \simeq \frac{\pi}{2}$, the coupler inertia term will be very small and the pin force component may be given the approximate value

$$F_x = \frac{-I_4\alpha_4}{\ell_4 \sin(\theta_3-\theta_4)} \qquad (6.15)$$

Furthermore, in general when the follower is much more massive than the coupler (which situation will obtain in many of the cases under investigation since we are considering a flexible coupler and rigid follower) this approximate formula may be used. However, we must bear in mind the effect of this term upon the full equation of motion, equation (6.11), which we now write in non-dimensional form using the new variables $U_m = Y_m/\ell_3, \theta_2 = \omega_2 t$.

$$\frac{d^2U_m}{d\theta_2^2} + U_m\left\{\frac{EI}{\mu}\left(\frac{m\pi}{\ell_3}\right)^4 - \frac{\omega_3^2}{\omega_2^2} + \frac{F_x}{\mu\omega_2^2}\left(\frac{m\pi}{\ell_3}\right)^2\right\} \begin{cases} = \frac{2}{m\pi}\left\{\frac{2\ell_2}{\ell_3}\sin(\theta_2-\theta_3) - \frac{\alpha_3}{\omega_2^2}\right\} & (m \text{ odd}) \\ = \frac{2}{m\pi}\left\{\frac{\alpha_3}{\omega_2^2}\right\} & (m \text{ even}) \end{cases} \qquad (6.16)$$

This equation describes the m th mode of transverse vibration of the coupler but may also be considered in more general terms as describing the vibration of a pinned uniform beam, rotating at angular velocity ω_3 with angular acceleration α_3, subject to an end load F_x. This equation then, covers a wide range of situations but we will examine in detail only the case of the coupler of a crank and rocker linkage.

Considering again the coefficient of U_m, and writing the F_x term in full as follows,

$$\frac{F_x}{\mu\omega_2^2}\left(\frac{m\pi}{l_3}\right)^2 = \frac{I_3 m^2\pi^2}{\mu l_3^3}\left\{\frac{-\alpha_3}{\omega_2^2\tan(\theta_3-\theta_4)}\right\} + \frac{m^2\pi^2 t_3 l_2}{l_3^2}\left\{\frac{\sin(\theta_2-\theta_3)}{\tan(\theta_3-\theta_4)}\right\} + \frac{I_4 m^2\pi^2}{\mu l_3^2 l_4}\left\{\frac{-\alpha_4}{\omega_2^2\sin(\theta_3-\theta_4)}\right\}$$

$$= \epsilon_1 f_1(\theta_2) + \epsilon_2 f_2(\theta_2) + \epsilon_3 f_3(\theta_2)$$

we see that it contains in effect three periodic terms which are purely kinematic functions of the mechanism, and three parameters which are functions of the mass distributions of the coupler and follower. The full equation of motion may thus be written in the following symbolic form

$$\frac{d^2U_m}{d\theta_2^2} + \left\{m^4\lambda^2 - \phi(\theta_2) + m^2\left(\epsilon_1 f_1(\theta_2) + \epsilon_2 f_2(\theta_2) + \epsilon_3 f_3(\theta_2)\right)\right\}U_m = g_m(\theta_2)$$

where $$\lambda = \Omega/\omega_2 = \sqrt{\frac{\epsilon I}{\mu}}\cdot\left(\frac{\pi}{l_3}\right)^2\cdot\frac{1}{\omega_2} \qquad (6.17)$$

$$\phi(\theta_2) = \omega_3^2/\omega_2^2 \quad ;$$

$$\epsilon_1 = \frac{I_3\pi^2}{\mu l_3^3} \quad ; \qquad f_1(\theta_2) = \frac{-\alpha_3}{\omega_2^2\tan(\theta_3-\theta_4)} \quad ;$$

$$\epsilon_2 = \frac{\pi^2 t_3 l_2}{l_3^2} \quad ; \qquad f_2(\theta_2) = \frac{\sin(\theta_2-\theta_3)}{\tan(\theta_3-\theta_4)} \quad ;$$

$$\epsilon_3 = \frac{I_4\pi^2}{\mu l_3^2 l_4} \quad ; \qquad f_3(\theta_2) = \frac{-\alpha_4}{\omega_2^2\sin(\theta_3-\theta_4)} \quad ;$$

$$g_m(\theta_2) = \begin{cases} \dfrac{2}{m\pi}\cdot\left\{\dfrac{2l_2}{l_3}\sin(\theta_2-\theta_3) - \dfrac{\alpha_3}{\omega_2^2}\right\} & (m \text{ odd}) \\ \dfrac{2}{m\pi}\left\{\dfrac{\alpha'_3}{\omega_2^2}\right\} & (m \text{ even}) \end{cases}.$$

This equation is a special form of inhomogeneous Hill's equation containing four independent parameters in the coefficient of the dependent variable U_m. The examination of such an equation involves a great deal of lengthy and complicated analysis in the completely general case. However, because of the nature and relative magnitudes of the parameters involved, it will be seen that it is possible in many instances to make simplifying assumptions which render the equation more amenable to analysis.

Let us examine the coefficient of U_m in equation (6.17) and compare the magnitude of the various terms. The first term $m^4 \lambda^2$ represents the square of the ratio of the m th natural frequency of transverse vibration of the coupler to the driving frequency of the crank. The value of this term may theoretically range from zero to infinity corresponding to infinitely high and zero values of ω_2 respectively. In practice however, since we shall norrally have $\omega_2 << \Omega$, the value of λ will, in the great majority of instances, be much greater than unity. The second term, $\phi(\theta_2)$ is a purely kinematic term and will be determined entirely by the linkage dimensions.

From Chapter 2 we have

$$\phi(\theta_2) = \left(\frac{\omega_3}{\omega_2}\right)^2 = \frac{\ell_2^2 \sin^2(\theta_2 - \theta_4)}{\ell_3^2 \sin^2(\theta_3 - \theta_4)}$$

It is therefore not possible in general to make any estimate of the magnitude of this term other than to say that for the majority of crank and rocker mechanisms $\ell_2 < \ell_3$ and $\omega_3 < \omega_2$ so that in general $\phi(\theta_2) < 1$. It follows directly from the definition of $\phi(\theta_2)$ that the minimum value will be zero.

The remaining three terms are combinations of dynamic and kinematic functions and again it is difficult to generalise concerning amplitudes of the kinematic functions. However the contributions of the dynamic factors may be examined and comparisons made between them. The third term $\epsilon_1 f_1(\theta_2)$ arises from the inertia of the coupler, the parameter $\epsilon_1 = I_3 \pi^2 / \mu \ell_3^2$ being a function of the mass distribution of this link. Writing I_3 in terms of the radius of gyration

as $I_3 = (\mu \ell_3) k_3^2$ we obtain for ϵ_1,

$$\epsilon_1 = \frac{\pi^2 \, k_3^2}{\ell_3^2}$$

which, for a uniform coupler, becomes

$$\epsilon_1 = \frac{\pi^2}{3}$$

Should the coupler be partially or totally balanced about the crank pin, then the radius of gyration will be correspondingly larger but taking the uniform coupler case as typical, we obtain an approximate value of 3 for the parameter ϵ_1.

The next parameter $\epsilon_2 = \pi^2 + _3 \ell_2 / \ell_3^2$, if similarly treated is seen to have zero value for a coupler balanced at the crank pin ($+_3 = 0$) and a value of $\pi^2 \ell_2 / 2 \ell_3$ for a uniform coupler. Since $\ell_2 < \ell_3$, we have $\epsilon_2 < \pi^2/2$.

The final parameter ϵ_3 is a function of the mass distributions of coupler and follower. Writing $I_4 = M_4 k_4^2$ we have $\epsilon_3 = M_4 k_4^2 \pi^2 / M_3 \ell_3 \ell_4$ which, for a uniform follower gives $\epsilon_3 = \pi^2 M_4 \ell_4 / 3 M_3 \ell_3$. Furthermore, assuming that $\ell_3 \gtrsim \ell_4$ for the majority of practical cases, the parameter ϵ_3 takes the approximate value

$$\epsilon_3 \lesssim \frac{3M_4}{M_3}$$

We now have an assessment of the relative magnitudes of the parameters ϵ_i but there still remains the question of the relative amplitudes of the functions $f_i(\theta_2)$. As we have seen, it is not possible to quote figures in general and the best solution is to examine a number of examples of particular linkages and compare the magnitudes of the kinematic functions $f_i(\theta_2)$ and $\phi(\theta_2)$.

Figs. 27(a - e) show the functions $\phi(\theta_2)$ and $f_i(\theta_2)$ (for i = 1,2,3) for a representative number of mechanisms from which it can be seen that $f_3(\theta_2)$ is most often the predominating function. $f_1(\theta_2)$ and $f_2(\theta_2)$ become important in some cases but the angular velocity term $\phi(\theta_2)$ is comparatively small in all cases. Added to this is the contribution of the parameters ϵ_i all of which exceed unity and thereby increase the magnitudes of the $\epsilon_i f_i(\theta_2)$ terms in comparison with $\phi(\theta_2)$ in equation (6.17). Fig. 27(c) in particular shows

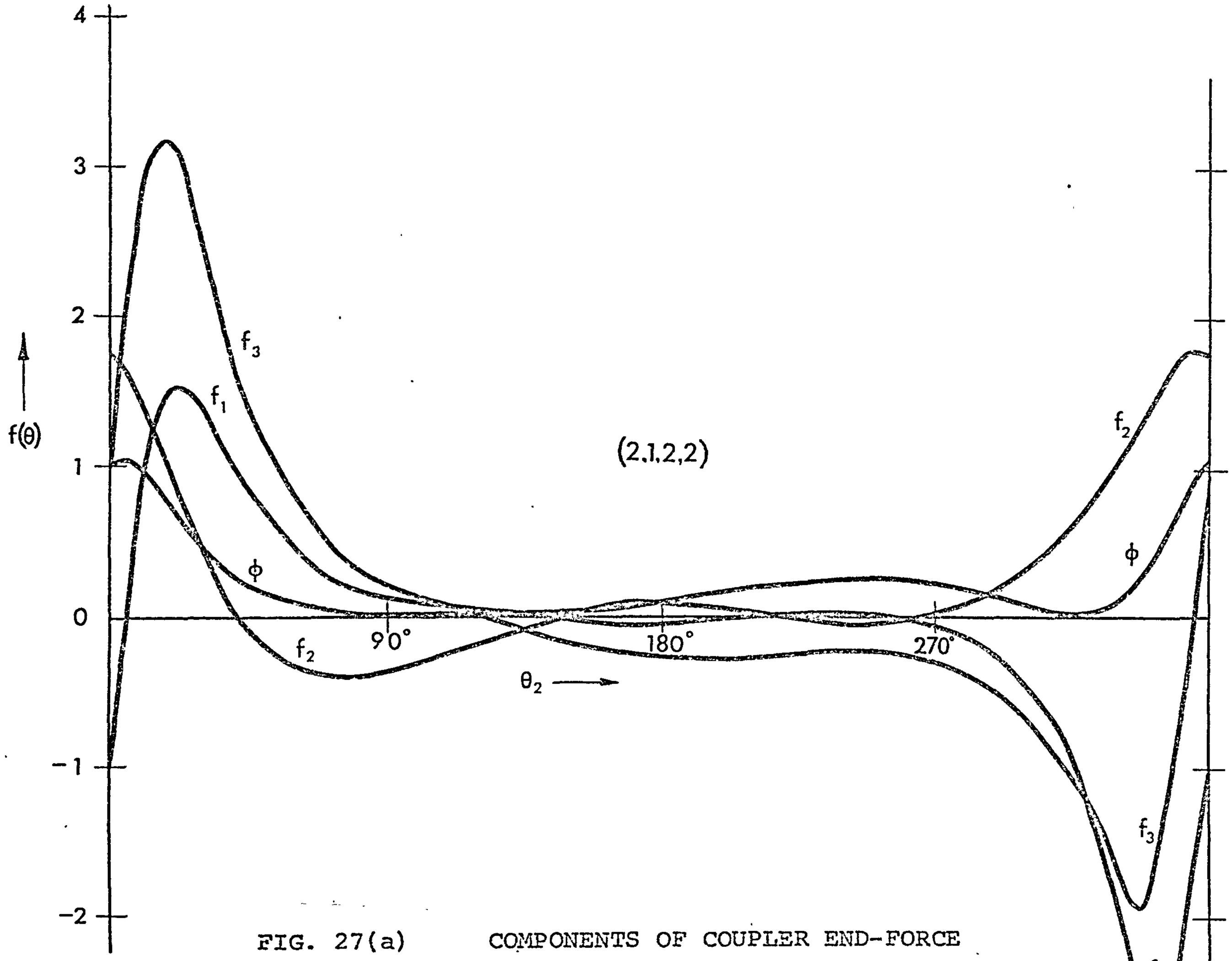

FIG. 27(a) COMPONENTS OF COUPLER END-FORCE

FIG. 27(b) COMPONENTS OF COUPLER END-FORCE

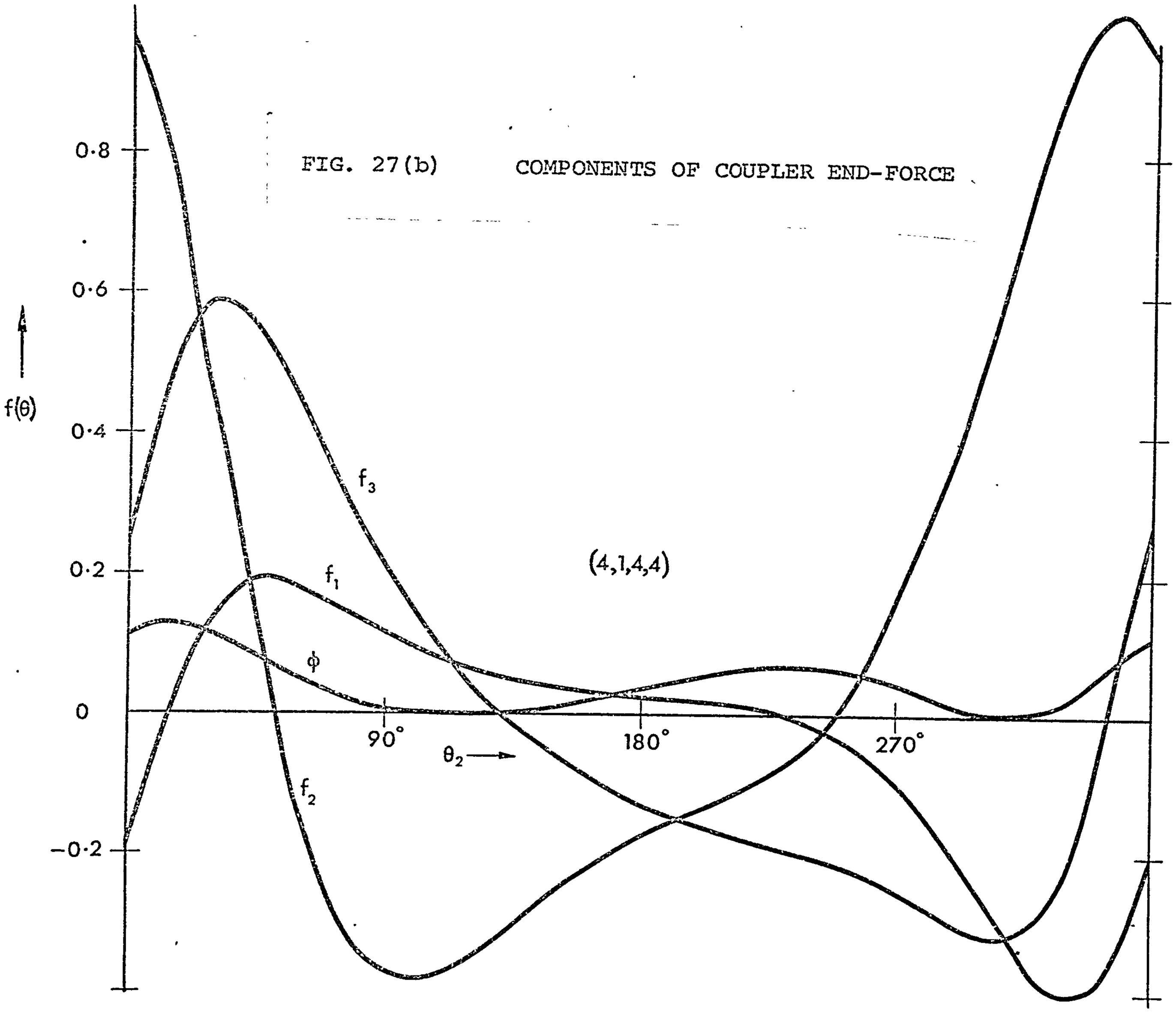

FIG. 27(c) COMPONENTS OF COUPLER END-FORCE

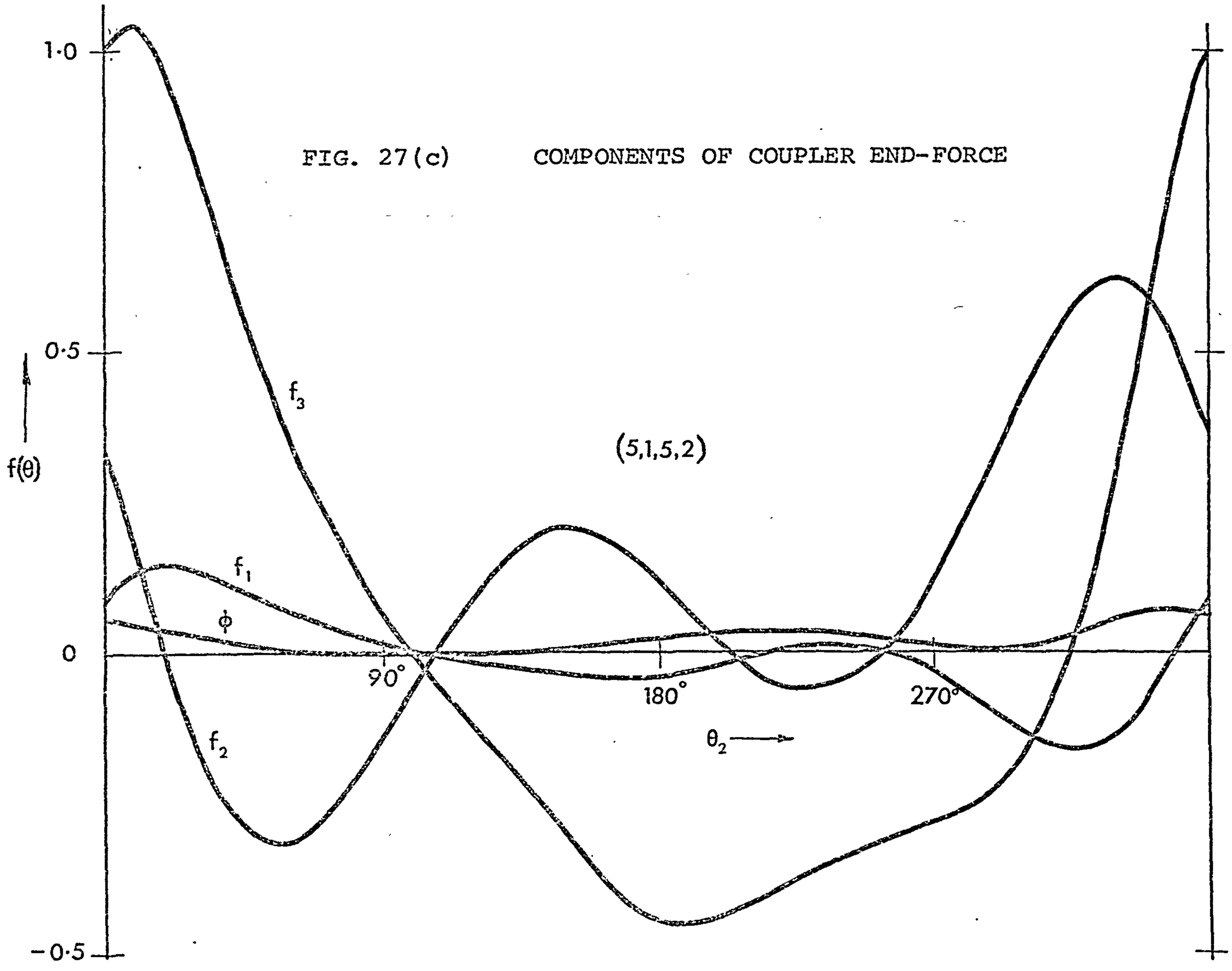

FIG. 27(d) COMPONENTS OF COUPLER END-FORCE

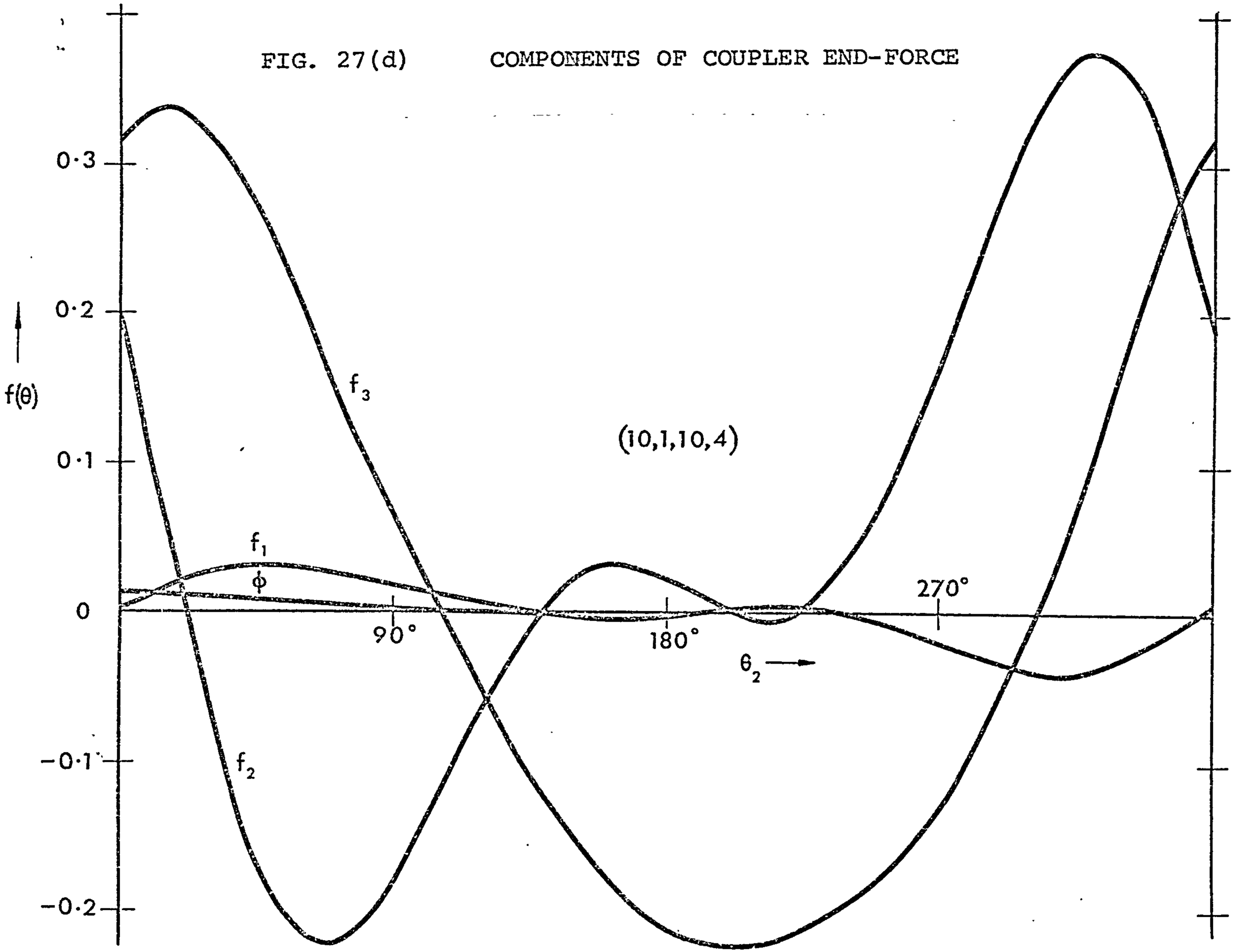

FIG. 27(e) COMPONENTS OF COUPLER END-FORCE

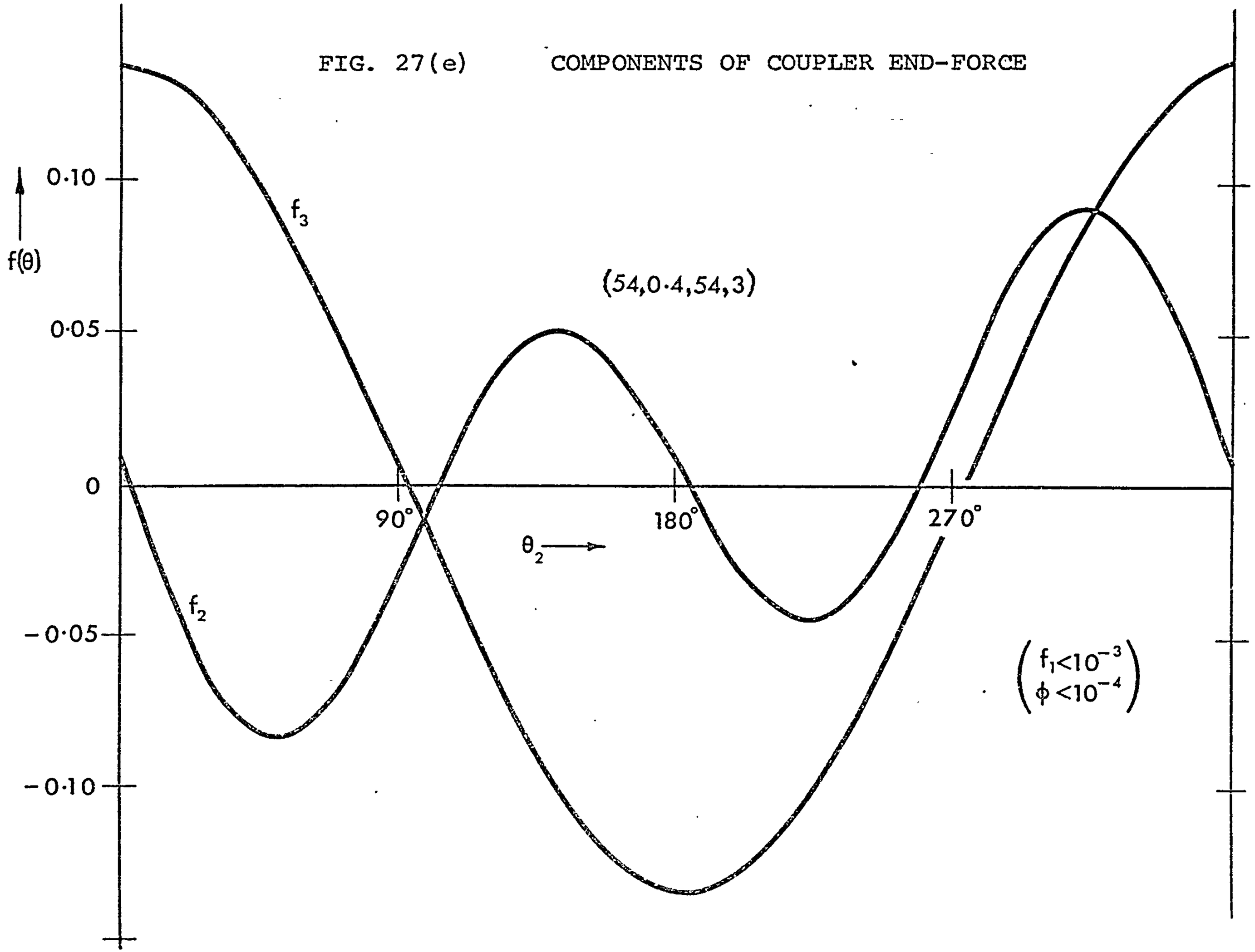

the periodic functions of the linkage used by Houben[11] in his stability investigations. The functions $f_1(\theta_2)$ and $\phi(\theta_2)$ are negligible with respect to the $f_2(\theta_2)$ and $f_3(\theta_2)$ which are themselves of comparable magnitudes. Houben however makes no mention of the term $f_2(\theta_2)$ and considers only the effect of $f_3(\theta_2)$ which he approximates quite justifiably to A cos θ_2 where the amplitude factor A is determined by the follower inertia.

We conclude therefore that in a wide range of crank and rocker mechanisms, the predominating periodic terms will be $f_2(\theta_2)$ and $f_3(\theta_2)$ and taking into account the relative magnitudes of ϵ_2 and ϵ_3 the equation may be written as follows

$$\frac{d^2U_m}{d\theta_2^2} + \left\{ m^4\lambda^2 + m^2 \epsilon_3 f_3(\theta_2) \right\} U_m = g_m(\theta_2) \qquad (6.18)$$

This is the form of the equation examined by many workers who have investigated the transverse vibrations of links in crank and rocker or crank and slider mechanisms and is equivalent to using the approximate form of the coupler end-force F_x

$$F_x = \frac{-I_4 \alpha_4}{\ell_4 \sin(\theta_3 - \theta_4)}$$

This form is assumed by Meyer zur Capellen[14] who obtains and equation of motion similar to equation[6.6] and describes an approximate method of solution using Fourier series. In a much more detailed investigation Houben[19] derives the full equation of motion and quotes the full form of the force F_x. However, by choosing to investigate experimentally a mechanism of extreme proportions, as we have seen, most of the periodic terms are reduced to a negligible level and the equation of motion is treated as a Mathieu equation in which the small parameter is considered to be a function of the follower inertia only.

One further step is possible which simplifies the examination of the equation and that is the restriction of the analysis to the principal mode of vibration (viz. m = 1 in equation (6.18)). Houben[19], Viscomi[17], Seevers

and Yang[20] have developed the equations of motion of systems essentially similar to the present one and have obtained a series of coupled equations describing all modes of vibration. The situation is then so complex that further analysis is only made possible by restricting attention to the first (and in some cases the second) mode. However it can be shown that the amplitude of the first mode is at least one order of magnitude greater than that of the second, which in turn is an order of magnitude greater than that of the third. In addition, the speeds of operation at which instabilities may be expected in the higher modes will be correspondingly higher than those occurring for the principal mode and will thus not severely restrict any investigation of instability at lower speeds.

A comparison of the amplitudes of typical modes will be made in the subsequent sections.

6.2.3 Solution by Digital Computation

6.2.3.1 Form of Solution

Equations similar in form to that of equation (6.16) (viz. second order differential equations in which the first differential is absent) may conveniently be solved using an algorithm due to de Vogelaere[23]. This algorithm forms the basis of a digital computer programme (see Appendix 4) used to solve equation (6.16) for a range of mechanism dimensions and parameter values on the KDF9 computer at Newcastle University.

In order to test the stability and accuracy of the algorithm, the system parameters were kept constant while the step length in the integration procedure was decreased gradually until no appreciable difference in consecutive computed solutions was evident. Fig. 28 shows the effect of step length upon the form of the solutions for a representative set of values. The fundamental wavelength of the solution in this particular case is equivalent to approximately 20^{o} of crank rotation. With a step length of 2^{o}, the amplitude of this component of the solution rapidly decays and, after one cycle of the crank, has almost disappeared. However, with a step length of 1.0^{o}, the solution remains approximately constant in amplitude. Further decreases in step length (down to 0.1^{o}) produce no

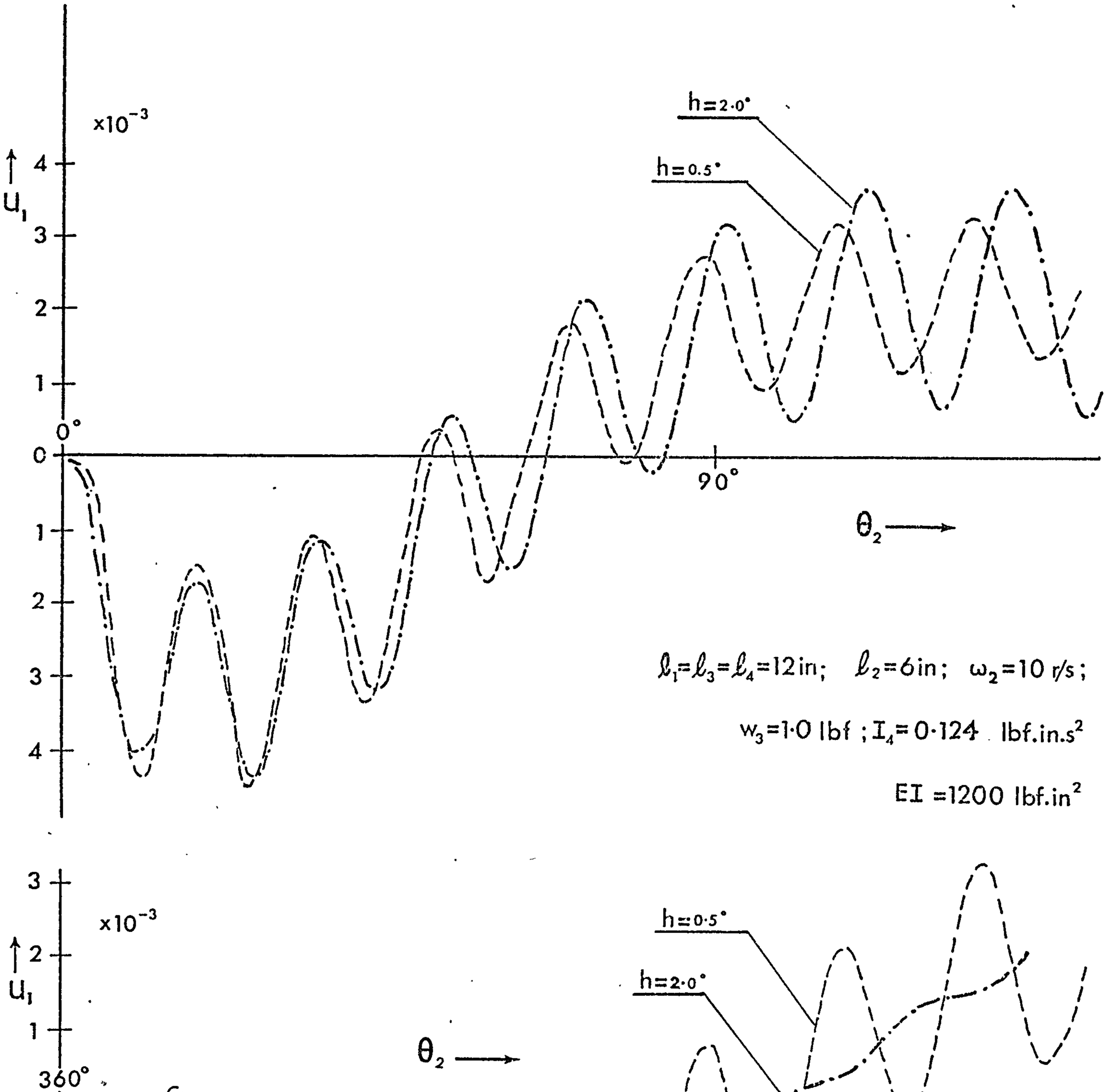

FIG.28. SOLUTION OF HILL'S EQUATION BY DIGITAL COMPUTER

Effect of Step-length

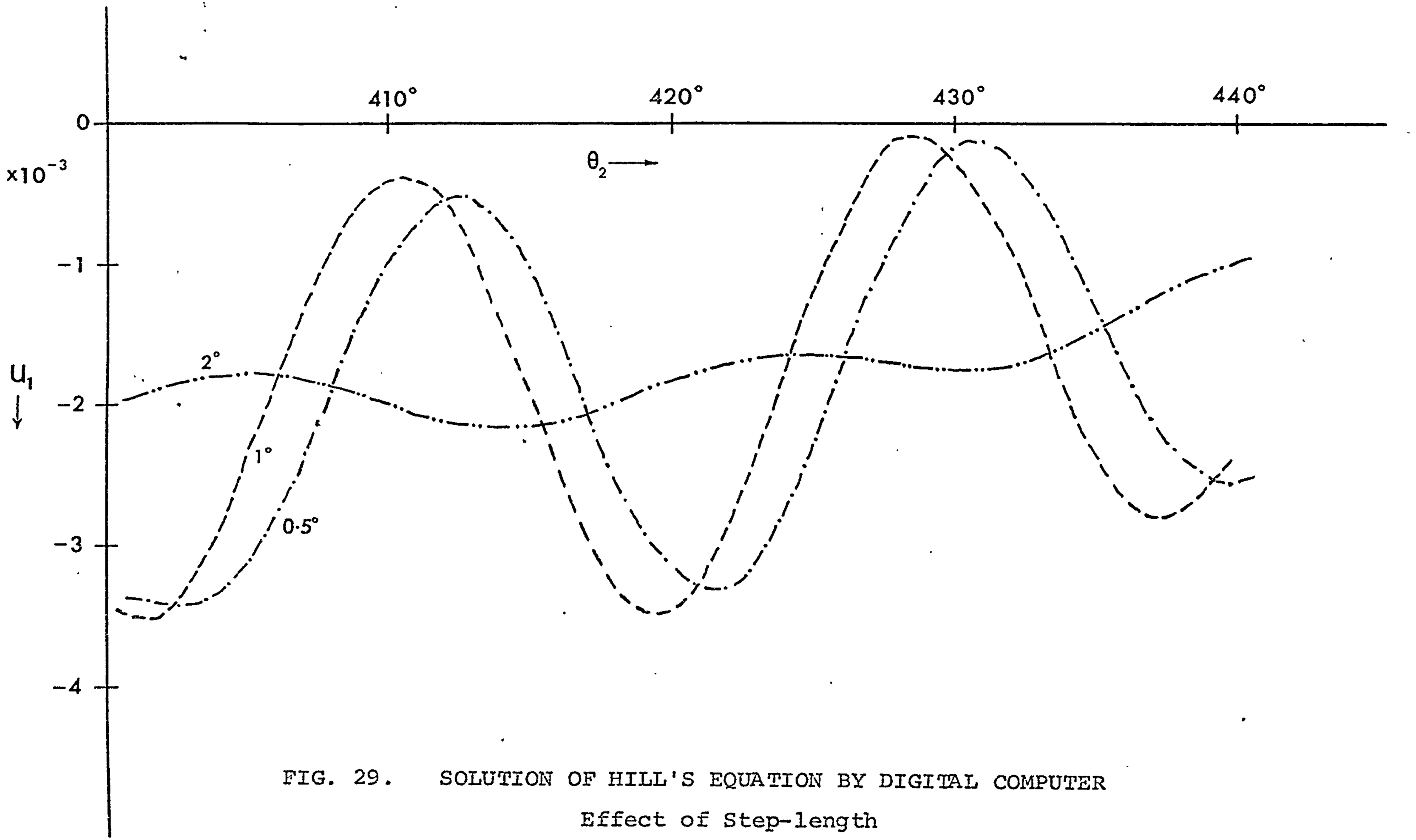

FIG. 29. SOLUTION OF HILL'S EQUATION BY DIGITAL COMPUTER

Effect of Step-length

(Data as for Fig. 28)

essential change in the form of the solution. With a step length of 0.5^{0}, the solution resembles closely that obtained with the 1.0^{0} step length. A slight phase change is observed after a few crank cycles which is of little consequence to the object of the investigation. (Fig. 29)

To ensure a valid representation of the solution therefore, the step length was restricted to a maximum possible value of one twentieth of the wavelength of the high frequency component in the solution.

This component corresponds closely to the natural frequency of the coupler so that it is a simple matter to compute a close approximation to the maximum permissible value of the step-length in degrees.

$$h_{max} \leq \frac{2\pi}{20\,\Omega_m} \qquad \text{where} \qquad \Omega_m = \frac{m^2\pi^2}{\ell_3^2}\cdot\sqrt{\frac{EI}{\mu}}$$

Working in terms of the crank angle θ_2 as independent variable, there will be λ oscillations of the fundamental mode for every crank cycle (where $\lambda = \Omega_1/\omega_2$. For the step-length h to be less than 1/20th of the wavelength $2\pi/\Omega_1$ we have

$$h < \frac{2\pi}{20\Omega_1} = \frac{\pi}{10\lambda\omega_2} = \frac{\pi}{10\lambda(2\pi f)} = \frac{\ell}{20\lambda}$$

where ℓ is "wavelength" of the crank angle i.e. 360^{0}.

Hence the condition $h < \frac{18}{\lambda}$ determines the maximum value of step length in terms of the speed parameter of equation (6.18).

In general, for the m th mode, the maximum step length will be determined by the relation

$$h < \frac{18}{\lambda_m} \qquad (\text{where} \qquad \lambda_m = \frac{m^2\Omega}{\omega_2})$$

In order to establish the validity of the method of solution, the equation of motion was also solved using a standard Kutta-Merson procedure with variable step length. The solution is shown in Fig. 30 compared with that obtained using the de Vogelaere method. As in the comparison of two different step-length solutions using the de Vogelaere method, (Fig. 29) the solutions here are

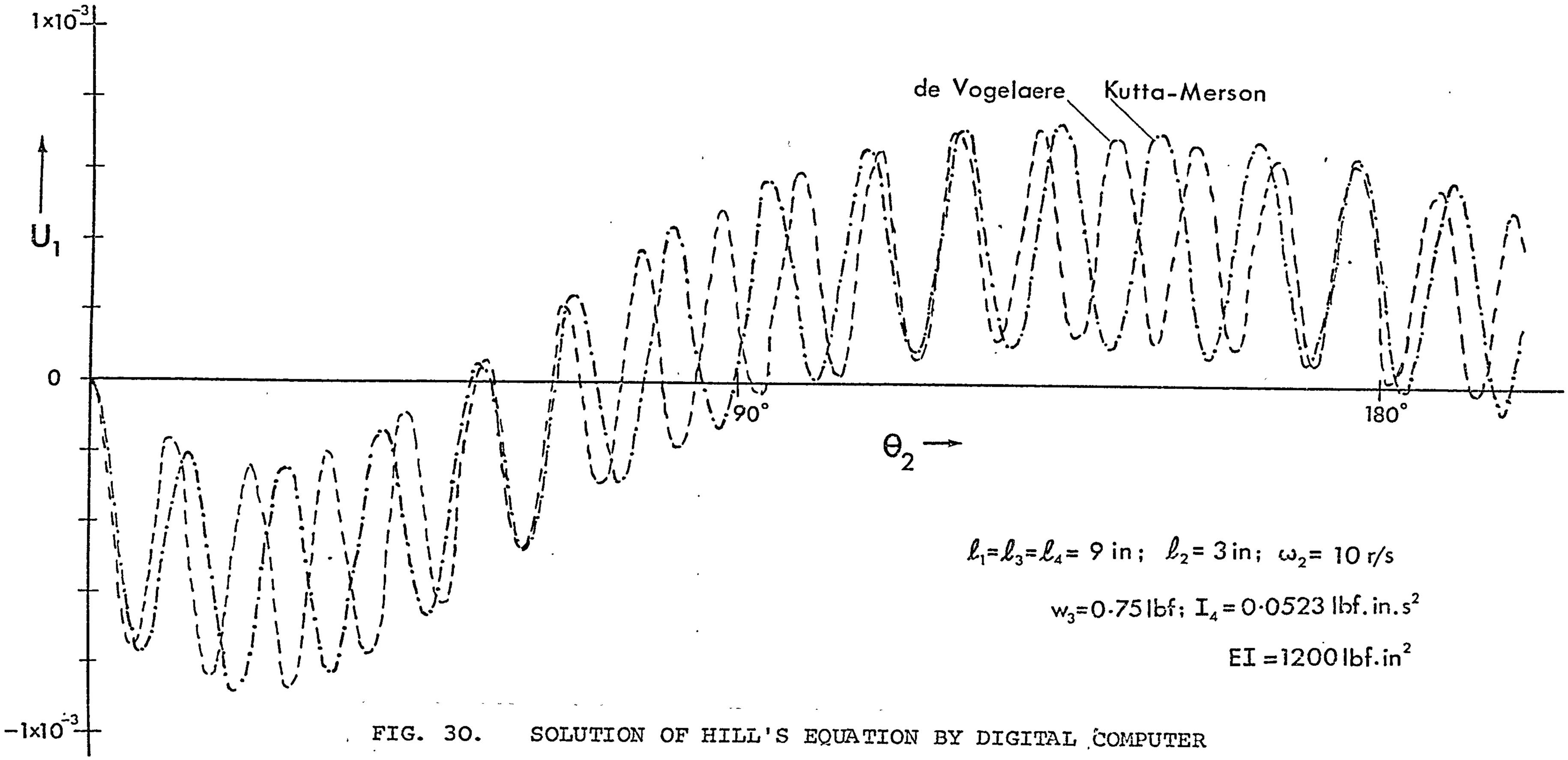

FIG. 30. SOLUTION OF HILL'S EQUATION BY DIGITAL COMPUTER
Comparison of KUTTA-MERSON and DE VOGELAERE Methods
(de Vogelaere step-length = 0.5°; Kutta-Merson variable)

essentially similar in form with a slight difference in the frequency of the high frequency component. This is an inevitable feature of the difference between the two methods, one having a fixed step length and the other having the facility for adjusting the step length at each integration step. As already stated, this is not a serious drawback since we are interested at this stage only in the general form of the solution of the equation of motion.

6.2.3.2 Higher Modes of Vibration

In problems of this type, it is customary to examine in detail only the fundamental mode of vibration since higher modes have very small amplitudes in comparison with that of the first[16,17,19]. Fig. 31 shows the amplitudes of the first three modes of equation (6.18). Considering only the amplitude of the high frequency components, it may be seen that there is more than an order of magnitude difference between first and second modes and approximately the same between second and third.

The corresponding low frequency components also bear a similar relationship to each other.

It should be noted here that these low frequency components are similar in form in the first and third (i.e. odd) modes but differ from that in the second (i.e. even) mode. Reference to equation (6.14) shows this to be a result of the nature of the "forcing function". The low frequency components are a result of this function (the transverse inertia force term) which has the effect of displacing the high frequency component from the mean position as in Fig. 28. Typical right hand side functions of equation (6.14) for the first and second modes are shown in Fig. 32.

6.2.3.3 Stability of Solutions

A feature of equations of the Hill type is that for a particular ϵ (equation (6.15)) there exists an infinite number of ranges of values of the parameter λ^2 for which the corresponding solution $u(\theta_2)$ is unstable, viz. the amplitude increases without bounds with increase of the independent variable θ_2.

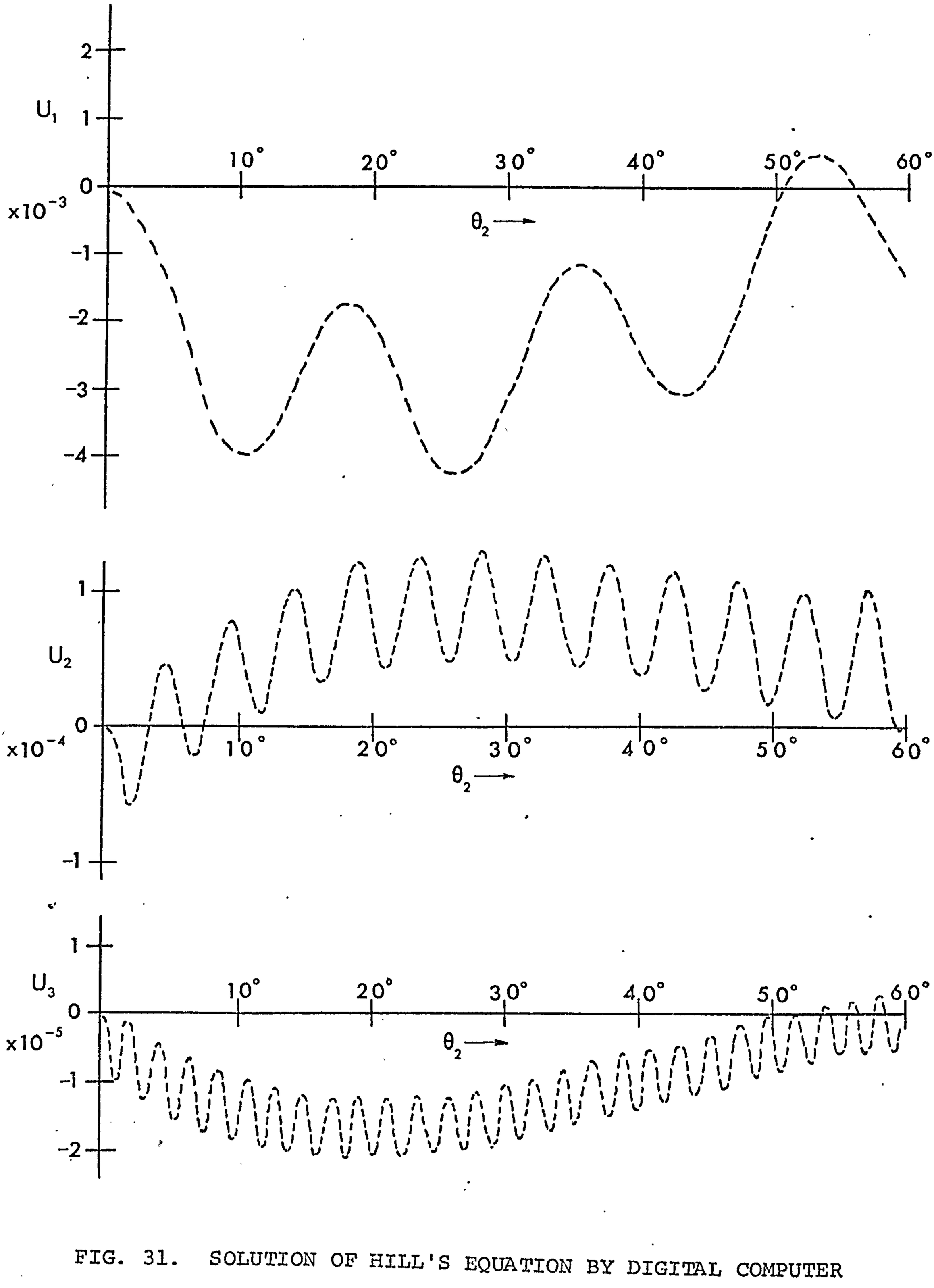

FIG. 31. SOLUTION OF HILL'S EQUATION BY DIGITAL COMPUTER

Relative Amplitudes of First Three Modes of Vibration

(Data as for FIG. 28)

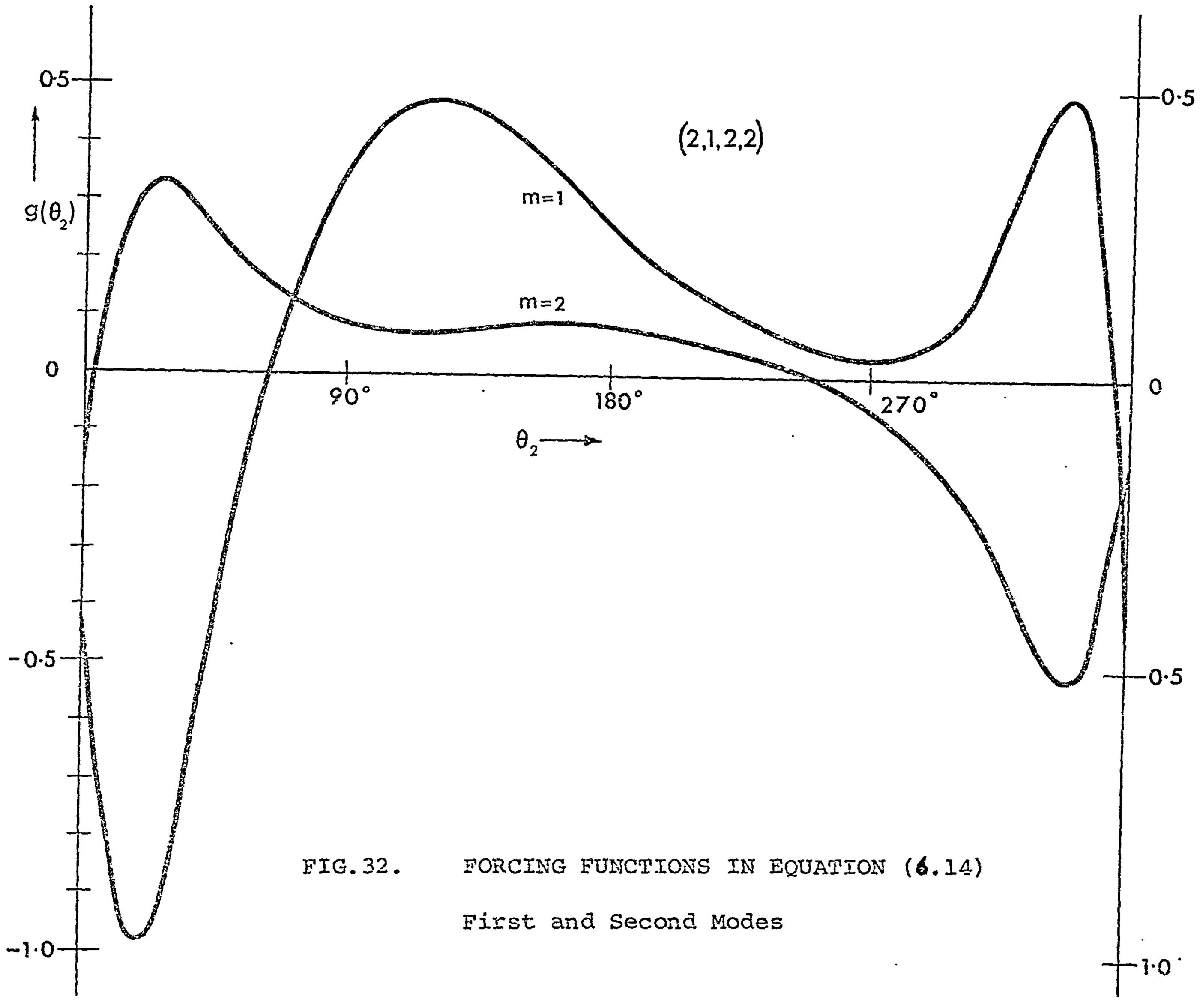

FIG.32. FORCING FUNCTIONS IN EQUATION (6.14)

First and Second Modes

In Chapter 7 we will seek to determine theoretically those values which yield stable or unstable solutions. For the present however we may investigate briefly whether the numerical method of solving the equation will yield stable and unstable forms of the solution for different values of the parameters λ^2 and ϵ . For small ϵ , unstable vibrations may be expected in the vicinity of $\lambda^2 = (\frac{n}{2})^2$ (see (31)). Fig. 33 shows examples of computed solutions of equation (6.15) for $\lambda^2 = 0.25, 1.0, 2.25$ all of which exhibit rapidly increasing amplitudes. Also shown in the figure are solutions with $\lambda^2 = 0.5, 1.5, 3.0$ (i.e. values between the expected unstable regions near $(\frac{n}{2})^2$) all of which have oscillating but bounded amplitudes.

The method of solution thus gives stable or unstable solutions as expected from a very brief examination of the theory of Hills equation. A more thorough investigation will be possible when the theoretical stability criteria have been determined in the next chapter.

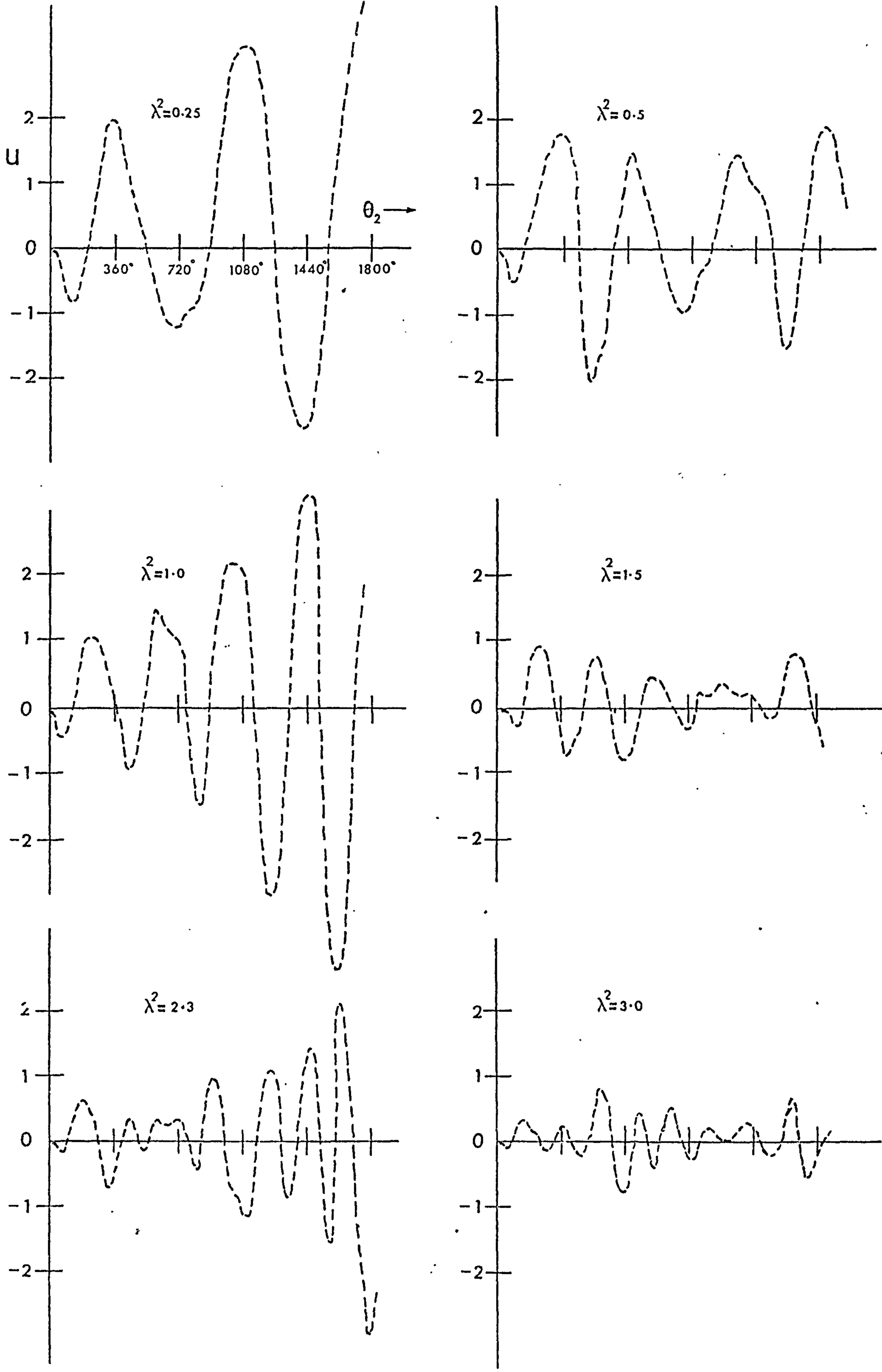

FIG. 33. STABLE AND UNSTABLE SOLUTIONS OF EQUATION (6.15)
Effect of change of stability parameters.

CHAPTER 7

THE STABILITY PROBLEM

7.1 Stability Criteria

7.1.1 Introduction

Hill's equation is commonly written in the following form[22]

$$\frac{d^2y}{dx^2} + \left\{ \lambda^2 + Q(x) \right\} y = 0 \qquad (7.1)$$

in which λ^2 is a constant and $Q(x)$ is a periodic (usually even) function of x of period π or 2π. By the introduction of an amplitude factor defined by $Q(x) = \mu . q(x)$ equation (7.1) becomes

$$y'' + \left\{ \lambda^2 + \mu \cdot q(x) \right\} y = 0 \qquad (7.2)$$

and now represents a two parameter problem in which the (λ, μ) plane must be divided into stable and unstable regions. The main problem in dealing with equations of this type therefore is the determination of the stability criteria in terms of the two parameters λ and μ, viz. the determination of the equations of the boundaries dividing the stable and unstable regions.

7.1.2 General Theory

The general Floquet theory describing the nature of the solutions of Hill's equation has been described fully in the literature of which a good summary is given by Magnus and Winkler[22]. Enough will be given here to make clear what follows.

Floquet's theorem states that Hill's equation will in general possess two independent solutions

$$y_1(x) = e^{i\alpha x} . p_1(x) \quad , \quad y_2(x) = e^{-i\alpha x} . p_2(x)$$

where p_1, p_2 are periodic functions of x. We refer to y_1, y_2 as the normalised solutions of equation (7.2) if

$$\left.\begin{aligned} y_1(0) &= 1 \quad , \quad y_1'(0) = 0 \quad , \\ y_2(0) &= 0 \quad , \quad y_2'(0) = 1 \end{aligned}\right\} \qquad (7.3)$$

If we assume $q(x)$ has period π in equation (7.2) then $y_1(x + \pi)$ and $y_2(x + \pi)$ will both be solutions and since $y_1(x)$, $y_2(x)$ are also solutions, it must be possible to express the former as linear combinations of the latter.

$$\left.\begin{aligned} y_1(x+\pi) &= a_1 y_1(x) + a_2 y_2(x) \\ y_2(x+\pi) &= a_3 y_1(x) + a_4 y_2(x) \end{aligned}\right\} \qquad (7.4)$$

Using initial conditions (7.3) we find immediately that

$$\begin{aligned} a_1 &= y_1(\pi) \\ a_2 &= y_1'(\pi) \\ a_3 &= y_2(\pi) \\ a_4 &= y_2'(\pi) \end{aligned} \qquad (7.5)$$

We now consider the general solution $y(x) = Ay_1(x) + By_2(x)$ and assume it is of a form such that

$$y(x + \pi) = p \cdot y(x) \qquad (7.6)$$

where p is a constant which determines the stability of the solution.

Putting $x = \pi$ in the general solution and using (7.6) we obtain

$$\begin{aligned} Ay_1(\pi) - Ap + By_2(\pi) &= 0 \\ y_1'(\pi)A + y_2'(\pi) \cdot B - Bp &= 0 \end{aligned} \qquad (7.7)$$

which is satisfied for nontrivial A, B if

$$\begin{vmatrix} y_1(\pi) - p & y_2(\pi) \\ y_1'(\pi) & y_2'(\pi) - p \end{vmatrix} = 0 \qquad (7.8)$$

This reduces to the form

$$p^2 - 2Xp + W = 0$$

$$\text{where} \quad X = \tfrac{1}{2}(y_1(\pi) + y_2'(\pi)) \qquad (7.9)$$

$$W = y_1(\pi) \cdot y_2'(\pi) - y_1'(\pi) \cdot y_2(\pi)$$

W is known as the Wronskian and may be shown[21] to have the value of unity for all x. Hence (7.9) becomes

$$p^2 - 2Xp + 1 = 0 \qquad (7.10)$$

which has roots p_1 , p_2 related by $p_1 \cdot p_2 = 1$

By comparison of the postulated forms of $y_1(x)$, $y_2(x)$ and the equation (7.6), it may be shown that the two values of the roots of the characteristic equation (7.10) are

$$p_1 = e^{i\gamma\pi} \quad , \quad p_2 = e^{-i\gamma\pi}$$

where γ is the characteristic exponent.

In general $p_1 \neq p_2$ and one of the solutions y_1 or y_2 will be unstable (since either $p_1 > 1$ or $p_2 > 1$) so that the complete solution will be unstable. In the case when $p_1 = p_1$ the complete solution will be stable (sometimes referred to as neutrally stable) with a period of π if $p = +1$ or of 2π if $p = -1$.

In what follows, we shall be interested mainly in investigating the condition necessary for a neutrally stable solution rather than determining the value of the characteristic exponent.

7.1.3 Determination of Bounds of Stability

7.1.3.1 Perturbation Method

It is well known that for small values of μ the values of λ^2 corresponding to solutions of period π will be in the vicinity of $(\frac{n}{2})^2$ for n = 1, 3, 5 ..... and for solutions of period 2π , in the vicinity of $(\frac{n}{2})^2$ for n = 2, 4, 6 ..... Before going further, we must recognise that what has been said in the foregoing section applies to periodic functions Q (x) and q (x) of period π . In what follows, the periodic function will have period 2π in the independent variable θ which has the effect of producing solutions of period 2π or 4π rather than of π or 2π .

To obtain equations describing the stability boundaries, we use a perturbation method in which λ^2 is expressed as a power series in the small parameter μ and seek a periodic solution in series form. Writing equation (7.2) as follows

$$\frac{d^2y}{d\theta^2} + \left\{ \lambda^2 + \mu f(\theta) \right\} y = 0 \qquad (7.11)$$

where f (θ) is periodic in θ of period 2π , we write

$$\lambda^2 = (\tfrac{n}{2})^2 + \alpha_1 \mu + \alpha_2 \mu^2 + \ldots \quad (n = 1, 2, 3 \ldots) \tag{7.12}$$

and attempt to find the coefficients α_i which will define the stability boundaries in the region of $\lambda^2 = (\frac{n}{2})^2$. For zero μ, we have the solution

$$y_o = A_1 \cos(\tfrac{n}{2})\theta + B_o \sin(\tfrac{n}{2})\theta \tag{7.13}$$

which has period 2π or 4π corresponding to even or odd n.

Assuming a solution to (7.11) of the form

$$y = y_o + \mu y_1 + \mu^2 y_2 + \ldots \tag{7.14}$$

and substituting this and (7.12) into (7.11) we obtain

$$\frac{d}{d\theta^2}\left(y_0 + \mu y_1 + \mu^2 y_2 + \cdots\right) + \left\{(\tfrac{n}{2})^2 + \alpha_1\mu + \alpha_2\mu^2 + \cdots + \mu f(\theta)\right\}\left\{ y_0 + \mu y_1 + \mu^2 y_2 + \cdots \right\} = 0 \tag{7.15}$$

which yields an infinite set of equations in y_i when like powers of μ are equated to zero.

$$\frac{d^2 y_o}{d\theta^2} + (\tfrac{n}{2})^2 y_o = 0 \tag{7.16}$$

$$\frac{d^2 y_1}{d\theta^2} + (\tfrac{n}{2})^2 y_1 = -\alpha_1 y_o - f(\theta) \cdot y_o \tag{7.17}$$

$$\frac{d^2 y_2}{d\theta^2} + (\tfrac{n}{2})^2 y_2 = -\alpha_1 y_1 - f(\theta) \cdot y_1 - \alpha_2 y_o \tag{7.18}$$

7.1.3.2 First Order Terms

The solution to (7.16) is the zero'th order solution (7.13) with arbitrary constants A_o, B_o. Equation (7.17) then becomes

$$\frac{d^2 y_1}{d\theta^2} + \left(\frac{n}{2}\right)^2 y_1 = -\left\{\alpha_1 + f(\theta)\right\} \cdot \left\{ A_o \cos\left(\frac{n}{2}\right)\theta + B_o \sin\left(\frac{n}{2}\right)\theta \right\} \tag{7.19}$$

The periodic function $f(\theta)$ must now be expressed in some form which allows the right hand side of (7.19) to be evaluated and thus make the integration of the equation possible. Malkin[24] has described a method in which the periodic function is itself expressed as a power series in the small parameter. This is not possible in the present case however, since the periodic functions of equation (6.15) are purely kinematic functions of the linkage whereas the small parameter is a function of kinematic and dynamic properties. To express the periodic functions explicitly in terms of the independent variable θ_2 (the crank angle) is a most difficult task in itself. Freudenstein[25] has described a method of harmonic analysis of the four bar linkage in which lengthy and complex expressions are derived which give the output angle (θ_4) in terms of harmonics of the crank angle (θ_2). To extend this work further in order to obtain similar expressions for the functions $f_i(\theta)$, $\phi(\theta)$ as defined by (6.16) and (6.17) would be unnecessarily tedious.

It is a much simpler matter to write the functions in terms of their Fourier Components which are assumed known. These may easily be calculated for any particular mechanism under examination by digital computer techniques using any of a wide variety of integration procedures (see Appendix 3). Accordingly, we write

$$f(\theta) = \sum_{m=0}^{\infty} \left(a_m \cos m\theta + b_m \sin m\theta \right) \qquad (7.20)$$

and substitute this into the right hand side of equation (7.19) with the following result.

$$\begin{aligned} \frac{d^2 y_1}{d\theta^2} + \left(\frac{n}{2}\right)^2 y_1 = & -\alpha_1 A_0 \cos\left(\tfrac{n}{2}\right)\theta - \alpha_1 B_0 \sin\left(\tfrac{n}{2}\right)\theta \\ & -\frac{1}{2}\sum_{m=0}^{\infty}\Big\{ (a_m A_0 - b_m B_0)\cos\left(m+\tfrac{n}{2}\right)\theta + (a_m A_0 + b_m B_0)\cos\left(m-\tfrac{n}{2}\right)\theta \\ & + (a_m B_0 + b_m A_0)\sin\left(m+\tfrac{n}{2}\right)\theta - (a_m B_0 - b_m A_0)\sin\left(m-\tfrac{n}{2}\right)\theta \Big\} . \end{aligned} \qquad (7.21)$$

Since we are seeking a periodic solution, all components y_i of the solution must themselves be periodic. Consequently, there must be no terms on the right hand side of equation (7.21) in $\sin(\frac{n}{2})\theta$ or $\cos(\frac{n}{2})\theta$ By equating the coefficients of such terms to zero, we obtain two simultaneous equations.

$$\left.\begin{aligned} -\alpha_1 A_o - \tfrac{1}{2}(2A_o a_o + A_o a_n + B_o b_n) &= 0 \\ -\alpha_1 B_o - \tfrac{1}{2}(2B_o a_o + A_o b_n - B_o a_n) &= 0 \end{aligned}\right\} \qquad (7.22)$$

which may be solved for α_1 and either of the arbitrary constants. If we choose A_o arbitrarily, then equations (7.22) will yield values of α_1 and B_o. Re-arranging as follows,

$$A_o(\alpha_1 + a_o + \frac{a_n}{2}) + B_o\frac{b_n}{2} = 0$$

$$A_o\frac{b_n}{2} + B_o(\alpha_1 + a_o - \frac{a_n}{2} = 0$$

we see that for a non-trivial solution, the determinant of these equations must have zero value which gives

$$(\alpha_1 + a_o)^2 - (\frac{a_n}{2})^2 - (\frac{b_n}{2})^2 = 0 \qquad (7.23)$$

$$\therefore \alpha_1 = -a_o \pm \tfrac{1}{2}\sqrt{a_n^2 + b_n^2}$$

Substitution into the original equation also yields a value for B_o

$$B_o = \frac{-A_o}{b_n}\left\{a_n \pm \sqrt{a_n^2 + b_n^2}\right\} \qquad (7.24)$$

We have thus determined the zero order solution y_o, the amplitude of which is governed by the choice of A_o the arbitrary constant. Furthermore, the first coefficient α_1 in the equation (7.12), is now known and to a first order approximation, the boundaries of the n^{th} unstable region are given by

$$\lambda'^2 = (\frac{n}{2})^2 + \alpha_1' \mu$$

$$\text{and} \qquad \lambda''^2 = (\frac{n}{2})^2 + \alpha_1'' \mu \qquad (7.25)$$

where α_1' , α_1'' are the values of α_1 obtained from equation (7.23) taking the positive and negative square root values respectively.

7.1.3.7 Second Order Terms

In order to obtain higher order approximations, equation (7.17) is now solved for y_1 and the resulting expression substituted into equation (7.18). Applying the periodicity condition enables the second coefficient α_2 to be determined, two values α_2', α_2'' being obtained corresponding to α_1' and α_1'' respectively. This process may be continued for higher order approximations but the complexity of the operation increases extremely rapidly for the completely general case considered here. Accordingly, only the second order terms will be evaluated in detail.

Equation (7.21) may now be re-written excluded all terms in $\begin{matrix}\sin\\ \cos\end{matrix}(\frac{n}{2})\theta$ on the right hand side

$$\frac{d^2y_1}{d\theta^2} + \left(\frac{n}{2}\right)^2 y_1 = -\frac{1}{2}\sum_{m=1}^{\infty}\left\{\left(a_m A_0 - b_m B_0\right)\cos\left(m+\tfrac{n}{2}\right)\theta + \left(a_m B_0 + b_m A_0\right)\sin\left(m+\tfrac{n}{2}\right)\theta\right\}$$

$$-\frac{1}{2}\sum_{\substack{m=1\\ m\neq n}}^{\infty}\left\{\left(a_m A_0 + b_m B_0\right)\cos\left(m-\tfrac{n}{2}\right)\theta - \left(a_m B_0 - b_m A_0\right)\sin\left(m-\tfrac{n}{2}\right)\theta\right\} \qquad (7.26)$$

Although this equation is now in integrable form, it is convenient at this stage to re-arrange the summation terms as follows. The second summation term in equation (7.26) includes terms in $\begin{matrix}\sin\\ \cos\end{matrix} j\,\theta$ where j takes the following values:-

$$\left(1-\tfrac{n}{2}\right), \left(2-\tfrac{n}{2}\right), \ldots\ldots \left(\tfrac{n}{2}-2\right), \left(\tfrac{n}{2}-1\right), \left(\tfrac{n}{2}+1\right), \left(\tfrac{n}{2}+2\right), \ldots\ldots$$

If n is even, then the lowest terms to occur will be in $\begin{matrix}\sin\\ \cos\end{matrix} 0$ otherwise if n is odd, the lowest terms will be in $\begin{matrix}\sin\\ \cos\end{matrix} \pm\tfrac{1}{2}\theta$. For $m < n$ there will be present terms in $\begin{matrix}\sin\\ \cos\end{matrix} 0$ up to $\begin{matrix}\sin\\ \cos\end{matrix} \pm(\frac{n}{2}-1)\theta$ for even n and $\begin{matrix}\sin\\ \cos\end{matrix}(\pm\frac{1}{2}\theta)$ up to $\begin{matrix}\sin\\ \cos\end{matrix} \pm(\frac{n}{2}-1)\theta$ for odd n. For $m > n$, (say $m = n + r$) terms will be in $(m - \frac{n}{2}) = (r + \frac{n}{2})$ for $r = 1, 2, 3 \ldots\ldots$ We may therefore collect these latter terms and include them in the first summation of equation (7.26) and re-arrange the remaining terms in descending order of magnitude whence equation (7.26) becomes

$$\frac{d^2y_1}{d\theta^2} + \left(\frac{n}{2}\right)^2 y_1 = -\frac{1}{2}\sum_{m=1}^{\infty}\left\{\left[A_o(a_m + a_{m+n}) - B_o(b_m - b_{m+n})\right]\cos\left(m+\frac{n}{2}\right)\theta\right. \tag{7.27}$$

$$\left. + \left[A_o(b_m + b_{m+n}) + B_o(a_m - a_{m+n})\right]\sin\left(m+\frac{n}{2}\right)\theta\right\}$$

$$-\frac{1}{2}\sum_{m=1}^{N}\left\{\left[A_o(a_m + a_{n-m}) + B_o(b_m + b_{n-m})\right]\cos\left(\frac{n}{2}-m\right)\theta\right.$$

$$\left. - \left[A_o(b_m - b_{n-m}) - B_o(a_m - a_{n-m})\right]\sin\left(\frac{n}{2}-m\right)\theta\right\}$$

$$-\frac{1}{2}\left[A_o a_{\frac{n}{2}} + B_o b_{\frac{n}{2}}\right]$$

where $N \begin{cases} = (n-1)/2 & \text{if n odd} \\ = (n-2)/2 & \text{if n even} \end{cases}$

and where the last term exists only for even n .

It is convenient now to introduce the following notation

$$P_{m,n} = A_o(a_m + a_{m+n}) - B_o(b_m - b_{m+n})$$

$$Q_{m,n} = A_o(b_m + b_{m+n}) + B_o(a_m - a_{m+n})$$

$$R_{m,n} = A_o(a_m + a_{n-m}) + B_o(b_m + b_{n-m}) \tag{7.28}$$

$$S_{m,n} = A_o(b_m - b_{n-m}) - B_o(a_m - a_{n-m})$$

$$T_n = A_o a_{\frac{n}{2}} + B_o b_{\frac{n}{2}} \qquad \text{if n even}$$

$$= 0 \qquad \text{if n odd}$$

which enables equation (7.27) to be written as

$$\frac{d^2y_1}{d\theta^2} + \left(\frac{n}{2}\right)^2 y_1 = -\frac{1}{2}\sum_{m=1}^{\infty}\left\{P_{m,n}\cos\left(m+\frac{n}{2}\right)\theta + Q_{m,n}\sin\left(m+\frac{n}{2}\right)\theta\right\} \tag{7.29}$$

$$-\frac{1}{2}\sum_{m=1}^{N}\left\{P_{m,n}\cos\left(\frac{n}{2}-m\right)\theta - S_{m,n}\sin\left(\frac{n}{2}-m\right)\theta\right\}$$

$$-\frac{1}{2}T_n$$

The solution of this is

$$
\begin{aligned}
y_1 &= \frac{1}{2}\sum_{m=1}^{\infty}\left\{P'_{m,n}\cos\left(m+\tfrac{n}{2}\right)\theta + Q'_{m,n}\sin\left(m+\tfrac{n}{2}\right)\theta\right\} \\
&+\frac{1}{2}\sum_{m=1}^{N}\left\{R'_{m,n}\cos\left(\tfrac{n}{2}-m\right)\theta - S'_{m,n}\sin\left(\tfrac{n}{2}-m\right)\theta\right\} \\
&-\frac{1}{2}\left(\frac{2}{n}\right)^2 T_n + A_1\cos\left(\tfrac{n}{2}\right)\theta + B_1\sin\left(\tfrac{n}{2}\right)\theta .
\end{aligned}
\tag{7.30}
$$

where $P'_{m,n} = P_{m,n} / \left\{ (m+\frac{n}{2})^2 - (\frac{n}{2})^2 \right\} = P_{m,n} / m(m+n)$

$$Q'_{m,n} = Q_{m,n} / \left\{ (m+\frac{n}{2})^2 - (\frac{n}{2})^2 \right\} = Q_{m,n} / m(m+n)$$

$$R'_{m,n} = R_{m,n} / \left\{ (\frac{n}{2}-m)^2 - (\frac{n}{2})^2 \right\} = -R_{m,n} / m(n-m)$$

$$S'_{m,n} = S_{m,n} / \left\{ (\frac{n}{2}-m)^2 - (\frac{n}{2})^2 \right\} = -S_{m,n} / m(n-m)$$

and A_1, B_1 are the arbitrary constants of the first order complementary function.

Having now determined the first order solution y_1 we refer back to equation (7.18) and see that by substituting the known quantities y_0, y_1 and α_1 into the right hand side we will obtain two simultaneous equations in α_2 and either A_1 or B_1 by applying the periodicity condition. The main difficulty in carrying out this operation is the evaluation of the product $y_1.f(\theta)$ and the determination of the coefficients of $\begin{matrix}\sin\\ \cos\end{matrix}(\frac{n}{2})\theta$.

The product $y_1 . f(\theta)$ is evaluated as follows:

$$
\begin{aligned}
y_1 . f(\theta) &= \left\{ A_1\cos\left(\tfrac{n}{2}\right)\theta + B_1\sin\left(\tfrac{n}{2}\right)\theta - \frac{1}{2}\left(\frac{2}{n}\right)^2 T_n \right. \\
&+\frac{1}{2}\sum_{m=1}^{\infty}\left(P'_{m,n}\cos\left(m+\tfrac{n}{2}\right)\theta + Q'_{m,n}\sin\left(m+\tfrac{n}{2}\right)\theta\right) \\
&\left.+\frac{1}{2}\sum_{m=1}^{N}\left(R'_{m,n}\cos\left(\tfrac{n}{2}-m\right)\theta - S'_{m,n}\sin\left(\tfrac{n}{2}-m\right)\theta\right)\right\} \\
&\times\left\{\sum_{m=0}^{\infty}\left(a_m\cos m\theta + b_m\sin m\theta\right)\right\}
\end{aligned}
$$

$$= \frac{1}{2}\sum_{m=0}^{\infty}\left\{(A_1 a_m - B_1 b_m)\cos(m+\tfrac{n}{2})\theta + (A_1 b_m + B_1 a_m)\sin(m+\tfrac{n}{2})\theta + (A_1 a_m + B_1 b_m)\cos(m-\tfrac{n}{2})\theta + (A_1 b_m - B_1 a_m)\sin(m-\tfrac{n}{2})\theta\right\}$$

$$-\frac{1}{2}\left(\frac{2}{m}\right)^2 T_n \sum_{m=0}^{\infty}\left(a_m \cos m\theta + b_m \sin m\theta\right)$$

$$+\frac{1}{4}\sum_{r=0}^{\infty}\sum_{m=1}^{\infty}\left\{(a_r P'_{m,n} - b_r Q'_{m,n})\cos(m+\tfrac{n}{2}+r)\theta + (a_r P'_{m,n} + b_r Q'_{m,n})\cos(m+\tfrac{n}{2}-r)\theta\right.$$

$$\left. + (a_r Q'_{m,n} + b_r P'_{m,n})\sin(m+\tfrac{n}{2}+r)\theta + (a_r Q'_{m,n} - b_r P'_{m,n})\sin(m+\tfrac{n}{2}-r)\theta\right\}$$

$$+\frac{1}{4}\sum_{r=0}^{\infty}\sum_{m=1}^{N}\left\{(a_r R'_{m,n} - b_r S'_{m,n})\cos(m-\tfrac{n}{2}+r)\theta + (a_r R'_{m,n} + b_r S'_{m,n})\cos(m-\tfrac{n}{2}-r)\theta\right.$$

$$\left. + (a_r S'_{m,n} + b_r R'_{m,n})\sin(m-\tfrac{n}{2}+r)\theta + (a_r S'_{m,n} - b_r R'_{m,n})\sin(m-\tfrac{n}{2}-r)\theta\right\}$$

We now equate the coefficients of $\begin{matrix}\sin\\ \cos\end{matrix}(\frac{n}{2})\theta$ in the right hand side of equation (7.18) to zero. Taking the cosine terms first we have

$$-\alpha_2 A_0 - \alpha_1 A_1 - \frac{1}{2}(2A_1 a_0 + A_1 a_n + B_1 b_n) + \frac{1}{2}\left(\frac{2}{m}\right)^2 T_n\, a_{\frac{n}{2}}$$

$$-\frac{1}{4}\sum_{m=1}^{\infty}\left\{(a_m + a_{m+n})P'_{m,n} + (b_m + b_{m+n})Q'_{m,n}\right\} - \frac{1}{4}\sum_{m=1}^{N}\left\{(a_{n-m} + a_m)R'_{m,n} - (b_{n-m} - b_m)S'_{m,n}\right\} = 0 \qquad (7.31)$$

and for the sine terms,

$$-\alpha_2 B_0 - \alpha_1 B_1 - \frac{1}{2}(2B_1 a_0 + A_1 b_n - B_1 a_n) + \frac{1}{2}\left(\frac{2}{m}\right)^2 T_n\, b_{\frac{n}{2}}$$

$$-\frac{1}{4}\sum_{m=1}^{\infty}\left\{(a_m - a_{m+n})Q'_{m,n} - (b_m - b_{m+n})P'_{m,n}\right\} - \frac{1}{4}\sum_{m=1}^{N}\left\{(a_{n-m} - a_m)S'_{m,n} + (b_{n-m} + b_m)R'_{m,n}\right\} = 0. \qquad (7.32)$$

Here again, the fourth terms in equations (7.31) and (7.32) exist only for even n.

Making use of the following abbreviations,

$$\sigma = -A_1\left\{\alpha_1 + a_o + \frac{a_n}{2}\right\} + \tfrac{1}{2}\left(\frac{2}{n}\right)^2 T_n \frac{a_n}{2} - \left\{\text{Summation terms in (7.31)}\right\}$$

$$\tau = -A_1 \frac{b_n}{2} + \tfrac{1}{2}\left(\frac{2}{n}\right)^2 T_n \frac{b_n}{2} - \left\{\text{Summation terms in (7.32)}\right\} \qquad (7.33)$$

the simultaneous equations in α_2 and B_1 may now be written as

$$\left.\begin{aligned} \frac{b_n}{2} B_1 + A_o \alpha_2 - \sigma &= 0 \\ \left(\alpha_1 + a_o - \frac{a_n}{2}\right) B_1 + B_o \alpha_2 - \tau &= 0 \end{aligned}\right\} \qquad (7.34)$$

The solutions to these equations are

$$\left.\begin{aligned} B_1 &= \frac{A_o \tau - B_o \sigma}{\left(\alpha_1 + a_o - \frac{a_n}{2}\right)A_o - \frac{b_n}{2} B_o} \\ \alpha_2 &= \frac{\left(\alpha_1 + a_o - \frac{a_n}{2}\right)\sigma - \frac{b_n}{2}\tau}{\left(\alpha_1 + a_o - \frac{a_n}{2}\right)A_o - \frac{b_n}{2} B_o} \end{aligned}\right\} \qquad (7.35)$$

which may be somewhat simplified in form by use of equations (7.23) and (7.24) with the following result

$$\left.\begin{aligned} B_1 &= \frac{A_o \tau - B_o \sigma}{A_o \sqrt{a_n^2 + b_n^2}} \\ \alpha_2 &= \frac{\sigma}{2A_o} - \frac{a_n \sigma + b_n \tau}{2A_o \sqrt{a_n^2 + b_n^2}} \end{aligned}\right\} \qquad (7.36)$$

Values of B_1 and α_2 obtained from these equations correspond to the values of B_0 and α_1 from equations (7.23) and (7.24). The positive value of the square root yields α'_1, α'_2 and the negative value yields α''_1 and α''_2 which define the stability boundaries of the n^{th} unstable region as

$$\lambda'^2 = (\tfrac{n}{2})^2 + \alpha'_1\mu + \alpha'_2 \cdot \mu^2 + 0(\mu^3) \qquad (7.37)$$

$$\lambda''^2 = (\tfrac{n}{2})^2 + \alpha''_1\mu + \alpha''_2 \cdot \mu^2 + 0(\mu^3)$$

Fig. 34 shows the second order stability boundaries for a typical mechanism while Fig. 35 illustrates the effect upon the size of the unstable regions of changing the dimensions of the linkage. (The dimensions chosen to demonstrate this point are similar in character to those chosen for Figs. 17 - 19, in which the lengths of coupler, follower and fixed link are identical, the crank length being changed as shown in the figure).

As the length of the crank is increased in relation to that of the other links, accompanied by an increase in the forces developed in the mechanism, the speed ranges in which unstable motion may be expected grow in extent. For small values of crank length the coupler will experience relatively small forces so that only at high speeds will any instability occur. This is shown in Fig. 35 in which the first unstable region is the only one not of negligible proportions. The presence of damping will also further reduce the possibility of instability at lower speeds, the effect of which we shall now examine.

7.1.4 Effect of Damping

7.1.4.1 Floquet Theory

We now consider the effect upon the stability boundaries of the presence of a viscous damping term in equation (7.11). The equation now takes the form

$$\frac{d^2y}{d\vartheta^2} + 2K\frac{dy}{d\theta} + \left\{\lambda^2 + \mu f(\theta)\right\} y = 0 \qquad (7.38)$$

where K is the damping coefficient. This equation may be transformed into a form similar to that of equation (7.11) by writing

FIG. 34. STABILITY CHART

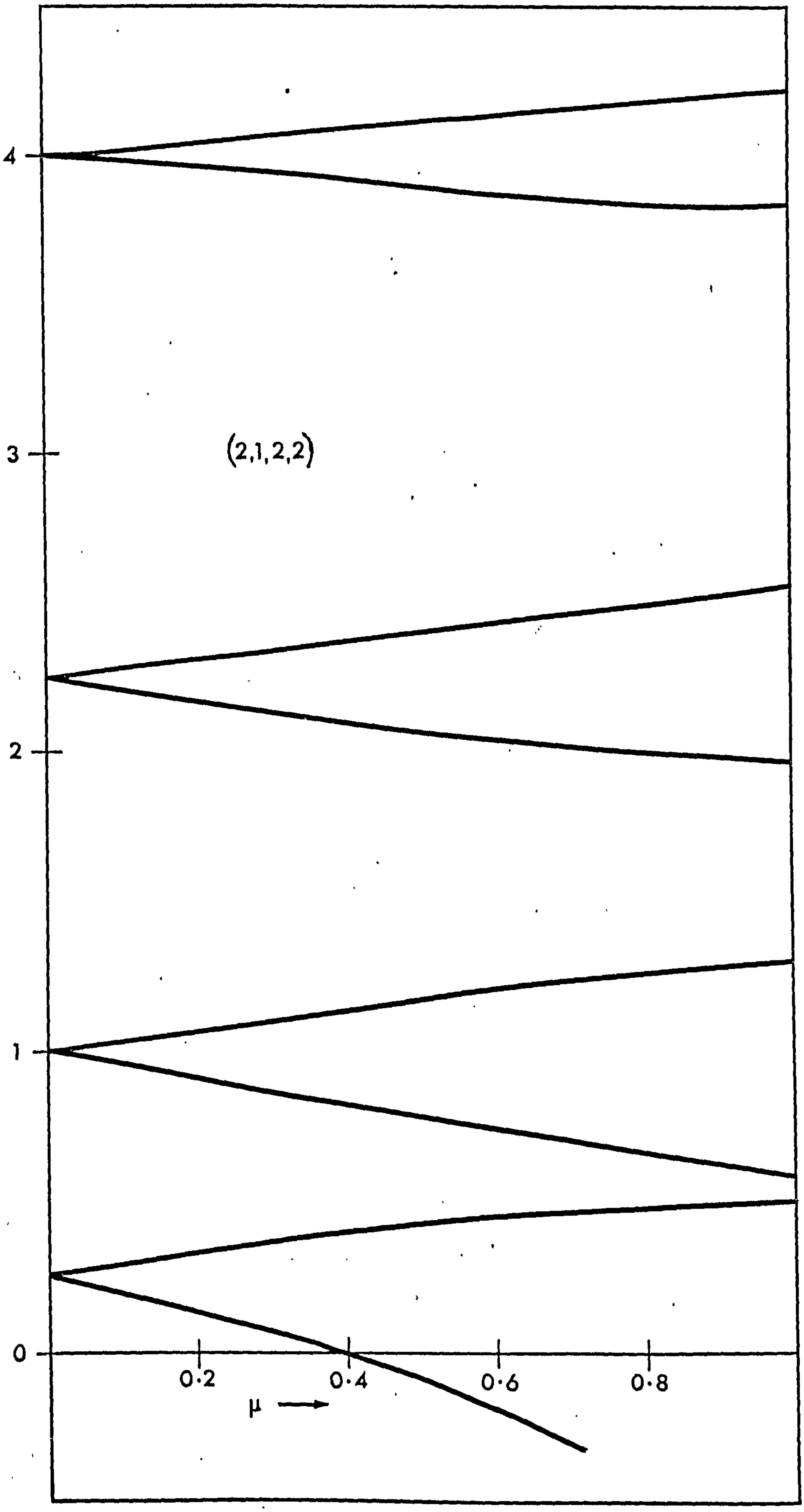

FIG. 35. STABILITY CHART

(Effect of change of dimensions)

($\ell_1 = \ell_3 = \ell_4 = 6$. ℓ_2 as shown)

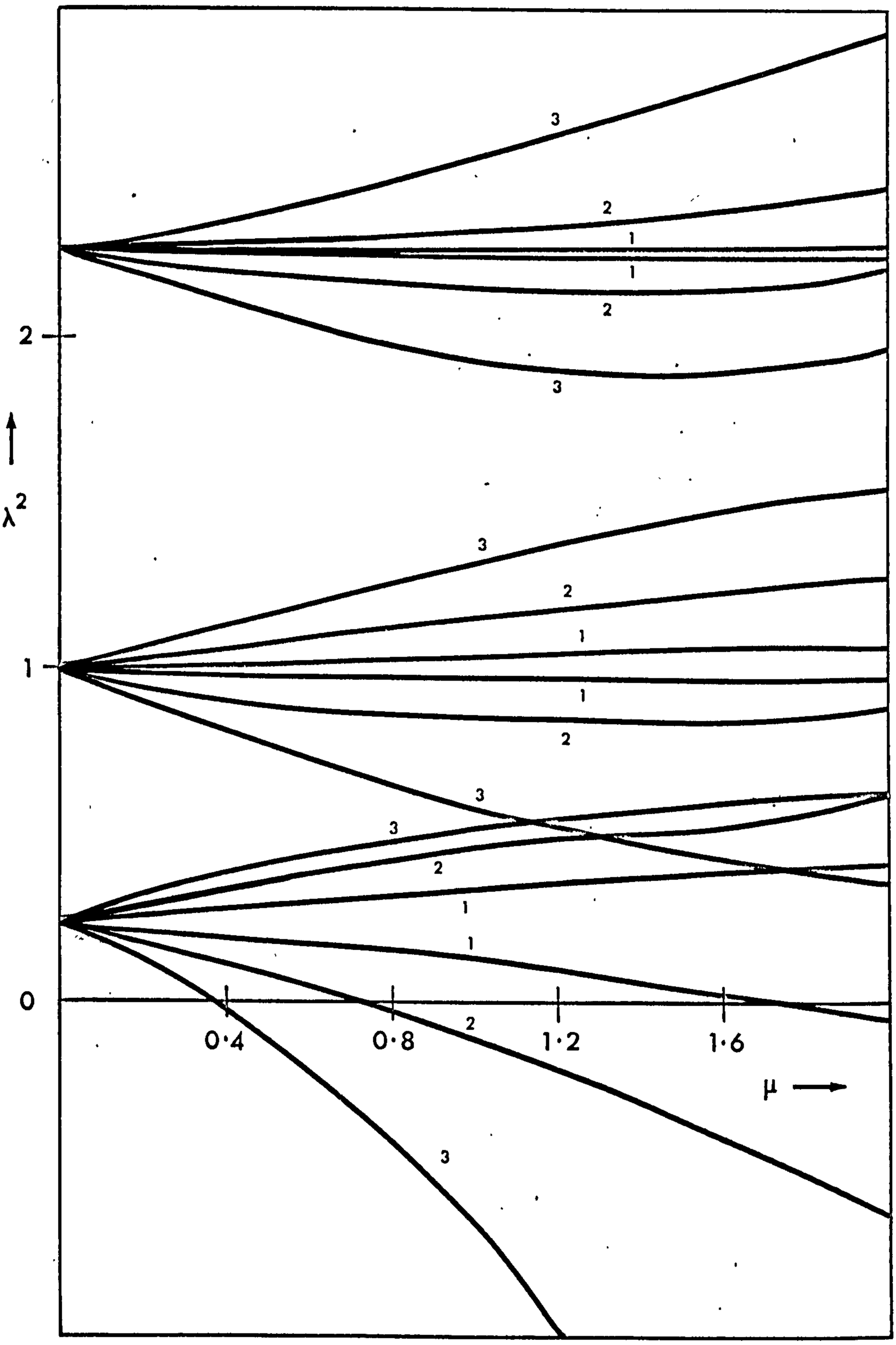

$$y(\theta) = e^{-K\theta} \cdot u(\theta) \tag{7.39}$$

which yields, after substitution into equation (7.38), an equation in $u(\theta)$

$$\frac{d^2u}{d\theta^2} + \left\{ (\lambda^2 - K^2) + \mu f(\theta) \right\} u = 0 \tag{7.40}$$

The stability of the new variable $u(\theta)$ is now determined in terms of the parameters $(\lambda^2 - K^2)$ and μ as in the preceding section. From Floquet's theory, the solution will have the form

$$u(\theta) = e^{\nu\theta} \cdot p(\theta)$$

where $p(\theta)$ is a periodic function of θ and the stability of $u(\theta)$ is determined by the magnitude of ν. It may be seen from the definition of $y(\theta)$ (equation 7.39) that it is possible for $y(\theta)$ to be stable while $u(\theta)$ is unstable if $K > \nu$, since in that case

$$y(\theta) = e^{-K\theta} \cdot u(\theta) = e^{-(K-\nu)\theta} \cdot p(\theta)$$

The determination of the criteria of stability for $y(\theta)$ then rests upon the calculation of ν which is in general a problem of great complexity and it is more instructive to approach the problem from another point of view.

7.1.4.2 Perturbation Method

Consider equation (7.38) in which μ is a small parameter. We express the damping coefficient K in terms of this parameter by choosing a suitable constant β such that $K = \beta\mu$ (33). Now, as in the case without damping, we seek a periodic solution of the form of equation (7.14) and express λ^2 as a power series in μ as in equation (7.12). Substitution of these expressions into equation (7.38) leads to the following

$$\sum_{i=0}^{\infty} \frac{d^2y_i}{d\theta^2}\mu^i + 2\beta\mu\sum_{i=0}^{\infty} \frac{d^2y_i}{d\theta}\mu^i + \left\{\left(\frac{n}{2}\right)^2 + \sum_{j=1}^{\infty} \alpha_j\mu^j + \mu f(\theta)\right\}\sum_{i=0}^{\infty} y_i\mu^i = 0 \tag{7.41}$$

Equating similar powers of to zero, a series of equations in y_i is obtained:-

$$\frac{d^2y_o}{d\theta^2} + (\frac{n}{2})^2 y_o = 0$$

$$\frac{d^2y_1}{d\theta^2} + (\frac{n}{2})^2 y_1 = - \alpha_1 y_o - f(\theta) . y_o - 2\beta \frac{dy_o}{d\theta}$$

$$\frac{d^2y_2}{d\theta^2} + (\frac{n}{2})^2 y_2 = - \alpha_2 y_o - \alpha_1 y_1 - f(\theta) . y_1 - 2\beta \frac{dy_1}{d\theta} \qquad (7.42)$$

The zero order solution is, as before

$$y_o = A_o \cos (\frac{n}{2})\theta + B_o \sin (\frac{n}{2})\theta$$

We now substitute this zero order solution into the second of equations (7.42) and evaluate the right hand side

$$\begin{aligned} \frac{d^2y_1}{d\theta^2} + \left(\frac{n}{2}\right)^2 y_1 = & - \alpha_1 \left(A_o \cos\left(\frac{n}{2}\right)\theta + B_o \sin\left(\frac{n}{2}\right)\theta\right) \\ & -2\beta\left(\frac{n}{2}\right)\left(-A_o \sin\left(\frac{n}{2}\right)\theta + B_o \cos\left(\frac{n}{2}\right)\theta\right) \\ & -\left(A_o \cos\left(\frac{n}{2}\right)\theta + B_o \sin\left(\frac{n}{2}\right)\theta\right) \cdot \sum_{n=0}^{\infty} \left(a_m \cos m\theta + b_m \sin m\theta\right). \end{aligned} \qquad (7.43)$$

Equating coefficients of $\begin{matrix}\sin \\ \cos\end{matrix}$ $(\frac{n}{2})\theta$ to zero as before, yields two simultaneous equations in α_1 and A_o or B_o.

$$\left.\begin{aligned} -\alpha_1 A_o - \tfrac{1}{2}\left(2A_o a_o + A_o a_n + B_o b_n\right) - 2\beta\left(\tfrac{n}{2}\right) B_o &= 0 \\ -\alpha_1 B_o - \tfrac{1}{2}\left(2B_o a_o + A_o b_n - B_o a_n\right) + 2\beta\left(\tfrac{n}{2}\right) A_o &= 0 \end{aligned}\right\} \qquad (7.44)$$

Re-arranging these equations in terms of the arbitrary constants A_o and B_o we obtain

$$\begin{aligned} (\alpha_1 + a_o + \frac{a_n}{2}) A_o + (\beta n + \frac{b_n}{2}) B_o &= 0 \\ (\beta n - \frac{b_n}{2}) A_o - (\alpha_1 + a_o - \frac{a_n}{2}) B_o &= 0 \end{aligned} \qquad (7.45)$$

The determinant of these equations is equated to zero, for a non-trivial solution and a value for α_1 results.

$$\alpha_1 = -a_o \pm \tfrac{1}{2}\sqrt{a_n^2 + b_n^2 - 4\beta^2 n^2} \tag{7.46}$$

The corresponding B_o is

$$B_o = \frac{-(a_n \pm \sqrt{a_n^2 + b_n^2 - 4\beta^2 n^2})\,A_o}{(b_n + 2\beta n)} \tag{7.47}$$

We see immediately that when $\beta = 0$ these formulae reduce to the corresponding values obtained in the previous section.

The first order stability boundaries in the damped case are given by

$$\lambda'^2 = (\tfrac{n}{2})^2 + \alpha_1' \mu$$

$$\lambda''^2 = (\tfrac{n}{2})^2 + \alpha_1'' \mu \tag{7.48}$$

where the values of α_1 are obtained from equation (7.46) taking the positive and negative values of the square root respectively. Combining equations (7.48) we have

$$\lambda^2 = (\tfrac{n}{2})^2 + \alpha_1 \mu$$

$$= (\tfrac{n}{2})^2 + \mu(-a_o \pm \tfrac{1}{2}\sqrt{a_n^2 + b_n^2 - 4\beta^2 n^2}) \tag{7.49}$$

Obviously, α_1 is real only if

$$a_n^2 + b_n^2 \geq 4\beta^2 n^2 \tag{7.50}$$

When the equality holds, the stability boundaries coincide and the region of instability disappears i.e. the damping present is sufficient to stabilise the vibration.

Fig. 36 shows the first order approximation to the boundaries of the principal unstable region of equation (7.38) for a range of values of the damping coefficient together with the boundaries for the undamped case. The periodic function $f(\theta)$ was taken to be $f_3(\theta)$ as defined in Chapter 6. For any

FIG.36. STABILITY CHART. Boundaries of Principal Unstable Region.(First Order).

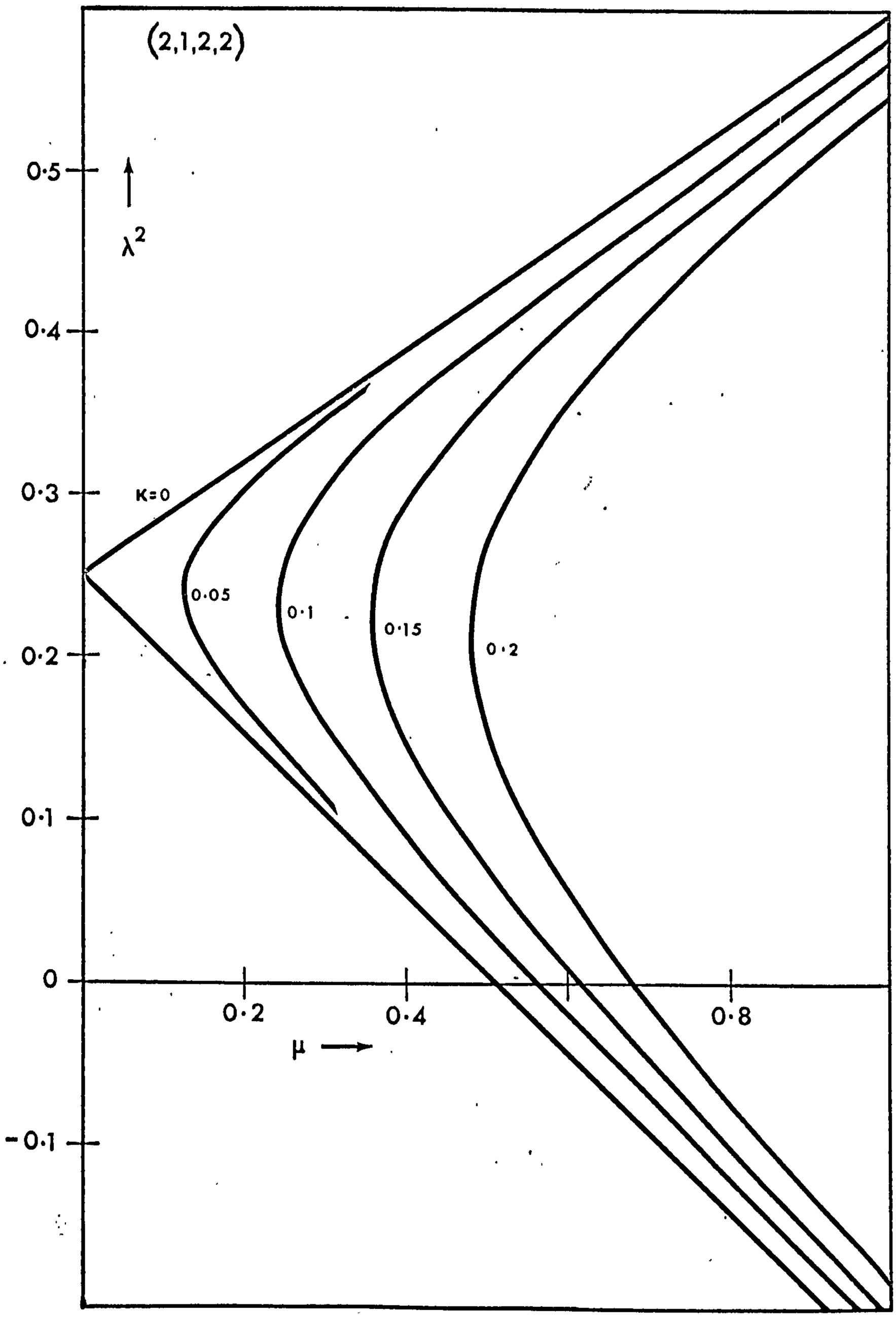

given value of the damping coefficient K, there is a minimum value of below which no unstable motion occurs. This minimum value increases with increased K. In the higher unstable regions (corresponding to lower values of the crank velocity ω_2) the effect of damping becomes increasingly great, viz. a larger value of μ is required in order to produce unstable motion (Fig. 37).

From condition (7.50) we obtain the minimum value of as

$$\mu_{min} \geqslant \frac{2Kn}{\sqrt{a_n^2 + b_n^2}} \tag{7.51}$$

so that the value of μ_{min} for a given K increases with n but is also inversely proportional to the amplitude of the n^{th} Fourier component. Since these components generally decrease rapidly in amplitude with increased n, the values of μ_{min} increase so that when even a small amount of damping is present, only a few unstable regions may be expected to exist for sufficiently low values of the parameter μ.

FIG. 37. STABILITY CHART.

Effect of increasing damping coefficient.

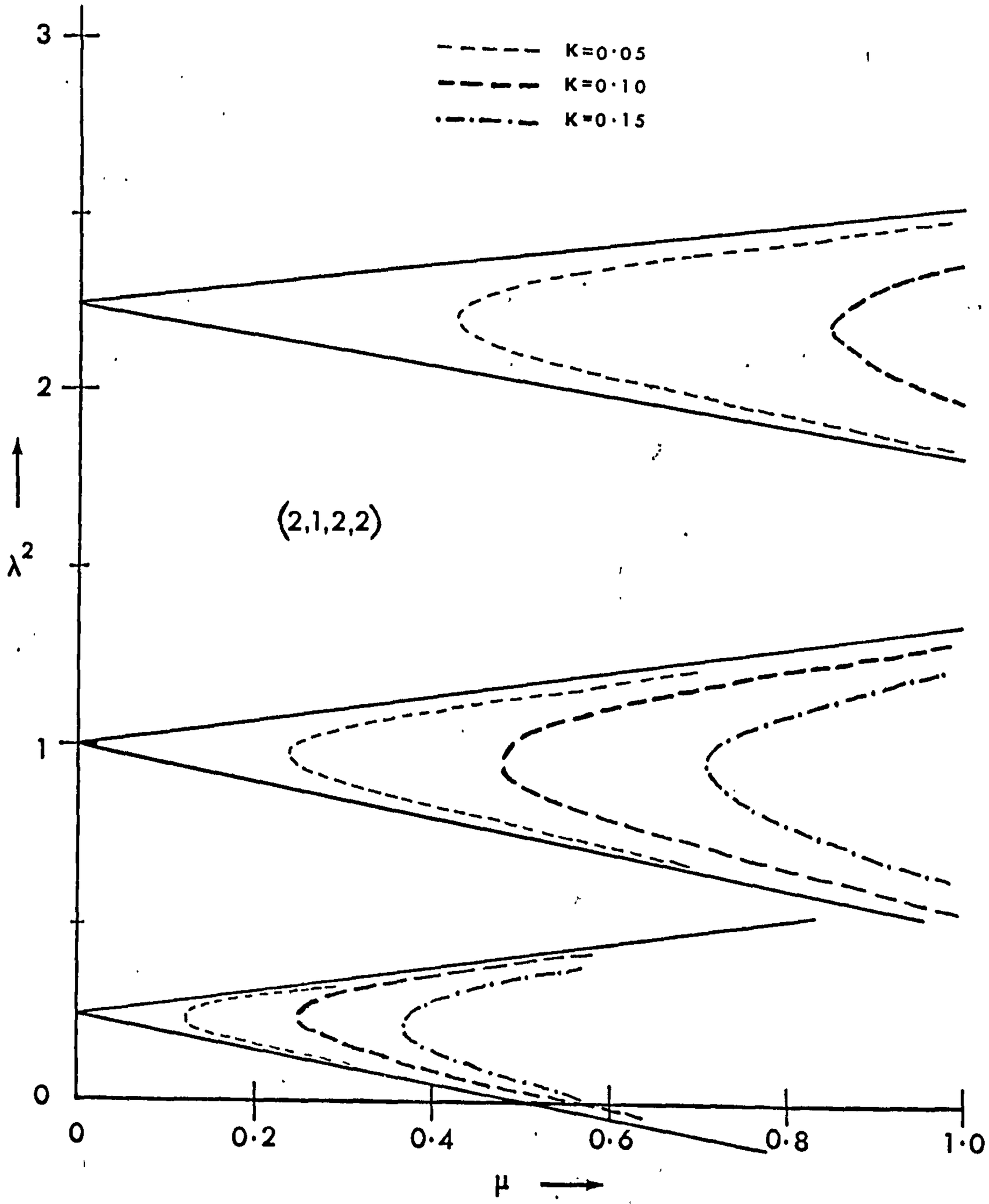

CHAPTER 8

STABILITY OF HILL'S EQUATION WITH MORE THAN TWO INDEPENDENT PARAMETERS

8.1 Introduction

In Chapter 7 we examined the stability of equation (7.11) which is in the standard form of Hill's equation. However equation (7.11) is only an approximation to the full equation of motion for the flexible coupler of a four-bar linkage which, as derived in Chapter 6, contains additional periodic terms and may be written in the following form

$$\frac{d^2y}{d\theta_2^2} + \left\{ \lambda^2 - \phi(\theta_2) + \epsilon_1 f_1(\theta_2) + \epsilon_2 f_2(\theta_2) + \epsilon_3 f_3(\theta_2) \right\} y = g(\theta_2) \qquad (8.1)$$

(This is effectively equation (6.17) with $m = 1$ i.e. the equation of the principal mode).

There are thus four independent parameters λ^2, ϵ_1, ϵ_2, ϵ_3 which determine whether the solution $y(\theta_2)$ is stable or unstable together with the periodic function $\phi(\theta_2)$ the coefficient of which is unity. In general terms, this may be considered to be a fifth independent parameter.

For convenience, the equations defining the parameters of equation (6.17) are quoted again:

$$\lambda^2 = \frac{\Omega^2}{\omega_2^2} \quad , \quad \phi(\theta_2) = \frac{\omega_3^2}{\omega_2^2}$$

$$\epsilon_1 = \frac{I_3 \pi^2}{\mu \ell_3^2} \quad , \quad f_1(\theta_2) = \frac{-\alpha_3}{\omega_2^2 \tan(\theta_3 - \theta_4)}$$

$$\epsilon_2 = \frac{\pi^2 r_3 \ell_2}{\ell_3^2} \quad , \quad f_2(\theta_2) = \frac{\sin(\theta_2 - \theta_3)}{\tan(\theta_3 - \theta_4)}$$

$$\epsilon_3 = \frac{I_4 \pi^2}{\mu \ell_3^2 \ell_4} \quad , \quad f_3(\theta_2) = \frac{-\alpha_4}{\omega_2^2 \sin(\theta_3 - \theta_4)}$$

Some discussion of the relative magnitudes of these parameters and their associated periodic terms has been given in Chapter 6 after which the stability of the reduced equation (7.11) was examined in Chapter 7. We now examine the

effect upon the system stability of retaining further terms in the equation of motion. This is equivalent to examining the effect of the properties of the coupler itself upon the stability of the mechanism. If we consider mechanisms in which the coupler is balanced at the crank pin ($r_3 = 0$) and for which the angular velocity term $\phi(\theta_2)$ is negligible in comparison with the remaining terms (see Fig. 27) then the equation of motion becomes

$$\frac{d^2y}{d\theta_2^2} + \left\{ \lambda^2 + \epsilon_1 f_1(\theta_2) + \epsilon_3 f_3(\theta_2) \right\} y = g(\theta_2) \qquad (8.2)$$

This is a form of Hill's equation with three independent parameters and two general periodic functions each of period 2π in θ_2.

Klotter and Kotowski[26] have examined the stability of such an equation in which the periodic terms were simple cosines. Stability boundaries (which are effectively surfaces in the 3-dimensional parameter space) are calculated for a range of parameter values and photographs of a model of the 'stability space' are presented. Strutt[27] has given a most detailed geometrical treatment of this type of equation concentrating on the eigenvalue problem, whereas in a more recent paper, Rand[28] has applied the perturbation technique to one special type of equation. This has four independent parameters in which, as in (26), all of the periodic terms are cosines of the independent variable or its multiples. . However, the examples quoted by Rand all reduce to <u>two</u> parameter stability problems, which may then be treated by the usual method. In the completely general situation, i.e. when odd <u>and</u> even or mixed periodic functions are present in the equation, this familiar perturbation approach cannot be applied - as has been pointed out by Smith[29] and Hamer and Smith[30].

In equation (8.2) the periodic functions will in general be neither odd nor even and as a direct consequence of this, a modification to the perturbation method is necessary.

We will now attempt to apply the standard perturbation method of analysis to equation (8.2) in order to demonstrate this point.

8.2 Stability Analysis by the Standard Perturbation Method

8.2.1 Application of the Method

We examine equation (8.2) initially by using the perturbation technique modified to take account of the second small parameter ϵ_2. Writing the equation in its homogeneous form we have

$$\frac{d^2y}{d\theta^2} + \left\{\lambda^2 + \epsilon_1 f_1(\theta) + \epsilon_2 f_2(\theta)\right\} y = 0 \qquad (8.3)$$

where the subscript of the independent variable has been omitted for brevity and the third term in the coefficient of y has been renumbered for convenience in handling the following analysis.

Applying the perturbation method, we express λ^2 as a power series in the two small parameters as follows:-

$$\lambda^2 = \sum_{i=0}^{\infty} \sum_{j=0}^{\infty} \alpha_{ij} \epsilon_1^i \epsilon_2^j \quad \text{with} \quad \alpha_{oo} = \left(\frac{n}{2}\right)^2 \qquad (8.4)$$

and seek a solution in the form

$$y = \sum_{i=0}^{\infty} \sum_{j=0}^{\infty} y_{ij} \epsilon_1^i \epsilon_2^j . \qquad (8.5)$$

Substitution of (8.4) and (8.5) into (8.2) yields an equation in the y_{ij} which may be treated as an infinite number of equations by setting successive powers of ϵ_1 and ϵ_2 equal to zero. These equations are

$$\frac{d^2y_{oo}}{d\theta^2} + \left(\frac{n}{2}\right)^2 y_{oo} = 0 \qquad (8.6)$$

$$\frac{d^2y_{10}}{d\theta^2} + \left(\frac{n}{2}\right)^2 y_{10} = -\left\{\alpha_{10} + f_1(\theta)\right\} y_{oo} \qquad (8.7)$$

$$\frac{d^2y_{01}}{d\theta^2} + \left(\frac{n}{2}\right)^2 y_{01} = -\left\{\alpha_{01} + f_2(\theta)\right\} y_{oo} \qquad (8.8)$$

$$\frac{d^2y_{20}}{d\theta^2} + \left(\frac{n}{2}\right)^2 y_{20} = -\left\{\alpha_{10} + f_1(\theta)\right\} y_{10} - \alpha_{20} y_{00} \qquad (8.9)$$

$$\frac{d^2y_{02}}{d\theta^2} + \left(\frac{n}{2}\right)^2 y_{02} = -\left\{\alpha_{01} + f_2(\theta)\right\} y_{01} - \alpha_{02} y_{00} \qquad (8.10)$$

$$\frac{d^2y_{11}}{d\theta^2} + \left(\frac{n}{2}\right)^2 y_{11} = -\left\{\alpha_{10} + f_1(\theta)\right\} y_{01} - \left\{\alpha_{01} + f_2(\theta)\right\} y_{10} - \alpha_{11} y_{00} \qquad (8.11)$$

. . . .

. . . .

. . . .

. . . .

8.2.2 First Order Terms

Equations (8.7) and (8.8) are essentially similar in form to equation (7.17) and may be treated in an exactly similar manner. Applying the periodicity condition to y_{10} in equation (8.7) yields two values for the coefficient α_{10} and similarly, equation (8.8) yields two values for α_{01}.

Defining the zero order solution as

$$y_{00} = A_{00} \cos\left(\frac{n}{2}\right)\theta + B_{00} \sin\left(\frac{n}{2}\right)\theta \qquad (8.12)$$

and writing the functions $f_1(\theta)$ and $f_2(\theta)$ in terms of their Fourier coefficients as

$$\left.\begin{aligned} f_1(\theta) &= \sum_{m=0}^{\infty} \left(a_m \cos m\theta + b_m \sin m\theta \right) \\ f_2(\theta) &= \sum_{m=0}^{\infty} \left(c_m \cos m\theta + d_m \sin m\theta \right) \end{aligned}\right\} \qquad (8.13)$$

we have, for the coefficients α_{10}, α_{01}

$$\left.\begin{aligned} \alpha_{10} &= -a_o \pm \tfrac{1}{n}\sqrt{a_n^2 + b_n^2} \\ \alpha_{01} &= -c_o \pm \tfrac{1}{n}\sqrt{c_n^2 + d_n^2} \end{aligned}\right\} \qquad (8.14)$$

as obtained for the single parameter case in Chapter 7. However, the analysis also yields values for the arbitrary constant B_{oo} in terms of A_{oo}.

From equation (8.7) we obtain

$$\frac{B_{oo}}{A_{oo}} = -\left\{\frac{a_n \pm\sqrt{a_n^2 + b_n^2}}{b_n}\right\} \qquad (8.15)$$

and from equation (8.8)

$$\frac{B_{oo}}{A_{oo}} = -\left\{\frac{c_n \pm\sqrt{c_n^2 + d_n^2}}{d_n}\right\} \qquad (8.16)$$

Clearly, for equations (8.15) and (8.16) to be consistant we must have

$$\frac{a_n \pm\sqrt{a_n^2 + b_n^2}}{b_n} = \frac{c_n \pm\sqrt{c_n^2 + d_n^2}}{d_n}$$

which may be reduced to the conditions

$$b_n = d_n = 0 \quad \text{or} \quad \frac{a_n}{b_n} = \frac{c_n}{d_n} \qquad (8.17)$$

The first of these conditions is satisfied if both functions $f_1(\theta)$ and $f_2(\theta)$ are even. Furthermore, the second condition will be satisfied if $a_n = c_n = 0$ i.e. if the functions are odd. In the slightly more general case, the second condition is satisfied only for special types of function which will not occur in the majority of mechanisms dealt with here. We see then that this method of analysis will work successfully for odd or even functions but in the completely general case, when neither of conditions (8.17) is satisfied, the only other conclusion we may reach from a consideration of equations (8.15) and (8.16) is that $A_{oo} = B_{oo} = 0$. This gives

immediately $y_{oo} = 0$ viz. there is no stable zero order solution which is clearly unacceptable. We conclude therefore that the present method fails in the completely general case when functions $f_1(\theta)$ and $f_2(\theta)$ are neither odd nor even. (It can further be shown that if $c_n/b_n \neq o_n/d_n$ then similar anomalies occur in the higher approximations and this method predicts $y_{10} = y_{01} = y_{11} = 0$.)

Since the difficulty in obtaining meaningful results appears to arise from the presence of the n th Fourier terms in $f_1(\theta)$ and $f_2(\theta)$, we shall re-examine equation (8.3) and write it in the form

$$\frac{d^2y}{d\theta^2} + \left\{\lambda^2 + \epsilon_1 \overline{f}_1(\theta) + \epsilon_2 \overline{f}_2(\theta) + \delta_n \cos(n\theta - \psi_n)\right\} y = 0 \qquad (8.18)$$

where $\overline{f}_1(\theta) = f_1(\theta) - (a_n \cos n\theta + b_n \sin n\theta)$

$\overline{f}_2(\theta) = f_2(\theta) - (c_n \cos n\theta + d_n \sin n\theta)$

The functions $\overline{f}_1(\theta)$, $\overline{f}_2(\theta)$ thus contain no terms in $\begin{matrix}\sin \\ \cos\end{matrix}$ (nθ). These terms are collected in the last term of the coefficient of y in the equation and δ_n and ψ_n are defined accordingly. Writing the n th order terms we have

$$\epsilon_1(a_n \cos n\theta + b_n \sin n\theta) + \epsilon_2(c_n \cos n\theta + d_n \sin n\theta)$$
$$= (\epsilon_1 a_n + \epsilon_2 c_n) \cos n\theta + (\epsilon_1 b_n + \epsilon_2 d_n) \sin n\theta$$
$$= \delta_n \cos(n\theta - \psi_n)$$

where $\delta_n = \sqrt{(\epsilon_1 a_n + \epsilon_2 c_n)^2 + (\epsilon_1 b_n + \epsilon_2 d_n)^2}$ (8.19)

and $\tan \psi_n = \dfrac{\epsilon_1 b_n + \epsilon_2 d_n}{\epsilon_1 a_n + \epsilon_2 c_n}$

δ_n may now be considered as a fourth parameter in equation (8.18) since, if $\frac{a_n}{b_n} \neq \frac{c_n}{d_n}$, it cannot be written as a series of powers and products of ϵ_1 and ϵ_2. As we have seen, if $\frac{a_n}{b_n} = \frac{c_n}{d_n}$, this extra parameter is not required and may incidentally be expressed as

$$\delta_n = \left(1 + \frac{b_n^2}{a_n^2}\right)^{\frac{1}{2}} . (\epsilon_1 a_n + \epsilon_2 b_n)$$

8.3 Modified Perturbation Method

8.3.1 Application of the Method

We now proceed with the analysis of equation (8.18) in terms of the three parameters ϵ_1 , ϵ_2 and δ_n and write

$$\lambda^2 = \sum_{i=0}^{\infty} \sum_{j=0}^{\infty} \sum_{k=0}^{\infty} \alpha_{ijk} \epsilon_1^i \epsilon_2^j \delta_n^k \quad \text{with} \quad \alpha_{000} = \left(\frac{n}{2}\right)^2 \tag{8.20}$$

and

$$y = \sum_{i=0}^{\infty} \sum_{j=0}^{\infty} \sum_{k=0}^{\infty} y_{ijk} \epsilon_1^i \epsilon_2^j \delta_n^k \tag{8.21}$$

Substitution of these expressions into equation (8.18) gives the following equation for y_{ijk} .

$$\sum_{i=0}^{\infty} \sum_{j=0}^{\infty} \sum_{k=0}^{\infty} \frac{d^2 y_{ijk}}{d\theta^2} \epsilon_1^i \epsilon_2^j \delta_n^k + \left\{ \sum_{i=0}^{\infty} \sum_{j=0}^{\infty} \sum_{k=0}^{\infty} \alpha_{ijk} \epsilon_1^i \epsilon_2^j \delta_n^k + \epsilon_1 \sum_{\substack{m=0 \\ m \neq n}}^{\infty} \left(a_m \cos m\theta + b_m \sin m\theta\right) \right.$$

$$\left. + \epsilon_2 \sum_{\substack{m=0 \\ m \neq n}}^{\infty} \left(c_m \cos m\theta + d_m \sin m\theta\right) + \delta_n \cos(n\theta - \psi_n) \right\} \sum_{i=0}^{\infty} \sum_{j=0}^{\infty} \sum_{k=0}^{\infty} y_{ijk} \epsilon_1^i \epsilon_2^j \delta_n^k = 0 \tag{8.22}$$

Equating powers of ϵ_1, ϵ_2 and δ_n to zero yields an infinite set of equations the first of which are

$$\frac{d^2 y_{000}}{d\theta^2} + \left(\frac{n}{2}\right)^2 y_{000} = 0 \qquad (8.23)$$

$$\frac{d^2 y_{100}}{d\theta^2} + \left(\frac{n}{2}\right)^2 y_{100} = - \left\{\alpha_{100} + \bar{F}_1(\theta)\right\} \cdot y_{000} \qquad (8.24)$$

$$\frac{d^2 y_{010}}{d\theta^2} + \left(\frac{n}{2}\right)^2 y_{010} = - \left\{\alpha_{010} + \bar{F}_2(\theta)\right\} \cdot y_{000} \qquad (8.25)$$

$$\frac{d^2 y_{001}}{d\theta^2} + \left(\frac{n}{2}\right)^2 y_{001} = - \left\{\alpha_{001} + \cos(n\theta - \psi_n)\right\} \cdot y_{000} \qquad (8.26)$$

8.3.2 First Order Terms

As before, the zero order equation is solved immediately and we may write

$$y_{000} = A_{000} \cos\left(\frac{n}{2}\right)\theta + B_{000} \sin\left(\frac{n}{2}\right)\theta$$

The values of α_{100} and α_{010} are now determined quite simply from the periodicity condition applied to y_{100} and y_{010} respectively. Accordingly, for y_{100} to be periodic (viz. the right hand side of equation (8.24) contains no terms in $\begin{matrix}\sin \\ \cos\end{matrix}\left(\frac{n}{2}\right)\theta$) we find

$$\alpha_{100} = - a_0$$

Similarly from equation (8.25)

$$\alpha_{010} = - c_0$$

In order to obtain a value for the coefficient α_{001}, we rewrite the zero order solution in terms of new arbitrary constants as

$$y_{000} = A'_{000} \cos\left(\frac{n}{2}\theta - \frac{\psi_n}{2}\right) + B'_{000} \sin\left(\frac{n}{2}\theta - \frac{\psi_n}{2}\right)$$

Equation (8.26) now becomes

$$\frac{d^2 y_{001}}{d\theta^2} + (\tfrac{n}{2})^2 y_{001} = -\alpha_{001}\left\{A'_{000}\cos\tfrac{1}{2}(n\theta - \psi_n) + B'_{000}\sin\tfrac{1}{2}(n\theta - \psi_n)\right\}$$

$$-\frac{A'_{000}}{2}\left\{\cos\tfrac{3}{2}(n\theta - \psi_n) + \cos\tfrac{1}{2}(n\theta - \psi_n)\right\}$$

$$\frac{-B'_{000}}{2}\left\{\sin\tfrac{3}{2}(n\theta - \psi_n) - \sin\tfrac{1}{2}(n\theta - \psi_n)\right\}$$

from which the periodicity condition for y_{001} yields

$$\left.\begin{aligned} A'_{000}\,(\alpha_{001} + \tfrac{1}{2}) &= 0 \\ B'_{000}\,(\alpha_{001} - \tfrac{1}{2}) &= 0 \end{aligned}\right\} \qquad (8.27)$$

This may be re-stated as

$$\left.\begin{aligned} &\text{If } A'_{000} = 0\text{ , then } \alpha_{001} = +\tfrac{1}{2}\text{ ; } B'_{000}\text{ arbitrary} \\ &\text{If } B'_{000} = 0\text{ , then } \alpha_{001} = -\tfrac{1}{2}\text{ ; } A'_{000}\text{ arbitrary} \end{aligned}\right\} \qquad (8.28)$$

We now have values for the three first order coefficients in equation (8.20) which becomes

$$\lambda^2 = (\tfrac{n}{2})^2 - \epsilon_1 a_0 - \epsilon_2 c_0 \pm \tfrac{i}{2}\,\delta_n + O(2)\ . \qquad (8.29)$$

This defines the boundaries of the n^{th} unstable region to first order. The method may also be applied to equations with additional independent parameters with similar results.

It may be pointed out here too that if $\epsilon_2 = 0$, equation (8.29) reduces immediately to a form similar to equation (7.25) which defines stability boundaries in the single parameter case.

8.3.3 Second Order Terms

The six second order equations obtained from equation (8.22) are

$$\frac{d^2y_{200}}{d\theta^2} + \left(\frac{n}{2}\right)^2 y_{200} = -\alpha_{200}\, y_{000} - \left\{\alpha_{100} + \bar{f}_1(\theta)\right\} y_{100} \qquad (8.30)$$

$$\frac{d^2y_{020}}{d\theta^2} + \left(\frac{n}{2}\right)^2 y_{020} = -\alpha_{020}\, y_{000} - \left\{\alpha_{010} + \bar{f}_2(\theta)\right\} y_{010} \qquad (8.31)$$

$$\frac{d^2y_{002}}{d\theta^2} + \left(\frac{n}{2}\right)^2 y_{002} = -\alpha_{002}\, y_{000} - \left\{\alpha_{001} + \cos(n\theta - \psi_n)\right\} y_{001} \qquad (8.32)$$

$$\frac{d^2y_{110}}{d\theta^2} + \left(\frac{n}{2}\right)^2 y_{110} = -\alpha_{110}\, y_{000} - \left\{\alpha_{100} + \bar{f}_1(\theta)\right\} y_{010} - \left\{\alpha_{010} + \bar{f}_2(\theta)\right\} y_{100} \qquad (8.33)$$

$$\frac{d^2y_{101}}{d\theta^2} + \left(\frac{n}{2}\right)^2 y_{101} = -\alpha_{101}\, y_{000} - \left\{\alpha_{100} + \bar{f}_1(\theta)\right\} y_{001} - \left\{\alpha_{001} + \cos(n\theta - \psi_n)\right\} y_{100} \qquad (8.34)$$

$$\frac{d^2y_{011}}{d\theta^2} + \left(\frac{n}{2}\right)^2 y_{011} = -\alpha_{011}\, y_{000} - \left\{\alpha_{010} + \bar{f}_2(\theta)\right\} y_{001} - \left\{\alpha_{001} + \cos(n\theta - \psi_n)\right\} y_{010} \qquad (8.35)$$

These equations may be solved as before but, due to the increased number of parameters, the complexity of the operation is considerably greater. Equations (8.30) and (8.31) are treated in a manner exactly analogous to that used for the single parameter case in Chapter 7. The right hand sides of the equations must be evaluated in order to determine the coefficients of $\begin{matrix}\sin\\ \cos\end{matrix}(\frac{n}{2})\theta$ terms. This entails the solving of the first order equations for y_{100} and y_{010}. We will examine only equation (8.30) and its method of solution to illustrate the method.

In order to evaluate the right hand side of equation (8.30), it is necessary to solve equation (8.24) for y_{100} and then carry out the multiplication of terms so as to identify the coefficients of terms in $(\frac{n}{2})\theta$. Equation (8.24) may be written as

$$\frac{d^2y_{100}}{d\theta^2}+\left(\frac{n}{2}\right)^2 y_{100} = -\sum_{\substack{m=1\\ m\neq n}}^{\infty}(a_m\cos m\theta + b_m \sin m\theta)\cdot\left\{A_{000}\cos\left(\frac{n}{2}\right)\theta + B_{000}\sin\left(\frac{n}{2}\right)\theta\right\} \tag{8.36}$$

which, after carrying out the multiplication, is exactly similar in form to equation (7.26) with y_{100} replacing y_1 and A_{000}, B_{000} replacing A_0, B_0. It is thus possible to write down the equation for y_{100} by a direct comparison with equation (7.30).

Hence

$$\begin{aligned} y_{100} &= \frac{1}{2}\sum_{m=1}^{\infty}\left\{P^{*1}_{m,n}\cos\left(m+\frac{n}{2}\right)\theta + Q^{*1}_{m,n}\sin\left(m+\frac{n}{2}\right)\theta\right\} \\ &\quad +\frac{1}{2}\sum_{m=1}^{N}\left\{R^{*1}_{m,n}\cos\left(\frac{n}{2}-m\right)\theta - S^{*1}_{m,n}\sin\left(\frac{n}{2}-m\right)\theta\right\} \\ &\quad -\frac{1}{2}\left(\frac{2}{n}\right)^2 T^{*}_{n} + A_{100}\cos\left(\frac{n}{2}\right)\theta + B_{100}\sin\left(\frac{n}{2}\right)\theta \end{aligned} \tag{8.37}$$

where $P^{*1}_{m,n}$, etc are defined as $P'_{m,n}$, etc (equation (7.28)) with A_0, B_0 replaced by A_{000}, B_{000} and where a_m, b_n are now the Fourier coefficients of $\bar{f}_1(\theta)$.

The right hand side of equation (8.30) may now be evaluated in order to determine the coefficients of $(\frac{n}{2})\theta$ terms by carrying out the multiplication. This leads again to lengthy expressions of some complexity arising from the term $\bar{f}_1(\theta)$. y_{100} but nevertheless y_{200} may be found by straightforward means. y_{020} and y_{002} are similarly found and at the same time, the second order coefficients α_{200}, α_{020} and α_{002} are obtained.

The method of calculating the remaining second order components is now familiar but the task of constructing the complete second order solution is exceedingly lengthy in the completely general case. This method is perhaps more suited to application to equations in which there are relatively few

Fourier components in the periodic terms $f_1(\theta)$. The use of this method in such cases has been described by Hamer and Smith[30].

It should be made clear in conclusion that the main object of the analysis of the equation of motion (8.3) is to obtain expressions for the boundaries of stability in the form of equation (8.20) rather than to evaluate the solution itself. Application of the method produces formulae for the zero'th order solution, the first order α coefficients, the first order solutions, the second order coefficients, etc in succession. In general therefore, to obtain the k^{th} order approximation to the equation for the stability boundaries, it is necessary to carry out the calculations only up to the $(k-1)^{th}$ order solutions. In particular, the second order approximation to equation (8.20) will be obtained by evaluating only the zero'th and first order solutions to equation (8.18).

8.4 Alternative Method

8.4.1 First Order Terms

As an alternative to the method of analysis applied to the equations with three independent parameters, the following modification works well to first order and simplifies the work involved.

Consider an equation of the form

$$\frac{d^2y}{d\theta^2} + \left\{ \lambda^2 + \epsilon_1 f_1(\theta) + \epsilon_2 f_2(\theta) \right\} y = 0 \qquad (8.38)$$

(This is equation (8.3) quoted again here for convenience)

By defining a new periodic term $h(\theta)$ as follows

$$h(\theta) = f_1(\theta) + \frac{\epsilon_2}{\epsilon_1} \cdot f_2(\theta) \qquad (8.39)$$

the equation may be re-written as

$$\frac{d^2y}{d\theta^2} + \left\{ \lambda^2 + \epsilon_1 h(\theta) \right\} y = 0 \qquad (8.40)$$

so that the situation has been formally reduced to a two-parameter stability problem. Applying the standard technique to equation (8.40) we obtain an expression for the first order stability boundaries as follows:

$$\lambda^2 = \left(\frac{n}{2}\right)^2 + \alpha_1 \epsilon_1 \tag{8.41}$$

where $\alpha_1 = -r_0 \pm \frac{1}{2}\sqrt{r_n^2 + s_n^2}$

The coefficient α_1 is now defined in terms of the Fourier coefficients of $h(\theta)$ which themselves are defined from equation (8.39) as

$$\left.\begin{aligned} r_i &= a_i + \frac{\epsilon_2}{\epsilon_1} c_i \\ s_i &= b_i + \frac{\epsilon_2}{\epsilon_1} d_i \end{aligned}\right\} \tag{8.42}$$

a_i, b_i and c_i, d_i are the Fourier coefficients of $f_1(\theta)$ and $f_2(\theta)$ as before.

Substituting these values into equation (8.41) we obtain

$$\lambda^2 = \left(\frac{n}{2}\right)^2 + \epsilon_1 \left\{ -a_0 - \frac{\epsilon_2}{\epsilon_1} c_0 \pm \frac{1}{n}\sqrt{\left(a_n + \frac{\epsilon_2}{\epsilon_1} c_n\right)^2 + \left(b_n + \frac{\epsilon_2}{\epsilon_1} d_n\right)^2} \right\}$$

$$= \left(\frac{n}{2}\right)^2 - a_0 \epsilon_1 - c_0 \epsilon_2$$

$$\pm \frac{1}{n}\sqrt{\left\{\epsilon_1^2(a_n^2 + b_n^2) + \epsilon_2^2(c_n^2 + d_n^2) + 2\epsilon_1\epsilon_2(a_n c_n + b_n d_n)\right\}} \tag{8.43}$$

This equation is equivalent to equation (8.29) obtained by using the subsidiary parameter δ_n and thus achieves the same result by a convenient and more direct method, at the same time justifying the use of equation (8.39).

It is of interest to examine the behaviour of the stability boundaries as one of the small parameters becomes vanishingly small. We see from equation (8.43) that as $\epsilon_2 \to 0$, we have

$$\lambda^2 = \left(\frac{n}{2}\right)^2 - a_0 \epsilon_1 \pm \frac{1}{2}\sqrt{(a_n^2 + b_n^2)\,\epsilon_1^2}$$

$$= \left(\frac{n}{2}\right)^2 + \epsilon_1 \left\{ -c_0 \pm \frac{1}{2}\sqrt{a_n^2 + b_n^2} \right\} \tag{8.44}$$

This is the equation for the stability boundaries of the two-parameter stability problem examined in the previous chapter. However, we may interpret this equation in another way by considering this to be a special case of the three-parameter problem. The stability chart is in this instance a three-dimensional structure in which the boundaries of instability are surfaces in $(\lambda^2, \epsilon_1, \epsilon_2)$ space and equation (8.44) defines the intersection of those

surfaces with the $\epsilon_2 = 0$ plane. For small non-zero values of ϵ_1 therefore there will exist a finite region of instability the width of which will be equal to $\epsilon_1 \sqrt{a_n^2 + b_n^2}$. In addition, the centre of this unstable region will be located at $\left\{(\frac{n}{2})^2 = a_0 \epsilon_1\right\}$ on the λ^2 - axis.

Fig. 38 illustrates this point showing diagrammatically the first-order stability boundaries of the n'th region and their intersections with the $\epsilon_1 = 0$ and $\epsilon_2 = 0$ planes. The existence of finite ranges of values of the parameter λ^2 on those surfaces is a feature of this type of equation which appears to have received little attention. The most notable exception is perhaps the paper by Klotter and Kotowski[26] in which an equation of this type is examined and its "stability space" constructed. As has already been pointed out however, the periodic functions in the equation examined are cosine functions only so that the analysis is considerably simplified.

Examining Fig. 38 which shows the n'th region of instability originating at point P on the λ^2 - axis, we see that for $\epsilon_1 = 0$, the stability boundaries are PC a nd PD, the width of the region being defined by

$$CD = \epsilon_2 \sqrt{c_n^2 + d_n^2}$$

and the axis PH of the region being defined by the equation

$$\lambda^2 = (\frac{n}{2})^2 - a_0 \epsilon_2$$

Similarly, for $\epsilon_2 = 0$, the stability boundaries are PA and PB with

$$AB = \epsilon_1 \sqrt{a_n^2 + b_n^2}$$

and the equation of PG is

$$\lambda^2 = (\frac{n}{2})^2 - a_0 \epsilon_1$$

For finite values of ϵ_1 and ϵ_2 the width of the unstable region will be EF defined from equations (8.43) and (8.29) as

$$EF = \delta_n = \sqrt{\epsilon_1^2(a_1^2 + b_n^2) + \epsilon_2^2(c_n^2 + d_n^2) + 2\epsilon_1\epsilon_2(a_n c_n + b_n d_n)}$$

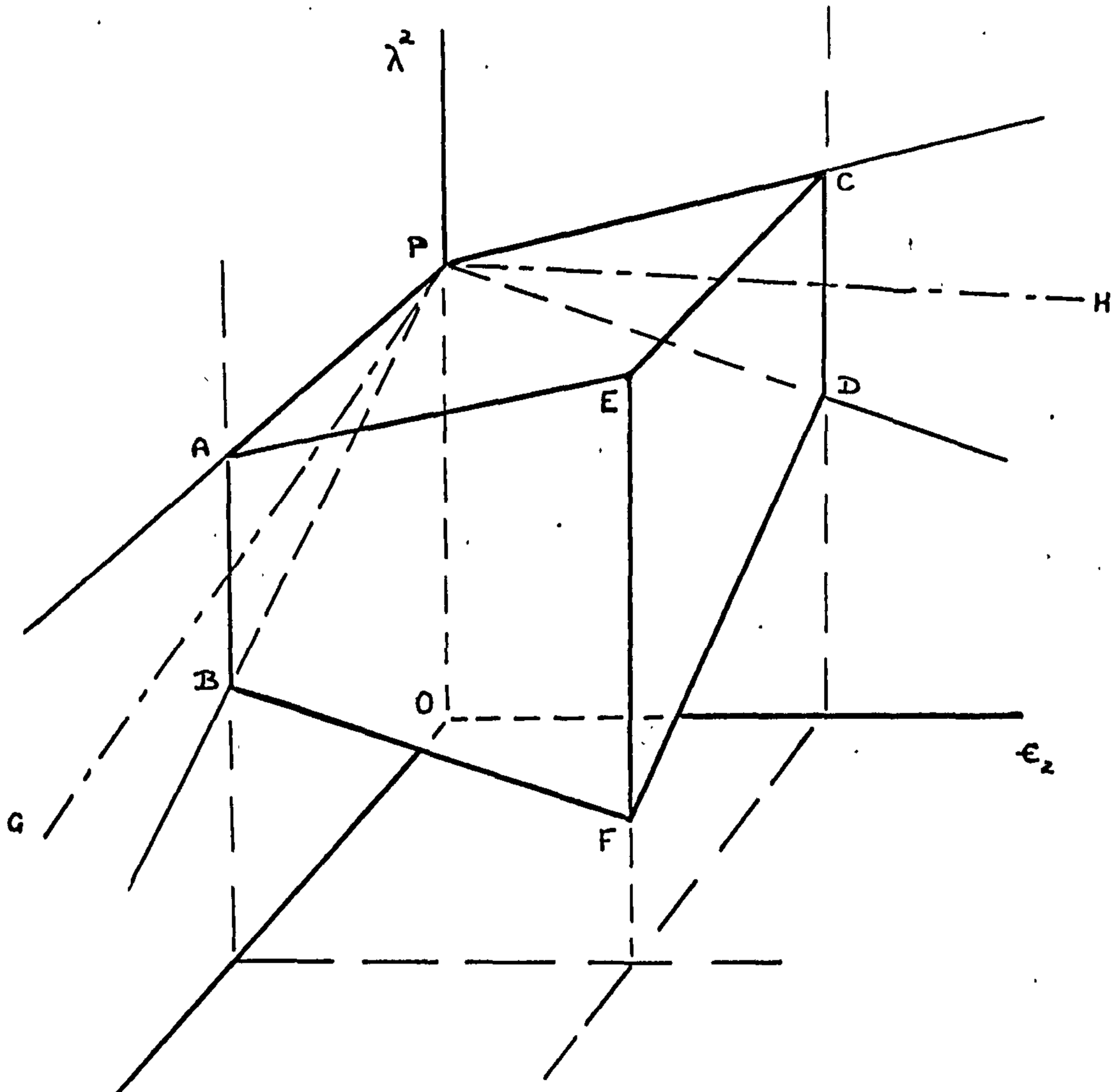

$$OP = \left(\frac{n}{2}\right)^2$$

$$AB = \epsilon_1 \sqrt{a_n^2 + b_n^2}$$

$$CD = \epsilon_2 \sqrt{c_n^2 + d_n^2}$$

$$EF = \delta_n$$

Equation of PG : $\lambda^2 = \left(\frac{n}{2}\right)^2 - a_0 \epsilon_1$

Equation of PH : $\lambda^2 = \left(\frac{n}{2}\right)^2 - c_0 \epsilon_2$

FIG. 38. CHARACTERISTIC STABILITY SPACE for Hill's Equation with Three Independent Parameters.

The widths of the unstable regions on the $\epsilon_1 = 0$ and $\epsilon_2 = 0$ planes are thus proportional to the amplitude of the n'th Fourier component of the corresponding periodic function which in general will decrease rapidly with increasing n .

8.5 Conclusion

The stability analysis of Hill-type equations containing more than two independent parameters has been examined and the familiar perturbation method has been shown to fail in the case of general periodic functions. A modification to this method, being effectively the introduction of an additional parameter, has been demonstrated and shown to work well in producing first order formulae for the stability boundaries. The complexity of this method increases greatly however when more than three parameters are present and also in deriving the second order solutions. An advantage of this method, on the other hand, is that the order of the approximation to the stability boundaries is always one greater than that of the solutions. This particular method is particularly useful in equations containing relatively few Fourier coefficients as has been demonstrated elsewhere[30].

An alternative method of analysis for the three parameter case has also been described which gives results similar to those of the first method. The effect of the presence of a third parameter upon the stability of the equation has been discussed and attention brought to various features of the stability characteristics which appear to have received little attention hitherto.

The alternative method of analysis and its application to equation (8.1) in connection with the study of stability in mechanisms has been reported by Smith and Maunder in the Journal of Mechanical Engineering Science[35].

PART IV

EXPERIMENTAL WORK

CHAPTER 9

EXPERIMENTAL WORK

9.1 Introduction

The experimental investigations carried out in connection with the work described in this thesis are concerned entirely with the content of Part III. Since the inertia forces generated in linkage mechanisms may be calculated exactly by straightforward methods, no attempt has been made here to obtain any experimental verification of the content of Parts I or II. Part III however, which deals with the dynamic stability of linkages with flexible elements, contains approximate methods of analysis of the equations of motion for which some experimental justification is desirable. This chapter describes the results obtained from experiments carried out on a number of crank-rocker type mechanisms of various dimensions, comparison being made with computed results based on the theoretical predictions of vibration and stability characteristics.

9.2 Design of Experiments

Theoretical examination of the transverse vibrations of the coupler in a crank-rocker linkage has shown that the nature of the vibrations is governed by certain kinematic and dynamic parameters of the linkage. These parameters, being well-defined functions of the linkage geometry and of the physical properties of the individual links, form the basis upon which the experimental work is organised. Those parameters which are purely kinematic functions of the linkage will, in general, be common to all linkages of the same geometrical proportions (viz. linkages having the same link-length ratios). These functions are the periodic functions of the equation of motion, equation (8.1), and are determined entirely by the linkage geometry. Once the link-length ratios are determined, there remain those parameters which are functions of the individual link characteristics (coupler stiffness, follower inertia, etc) which may be changed independently of linkage geometry.

It is consequently convenient to choose these latter parameters as those which will be used as the independent variables in the investigation of the system vibrational characteristics. As has been demonstrated in Part III these parameters are also those in terms of which stability charts are normally constructed. Any stability chart is therefore unique to its particular mechanism, the location of the boundaries between regions of stable and unstable motion being determined by kinematic properties for any fixed values of the dynamic parameters.

The parameters which are independent of linkage proportions (i.e.kinematics) are λ^2, the "speed parameter", defined as the square of the ratio of the coupler natural frequency to the angular velocity of the crank, and the ϵ_j which appear as coefficients of the periodic functions in the equation of motion. The theoretical range of λ^2 is evidently from zero to infinity but will, in the great majority of practical cases, not fall below some value in the region of unity (corresponding to an operational speed of the same order as the principal mode of vibration of the coupler). This practical minimum value of λ^2 is determined not only by the operational speed ω_2, but also by Ω the coupler natural frequency which is itself dependent upon coupler stiffness and mass distribution.

Changing stiffness will have no effect upon other parameters in the system but an alteration to the mass of the coupler will produce a corresponding change in the parameter ϵ_3, defined as

$$\epsilon_3 = \frac{\pi^2 M_4 k_4^2}{M_3 \ell_3 \ell_4}$$

In addition, there may also be an effect upon ϵ_1

$$\epsilon_1 = \frac{\pi^2 k_3^2}{\ell_3^2}$$

if the mass distribution of the coupler is changed. However, both ϵ_1 and

ϵ_2 may be unaffected if the coupler remains uniform. (More strictly, if radius of gyration and location of centre of mass are unchanged.)

$$\epsilon_2 = \frac{\pi^2 + {}_3 l_2}{l_3^2}$$

In deciding upon the method of changing the values of these parameters λ^2, ϵ_1, ϵ_2, ϵ_3 one must therefore ensure either that each may be varied independently of the other or that the consequent effects upon other parameters are recognised.

From the definitions of the parameters ϵ_i, it is evident that any change in follower inertia I_4 will affect only ϵ_3 and, as has been discussed in Part III, in a great many linkage configurations the magnitude of the $\epsilon_3 f_3(\theta)$ term predominates over that of the $\epsilon_1 f_1(\theta)$ and $\epsilon_2 f_2(\theta)$ terms. Since we will be considering light couplers and relatively heavy follower links, the contribution of the terms which are functions of the coupler mass-distribution (ϵ_1 and ϵ_2) will be relatively small. Consequently, the two predominating parameters governing the behaviour of the flexible coupler will be the "speed parameter" λ^2 and the "load parameter" ϵ_3.

By using a number of uniform coupler links of different thickness, the coupler stiffness may be changed without affecting ϵ_1 or ϵ_2 and the appropriate range of operation of the linkage is thus determined entirely by Ω, the natural frequency of coupler vibration.

As has already been pointed out, the follower inertia may be varied by any convenient method without affecting the other system parameters.

By designing the follower link so that the inertia is initially small, it is possible to increase the moment of inertia about the fixed pivot by attaching a weight or weights to the link at points on its axis. This method is simple to use and, as will be described below, allowed the inertia to be changed quickly without necessitating the dismantling of any of the links.

The most important governing parameters of the system are thus seen to be the stiffness of the coupler, the speed of operation of the mechanism and the follower inertia. The first of these has a direct effect upon the coupler natural frequency and thus determines the practical range of the speed of operation. The follower inertia may be varied independently of the other two parameters, its range being defined mainly by design considerations.

The most logical and convenient method of examining the behaviour of the system is accordingly to observe the vibrations of the coupler in a particular linkage over the practical speed range for known values of stiffness and inertia. Changing the inertia will create a different pattern of behaviour with all other conditions unchanged. Having examined the vibrational behaviour over the complete range of follower inertia values, one may then examine either a linkage of similar proportions with a coupler of different stiffness or a linkage of different dimensions. In the former case, the behaviour of the coupler may be expected to resemble that of the first linkage examined for similar values of a non-dimensional speed parameter expressed in terms of the coupler natural frequency (ω_2/Ω). Results from these two experiments would then be treated as corroborative evidence for a situation in which the governing parameter values are identical while the experimental conditions differ in certain respects.

The alternative choice of changing the linkage dimensions brings about fundamental changes in the expected behaviour of the coupler and is therefore preferably treated as a separate set of experiments.

9.3 Description of Apparatus

9.3.1 Mechanical Components

Fig. 39 shows a general view of the apparatus. The linkage is mounted on a steel bed plate (1) supported on an angle-iron frame (2). The crank or input link takes the form of a flywheel (3) mounted in bearings located below the plate (Fig.40) which relieve side-thrust and end-load on the shaft of the drive motor (20) which is attached to the bearing housing (21).

FIG. 39

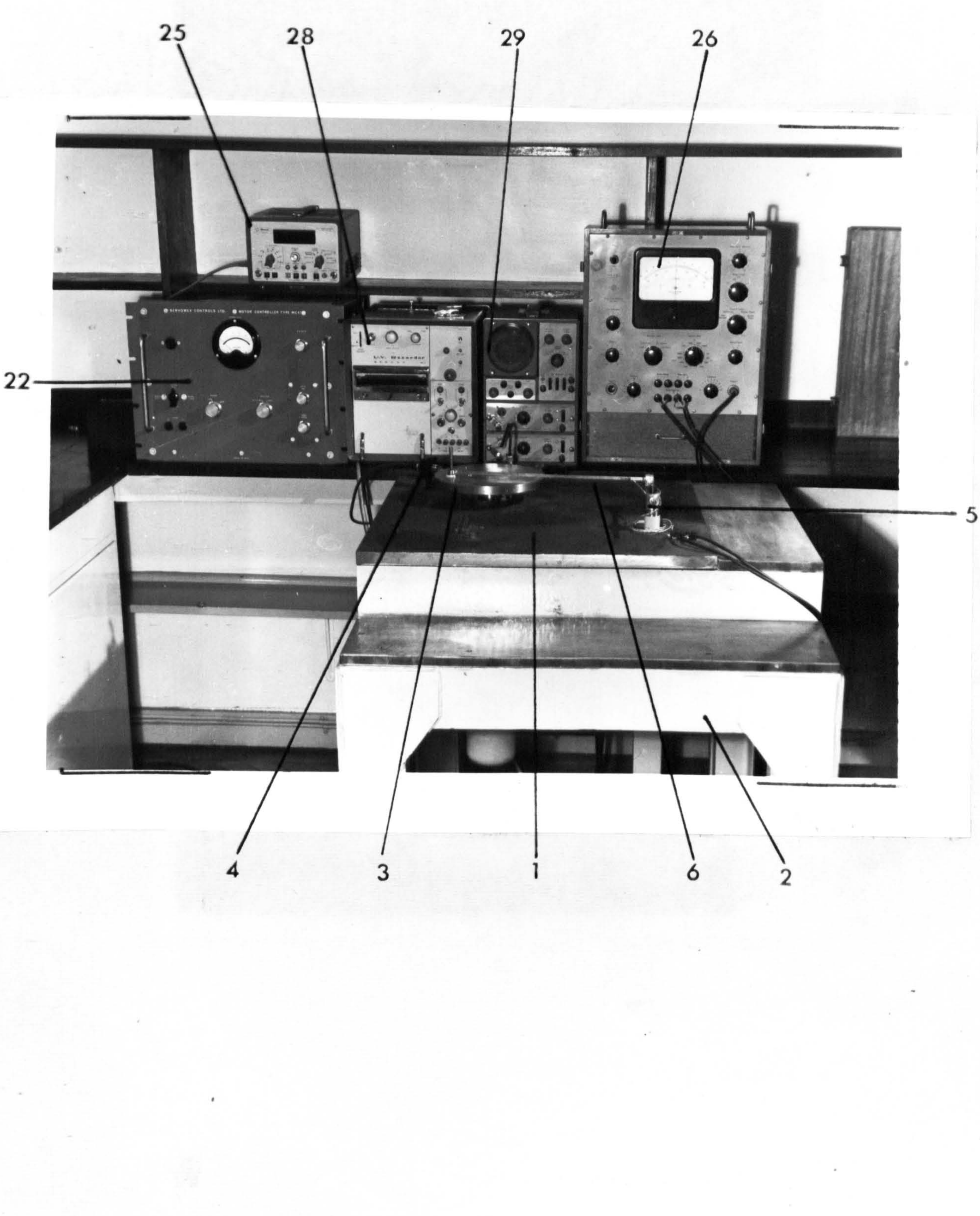

FIG. 40

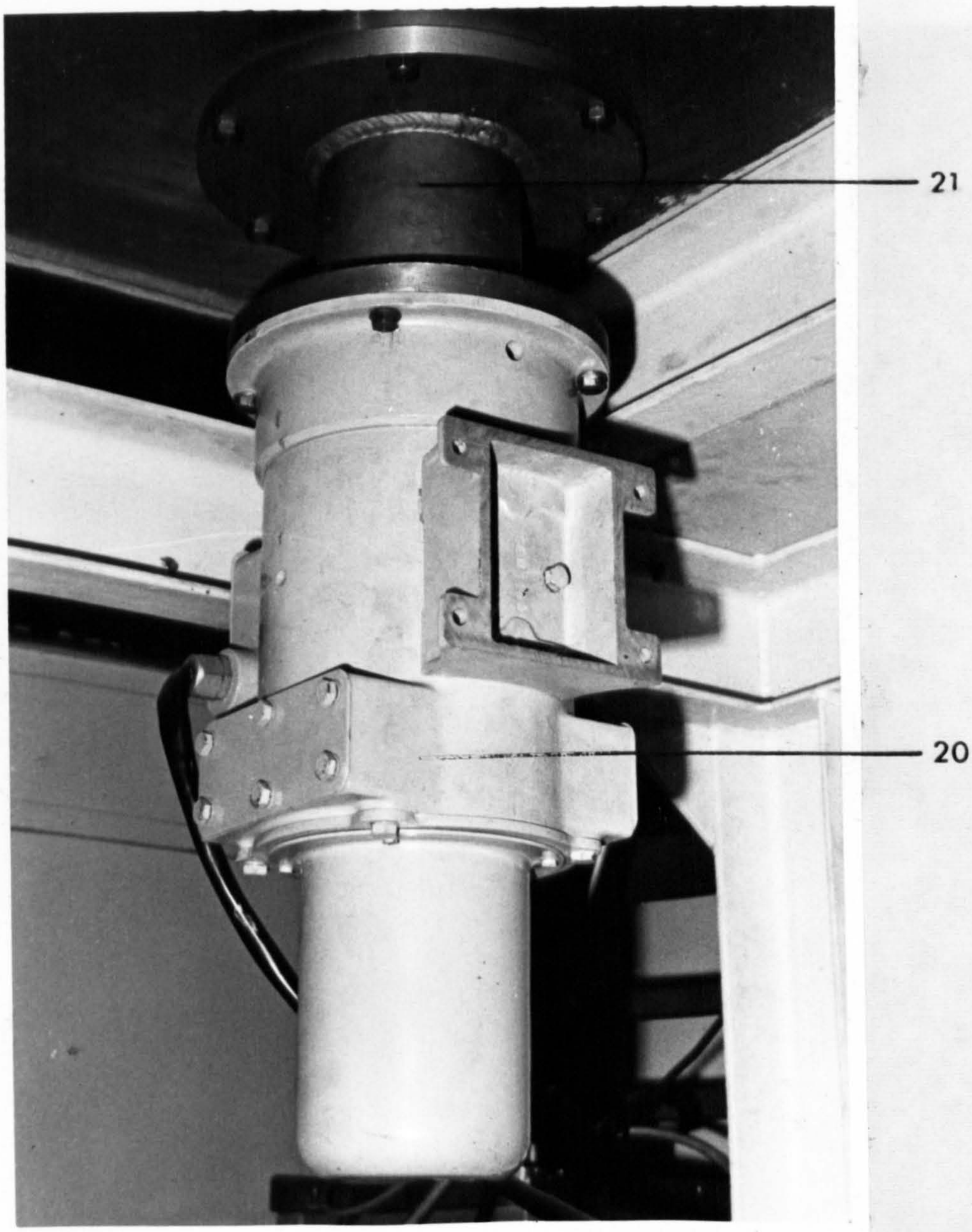

FIG. 41

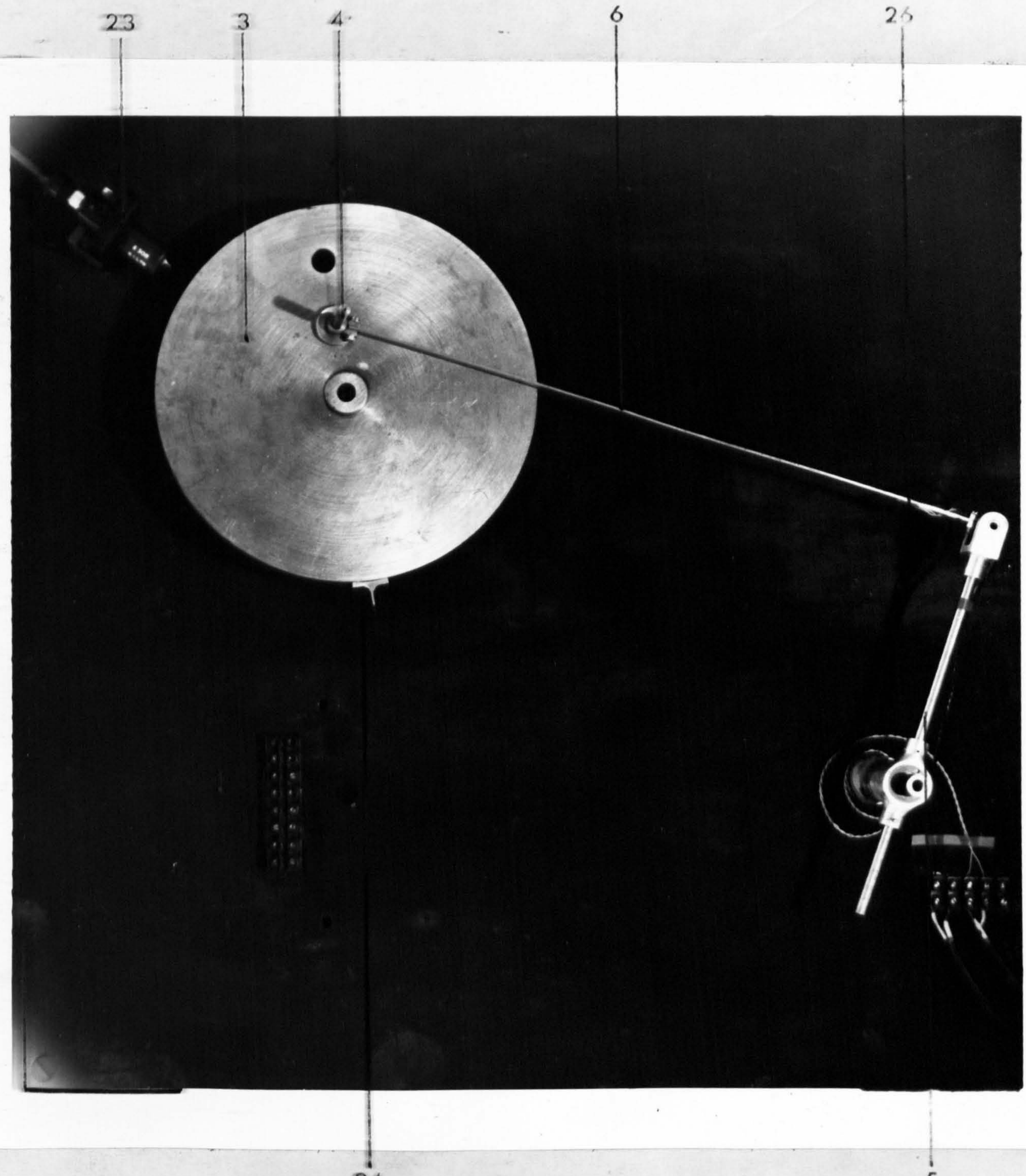

FIG. 42

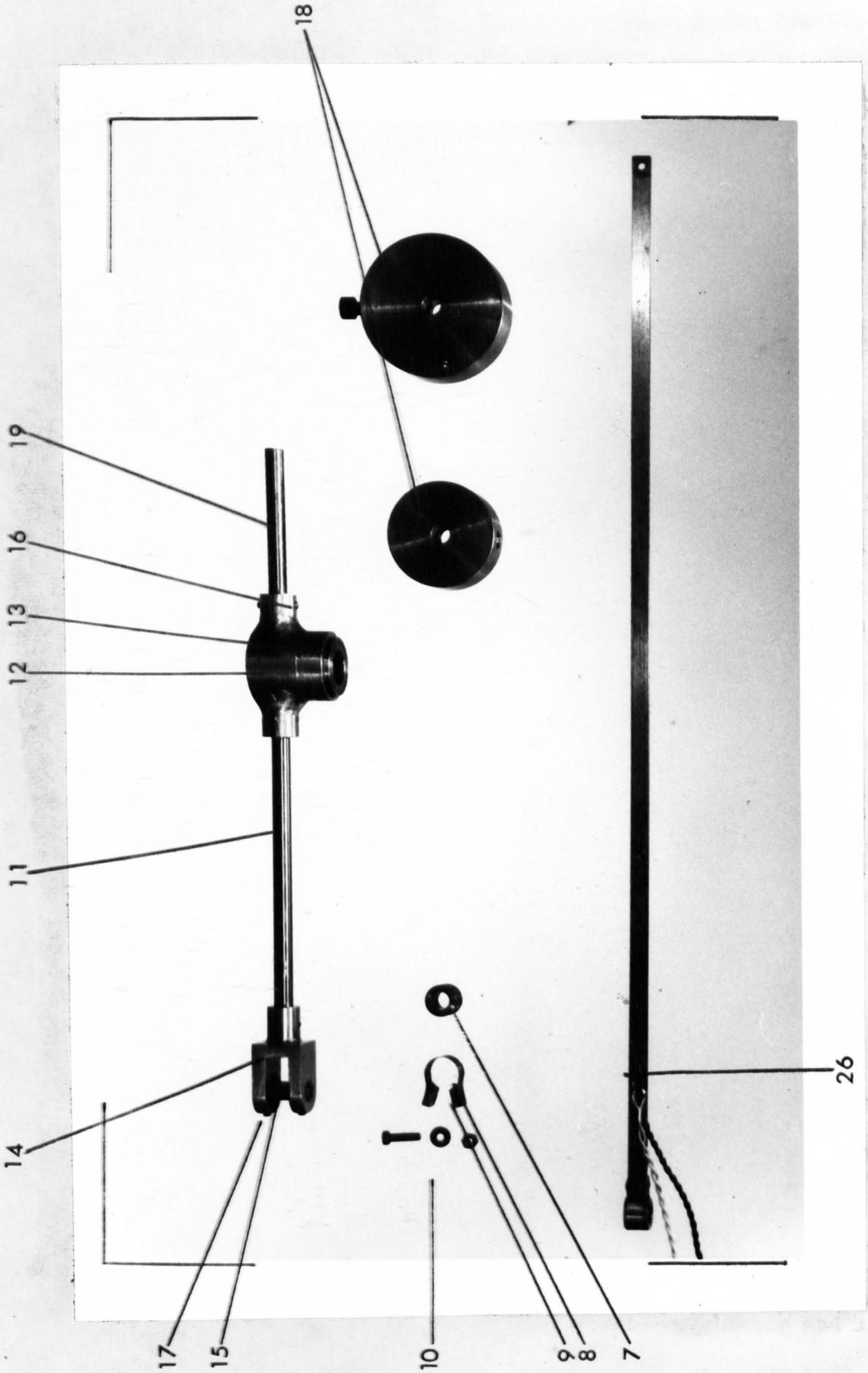

The crank pin (4) (see Fig.41) located in one of two possible positions on the flywheel (3) transmits motion to the follower (5) through the flexible coupler (6). The coupler-follower joint is a symmetrical fork to counteract torsional effects while the follower bearing is a rigid pin attached directly to the bedplate.

Fig. 42 shows details of the coupler and follower links. The couplers used are $\frac{1}{2}$"-wide strips of gauge plate of different thicknesses. The end-bearings are constructed so as to minimise end-effects on the coupler vibration and consist of bronze bushes (7) attached to the coupler by steel tapes (8) onto which spacers (9) are brazed. Each bush and tape is held in place by a nut and bolt (10). The spacers are designed to accommodate a nominal coupler thickness of 1/16 in. which was the thickest used. Thinner couplers were attached to the bearing assemblies using suitable shims. Two different views of the assembled coupler bearing may be seen in Figures 41 and 42.

The follower link and associated additional weights are also shown in Fig.42. The link is composed of a $\frac{1}{4}$ in. stainless steel tube (11) carried in an aluminium alloy boss (12) which is fitted with a copper bush (13). The coupler is attached to the follower by the aluminium alloy fork (14) in which a stainless steel tube (15) forms the pivot for the coupler bearing. The fork (14) and boss (12) are held in place by tapered pins (16) while the pivot pin (15) is held by grub screws (17) in the arms of the fork.

The additional weights (18) are brass cylinders which may be attached to the rearward extension of the follower (19) at predetermined positions in order to increase the moment of inertia.

9.3.2 Electrical Components

The linkage is driven by a 0.5 H.P. motor (Fig.40 (20)) attached to the crank bearing housing (21) mounted below the bed-plate. The motor and its associated control unit (Fig.39 (22)) (Type MJ 47, Servomex Controls Ltd) form a very flexible system which proved to be well suited to this particular application. The accuracy of speed control was in most instances

adequate using the control box scale (for which an accuracy of 1.5% is guaranteed by the manufacturers). Drift in the motor speed was very low and caused no difficulty since the linkage was not required to run for long periods at constant speed. In addition, the torque characteristics of the system are such that speed variation throughout one cycle was minimal so that a constant angular velocity could be assumed except at the lowest speeds (lower than those speeds at which any significant experimental observations were made).

As a secondary method of measuring speed of the motor, an inductive probe (S.I. Ltd., Type G.308) (Fig. 41(23)) was mounted adjacent to the circumference of the crank flywheel. A timing probe (24) mounted on the flywheel gave pulses corresponding to the beginning of each cycle ($\theta_2 = 0^\circ$) which were used in parallel with the signal from the strain gauge apparatus (see below) to relate vibrational amplitude to crank position.

The pulses from the probe could also be used in conjunction with an electronic counter (Fig. 39, (25)) as a check on crank speed but in practice it was found more convenient and sufficiently accurate to use the motor control box scale from which to read the motor speed directly.

Vibration of the coupler link was detected using two standard strain gauges (26) attached back-to-back directly to the coupler near to the follower-coupler joint. (Figures 41 and 42) The Bruel and Kjaer apparatus Type 1516 (Fig. 39, (27)) used in conjunction with the strain gauges enabled the overall sensitivity of the experimental apparatus to be controlled over a wide range. The signal fed to the ultra-violet recorder (28) could thus be amplified so as to produce full scale deflection for a range of sensitivity settings (see Calibration below).

The output signals from the strain gauge apparatus and timing probe were displayed simultaneously on the oscilloscope (29) and ultraviolet recorder (Type S.E. 2000). The former signal was passed through a simple R-C

FIG.43 CIRCUITRY

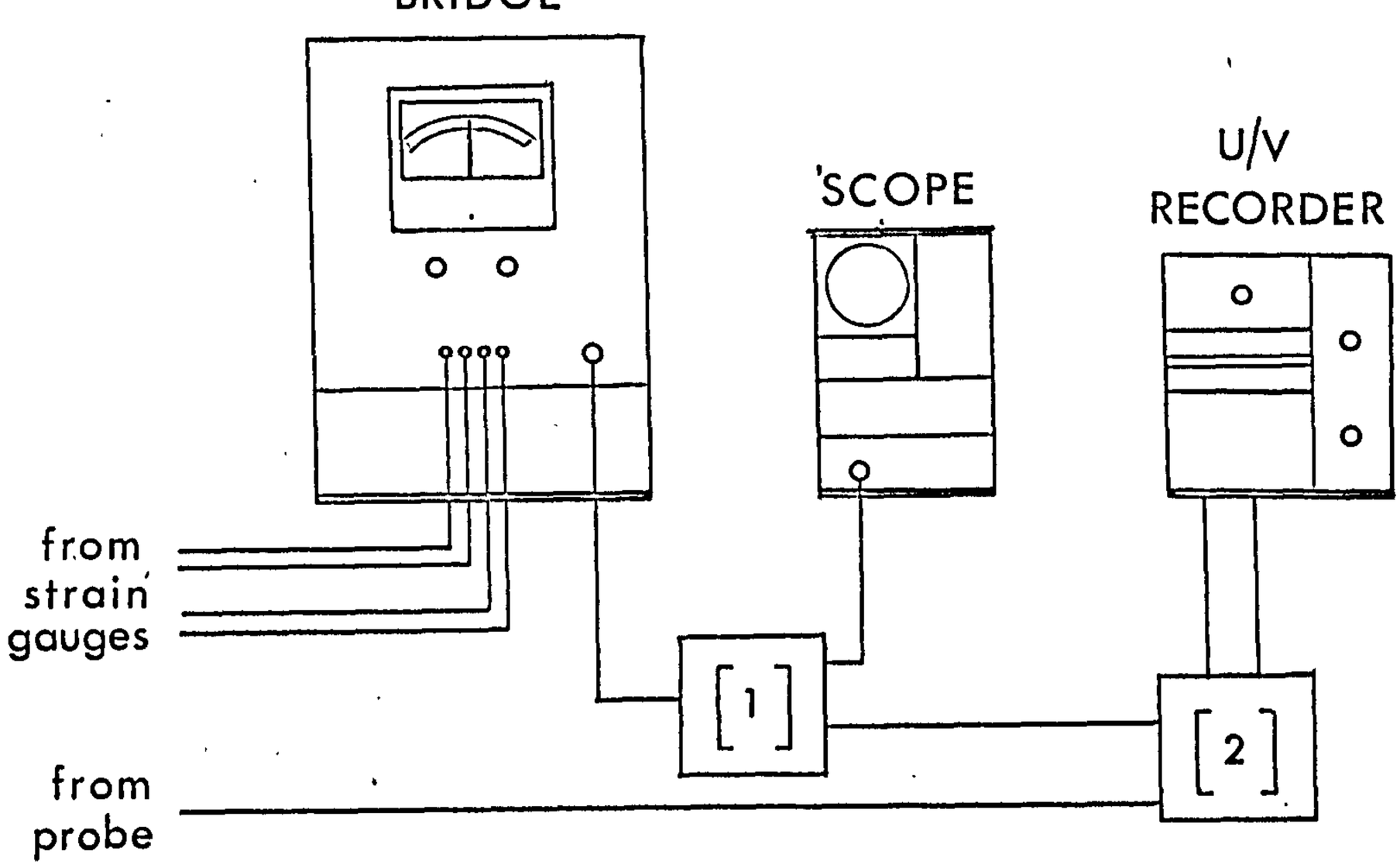

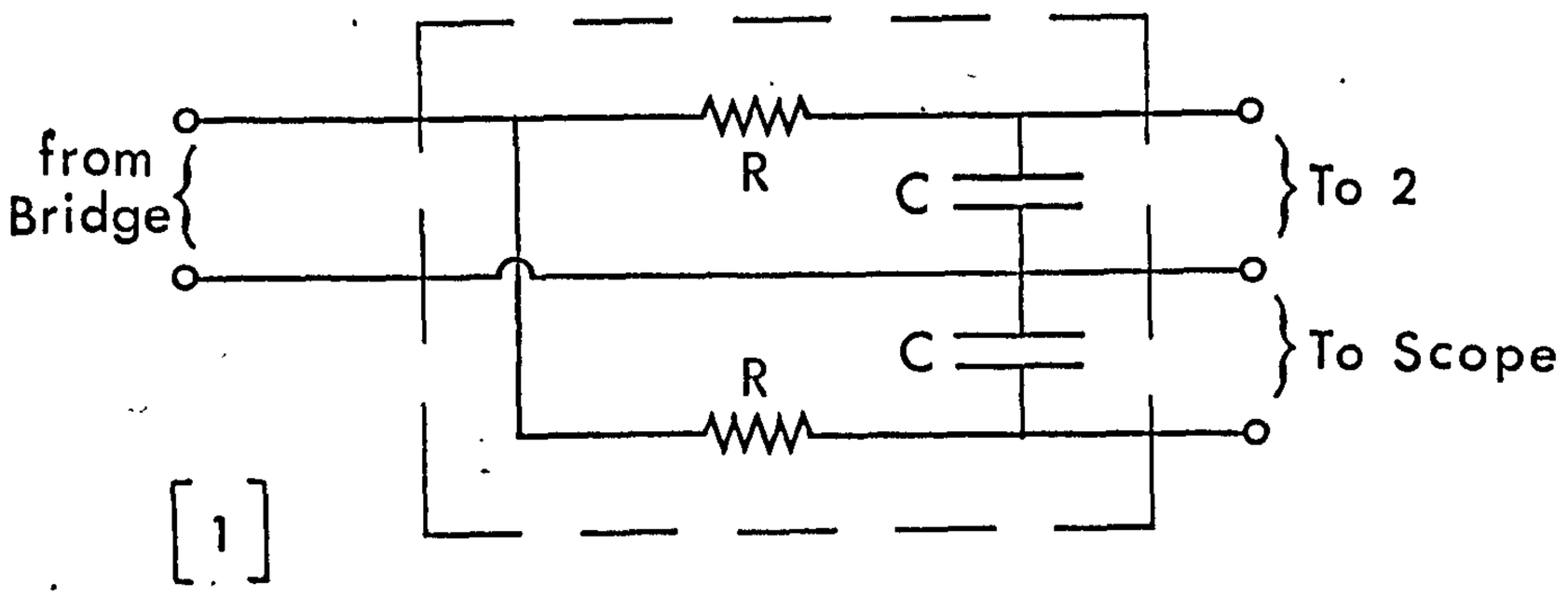

R = 100 kΩ

C = 0·25 μF

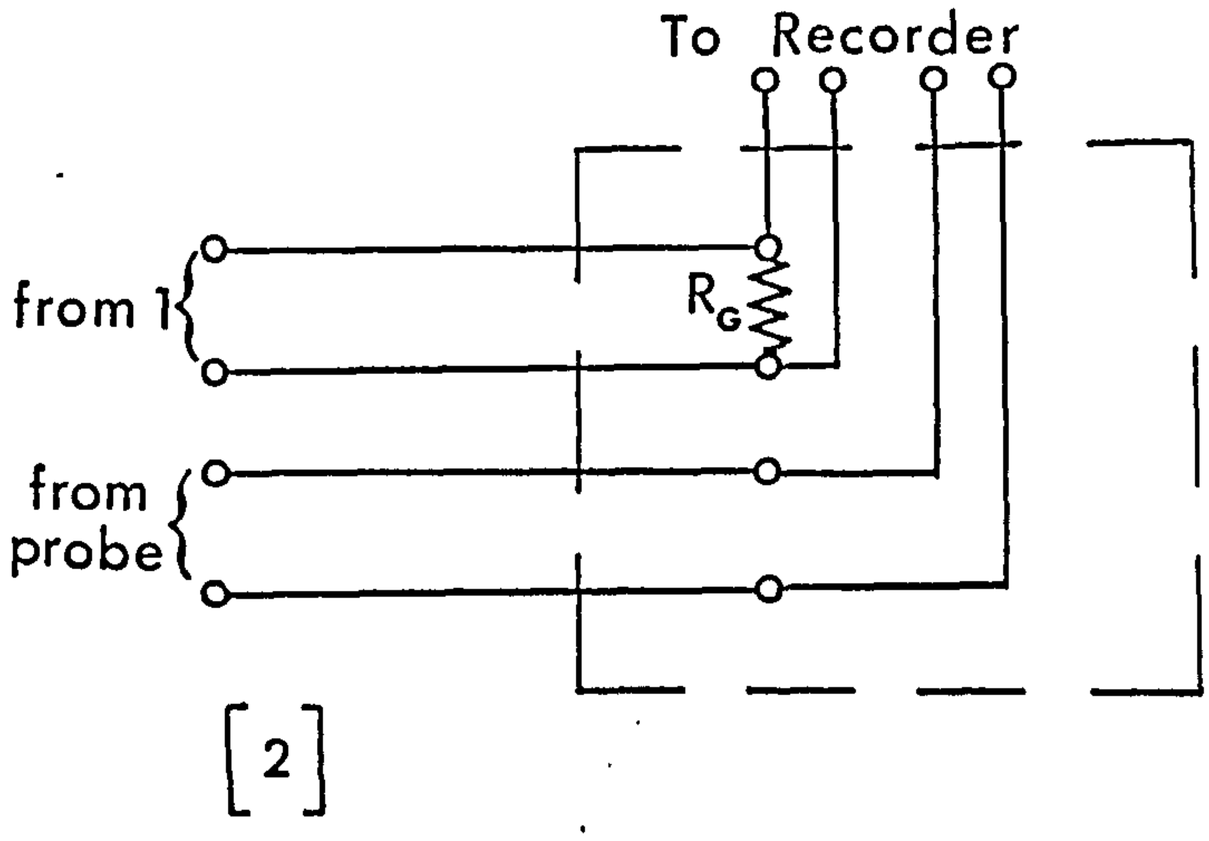

R_G = 270 Ω

filter unit to eliminate the carrier frequency and then to the u-v recorder via a junction box which contained the damping resistance for the galvanometer. The circuit diagram is shown schematically in Fig. 43 together with the details of filter unit and junction box.

9.4 Calibration

9.4.1 Follower Inertia

The moment of inertia of the follower about the fixed pivot was measured by suspending the link as a compound pendulum. In addition, by using a bifilar suspension, the inertia about the centre of gravity was determined and used as a check on the values obtained from the compound pendulum method.

Having determined the values of inertia for the follower alone ($I_{4\ MIN}$) and for the follower plus both additional weights at their extreme position ($I_{4\ MAX}$), a number of values approximately equally spaced between those two were chosen and the corresponding positions of the weights calculated by interpolation. The exact values of inertia for the follower plus weights in these positions were then determined by experiment, the smaller of the two weights being used for the lower values, the larger weight for intermediate values, and both weights for the higher values.

The table below shows the values obtained in this way which were used in the experiments to be described.

MOMENT OF INERTIA OF FOLLOWER ABOUT FIXED PIVOT	
Minimum Inertia (Follower alone)	0.0058 ± 0.0001 lbf. in. sec^2
Follower plus smaller weight	.0069 ± 0.0002
" " " "	.0079 ± 0.0002
" " " "	.0109 ± 0.0003
" " larger "	.0130 ± 0.0003
" " both weights	.0149 ± 0.0004
" " " "	.0164 ± 0.0004
" " " "	.0190 ± 0.0005

9.4.2 Coupler Stiffness

The stiffness of the couplers used were measured by determining the deflection due to an applied load. The coupler under investigation was supported horizontally between two knife-edges and an increasing central load applied. The stiffness was then simply determined from the slope of the resulting load/deflection curve.

Theoretical calculations, based upon the cross sectional area of the coupler and the modulus of elasticity of the material used, gave good agreement with the experimentally determined values.

Fig. 44 shows a typical load/deflection curve obtained in the manner described. For the case illustrated, (a coupler of $\frac{1}{16}$ in. thickness) the calculated value of stiffness obtained is (EI) = 171.5 lbf.in^2 which gives a theoretical natural frequency of transverse vibration of 26.5 Hz for a coupler of 15 in. length (neglecting end-effects). This is in close agreement with the frequency of the experimentally observed damped free vibration. As will be discussed later, the damped natural frequency of the coupler was found to be within 2% of the theoretical (undamped) value. Similar agreement was found with couplers of different thickness, the observed natural frequencies being in proportion to their thickness indicating that any end effects were minimal and could be neglected.

9.4.3 Vibrational Amplitude

The accurate determination of the amplitude of vibration of the coupler is required in the lower speed ranges when the experimental waveforms may be compared with computed results in order to verify the theoretical analysis. At the high end of the speed ranges, vibrational amplitude increases to a value at which the small deflection theory no longer holds and the detection of the onset of instability is of prime importance. In addition, non-linear effects become important and the mode shape may contain terms higher than the first. At all speeds except these however, the theory predicts that the predominating mode will be the fundamental so that higher harmonics may be ignored.

FIG.44 MEASUREMENT OF COUPLER STIFFNESS

(X LOAD INCREASING)
(O LOAD DECREASING)

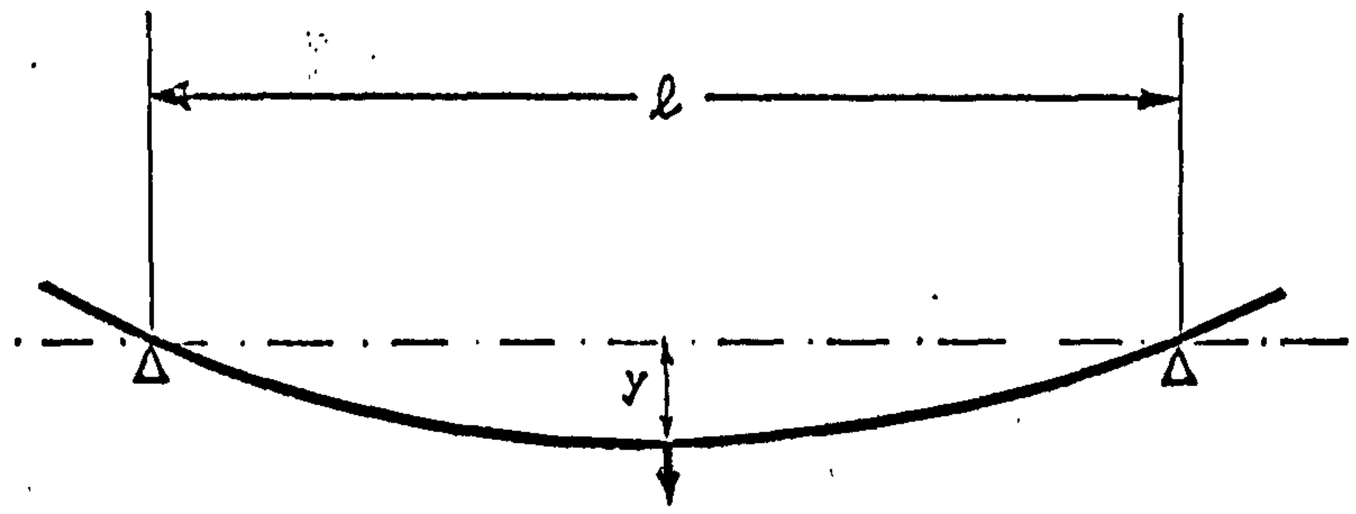

$$y = \frac{W \ell^3}{48 EI}$$

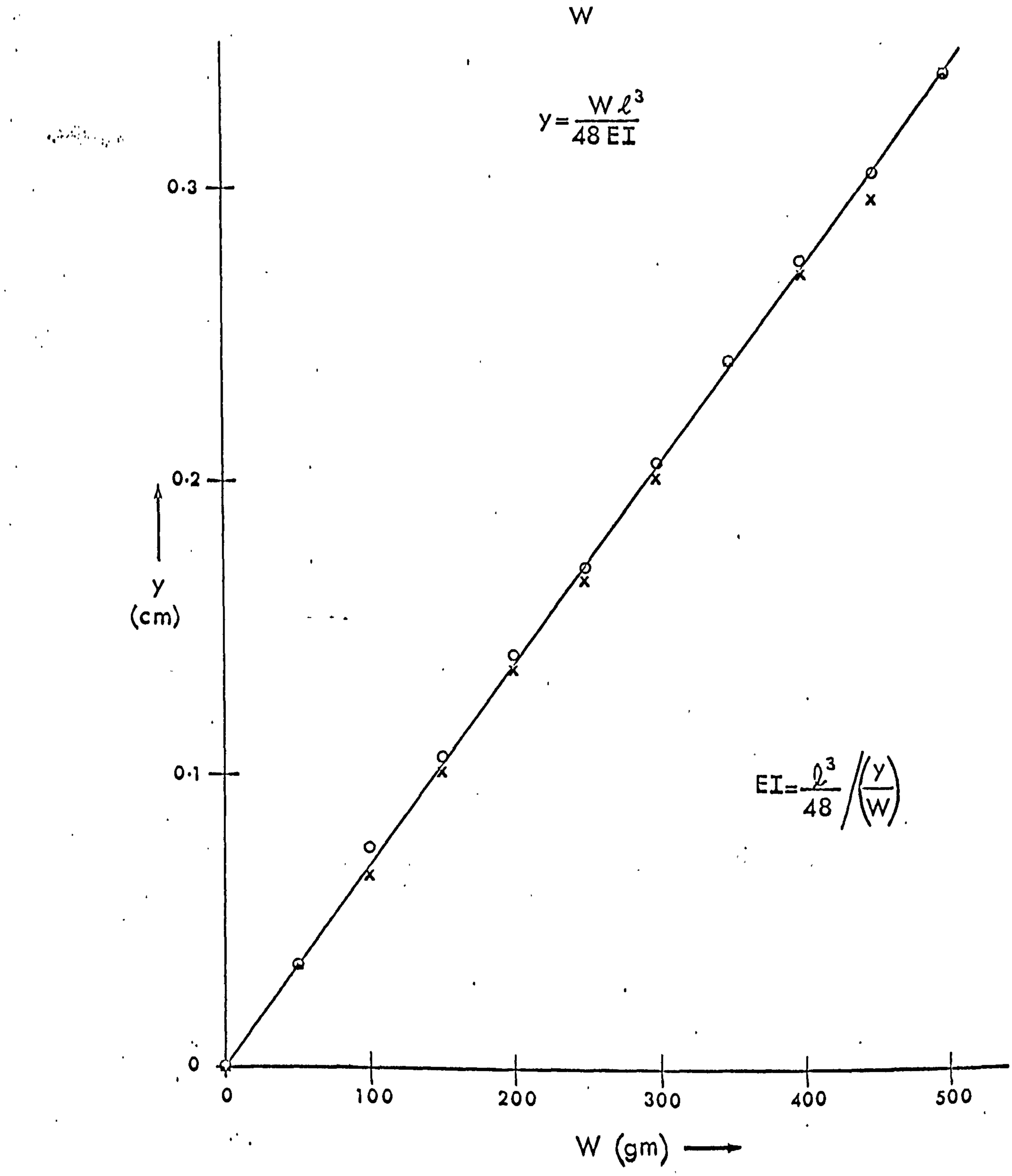

$$EI = \frac{\ell^3}{48} \Big/ \left(\frac{y}{W}\right)$$

The strain gauges placed back-to-back on the coupler are near the coupler-follower joint. Initial investigations with centrally placed gauges showed that over-straining occurred at comparatively low speeds together with failure of the cement bonding. Consequently, the gauges were placed near to one end of the coupler in a region of lower strain, the end nearer the follower being chosen as the most convenient for carrying the strain gauge signal to a point on the fixed frame via the follower link.

The calibration of the gauge-bridge-recorder system was carried out as follows. As previously described, the Bruel and Kjaer apparatus gives ample provision for sensitivity adjustment so that all that is required is the correlation of vibrational amplitude with scale deflection on the recorder. A static point-load method of deflecting the coupler was used which provided an acceptable approximation to the theoretical sinusoidal mode shape. Fig. 45 shows the close agreement between the deflected mode shape due to a central point load (non-dimensionalised so as to give unit maximum amplitude) and a sinusoidal mode shape for half the beam length.

The gauges are attached at a point approximately one tenth of the total length of the coupler from the coupler-follower joint. The corresponding difference between the two mode shapes here is less than 5%, the sinusoidal mode being the greater, indicating that the apparent amplitudes measured will be slightly larger than the true amplitudes. Some evidence will be presented in the next section to support this expected difference.

Fig.46 shows the calibration curves for three couplers of different thickness, each at three sensitivity settings of the Bruel and Kjaer apparatus. Deflection of the trace on the u-v recorder is plotted against corresponding mid-point deflection of the coupler, readings being taken of deflection in both positive and negative senses. As may be seen from the figure, most of the curves show a slight non-linearity to a greater or lesser extent, with sensitivity decreasing as amplitude increases. The thinnest coupler used shows the

FIG. 45. CALIBRATION OF VIBRATIONAL AMPLITUDE

Comparison of Point-Load and Sinusoidal Mode-Shapes.

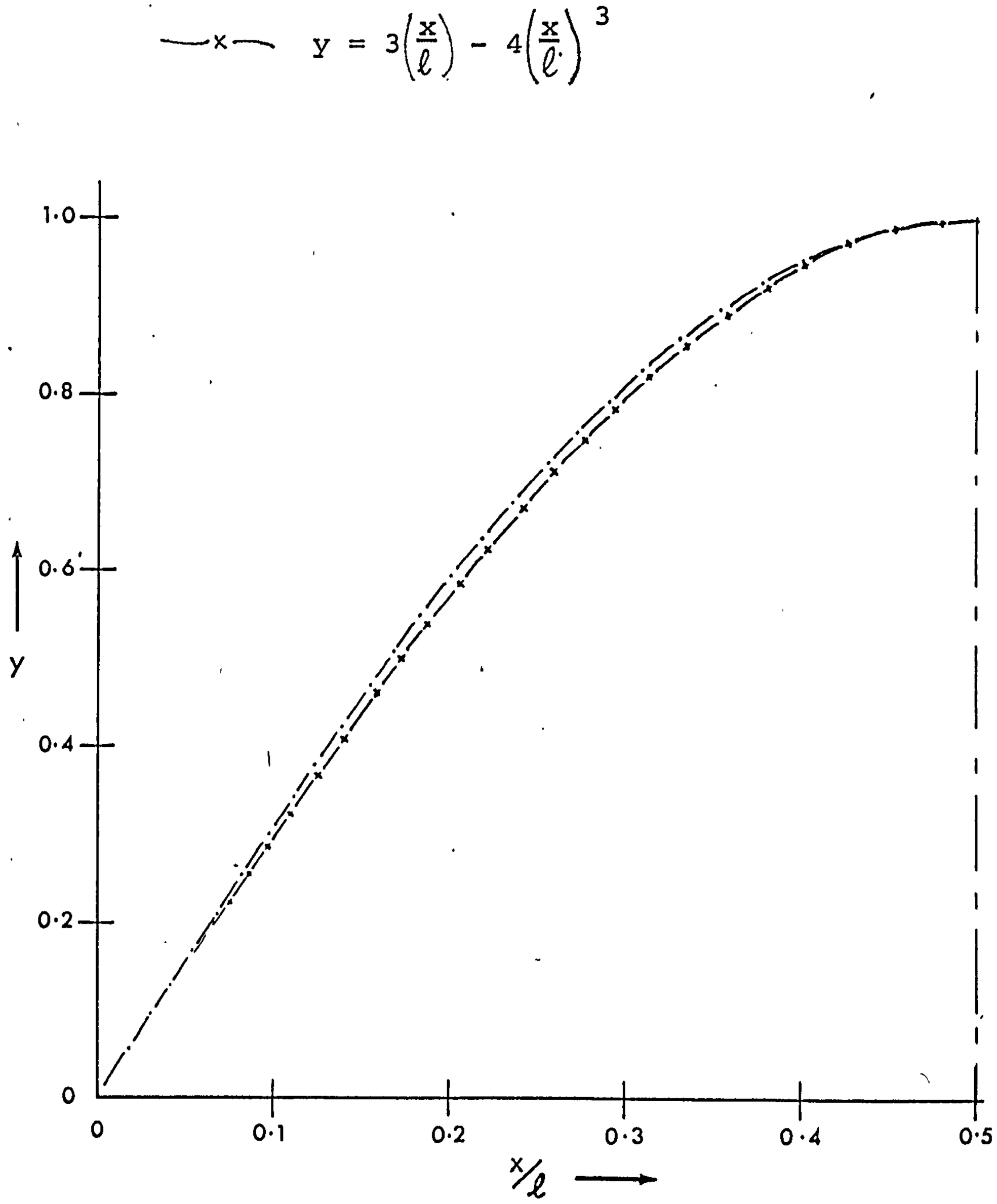

FIG. 46. CALIBRATION CURVES

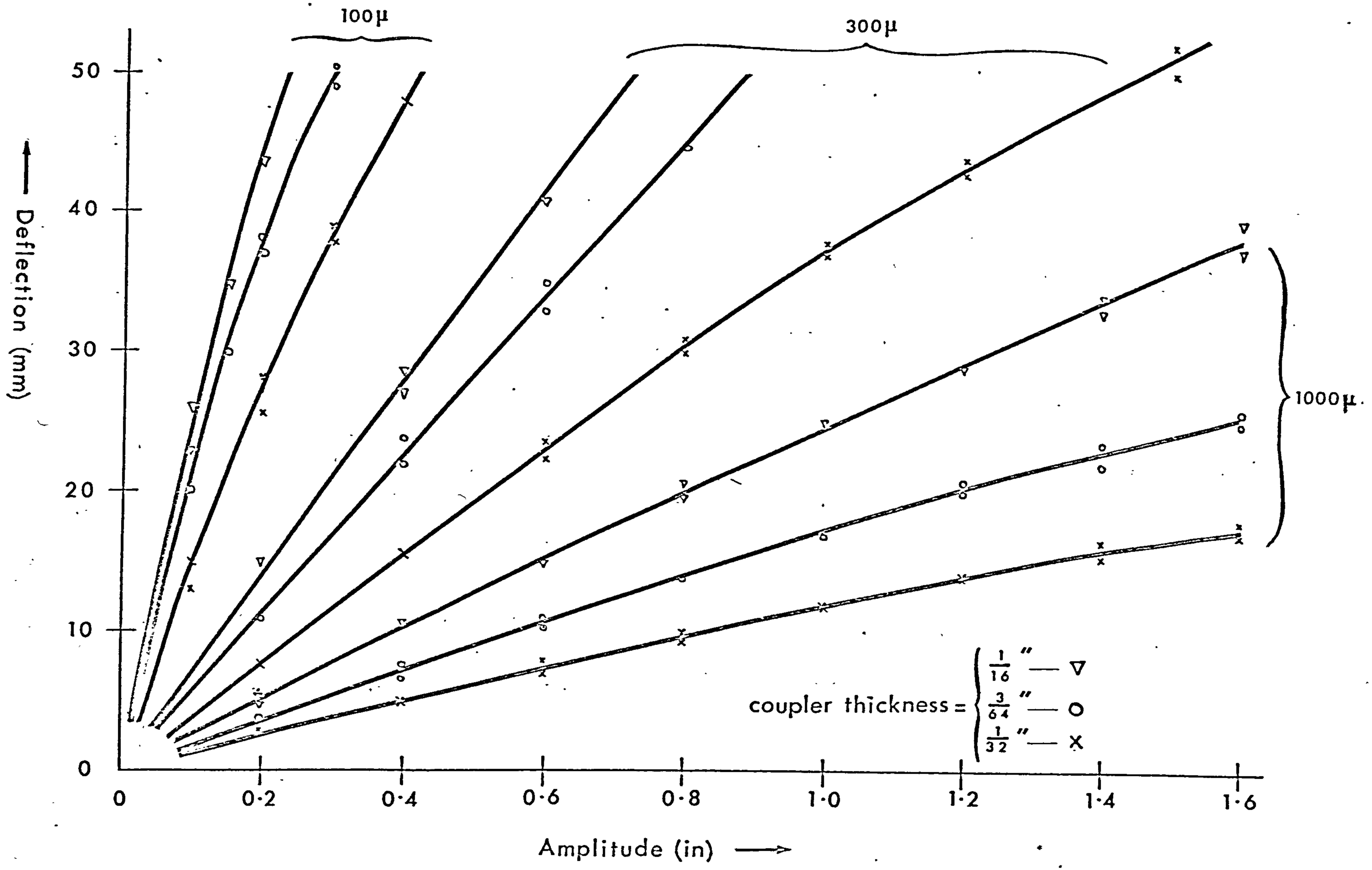

greatest deviation from linearity but the calibration is still sufficiently linear for the characteristics of the vibrations to be evident from the recorder traces, the calibration curves being necessary only when accurate measurements are desirable. The three sensitivity settings used are the 100μ , 300μ and 1000μ ranges on the Bruel and Kjaer apparatus with a bridge voltage of 3V.

9.5 Results

9.5.1 Introduction

It is possible to consider the experimental results in three separate ways each of which lays a slightly different emphasis on the interpretation of these results. Firstly, as a verification of the validity of the derived equation of motion together with the methods of solution by digital computation as described earlier in this thesis, the detailed nature of the observed vibration may be examined and compared with the theoretical wave-forms over a range of conditions. It is sufficient here to consider only one full cycle of the crank at the speed under investigation when dealing with stable periodic vibration. This aspect of the experimental work may thus be considered as a test of the validity of the equation of motion itself in describing the mode of coupler vibration.

In addition to examining the details of the vibration throughout one crank cycle, the general behaviour of the coupler may be examined over the complete speed range of any particular mechanism under a given set of conditions. This may be likened to the frequency response of that mechanism and a number of resonant frequencies will be detected at which the fundamental mode of vibration will be excited as a consequence of the harmonics present in the periodic forces generated by the mechanism motion. This is the second way in which the results may be considered and as in the first, the majority of the vibrations examined will be stable. The stability analysis outlined in the foregoing chapters deals mainly with the prediction of the speed at which unstable

vibrations will occur in any mechanism operating under predetermined conditions. It is not concerned with the nature of those vibrations although solutions to the equation of motion at the limit of stability (viz. on the stability boundaries of the stability chart) are produced as a consequence of the analytic process. The main emphasis in the examination of the system stability therefore will be on the speeds at which instability occurs and is in this way closely related to the determination of the speeds at which resonant vibrations occur as mentioned above.

These two latter aspects of the results may be viewed jointly by the construction of a set of response curves (one for each particular value of follower inertia in each linkage examined) the upper limit of which is the speed at which the vibration becomes unstable. As will be discussed below, it is sometimes possible to obtain stable vibrations at speeds higher than this by passing through the unstable region. Various factors affect the ease with which such conditions may be obtained, including the width of the relevant unstable region and the amplitude of the forced vibrations in adjacent stable regions.

The three aspects of the experimental results will now be discussed in more detail.

9.5.2 Vibrational Characteristics

The detailed nature of the stable vibrations of the couplers in three crank-rocker linkages of different link-length ratios was examined and compared with that of the corresponding theoretical wave-forms obtained by digital computation. As has been described in Chapter 6, two entirely different methods of solving the equation of motion were employed using two different computers. One of the methods used (on the KDF9 computer) is explained in Appendix 4 and is based on an algorithm due to de Vogelaere[23] solving the equation by a fixed-step method. The second method used a standard Kutta-Merson variable step-length procedure which is embodied in the Continuous System Modelling Program (C.S.M.P.) on the IBM 360 computer.

Figures 47 - 51 show a selection of typical results obtained in this way compared with corresponding experimentally observed vibrations over one cycle of the crank.

The vibrations represented in these figures all refer to a mechanism of proportions (5,1,5,2). Similar agreement was found to obtain for the other two linkages examined which were of relative proportions (2,1,2,2) and (10,1,10,4).

Figure 47 shows the resonant vibration observed at speed corresponding to one eighth of the coupler natural frequency. The experimental and theoretical wave-forms show close agreement in phase and amplitude with a small difference in mean level in the second half of the cycle. Figure 48 shows the same general agreement at a higher speed while in Fig. 49, at one quarter of the natural frequency, the amplitudes of all three curves are in very close agreement. At the next resonant speed, the increased amplitudes again agree while one of the computed solutions (the Kutta-Merson method) exhibits a small phase shift in relation to the other over approximately one wavelength of the fundamental vibration. It is evident that, in general, there is better agreement between the experimental curves and the computed curves using the de Vogelaere method than with the Kutta-Merson method.

Figure 51 shows the observed vibration at a non-resonant speed together with two computed solutions, one with damping taken into account and one without. The undamped wave-form shows the expected frequency relationship between the coupler vibration and crank rotation, there being 4.7 vibrations of the coupler per crank revolution, for a speed of $\omega_2 = \Omega/4.7$, and the general nature of the vibration correlates well with that of the adjacent resonant frequencies. Agreement between the damped theoretical wave-form and the observed vibration is poorer than in the previous figures however and is indicative of the partial failure of the assumption that damping is purely viscous. In computing the solutions to the damped equation of motion in this case, a range of values of the viscous damping coefficient was examined and curve shown in Fig. 51 is the

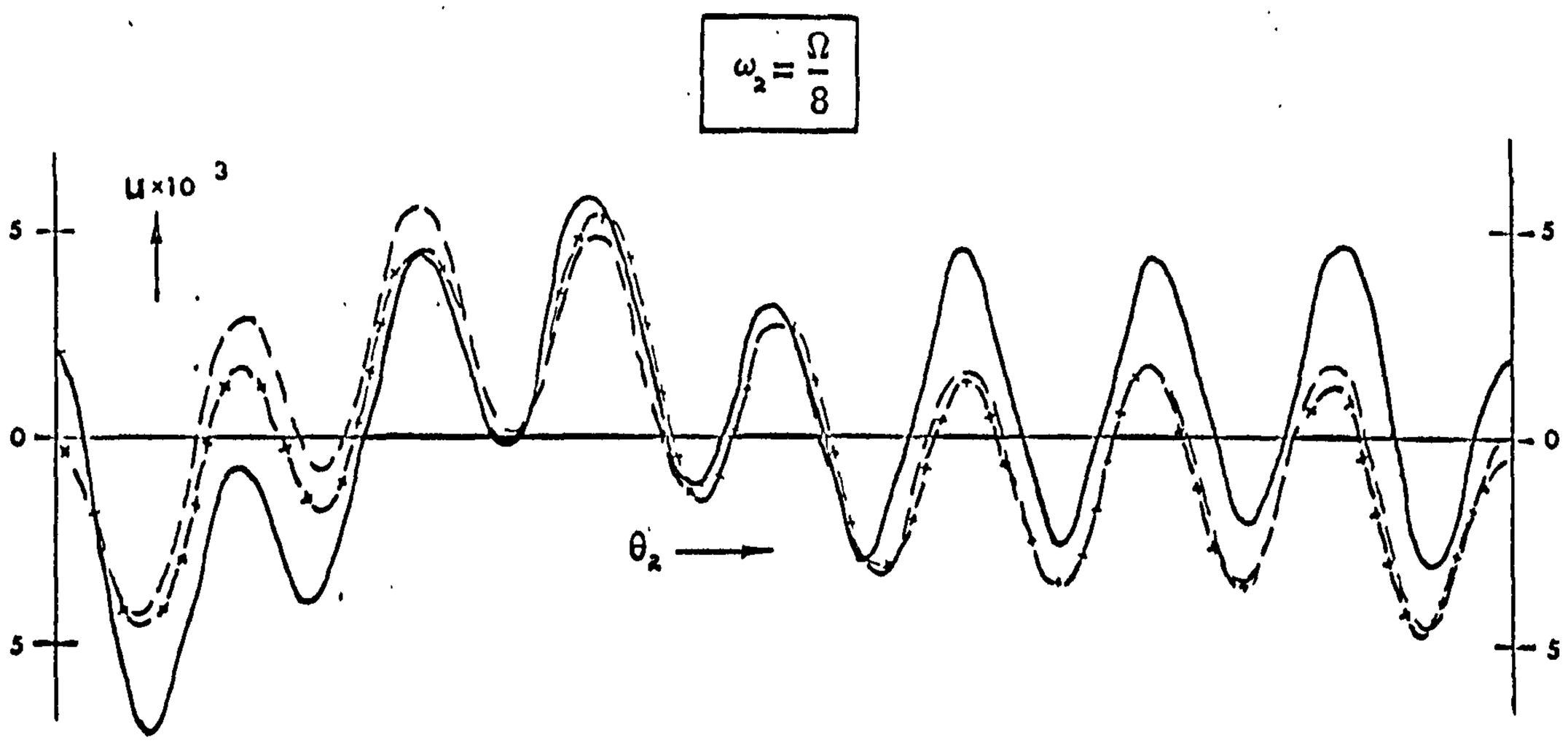

FIG.47. COMPARISON OF THEORETICAL AND EXPERIMENTAL WAVE-FORMS

REPRESENTATIVE RESULTS FOR ONE CRANK CYCLE

——— EXPERIMENTAL

— — — DE VOGELAERE METHOD

—×—×— KUTTA-MERSON METHOD

FIG. 48.

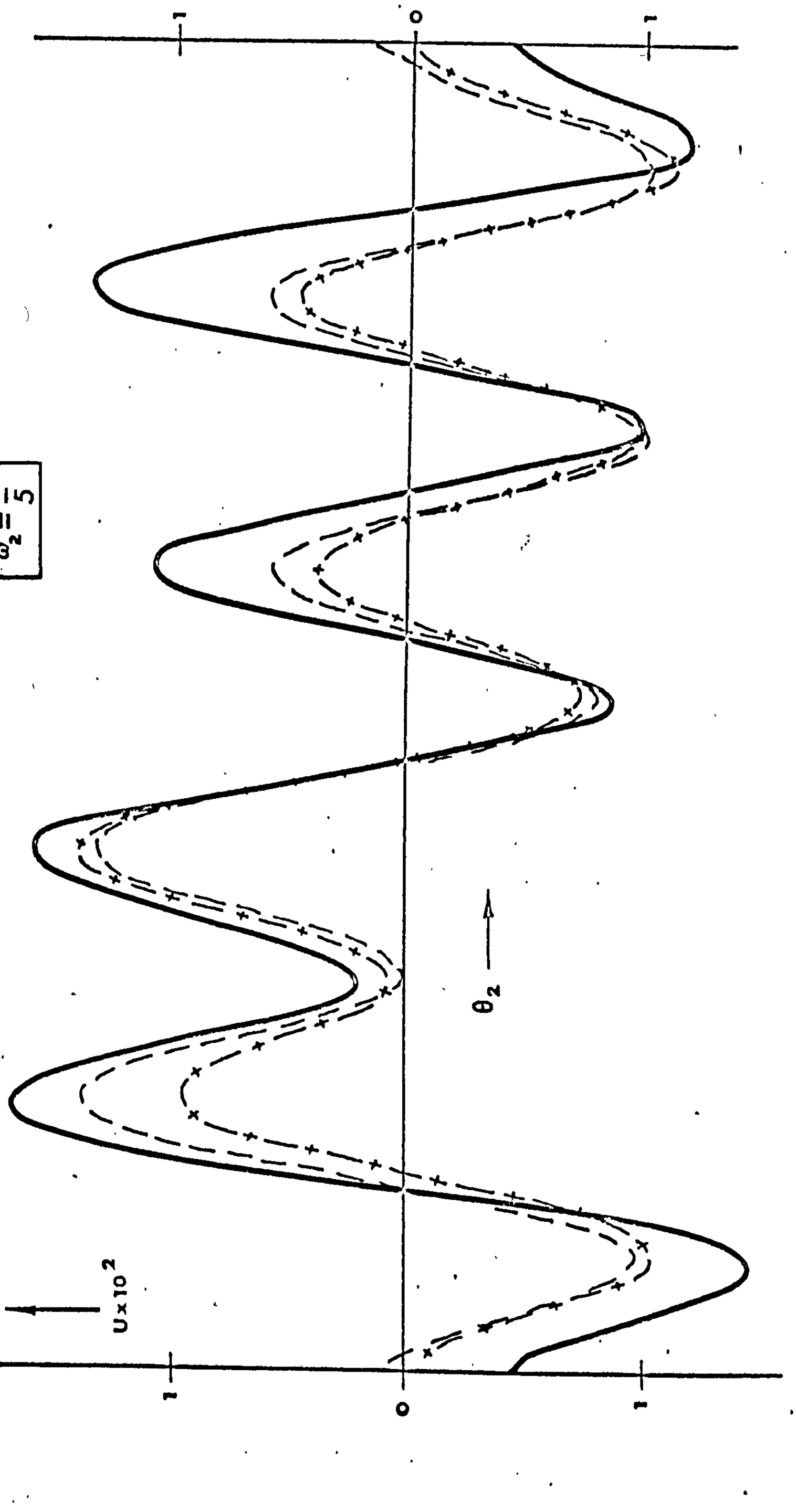

FIG. 49

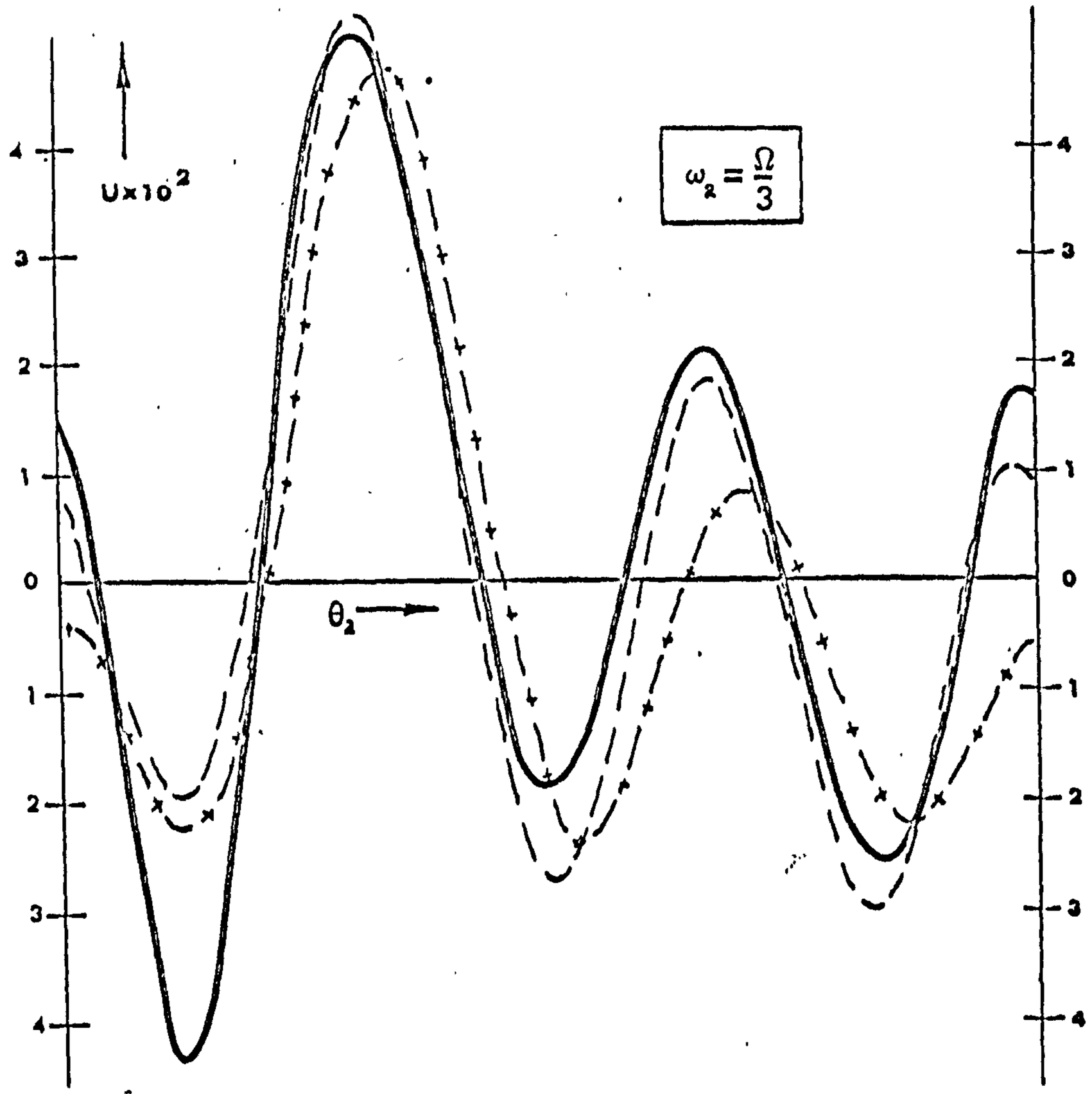
$\omega_2 = \frac{\Omega}{3}$
U×10²
θ₂
4
3
2
1
0
1
2
3
4

FIG. 50

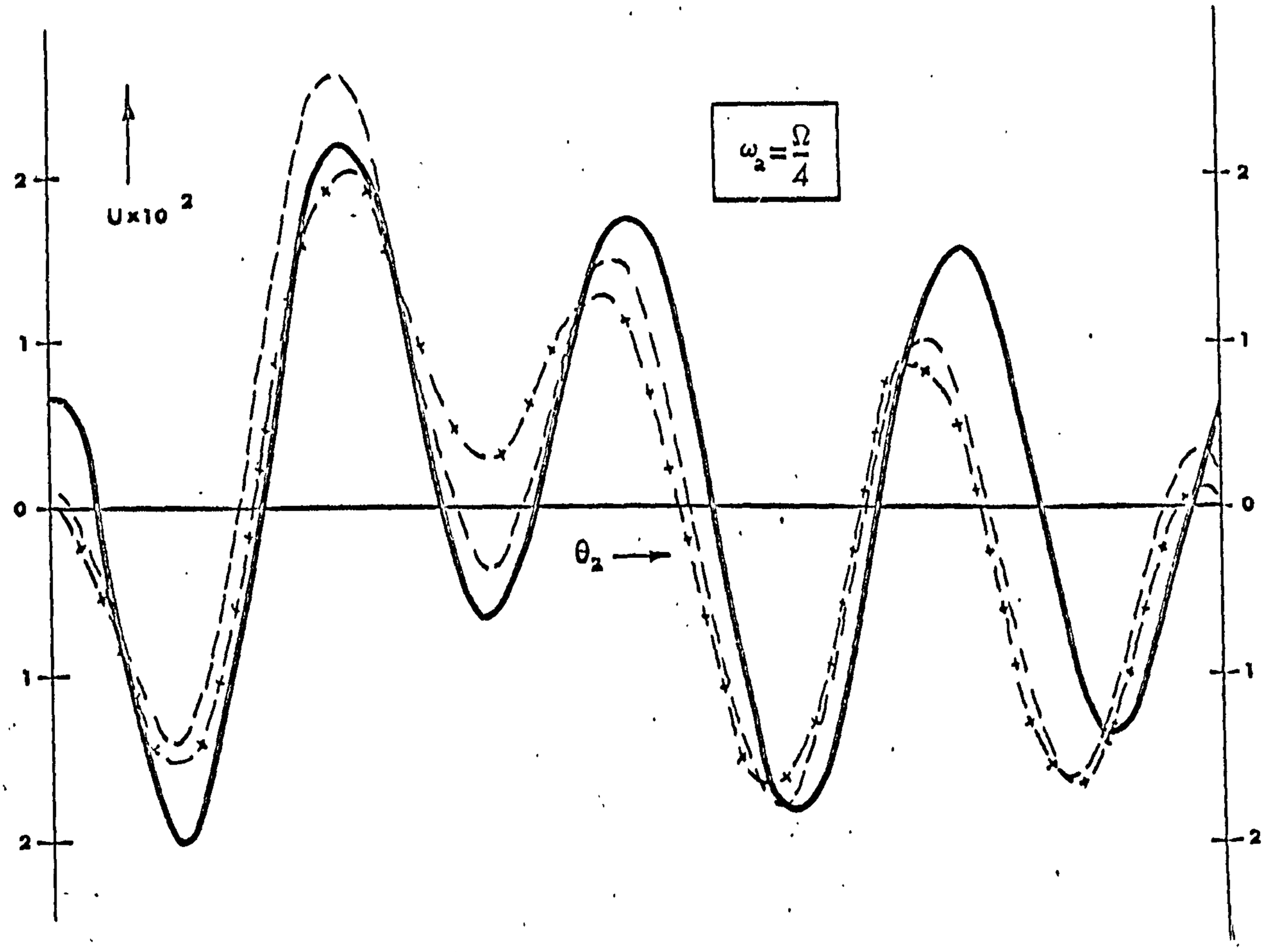
$\omega_2 = \frac{\Omega}{4}$
U×10²
θ₂
2
1
0
1
2

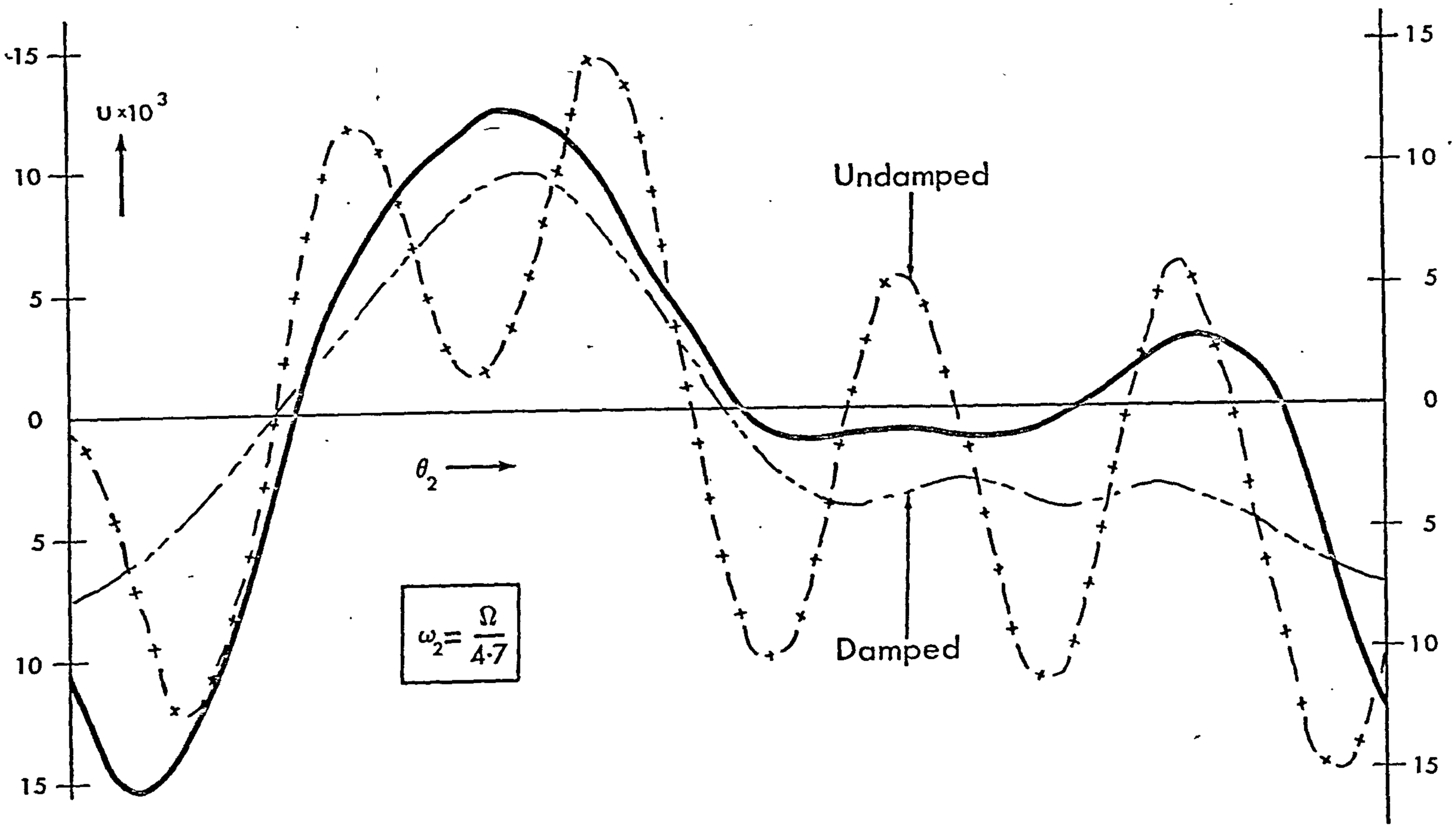

FIG. 51.

best fit obtained. The effects of damping upon resonance and instability will be further discussed later.

One general feature of the experimentally observed vibrations is that there is a tendency for the amplitude to exceed the theoretical amplitudes by a small amount (see for example Figs. 47 and 48). A contributing factor to this divergence is the method of calibrating the vibrational amplitude as has already been discussed.

However, this small effect is not sufficient to detract from the good agreement between all three wave-forms over a wide range of crank speeds.

As has been stated above, three linkages of different dimensions were used in these experiments, one of which has been used to illustrate the type of results obtained. The choice of linkage dimensions has a most important bearing upon the range throughout which resonant vibrations may be observed. If the dimensions are such that the accelerations of the driven links are high, then the inertia forces generated at quite low speeds will be sufficient to excite resonance. In a mechanism of relative proportions (2,1,2,2) for instance, resonant vibrations were detected at speeds down to one sixteenth of the coupler natural frequency. At the other end of the practical speed range however, the amplitude of vibration became too large to allow any sensible measurements to be made in the vicinity of the coupler natural frequency. Choosing dimensions of relative proportions (5,1,5,2), in which the inertia forces are reduced as a consequence of the comparatively lower accelerations, enabled the higher resonant regions to be examined with an accompanying loss of detectable resonance below approximately $\Omega/10$.

It is evident therefore that the choice of linkage dimensions is important not only in providing a wide range of experimentally detectable resonant regions but also in enabling the higher resonant and unstable regions to be examined.

It is customary, when analysing such systems as this, to consider special cases in which the dimensions chosen reduce the equation of motion to a Mathieu equation, viz. the disturbing force is approximated to a harmonic function.

As a consequence of this simplification a great deal of generality is lost at the expense of reduced analytical complexity. Houbon[11,19] for example chooses a crank-rocker mechanism of extreme proportions with which to acquire experimental verification of his simplified equations of motion. Minimal account is given of the experimental work itself, the majority of the two works quoted being concerned with theoretical considerations and analogue computer results.

The use of analogue computers in the examination of the stability of physical systems in which parametric vibrations occur has gained increasing popularity elsewhere. Seevers and Yang[20] for instance, have examined the vibrations of the connecting rod in a crank and slider (a simplified version of the crank-rocker) using analogue methods and produced stability charts in which the onset of instability was determined rather arbitrarily. Viscomi and Ayre[17] also examined the crank and slider in more detail, comparisons being made between the solutions of linearized and non-linearized equations obtained by analogue and digital means. Earlier work by Neubauer, Cohen and Hall[16] deals entirely with digital solutions.

There appears to be little reported experimental work on parametric vibrations in linkage mechanisms in which the forces are not purely or only approximately harmonic. For this reason the dimensions of the linkages examined in the present work were selected so as to preserve the non-harmonic nature of forces while enabling the vibrations to be observed over a reasonably wide range of operating speed. As already mentioned, the choice must be made so as to limit the resonant amplitudes in the high speed ranges which is accomplished to some extent by limiting the accelerations of the links to some acceptable level. This in itself is accompanied by the reduction of higher harmonics in the periodic function appearing in the equation of motion but as has been discussed in Part I, up to ten sine and cosine Fourier coefficients may be necessary to obtain an acceptable approximation to such non-harmonic functions.

The non-harmonic nature of the forces gives rise to non-harmonic responses which themselves create certain problems of interpretation as will be discussed in the next section.

9.5.3 Frequency Responses

The frequency responses of the linkages previously discussed were examined over the ranges of speed in which stable vibrations occurred. The upper limit of the practical speed of operation for the (2,1,2,2) linkage was restricted by the large forced vibrational amplitude and for this reason will not be discussed in detail in this or the next section. Attention will be concentrated on the behaviour of the remaining two linkage configurations (viz (5,1,5,2) and (10,1,10,4)) for which considerably wider speed ranges were obtainable.

The lower limit of the speed ranges examined was fixed arbitrarily at approximately 100 r.p.m. since in the majority of instances resonance could be detected down to this level while observations below this speed were of little relevance to the object of the investigations.

Figure 52 shows a typical "response curve" as obtained on the u-v recorder for the (5,1,5,2) linkage with a coupler of 3/64 in. thickness. A number of resonant frequencies are evident throughout the range shown corresponding to speeds of one tenth up to one third of the coupler natural frequency.

As a consequence of the non-harmonic nature of the vibration, there is apparent an "inner structure" of the trace as obtained with the compressed time scale used here in order to show as large a speed range as possible. Expanding the time scale allows individual resonances to be examined as for example in Fig. 53 which shows resonance near 350 r.p.m. in the (10,1,10,4) linkage. The total amplitude of vibration at speeds higher than this remains substantially constant while the inner amplitude reduces steadily with increased speed. (Values of crank speed ω_2 are shown at the right-hand edge of this and subsequent figures). A further increase in the time scale shows the details of the vibration as has been examined in previous sections. Comparison of the wave-forms at speeds above and below resonance with the resonant wave-form, as in Fig. 54 (for the (5,1,5,2) linkage with $\frac{1}{16}$ in. coupler), indicates clearly the

FIG. 52

(5,1,5,2)

3/64"

I_{MIN}

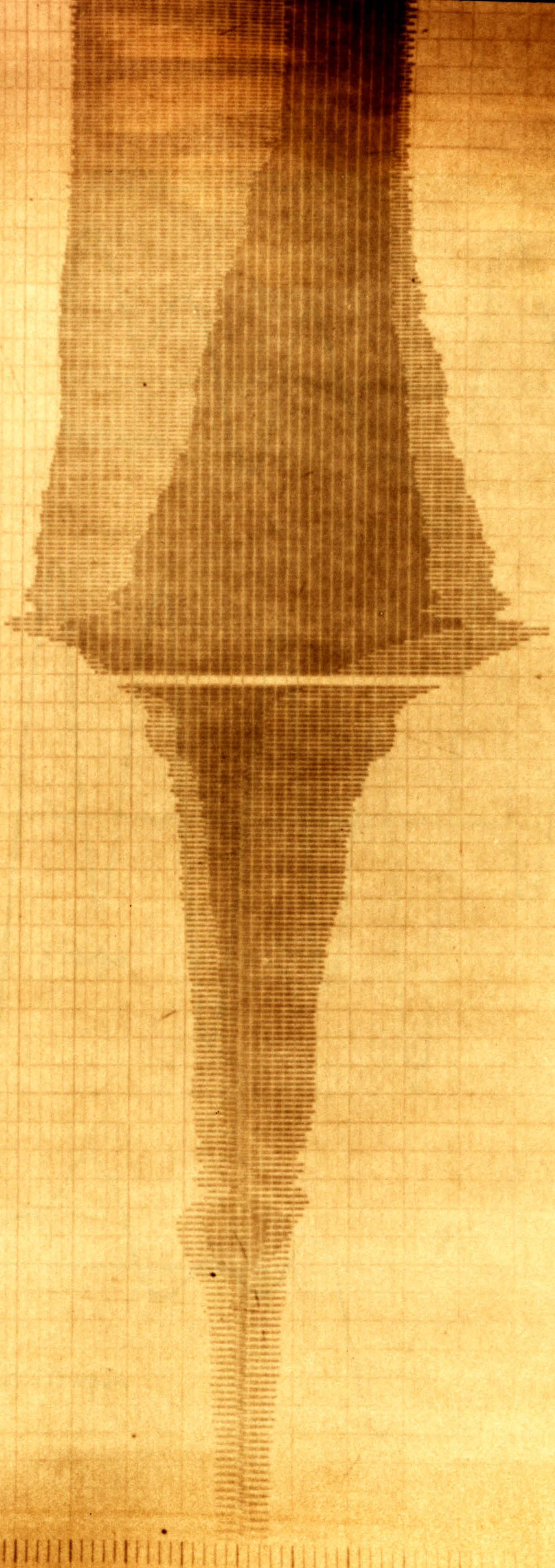

FIG. 53

(10, 1, 10, 4)

1/32"

I = 0.00788

FIG. 54.

CHANGE OF MODE SHAPE THROUGH RESONANCE

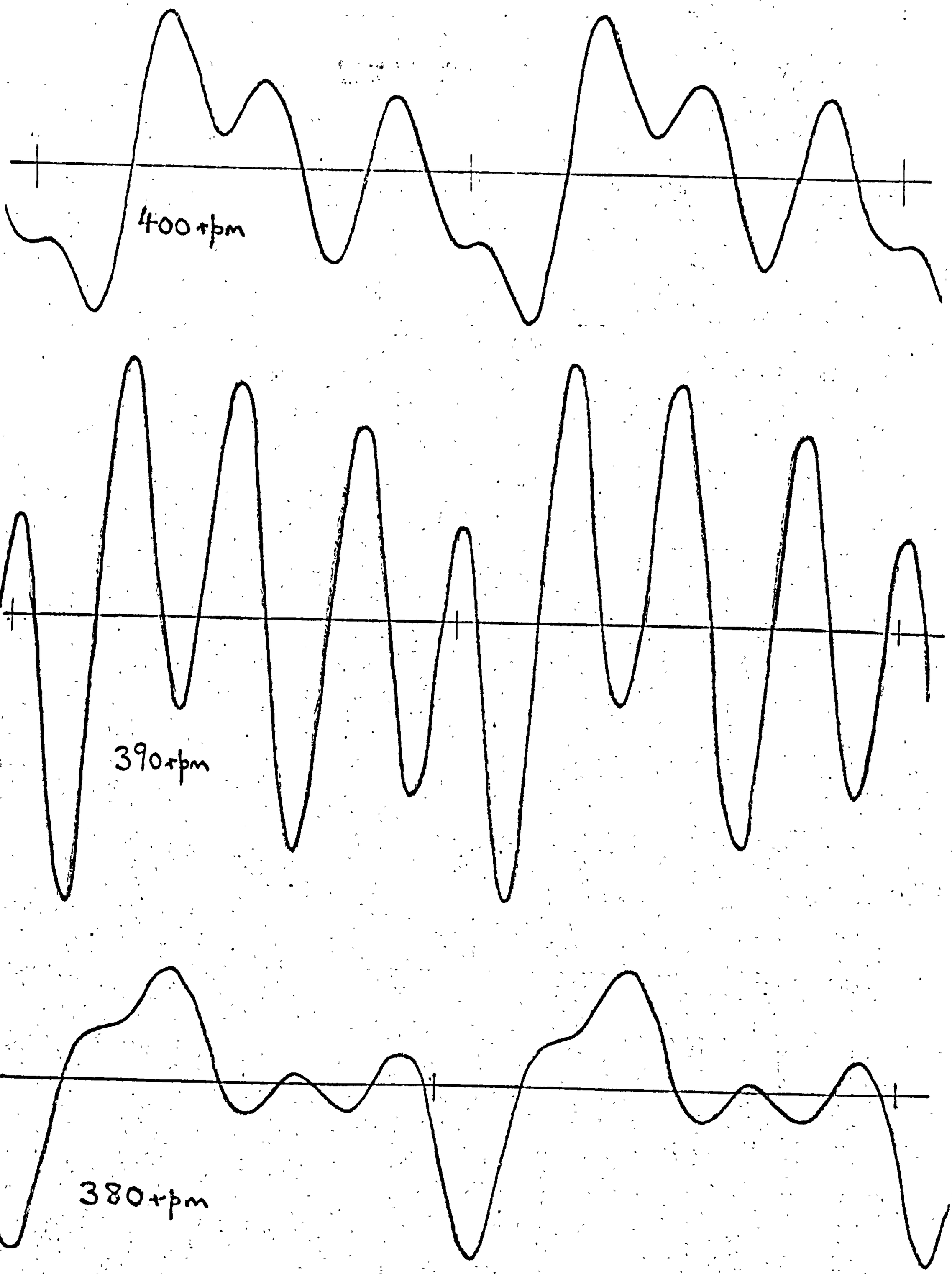

FIG. 55.

Effect of Follower Inertia Upon Coupler Vibration

(5, 1, 5, 2)

230 rpm

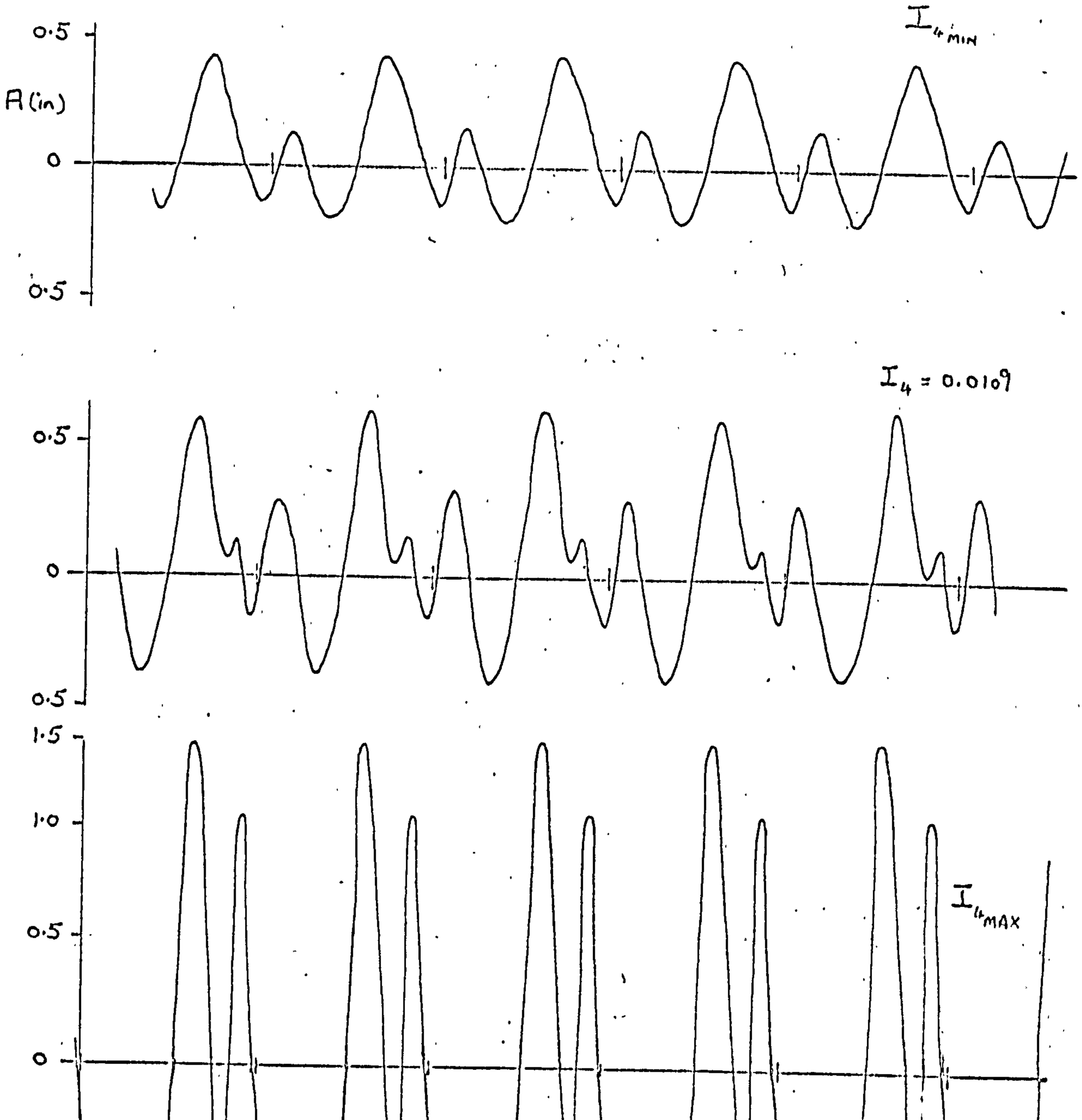

rapid increase in amplitude of the fundamental vibration of the coupler at resonance which brings about a corresponding increase in the total vibrational amplitude. At non-resonant speeds, the reduction in the fundamental vibration together with the changed phase relationship between this and the rotation of the crank, causes a change in the mode of vibration (as indicated by upper and lower traces in Fig. 54). This non-harmonic nature of the coupler vibration in general causes no difficulty in interpretation of the observed wave-forms except in a few isolated cases where the total amplitude attains a maximum value at a speed slightly different from that at which the amplitude of the inner structure attains its maximum. This phenomenon is associated with non-linear characteristics exhibited at higher speeds which will be dealt with below. The sample wave-forms shown in Figures 52, 53 and 54 serve to demonstrate the nature of the non-harmonic vibrations observed in the linkages and their effect upon the appearance of the response curves (Fig. 52). Different examples have been chosen for each of the figures to illustrate the general nature of the phenomenon in all linkage configurations.

In addition to the speed of operation of the linkage, the follower inertia has an important effect upon the coupler vibration. In general, increasing the inertia will increase the end-load on the coupler and produce correspondingly increased vibrational amplitude. The situation is considerably more complex than this however, due to the presence of regions of instability and this very general statement will only apply at speeds for which no unstable vibration occurs. Figure 55 shows the effect of follower inertia upon a stable vibration in the (5,1,5,2) linkage with a coupler of $\frac{1}{32}$ in. thickness and at a speed of 230 r.p.m. At speeds other than this, the vibration may become unstable as inertia is increased, a feature which will be discussed in the next section.

The experimentally obtained response curves for the (5,1,5,2) linkage with the thinnest coupler are shown in Figs. 56 - 61. The same sensitivity is used throughout so that resonances at the lower end of the speed range are less evident here than at the higher sensitivities which were used for the determination of these lower resonant speeds. Nevertheless the figures serve to

demonstrate the behaviour of the coupler over the particular speed range. For low values of follower inertia, the responses show a well-defined resonance near $\omega_2 = 250$ r.p.m. corresponding to the third sub-harmonic frequency. This resonance occurs at progressively lower speeds as the inertia increases being observed near $\omega_2 = 220$ r.p.m. for $I_{4\ MAX}$ (Fig. 61).

At higher speeds there is, with $I_{4\ MIN}$ (Fig. 56) a small rise in amplitude near $\omega_2 = 300$ r.p.m. which becomes a most considerable increase in amplitude following a single increment in follower inertia (Fig. 57). For higher inertia values, the vibration displays a non-periodic nature in the range 260 - 280 r.p.m. This is equivalent to the region of instability around $\omega_2 = \frac{2}{5}\Omega$ which will be considered in the next section.

Figures 62, 63 and 65 show a selection of similar responses for the (10,1,10,4) linkage, again with a coupler of $\frac{1}{32}$ in. thickness. Resonant amplitudes are, in general, smaller than the previous example due to the reduced inertial loads in the linkage. This allows correspondingly higher resonant regions to be examined with interesting results.

Figures 62 and 63 show the response of the (10,1,10,4) linkage with minimum follower inertia from 300 r.p.m. up to approximately 530 r.p.m. the vertical scale being continuous from Fig. 62 to Fig. 63. The resonances at 360 r.p.m. is clearly different in character from that in the region of 460 r.p.m., the latter being somewhat less "regular" in appearance than the former. Closer examination of the wave-form at 460 r.p.m. reveals that the periodicity is 4π (viz. two crank rotations per cycle of coupler vibration) as shown in Fig. 64. As described in Chapter 7, such a periodicity may be expected when $\Omega/\omega_2 = n/2$ if n is an odd integer. At this speed we are observing the vibration in the third region of instability ($n = 3$) corresponding to a crank speed of the order of two-thirds of the coupler natural frequency ($\omega_2 = 2\Omega/3$). The damping present in the system is sufficient to render the vibration stable although it is possible that if the linkage were to be run at this speed for some time, then the amplitude may be expected to increase exponentially. Under the conditions obtaining when the vibrations in Fig. 63 were observed, the crank speed was

slowly increasing so that a stable region was entered ($\omega_2 \geq 480$ r.p.m.) before any such instability occurred.

Figure 65 shows the response of the linkage for a slightly increased follower inertia. The resonance at 360 r.p.m. (corresponding to $\Omega/2$) is still present but now the vibration is unstable above 450 r.p.m. The damping present is no longer sufficient to stabilise the motion.

An interesting feature of the resonance at $\Omega/2$ is the non-linear character displayed in Figs. 62 and 65. The figures referred to so far have all been obtained with an increasing crank speed i.e. vibrations have been recorded by increasing the crank speed slowly from zero up to the practicable maximum. If however, the higher resonant regions are examined by decreasing through the resonant frequency, the non-linear character of the vibration becomes much more apparent. Figures 66 and 67 show the effect of decreasing the crank speed from 500 r.p.m. to below 300 r.p.m. Conditions are otherwise as for Figs. 62 and 63 (there is however a considerable overlap between Figs. 66 and 67 in order to show each region in its entirety. Figure 68 shows the analogous case applicable to conditions obtaining in Fig. 65.

The two speed ranges of interest in this particular case correspond to the $\Omega/2$ resonant region and the $2\Omega/3$ unstable region. In the former, instability is also possible whereas in the latter resonance does not occur. For this reason the characteristics of the vibration differ in certain respects, the main difference being the periodicity of the vibration. As has been shown, vibration in the unstable region has a period equivalent to two crank rotations and this is immediately obvious from Figs. 65 and 66. The shapes of the response curves are typical of a non-linear softening spring characteristic showing a rapid rise in amplitude followed by a gradual decrease when speed is increased through resonance and a gradual increase to a greater amplitude followed by a rapid fall when speed is decreased through resonance. Since the vibration near $2\Omega/3$ cannot strictly be described as a resonance, one must take care to distinguish between the inherent instability of the system under these conditions and the non-linear resonance with its own different type of

instability near $\Omega/2$. It is not intended in this thesis to examine in great detail the non-linearity of the vibrations in the higher speed ranges; its presence is merely demonstrated and commented upon. To illustrate the non-linearity more clearly, the responses in Figs. 62, 63 and 67 are plotted in the more conventional manner in Fig. 69. The amplitude values are peak-to-peak amplitudes taken directly from the u-v recorder traces, viz. no account is taken here of the calibration so that the figure does not strictly represent the amplitude of the coupler. However, this is of minor importance since the figure is itself meant solely as an illustration of the non-linear nature of higher resonances, in which the solid line drawn through the experimental points has no theoretical basis.

One further interesting aspect of these non-linear resonances is the oscillation in amplitude level observed in certain cases after the resonant frequency is passed. Figures 70 and 71 show such a case (the (5,1,5,2) linkage with $\frac{1}{16}$ in. coupler) in which the amplitude oscillates as the crank speed is raised and lowered through the $\Omega/3$ resonant region. This phenomenon is described by Bogoliubov and Mitropolsky[36] and is a consequence of the non-linear nature of the "stationary" response curve. By this latter term is meant the amplitude-frequency relationship obtained with a fixed frequency. The response of the system as obtained by the raising or lowering of the frequency though any particular resonant region will differ from the "stationary" response in important respects. Not only is there an oscillation of the observed amplitude whose frequency depends upon the rate of change of the forcing frequency (in this case the crank speed) but the maximum amplitudes will occur at frequencies different from those corresponding to the maximum "stationary" amplitudes. The governing factor here is again the rate of change of the forcing frequency and consequently the detailed examination of such non-linear phenomena is a most involved process. No attempt has been made here to analyse the system; the responses shown in Fig. 70 and 71 are presented only to demonstrate the nature of the phenomenon. Also evident in these figures is

a small change in mean level through the resonance which is a consequence of the change in mode shape as has been discussed above.

The frequency response of each linkage may be shown in terms of crank speed and follower inertia (rather than vibrational amplitude) on a stability chart in which no indication of amplitude is given. The presence of a resonance is indicated by a point appropriate to the speed at which it is detected for a particular value of follower inertia. In this way a concise picture may be built up to indicate the behaviour of the coupler in any linkage. The theoretical values of crank speed at which resonance may be expected are obtained, for the lower speeds, directly from determination of the natural frequency of the coupler. In the higher speed ranges the location of the regions of instability becomes important and the stability theory must be used to locate the relevant boundaries. The coupler natural frequencies were determined by calculation based upon stiffness measurements as previously described and also by observation of the damped free vibrations in situ. Figure 72 shows the damped free vibration of a 1/16 in. coupler from which the frequency is determined as 26 Hz, which is within 2% of the calculated value of 26.5 Hz, and correlates well with the speeds at which the sub-harmonic resonances were detected.

In Fig. 73 the corresponding vibration of a 3/64 in. coupler is shown from which the natural frequency is found to be 20 Hz. A selection of responses for this thickness of coupler in the (5,1,5,2) linkage is given in Figs. 74 - 78. The first of these shows the response over the range 200-600 rpm, at low sensitivity, in which the $\Omega/4$, $\Omega/3$ and $\Omega/2$ resonances are seen together with an apparent resonance in the $2\Omega/5$ unstable region. An unsymmetric resonant vibration is evident near 600 rpm ($\frac{\Omega}{2}$) which is due once again to the onset of the one-half subharmonic resonance, the mean level of which differs from the undeflected position. Figure 75 demonstrates, more clearly at increased sensitivity, the increase of forced amplitude with speed together with the superimposed resonances at 300, 400 and 500 rpm. Figure 76 shows the resonance detected at the lower speeds at a further increased sensitivity, an even higher

sensitivity being required for accurate determination of the speeds at which resonances occur below 150 rpm. At the other end of the speed range, there is again evidence of non-linearity of the response (Fig.74). Further examination of the vibration near 500 rpm (Figs 77, 78) shows again the typical "softening spring" characteristic as has already been described.

The final figuresin this section (Figs. 79, 80) show the response of the (5,1,5,2) linkage with 1/16 in. coupler over the speed range 200-900 rpm at one sensitivity setting, the vertical scale being continuous with slight overlap between the two figures. The large resonance in the centre of Fig. 80 is the one-half subharmonic resonance, the motion becoming unstable in the $2\Omega/3$ region above 900 rpm.

In this section, the frequency responses of couplers of three thicknesses have been examined in two linkages of different dimensions. A selection of the experimentally obtained responses has been shown to illustrate the nature of the observed vibrations together with some qualitative discussion of non-linearities observed at the higher speeds. Some consideration has inevitably been given to instability where appropriate and this will be discussed further in the following section.

2.5.4 Instability

The stability characteristics of the linkages are necessarily very closely associated with the response characteristics of the forced vibrations. Whereas the stability of such systems may be theoretically divorced from the forced vibration by considering only the homogeneous equation of motion, it is not possible to separate the two practically for experimental purposes except in certain specialised and simplified cases. As has been seen in the foregoing section, the non-linear nature of some of the higher resonances produces an instability which is characteristic of the "softening spring" type of response (Fig. 69). This instability differs in nature from parametric instability in that there is always a finite amplitude of vibration. The instability arises as a result of the possibility of there being either two or three different

vibrational amplitudes within certain speed ranges. In the case of parametric instability characteristic of Hill's equation, the vibrational amplitude increases exponentially in accordance with theory. In practical cases the vibration may be limited by damping in the system or, if the damping is insufficient to stabilise the motion, failure of one or more components may result.

The nature of parametric instability in the linkage mechanisms examined has already been described briefly in the previous section since it has usually been this which forms the upper speed limit of the frequency responses. Examination of the vibrational wave-form has shown that the periodicity is 4π (two crank cycles) in regions of (theoretical) instability where damping is just sufficient to stabilise the motion. In a number of instances it has been possible to increase the speed of operation of the linkage past such unstable regions so as to attain the next stable region (see for example Fig.58). Under different conditions however, instability may occur almost instantaneously with complete loss of periodicity of the previously stable vibrations. Figure 81 shows such an example. Crank speed is increased slowly in the stable region between the $2\Omega/5$ and $\Omega/2$ unstable regions. As the boundary of the latter region is crossed, the amplitude of vibration increases rapidly by approximately 300% and the motion of the linkage becomes violently unstable. In a number of such cases examined, the couplers became strained beyond the elastic limit due to the excessive amplitudes imposed upon them, whereas in other instances, the linkages could be stopped before such damage occurred. In these latter cases, instability was normally detected by direct observation of the linkage. In addition the change from periodic stable vibration to aperiodic unstable motion could be readily detected audibly and this was a further aid to the rapid reduction of crank speed to prevent undue damage to the linkage.

The majority of the information contained in the frequency response figures discussed in the previous section is given in condensed form in the stability charts shown in Figs. 82-87. A separate chart is shown for each linkage-coupler combination. It is possible to condense the results still

further onto two stability charts, one for each linkage, however the presentation of each set of results separately greatly clarifies the nature of the stability of the corresponding linkage-coupler arrangement. A combined non-dimensionalised chart which, while emphasising the point that the stability boundaries are determined entirely by the linkage dimensions, would create an unnecessarily complicated picture of the results.

The stability charts are plotted in terms of the crank speed ω_2 and follower inertia I_4. Also shown on the ω_2-axis are fractional values of the natural frequency Ω corresponding to resonant and unstable regions. The stability boundaries of regions in which true resonance may also be expected (i.e. for $\omega_2 = \frac{\Omega}{n}$) are indicated by dashed lines whereas those unstable regions in which no resonance may occur (i.e. for $\omega_2 = \frac{2\Omega}{n}$, n odd) are shown by much shorter dashes. Only one or two of these latter regions are indicated since damping effectively eliminates all but the highest.

These theoretical stability boundaries are calculated for the simplified equation of motion (equation (6.18)) in which the periodic terms which are functions of the coupler inertia and mass distribution are neglected with respect to the follower inertia term. In the linkages examined here, the coupler-dependent terms were all at least one order of magnitude smaller than the follower-dependent term, even for the minimum value of the latter. The boundaries of lower speed regions are given a preference to those of the adjacent higher speed regions in accordance with the theory since the intrinsic value of the parameter λ^2 will be greater for the lower speed boundaries.

Each point at which resonance was detected is represented by a circle while instability is indicated by a triangle. For some of the higher resonant regions, two circles are shown corresponding to the speeds at which resonance was detected with increasing and decreasing crank speed. As has been pointed out above the speeds at which maximum amplitudes occur in such non-linear resonant regions will be determined by the rate of change of crank speed. No attempt was made to examine this phenomenon in detail however and since this particular

effect is of little consequence to the detection of resonance, the results are presented on the stability charts to give some indication of the extent of the non-linearities present in the higher resonant regions.

In Fig.82 it may be seen that the $\frac{2\Omega}{7}$ unstable region is detected only for higher values of follower inertia. With the maximum inertia, instability occurs in this region but the proximity of the $\frac{\Omega}{3}$ region may also have some effect. The speeds at which unstable motion occurs in the $\frac{2\Omega}{5}$ region show good agreement with the theoretical curves, as do the two points, for lowest values of inertia, approaching the half-speed resonant region. By comparison, Fig.83 indicates a greater degree of damping present in that there is no experimental indication whatever of the presence of the $\frac{2\Omega}{7}$ region of instability. In addition instability in the $\frac{2\Omega}{5}$ region is only induced by increased inertia and it is poss ible to detect both sides of the half-speed resonant region, albeit for only one value of follower inertia. A similar pattern is seen in Fig.84 with the upper boundary of the $\frac{2\Omega}{5}$ region being detectable.

In all of the cases described above, i.e. for the (5,1,5,2) linkage, the highest observable region is the half-speed subharmonic resonance. In this region not only is there forced resonance present but there is the possibility of instability occurring. An increased amplitude in this region will therefore be inevitable whereas the onset of unstable vibrations depends upon the level of damping present. The adjacent region however is one of instability only, no resonance being expected at a speed between one half and one third of the natural frequency. The observation of any apparent resonance for low inertia values or instability for higher inertia values is therefore evidence in support of the theoretically predicted stability boundaries. In two of the three examples presented, this is the only non-resonant unstable region detected. In the third, the next lowest region ($\omega_2 = \frac{2\Omega}{7}$) is detected for the larger inertia values. The damping present in the linkages is sufficient to suppress all lower unstable regions within the range of inertia examined so that only the resonant regions ($\omega_2 = \frac{\Omega}{n}$) are observable at lower speeds.

By reducing the inertia forces in the linkage, it is possible to examine higher regions of instability since the accompanying resonant vibration will also be reduced. The (10,1,10,4) linkage stability charts are shown in Figs.85-87 from which it is seen that the $\frac{2\Omega}{3}$ region is now attainable. The highest region examined in these examples is now a true region of instability having no associated resonance. A consequence of the change of dimensions of the linkage is a narrowing of the regions of instability so that it is correspondingly simpler to cross, for example, the half-speed resonant region for any particular value of inertia. In addition, the effects of damping will be correspondingly greater and this too facilitates the examination of the higher unstable regions.

In Fig.85 the $\frac{2\Omega}{5}$ unstable region is detected for some of the higher inertia values only. (Compare this with Fig.82 in which it is observed throughout the whole range of inertia values). The non-linearity of the half-speed resonances is observed for the lower inertia values, the experimental "width" of the region agreeing quite well with the theoretical curves as in all other cases for the $\frac{\Omega}{3}$ resonance. With increased inertia, the $\frac{\Omega}{2}$ region becomes unstable with the experimental points lying close to the theoretical boundary. Similarly, in Figs. 86 and 87 the $\frac{\Omega}{2}$ region becomes unstable for the higher values of inertia while a few points indicate the presence of the $\frac{2\Omega}{5}$ region. In Fig.87 (the thickest ecupler) instability occurs on the high speed side of the $\frac{\Omega}{2}$ region which, for higher inertia values, lies close to the $\frac{2\Omega}{3}$ region. In this region too, instability occurs on the high speed side for low inertia values, an increase in amplitude being noted at the low speed side.

In the majority of cases then, the experimental points lie close to the theoretical stability boundaries. In the case of the (10,1,10,4) linkage especially, the detection of apparent resonance or instability in the region of $\omega_2 = \frac{2}{3}\Omega$ is a satisfactory justification of the theoretical predictions, more so perhaps than in the case of the (5,1,5,2) linkage where the upper limit is near $\omega_2 = \frac{\Omega}{2}$ where large resonant amplitudes would also be expected. A few

points may be seen to lie above the upper unstable regions examined (Fig.84,85,87) rather than on the boundaries of those regions. All of these points were detected with low values of follower inertia there being only an increased amplitude rather than instability noted as the highest observable region was passed. Since instability then occurred at speeds much below the next unstable region in the case of the (10,1,10,4) linkage, the most probable explanation for this is that the greatly increased amplitude produced at this high speed caused failure of the coupler. A high-speed ciné film of the linkage at the point of becoming unstable showed the behaviour of the coupler in greater detail. A selection of frames from this film is shown in Figs.88 and 89. Initially, the coupler vibrates in a stable periodic manner until instability occurs. The amplitude then increases rapidly and higher modes of vibration may be seen (in the examples shown both the second and third modes are visible). Under such conditions of excessively large amplitude, the follower may "snap through" so that the linkage takes up its alternative orientation (viz. the alternative position in which coupler and follower may be corrected. See Fig.3 and last frame of Fig.89.). When examining the behaviour of the thinnest coupler under such conditions, it was found that such "snap-through" changes occurred in an apparently random fashion while the motion remained unstable. A reduction in speed restored the stable vibration of the coupler despite the over-straining to which it had been subjected during the "snap-through".

9.5.5 Damping

The effect of damping upon the stability has been mentioned briefly in a qualitative manner in this and the previous section. In Chapter 7 the effect of damping upon the theoretical stability charts has been examined, the nature of damping being assumed to be purely viscous. As we have seen, this is not often the only type of damping present in practice and indeed in the present system, there will be frictional and viscous damping in the coupler bearings in addition to the internal damping of the coupler itself.

The estimation of the damping affecting the free vibration of individual couplers is a comparatively simple task in the stationary case and Figs.72 and 73

show typical damped vibrations. Measurement of the logarithmic decrement of such vibration gave values of between 0.15 and 0.30 for the $\frac{1}{32}$ in. coupler, between 0.10 and 0.27 for the $\frac{3}{64}$ in. coupler and a much lower value of 0.05 to 0.10 for the $\frac{1}{16}$ in. coupler. These values serve merely to indicate orders of magnitude since the conditions under which the coupler vibrates while the linkage is in motion differ greatly from those obtaining with the linkage stationary. Not only are the journals rotating at varying speed in the coupler bearings but the loads on these bearings are also varying. The estimation of effective damping in such a situation is an extremely difficult practical problem and will not be persued at length here. One method of obtaining some rough estimate of damping in the linkages is to examine the stability charts and attempt to locate the appropriate damped stability boundary for a number of unstable regions. In Chapter 7, a first order estimation of the minimum value of the parameter μ is obtained below which motion will be stable for any given value of the damping coefficient K. Examination of, for example, the $\frac{2\Omega}{5}$ unstable region in Fig.82 shows that the motion becomes unstable when follower inertia is increased from 0.0069 to 0.0079 lbf. in. sec^2. The appropriate damped stability boundary must therefore lie between these two points and working from this assumption, it is possible to deduce an approximate value of the corresponding damping coefficient. In this case the value of K obtained is 0.02. Applying the same reasoning to the $\frac{\Omega}{5}$ region, a value of 0.01 results. Obviously such approximations can only be used as a very rough guide to indicate the level of effective damping since the calculations involved are subject to a number of widely differing assumptions. There does appear however to be some consistency in these figures to within less than an order of magnitude. The $\frac{\Omega}{2}$ and $\frac{2\Omega}{3}$ regions in Fig.85, for instance, yield values for the damping coefficient of 0.005 and 0.02 respectively.

In general, the accurate determination of the effective damping in such mechanisms as have been examined here is not of prime importance. The major problem is usually the location of the boundaries of the unstable regions and the presence of any damping is advantageous in reducing the size of those

regions in addition to having an overall stabilising effect upon the system. As has been demonstrated by reference to the stability charts, vibrations in a region of instability (not accompanied by a resonant region) can behave in a manner similar to those of non-linear resonant regions in so far as increased amplitudes will be produced over a range of operating speed. For this reason, the main aim of the analysis and accompanying experimental work is the prediction and detection of those areas on the stability charts in which large resonant or unstable vibrations may be expected. If in practice the unstable vibrations are limited to areas smaller than expected, due to the presence of damping, then this may be taken as a benefit to the theoretical predictions since one is then given a wider choice of stable conditions in which any particular mechanism may operate.

9.6 Summary, Conclusions and Suggestions for Further Work

The experimental work described in this chapter has been concerned solely with the verification of the theoretical work developed in Part III of this thesis. The equation of motion of the flexible coupler in a crank-rocker linkage has been derived in Chapter 6 and some consideration has been given to methods of solution by digital computation. Appendix 4 lists a programme suitable for this task and sample results have been presented together with experimentally observed wave forms which show good agreement with this and an alternative computer solution.

Chapter 7 deals with the determination of the location of the stability boundaries in terms of the operating speed of the mechanism and a parameter which is a function of the follower inertia. Experimentally obtained results show close agreement with the theoretical stability boundaries for the simplified equation in which coupler-dependent terms are neglected. These terms may be neglected in the present situation as a consequence of the choice of linkage dimensions which renders them small in comparison with the follower-dependent term. The periodic coefficients in this simplified equation are however not replaceable by harmonic functions as has been done by other workers (Neubauer et al[16], Houbon[19] and Meyer zur Capellen[14]). The analysis

is therefore correspondingly more prolonged due to the large number of Fourier terms which must be retained in order to obtain an acceptable approximation to these periodic functions.

Chapter 8 examines the stability of Hill-type equations with more than two independent parameters which appears to have received little attention elsewhere. Certain difficulties arise in the application of standard perturbation techniques and a modified method is proposed which works well to a first approximation.

Further work is desirable on problems of this type either by extension of existing perturbation analysis methods or by alternative means. The full linearised equation of motion for the coupler vibration contains four periodic terms (five independent parameters) and is thus a most difficult equation to analyse fully.

One additional aspect of the theory which is highlighted by the experimental work is the non-linear nature of the resonances at higher speeds. This has been described qualitatively but no quantitative work has been attempted. An examination of the non-linear terms in the full equation of motion may lead to a more thorough understanding of the characteristics of the coupler vibration at high speed (i.e. above approximately $\Omega/3$). Viscomi and Ayre[17] have reported some work on a closely associated problem using analogue computer techniques but there appears to be a lack of any experimental work on this topic.

The recording of the coupler vibrations by high-speed ciné film brought to light the presence of higher modes of vibration at the onset of instability. No evidence of the existence of these modes was found under stable conditions but it is possible that their presence may have important effects upon the stability characteristics in some cases. Again, no experimental work appears to have been reported while some theoretical analysis has been carried out by Seevers and Yang[20] who examine the effect of the second mode.

Among those working on various aspects of vibrations in linkage mechanisms, it has been almost universal practice to consider only vibrations in the plane of the mechanism. In many practical cases this is the mode of vibration most likely to be encountered and for this reason many mechanism links are

constructed to withstand bending in this plane while being comparatively flexible in the plane perpendicular to that of the mechanism. Vibrations in this plane are therefore worthy of examination, the corresponding equation of motion being similar to that which has been examined here but differing in some interesting respects in that certain terms are absent. The investigation of such vibrations would form an use parallel to the present work.

The majority of this section has concentrated on the content of Part III of this thesis since the content of Parts I and II are comparatively well known and have been investigated thoroughly. There are still however one or two aspects of mechanism dynamics worthy of further study in connection with the present work and these are listed below together with the topics previously mentioned.

Suggested topics for further study

1. Investigation of the effect upon stability of the presence of higher modes of vibration in the coupler.
2. Further examination of the non-linear terms in the equation of motion and their effect upon high-speed resonances.
3. Development of techniques for the analysis of Hill's equation with more than two independent parameters.
   (This may be considered a purely mathematical problem but it has a direct bearing upon problems such as that investigated here)
4. Examination of out-of-plane bending of mechanism links (especially the coupler).
5. Optimisation of pin-forces and torques in general planar linkage mechanisms (e.g. Reduction of pin-forces by change of mass distribution of individual links while avoiding accompanying increase in torque).

6. Examination of the effects of springs, flexible elements, balancing and possibly backlash in any combination to achieve special objectives (e.g. The reduction of the effects of clearance by the addition of springs).

FIG. 56

(5, 1, 5, 2)

1/32"

I = 0.0069

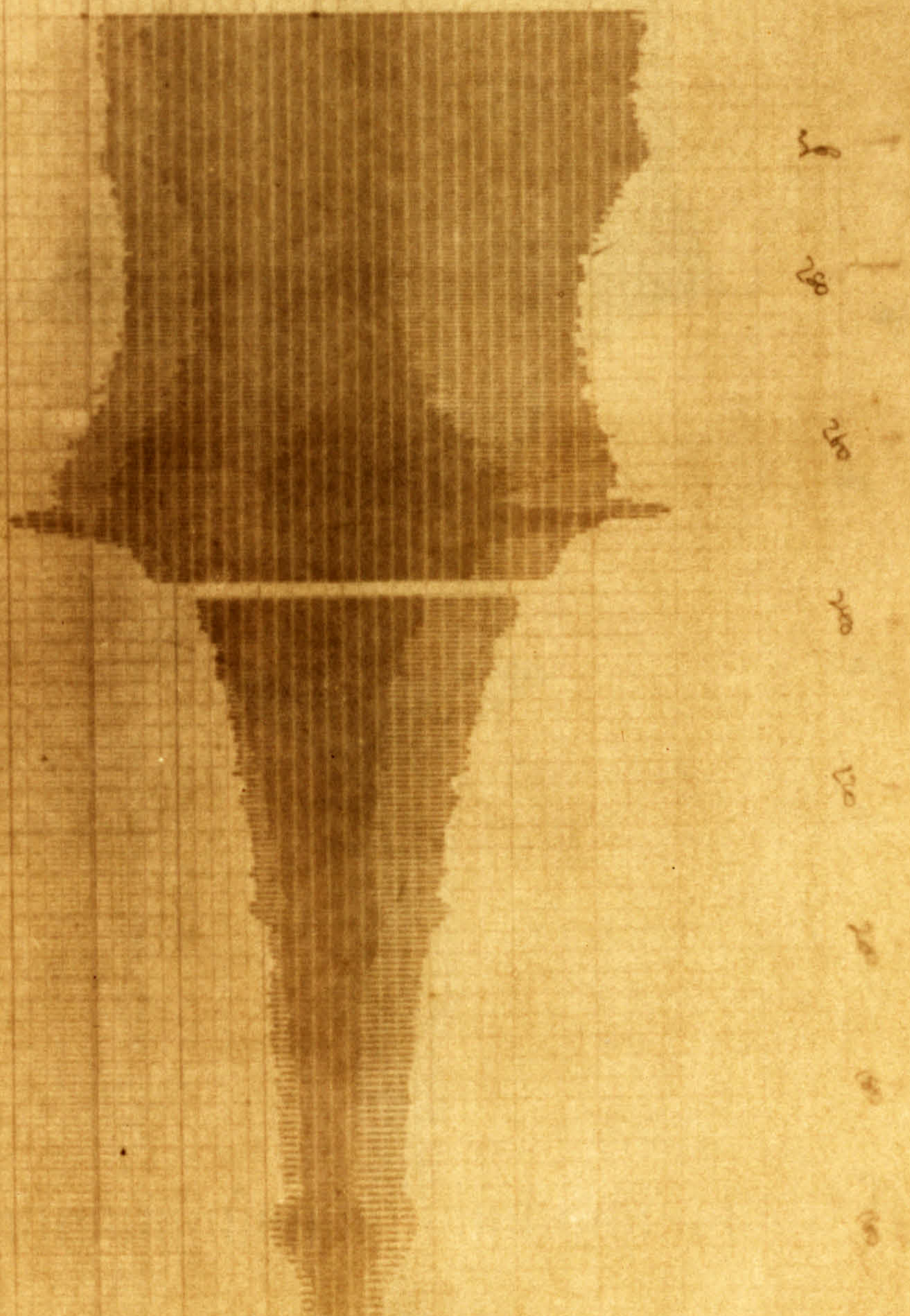

FIG. 57

(5,1,5,2)

1/32"

I = 0.0079

FIG. 58

(5.1, 5.2)

1/32"

I = 0.0109

FIG. 59

(5, 1, 5, 2)

1/32"

I = 0·0130

FIG. 60

(5, 1, 5, 2)

1/32"

I = 0.0149

FIG. 61

(5, 1, 5, 2)

1/32"

I_{MAX}

FIG. 62

(10, 1, 10, 4)

1/32"

I_{MIN}

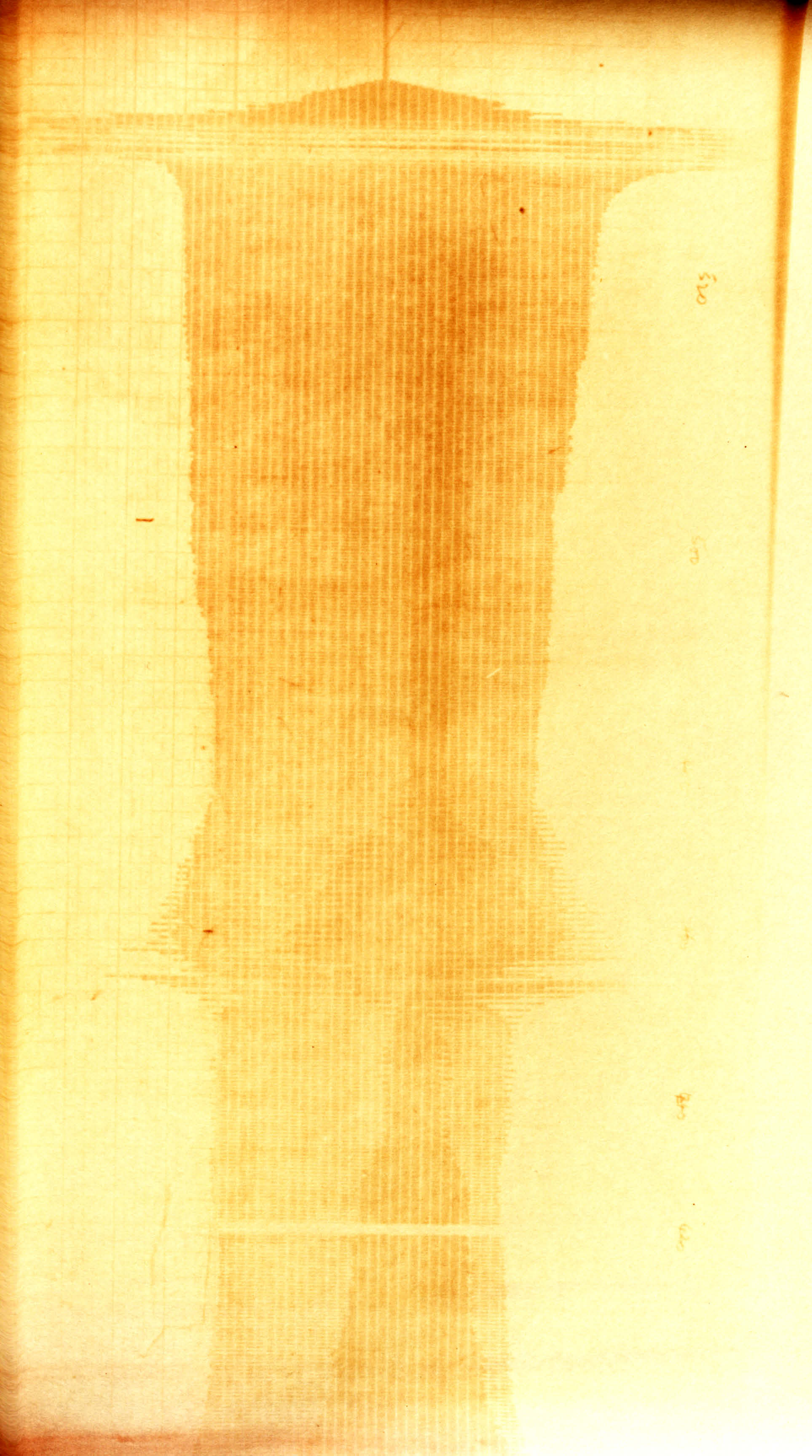

FIG. 63

(10, 1, 10, 4)

1/32"

I_{MIN}

FIG. 64

VIBRATION
OF
PERIOD 4π.

FIG. 65

(10, 1, 10, 4)

1/32"

I = 0.00788

FIG. 66

(10, 1, 10, 4)

1/32"

I_{min}

(SPEED DECREASING)

FIG. 67

(10, 1, 10, 4)

1/32"

I_{MIN}

(SPEED DECREASING)

FIG. 68

(10, 1, 10, 4)

1/32"

I = 0.00788

(SPEED

DECREASING)

FIG. 69.

NON-LINEAR RESONANCE AT $\Omega/2$

AND INSTABILITY AT $2\Omega/3$.

(See also Figs. 62, 63, 66, 67)

(10, 1, 10, 4)

I_{MIN}

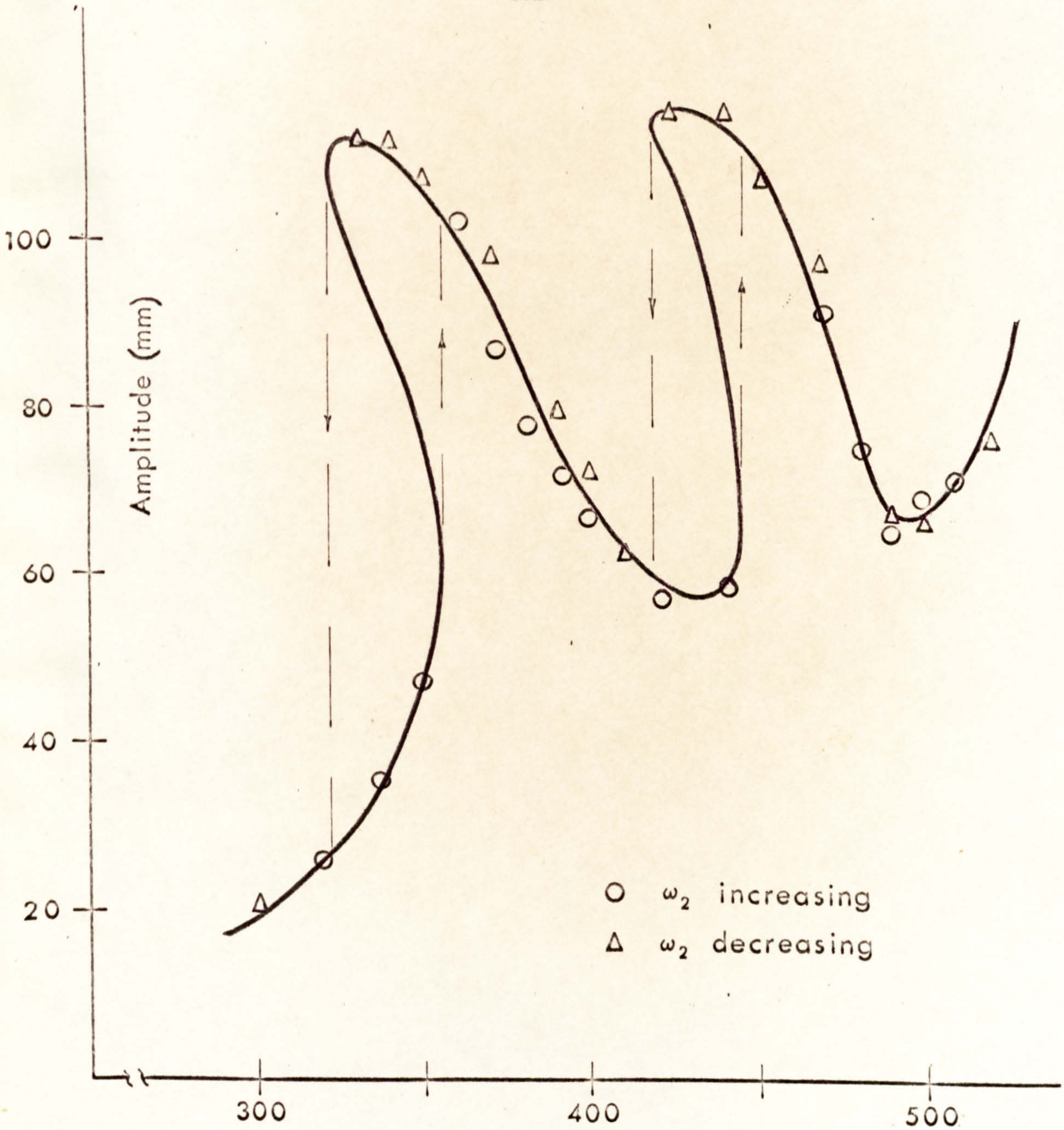

FIG. 70

(5,1,5,2)

1/16"

I_{min}

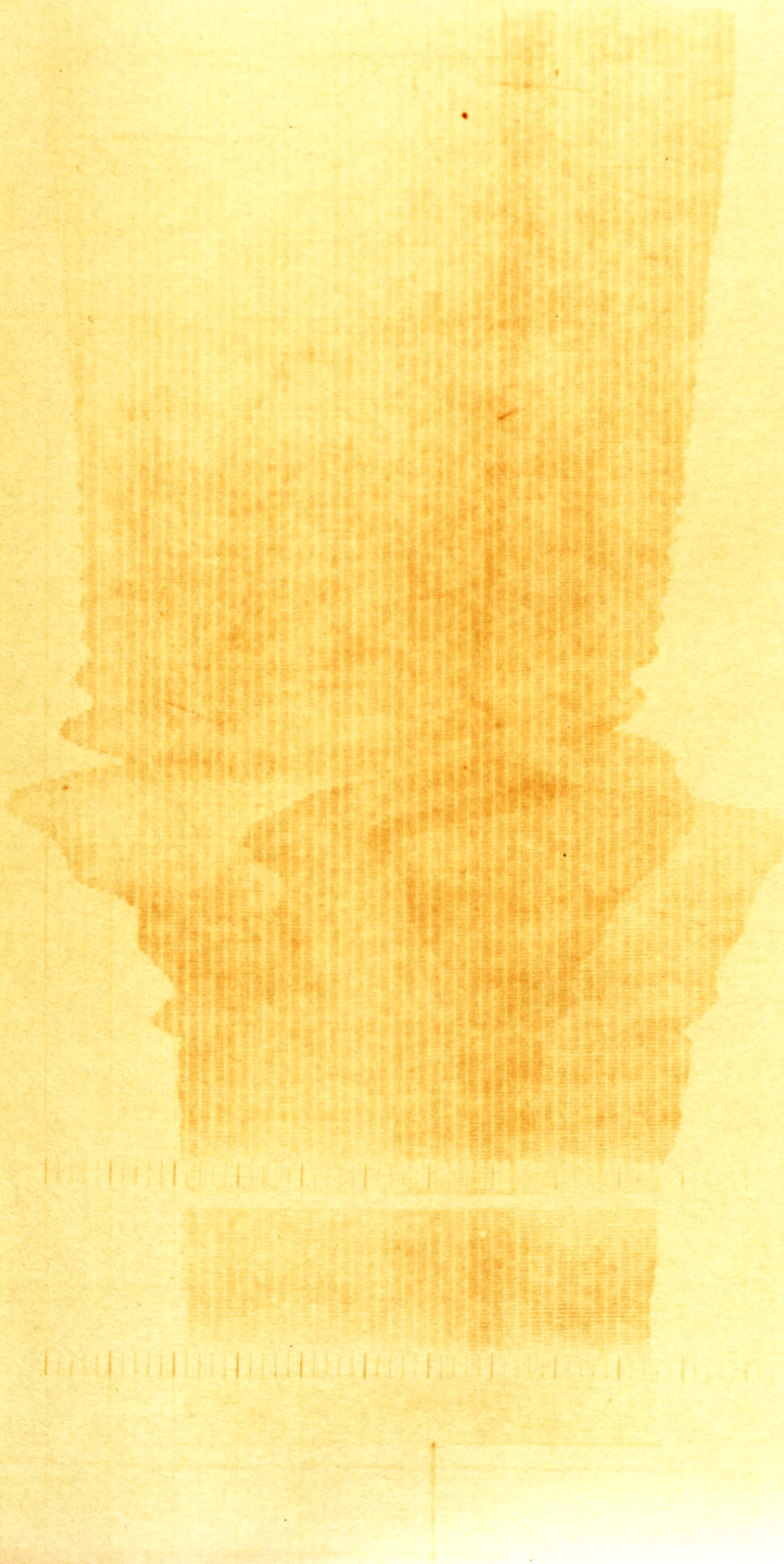

FIG. 71

(5, 1, 5, 2)

1/16"

I_{MIN}

(SPEED DECREASING)

FIG. 72

DAMPED FREE VIBRATION.

$\frac{1}{16}$" COUPLER.

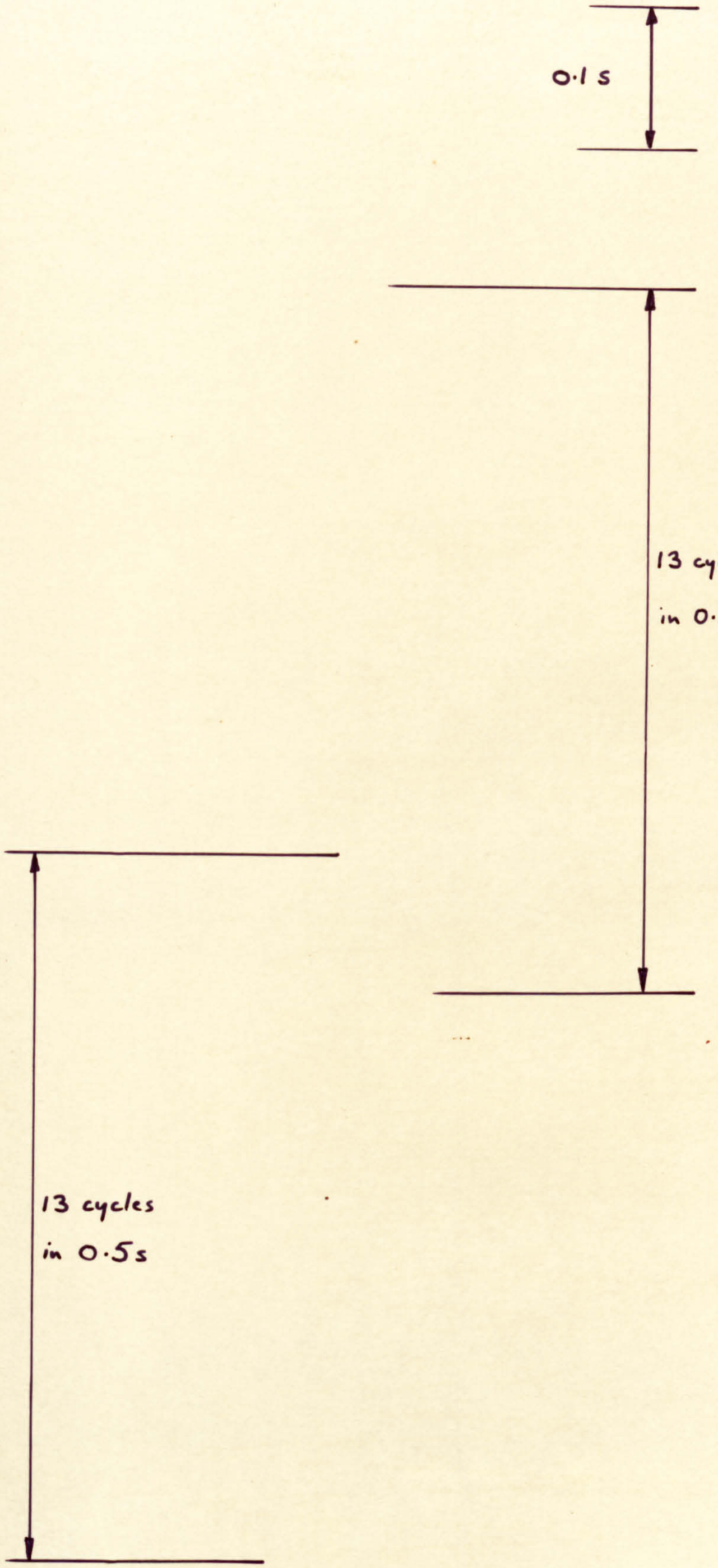

FIG. 73

DAMPED

FREE

VIBRATION.

$\frac{3}{64}$" COUPLER

FIG. 74

(5, 1, 5, 2)

3/64"

I_{MIN}

FIG. 75

(5, 1, 5, 2)

3/64"

I_{min}

Fig. 76

(5, 1, 5, 2)

3/64"

I = 0·0109

FIG. 77

(5, 1, 5, 2)

3/64"

I_{MIN}

FIG. 78

(5, 1, 5, 2)

3/64"

I_{MIN}

(SPEED
REDUCING)

FIG. 79

(5,1,5,2)

1/16"

I_{MIN}

FIG. 80

(5, 1, 5, 2)

1/16"

I_{MIN}

FIG. 81

(5,1,5,2)

1/32"

I_{MIN}

ONSET OF

INSTABILITY

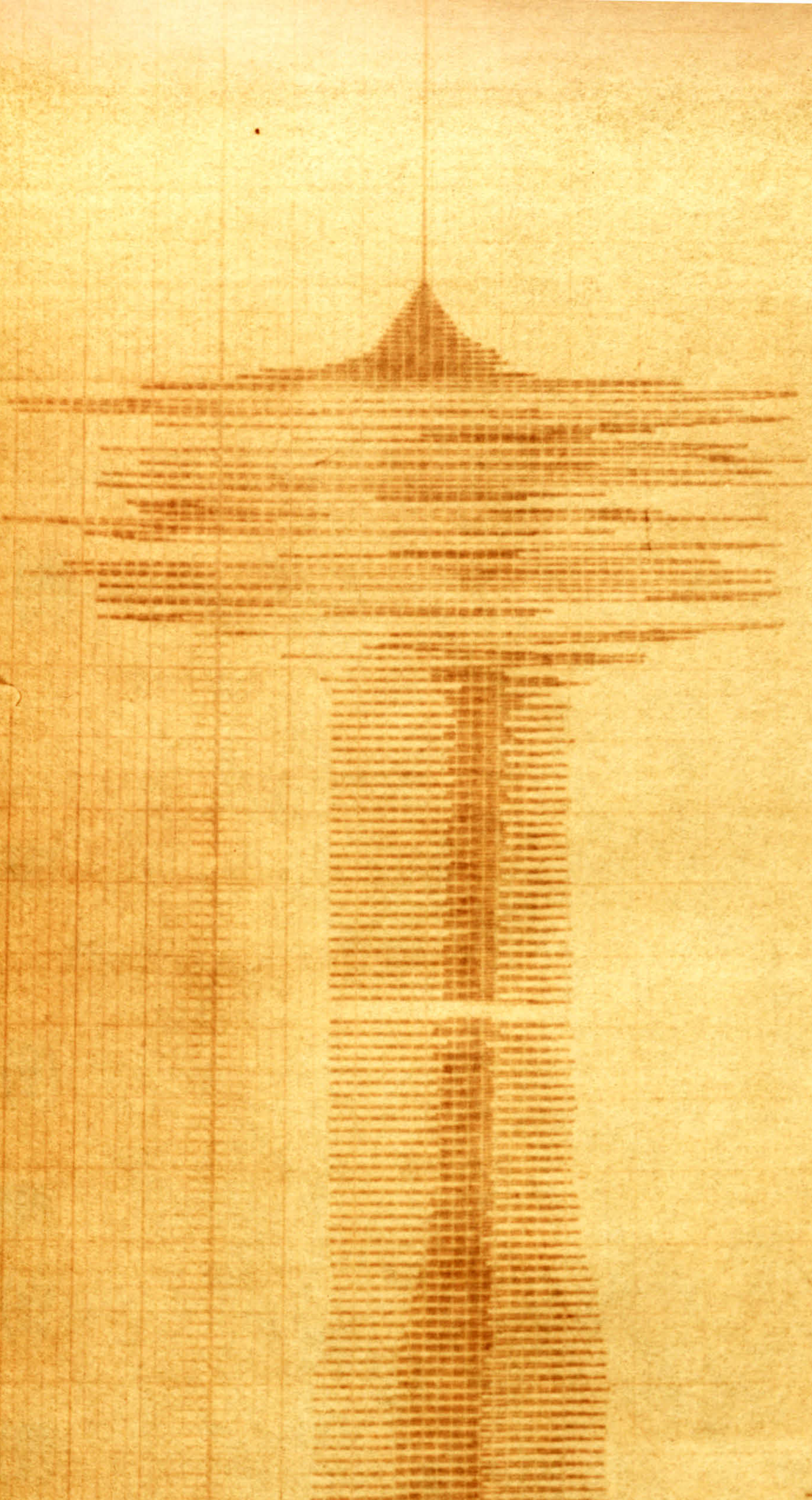

FIG.82 STABILITY CHART

(5, 1, 5, 2) $\frac{1}{32}$ in COUPLER

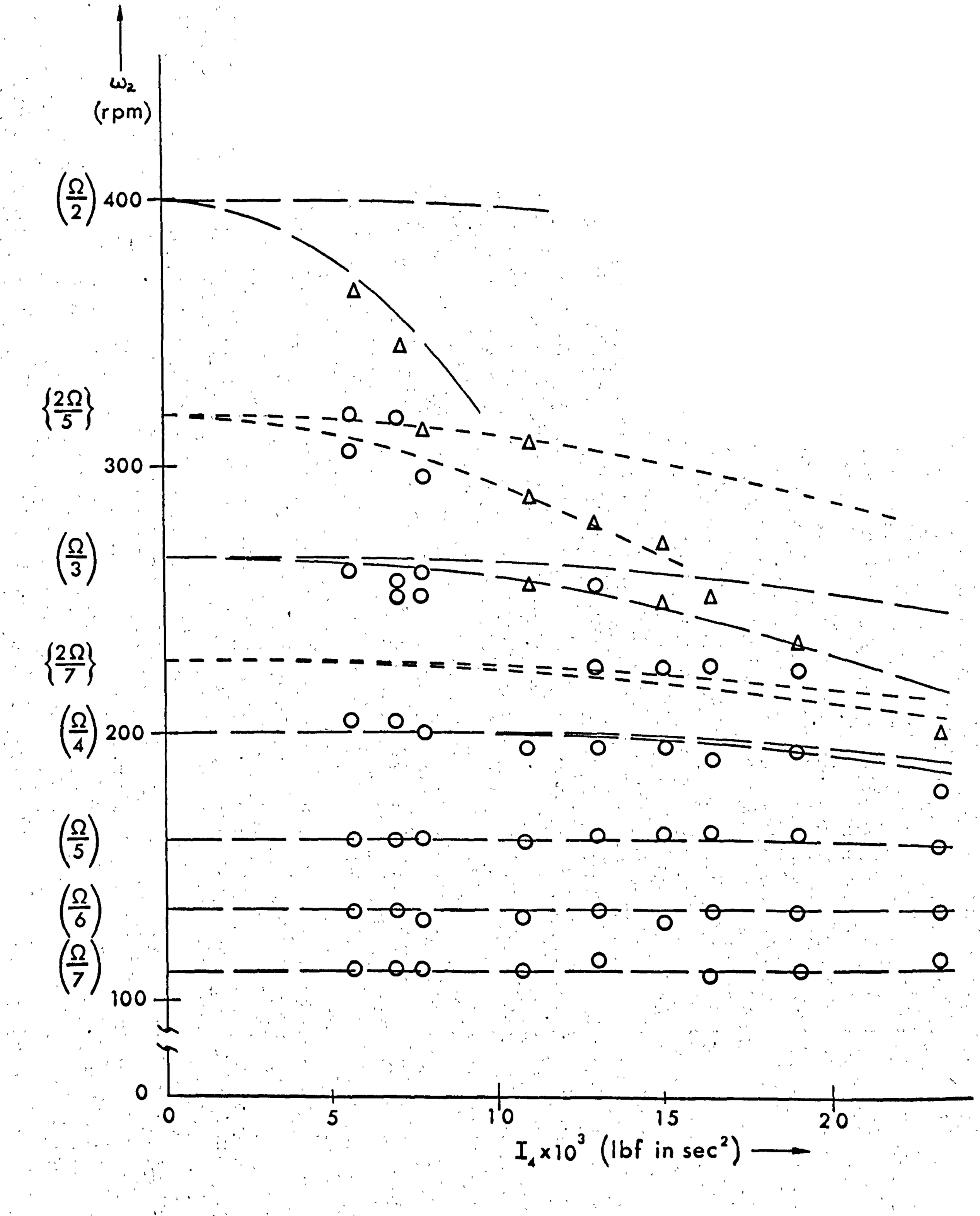

FIG. 84 STABILITY CHART

(5, 1, 5, 2) $\frac{1}{16}$ in COUPLER.

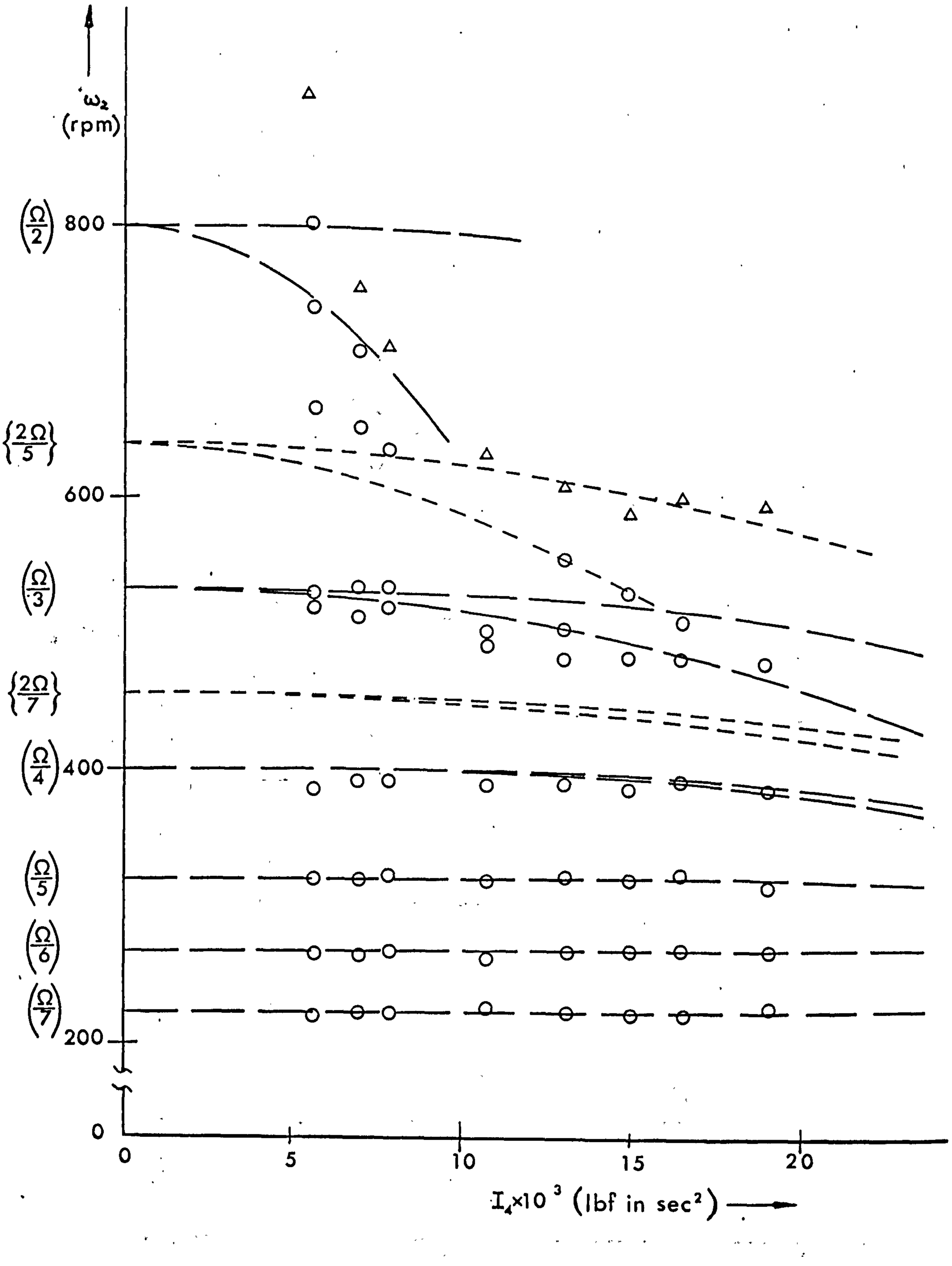

FIG. 85 STABILITY CHART

(10, 1, 10, 4) $\frac{1}{32}$ in COUPLER

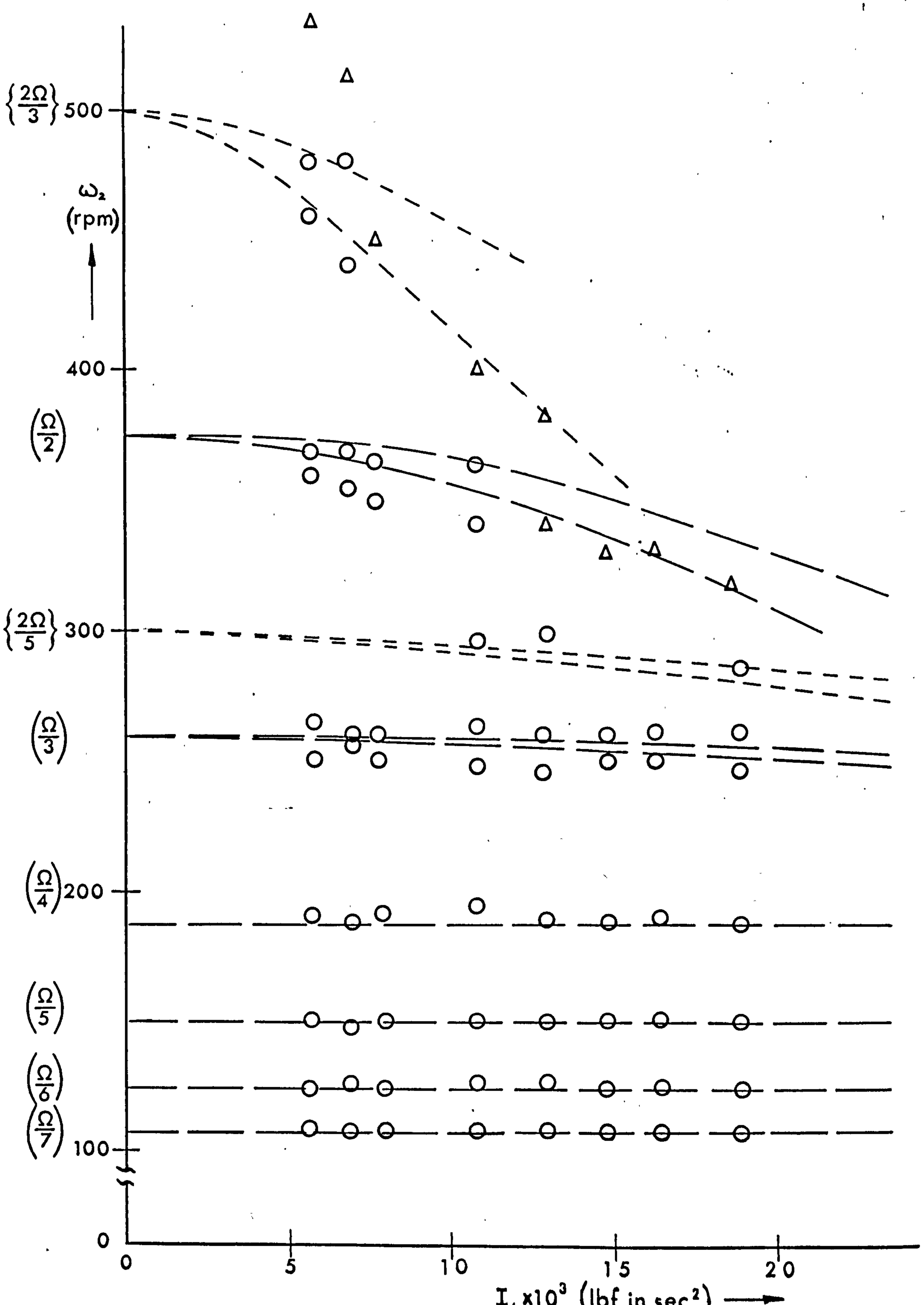

FIG.86 STABILITY CHART

(10, 1; 10, 4) $\frac{3}{64}$ in COUPLER.

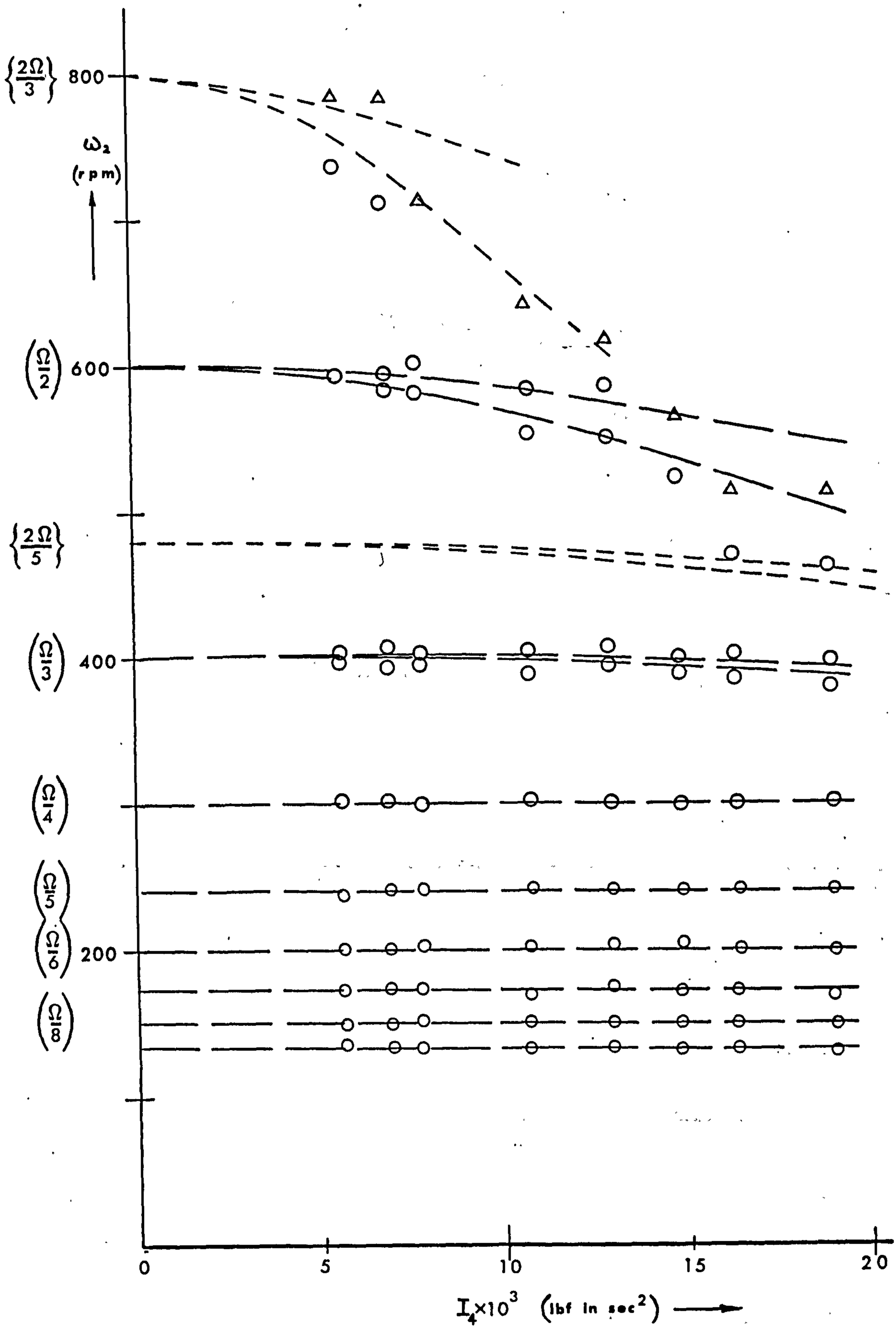

FIG.87 STABILITY CHART

(10, 1, 10, 4) $\frac{1}{16}$ in COUPLER

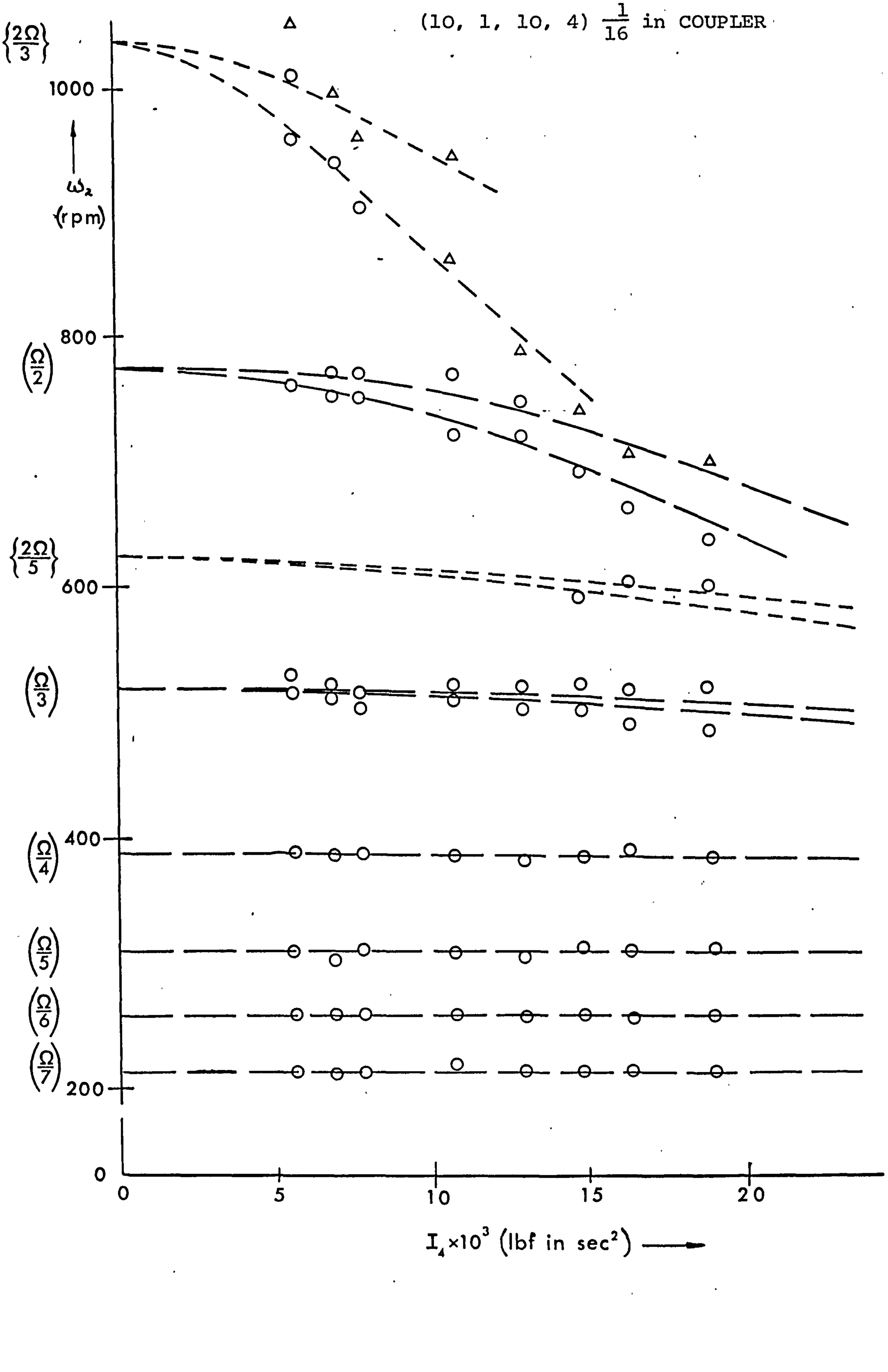

Fig. 88

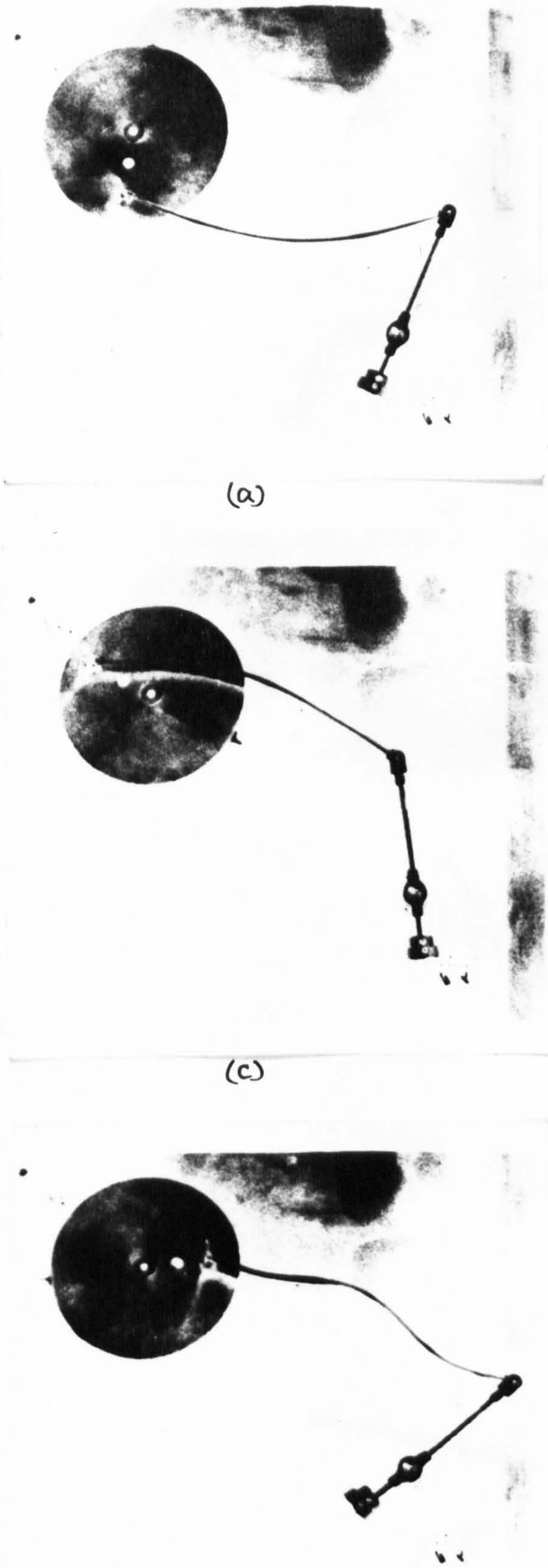

(a)

(b)

(c)

(d)

(e)

(f)

FIG. 89

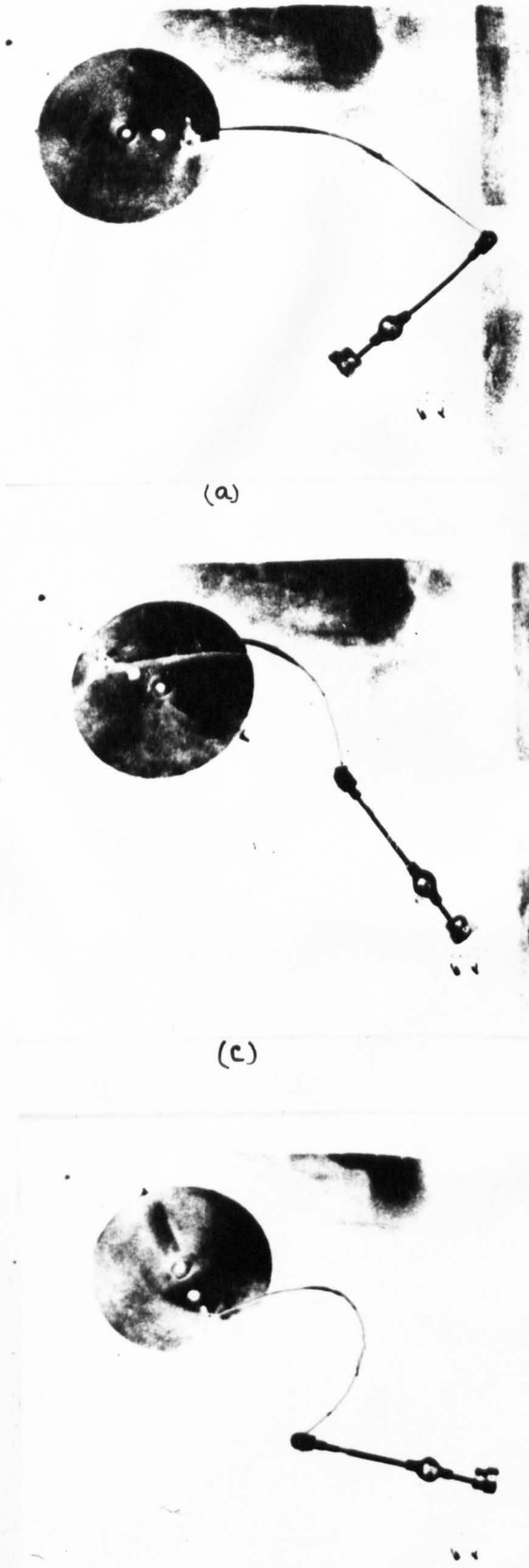

(a)

(b)

(c)

(d)

(e)

(f)

References

1. WILLIS, R. Principles of Mechanism. Longmans Green and Co., London (1841)

2. REULEUX, F. Kinematics of Machinery. (English Translation by A.B.W.Kennedy). Macmillan & Co., London (1876)

3. de JONGE, A.E.R. What is wrong with Kinematics and Mechanisms. MECH.ENG. 64, 4, 273-278 and 744-751, (1942)

4. SMITH, R. TRANS. ROY. SOC. EDIN. 32, 507, (1885)

5. BURMESTER, L. Lehrbuch der Kinematik. A.Felix Verlag, Leipzig, (1888).

6. FREUDENSTEIN, F. Trends in the Kinematics of Mechanisms, APP.MECH.REV. 12, No.9, (1959)

7. BOTTEMA, O. and FREUDENSTEIN, F., Kinematics and the Theory of Mechanisms. APP.MECH.REV. 19, No.4, (1966)

8. BLOKH, S.S. On the Synthesis of Four-Link Mechanisms. Izv. Akad.Nauk SSSR., OTD.TEKH.NAUK. 1, 47-54. (1940)

9. TALBOURDET, G.J. Mathematical Solution of Four-bar Linkages MACHINE DESIGN, 13, Nos.5,6,7, (1941)

10. SMITH, M.R., and MAUNDER, L., Inertia Forces in a Four-bar Linkage J.M.E.S. 9, No.3, 218-225, (1967)

11. HOUBEN, H. Über die Stabilitat von Schwingungen in Gelenkgetrieben FORSCH. des LANDES NORDRHEIN-WESTFALEN, No.1959,(1968)

12. GAYFER, J.R., and MILLS, B. Small Amplitude vibrations of the four-bar linkage chain. J.M.E.S. 7, No.3, 252-258, (1965)

13. MAHALINGHAM, S. Small-amplitude vibrations of a four-bar mechanism J.M.E.S. 8, No.4, 456-458, (1966)

14. MEYER ZUR CAPELLEN, W.
Biegungsschwingungen in der Koppel einer Kurbelschwinge. ÖST.ING.ARCH. 16, No.4, 341-348, (1962)

15. MEYER ZUR CAPELLEN, W., and HOUBEN, H.
Untersuchungen über elastische schwingungen in periodischen Getrieben. FORSCH. DES LANDES NORDRHEIN-WESTFALEN, No.1394, (1964)

16. NEUBAUER, A.H., COHEN, R., and HALL, A.S.
An analytical study of the dynamics of an elastic linkage. TRANS.A.S.M.E., J.ENG. for INDUS. 88, No.3, 311-317 (1966)

17. VISCOMI, B.V., and AYRE, R.S.
Nonlinear dynamic response of elastic slider-crank mechanism, TRANS.A.S.M.E., J. ENG. for INDUS. 93, No.1, 251-262 (1971)

18. MEYER ZUR CAPELLEN, W., and HOUBEN, H.,
Torsionsschwingungen im An- und Abtrieb von Viergelenkgetrieben. FORSCH. des LANDES NORDRHEIN - WESTFALEN No.1429 (1965)

19. HOUBEN, H. Untersuchungen über die Stabilität elastischer Bewegungen in der Koppel eines Viergelenkgetriebes. Dissertation, Tech.Hochschule, Aachen (1965)

20. SEEVERS, J.A., and YANG, A.T.
Dynamic Stability Analysis of Linkages with elastic members via analogue simulation
A.S.M.E. Paper 70-MECH-48. (1970)

21. McLAUGHLAN, N.W. Theory and application of Mathieu Functions
DOVER PUBLICATIONS INC., NEW YORK, (1964)

22. MAGNUS, W., and WINKLER, S.
Hill's Equation, INTERSCIENCE PUBLISHERS (1966)

23. DE VOGELAERE, R. A method for the numerical integration of differential equations of second order without explicit first derivatives. J.RES.NAT.BUR.STANDARDS. 54, 119-125, (1955)

24. MALKIN, I.G. On the stability of motion. MOSCOW-LENINGRAD (1952) Translation by U.S.ATOMIC ENERGY COMMISSION, OFFICE of TECHNICAL INFORMATION

25. FREUDENSTEIN, F. Harmonic Analysis of crank and rocker mechanisms with application. TRANS.A.S.M.E., J.APP.MECH., 26, No.4, 673-675, (1959)

26. KLOTTER, K., and KOTOWSKI, G. Über die Stabilität der Lösungen Hillscher Differentialgleichungen mit drei unabhängigen parametern. Z.A.M.M. 23, No.3, 149-155, (1943)

27. STRUTT, M.J.O. Reelle Eigenwerte verallgemeinerter Hillscher Eigenwertaufgaben 2. Ordnung. MAT.ZEIT. 49, 593-643, (1943-4)

28. RAND, R.H. On the stability of Hill's equation with four independent parameters. TRANS.A.S.M.E., J.APP.MECH. 36, No.4, 885-886, (1969)

29. SMITH, M.R. Determination of the stability of vibrations in mechanisms by a modified perturbation method. PROC.3rd WORLD CONG. for T.M.M., KUPARI, JUGOSLAVIA, VOL.B, 225-234, (1971)

30. HAMER, K., and SMITH, M.R. On the stability of the general Hill's equation with three independent parameters. TRANS. A.S.M.E. J.APP.MECH. 39, No.1, 276-278, (1972)

31. KOBRINSKII, A.E. Dynamics of mechanisms with elastic connections and impact systems. ILIFFE BOOKS LTD., London, (1969)

32. BOLOTIN, V.V. Dynamic Stability of elastic systems, HOLDEN-DAY INC. (1964)

33. PORTER, B. A Theoretical analysis of the torsional oscillation of a system incorporating a Hooke's joint. J.M.E.S. 3, No.4, 324-329, (1961)

34. WILSON, R. The Dynamics of the Slider Crank mechanism with clearance in the sliding bearing. Ph.D. Thesis University of Newcastle upon Tyne, Oct. 1971.

35. SMITH, M.R., and MAUNDER, L. Stability of a four-bar linkage with flexible coupler. J.M.E.S. 13, No.4, 237-242, (1971)

36. BOGOLIUBOV, N.N. and MITROPOLSKY, Y.A. Asymptotic methods in the theory of non-linear oscillations. (English Translation) Hindustan Publishing Corp., Delhi (1961)

Appendix 1

Planar Mechanism Kinematics

In Chapter 2, the kinematics of the four bar linkage are examined briefly and the equations giving angular position, velocity and acceleration of the links are quoted. They are obtained as follows.

Fig. 1 shows the four bar linkage and its parameters and Fig. 2 the equivalent vector representation. The horizontal and vertical projections of the vector polygon may be written as

$$\ell_2 \cos\theta_2 + \ell_3 \cos\theta_3 = \ell_1 + \ell_4 \cos\theta_4 \qquad \text{A.1}$$

$$\ell_2 \sin\theta_2 + \ell_3 \sin\theta_3 = \ell_4 \sin\theta_4 \qquad \text{A.2}$$

Elimination of θ_3 is achieved by re-arrangement as follows

$$\ell_3 \cos\theta_3 = \ell_1 - \ell_2 \cos\theta_2 + \ell_4 \cos\theta_4 \qquad \text{A.3}$$

$$\ell_3 \sin\theta_3 = -\ell_2 \sin\theta_2 + \ell_4 \sin\theta_4 \qquad \text{A.4}$$

Squaring and adding these equations yields

$$\ell_3^2 = \ell_1^2 + \ell_2^2 + \ell_4^2 - 2\,\ell_1\ell_2 \cos\theta_2 + 2\,\ell_1\ell_4 \cos\theta_4 - 2\ell_2\ell_4 \cos(\theta_2 - \theta_4) \qquad \text{A.5}$$

which is transformed to the well-known Freudenstein equation using the abbreviations

$$R_1 = \frac{\ell_1}{\ell_4}, \quad R_2 = \frac{\ell_1}{\ell_2}, \quad R_3 = \frac{\ell_1^2 + \ell_2^2 + \ell_4^2 - \ell_3^2}{2\,\ell_2\,\ell_4}$$

whence we obtain

$$R_1 \cos\theta_2 - R_2 \cos\theta_4 - R_3 = \cos(\theta_2 - \theta_4) \qquad \text{A.6}$$

However this is not the most convenient form of this equation for present purposes since θ_4 is required explicitly. Writing equation (A.5) as

$$\ell_1^2 + \ell_2^2 - \ell_3^2 + \ell_4^2 - 2\,\ell_1\ell_2 \cos\theta_2 = 2\,\ell_2\ell_4 \cos(\theta_2 - \theta_4) - 2\,\ell_1\ell_4 \cos\theta_4$$

$$= (2\,\ell_2\ell_4 \cos\theta_2 - 2\,\ell_1\ell_4) \cos\theta_4$$

$$+ (2\,\ell_2\ell_4 \sin\theta_2) \sin\theta_4$$

and using the notation

$$A = 2\,\ell_4\,(\ell_2 \cos\theta_2 - \ell_1)$$

$$B = \ell_3^2 - \ell_1^2 - \ell_2^2 - \ell_4^2 + 2\,\ell_1\,\ell_2 \cos\theta_2$$

$$C = 2\,\ell_2\,\ell_4 \sin\theta_2$$

we obtain

$$A \cos\theta_4 + B + C \sin\theta_4 = 0 \qquad \text{A.7}$$

Squaring this equation and re-arranging, a quadratic equation in $\cos\theta_4$ is produced which has the solution

$$\cos\theta_4 = \frac{-AB}{D^2} \pm \sqrt{\left(\frac{AB}{D^2}\right)^2 - \frac{B^2 - C^2}{D^2}} \qquad \text{A.8}$$

where $D^2 = A^2 + C^2$

A similar procedure may be followed to determine $\cos\theta_3$ when an analogous equation will be obtained. Alternatively equations (A.3) and (A.4) may be used in which case $\sin\theta_4$ is calculated from the appropriate value of $\cos\theta_4$ in (A.8).

APPENDIX 2.

DIGITAL COMPUTER PROGRAMME FOR CALCULATION OF LINKAGE KINEMATICS.

```
begin library A0,A6,A12;
open(20);
open(30);
write text(30,[[25s]FOUR*BAR*LINKAGE*KINEMATICS[2c]]);

begin   real X,Y,Z;

        procedure FORBAR 2(L2,L3,L4); comment  This procedure
         calculates the position, angular velocity and angular
        acceleration of the members of a four bar linkage in
        which L2 is the length of the crank , L3 that of the
        coupler and L4 that of the follower.
        The distance between the crank and follower pivots is
        taken as unity.The calculation is carried out in 10
        degree steps of the crank angle;

        value L2,L3,L4;          real L2,L3,L4;

        begin real a,b,c,d,e,k,th2,th3,th4,csth3,snth3,csth4,snth4,

                        omega3,omega4, alpha3,alpha4;

                integer i,x1,x2,y1,y2,f1,f2,f3,f4,f5;

                f1:=format([sndds]);
                f2:=format[4sndd]);
                f3:=format[3sdd]);
                f4:=format[4s+ndd.dddd]);
                f5:=format[ssnd.dd]);

                write(30,f5,L2);
                write(30,f5,L3);
                write(30,f5,L4);

                write text(30,[[2c]crank[5s]coupler[5s]coupler[6s]
                        coupler[5s]follower[5s]follower[5s]follower
                        [c]angle[6s]angle[6s]angular[6s]angular[6s]
                        angle[7s]angular[6s]angular[cs]deg[5s]deg
                        [2s]min[5s]velocity[5s]acceln[6s]deg[2s]min
                        [5s]velocity[5s]acceln[2c]]);

                k:=L3↑2-L2↑2-L4↑2-1;
                for i:= 0 step 1 until 36 do
                begin  th2:=0.174532925 x i;
                        a  :=2xL2xL4xcos(th2)-2xL4;
                        b  :=k+2xL2xcos(th2);
                        c  :=if abs(sin(th2))<10-3 then 0
                             else 2xL2xL4xsin(th2);
                        d  :=-axb/(a↑2+c↑2);
                        e  :=(b↑2-c↑2)/(a↑2+c↑2);
```

```
csth4  :=if c=0 then d else if th2 < arctan(1)x4
                then d+sqrt(d↑2-e)
                else d-sqrt(d↑2-e);
csth3  :=(1-L2xcos(th2)+L4xcsth4)/L3;
snth4  :=sqrt(1-(csth4)↑2);
snth3  :=sqrt(1-(csth3)↑2);
  th4  :=arctan(snth4/csth4);
  th3  :=arctan(snth3/csth3);

     x1:= entier(th3x180/3.1415926);
     y1:=((th3x180/3.1415926)-x1)x60;
     x2:= entier(th4x180/3.1415926);
     y2:=((th4x180/3.1415926)-x2)x60;

omega3:=L2x(snth4xcos(th2)-csth4xsin(th2))/
            (L3x(snth3xcsth4-csth3xsnth4));

omega4:=-L2x(snth3xcos(th2)-csth3xsin(th2))/
            (L4x(snth4xcsth3-csth4xsnth3));

alpha3:=+(L2x(csth4xcos(th2)+snth4xsin(th2))
            -(omega4)↑2xL4+(omega3)↑2x
            (csth3xcsth4+snth3xsnth4)xL3)/
            (L3x(snth4xcsth3-csth4xsnth3));

alpha4:=-(L2x(csth3xcos(th2)+snth3xsin(th2))
            +(omega3)↑2xL3-(omega4)↑2x
            (csth3xcsth4+snth3xsnth4)xL4)/
            (L4x(snth3xcsth4-csth3xsnth4));

            write(30,f1,10xi);
            write(30,f2,if x1<0 then 180+x1 else x1);
            write(30,f3,y1);
            write(30,f4,omega3);
            write(30,f4,alpha3);
            write(30,f2,if x2<0 then 180+x2 else x2);
            write(30,f3,y2);
            write(30,f4,omega4);
            write(30,f4,alpha4);
            newline(30,1);
        end;
end;

X:=read(20);
Y:=read(20);
Z:=read(20);

FORBAR2(X,Y,Z);
end;
close(20);
close(30);
end→
```

APPENDIX 3.

DIGITAL COMPUTER PROGRAMME FOR CALCULATION OF FOURIER COEFFICIENTS.

Below is listed a procedure FOUSIM which calculates the first M sine and cosine Fourier coefficients of the function f(z) which is considered periodic in z within the range $x \leq z \leq y$.

$$f(z) = a_0/2 + \sum_{m=1}^{M} (a_m \cos mz + b_m \sin mz)$$

Integration by Simpson's rule is carried out repeatedly until successive values of the coefficients differ by less than the desired accuracy parameter eps.

The m th cosine and sine coefficients are stored in the array elements a[m] and b[m] respectively.

```
procedure FOUSIM(x,y,f,M,eps);
value x,y; integer M; real x,y,eps; real procedure f;
begin real h,F,G,P; integer i,m,n,p;
        array A,B,C,D,I0,I1,I2,J0,J1,J2[0:M];
      for m:=0 step 1 until M do A[m]:=B[m]:=C[m]:=D[m]:=0;
      h:=(y-x)/2;
      n:=1;
      F:=f(x);          G:=f(y);
      for m:=0 step 1 until M do
      begin   I0[m]:=F×cos(m×x)+G×cos(m×y);
              J0[m]:=F×sin(m×x)+G×sin(m×y);
              I1[m]:=J1[m]:=0;
      end;
L1:   for i:=1 step 1 until n do
      begin   P:=f(x+(2×i-1)×h);
              for m:=0 step 1 until M do
              begin   B[m]:=B[m]+P×cos(m×(x+(2×i-1)×h));
                      D[m]:=D[m]+P×sin(m×(x+(2×i-1)×h));
              end;
      end;
      for m:=0 step 1 until M do
      begin   I2[m]:=h×(I0[m]+4×B[m]+2×A[m])/3;
              J2[m]:=h×(J0[m]+4×D[m]+2×C[m])/3;
      end;
      p:=0;
      for m:=0 step 1 until M do
      begin   if abs(I2[m]-I1[m])<eps and abs(J2[m]-J1[m])<eps
              then goto L3 else p:=p+1;
L3:   end;
      if p=0 then goto L2;
      for m:=0 step 1 until M do
      begin   I1[m]:=I2[m];
              J1[m]:=J2[m];
               A[m]:= A[m]+B[m];
               C[m]:= C[m]+D[m];
               B[m]:= D[m]:= 0;
      end;
      h:=h/2;
      n:=2×n;
      goto L1;

L2:   for m:=0 step 1 until M do
      begin   a[m]:=I2[m]/3.14159265;
              b[m]:=J2[m]/3.14159265;
      end;
              if m>M then a[m]:=b[m]:=0;
              a[0]:=a[0]/2;
end FOUSIM ;
```

Appendix 4

Computer Programme for Solution of Hill's Equation

The programme listed below integrates equations of the form

$$\frac{d^2y}{d\theta^2} + \lambda^2(1 + \mu F(\theta))y = g(\theta)$$

according to the algorithm due to de Vogelaere[23].

The procedure f(th,y) defines the second derivative of y in terms of th (theta, the independent variable) and y the dependent variable. Integration is carried out in steps of h which is initially given the value of 10^0 and then halved repeatedly until it is less than the derived maximum. (See Chapter 6).

The solution is printed out after every two steps together with the corresponding value of the independent variable (viz. crank angle in degrees).

The integration is terminated if y the non-dimensional amplitude exceeds unity but will otherwise proceed indefinitely.

Input requirements are as follows:-

$\ell_1, \ell_2, \ell_3, \ell_4$;	The mechanism link lengths.
ω_2	crank speed (r/s)
x_0, y_0, z_0	initial values of crank angle, θ, amplitude y, and slope $dy/d\theta$.
m	Mode of vibration ($m = 1$ for fundamental)
λ^2, μ	equation parameters.

```
begin library A0,A6,A12;
open(20);open(30);
write text(30,[SOLUTION*OF*DIFFERENTIAL*EQUATION*BY
                *DE*VOGELAERE*METHOD[2c]]);

begin real l1,l2,l3,l4,omega2,x0,y0,z0,h,x,p,q,r,s,t,lamsq,mu;
      integer m,n,f1,f2,f3,f4,f5,f6,f7;

      real procedure f(th,y);
            value   th,y;   real th,y;
             begin real a,b,c,d,e,k,snth3,snth4,csth3,csth4,
                        omega3,omega4,alpha3,alpha4;
                   k:=l3↑2-l1↑2-l2↑2-l4↑2;
                   a:=2×l2×l4×cos(th)-2×l1×l4;
                   b:=k+2×l1×l2×cos(th);
                   c:=if abs(sin(th))<10-3 then 0
                      else 2×l2×l4×sin(th);
                   d:=a×b/(a↑2+c↑2);
                   e:=(b↑2-c↑2)/(a↑2+c↑2);

csth4 := if abs(sin(th))<10-3 then d else
         if th < 4×arctan(1) then d-sqrt(d↑2-e)
         else d+sqrt(d↑2-e);
csth3 :=(l1-l2×cos(th)-l4×csth4)/l3;
snth4 :=-sqrt(1-(csth4)↑2);
snth3 :=+sqrt(1-(csth3)↑2);

         omega3 :=omega2×l2×(snth4×cos(th)-csth4×sin(th))/
                  (l3×(snth3×csth4-csth3×snth4));
         omega4 :=omega2×l2×(snth3×cos(th)-csth3×sin(th))/
                  (l4×(snth4×csth3-csth4×snth3));
         alpha3 :=((omega2)↑2×l2×(csth4×cos(th)+snth4×sin(th))
                  +(omega4)↑2×l4+(omega3)↑2×(csth3×csth4+snth3
                  ×snth4)×l3)/(l3×(snth4×csth3-csth4×snth3));
         alpha4 :=((omega2)↑2×l2×(csth3×cos(th)+snth3×sin(th))
                  +(omega3)↑2×l3+(omega4)↑2×(csth3×csth4+snth3
                  ×snth4)×l4)/(l4×(snth3×csth4-csth3×snth4));

f:=-y×lamsq×(1+mu×alpha4/(omega2↑2×(snth3×csth4-csth3×snth4)))+

      (if (m÷2×2-m)≠0 then 4×l2×(sin(th)×csth3-cos(th)×snth3)/

      (m×l3×3.14159265)-2×alpha3/(m×omega2↑2×3.14159265)

      else 2×alpha3/(m×omega2↑2×3.14159265));

      end;

   f1:=format([ndss]);      f2:=format([nd.ddss]);
   f3:=format([nd.dddds]); f4:=format([ndddddssss]);
   f5:=format([nds]);       f6:=format([d]);
   f7:=format([3sndd.ddd]);

   l1:=read(20);   l2:=read(20);   l3:=read(20);   l4:=read(20);
omega2:=read(20);  x0:=read(20);   y0:=read(20);   z0:=read(20);
    m:=read(20);lamsq:=read(20);   mu:=read(20);
```

```
        h:=10;
L2:  if h >18/sqrt(lamsq) then begin   h:=h/2;   goto L2;  end;
write text(30,[[c10s]L1[2s]L2[2s]L3[2s]L4[3s]W2[4s]xo[s]yo[s]
zo[2s]h[4s]m[s]lamsq[2s]mu[c10s]in[2s]in[2s]in[2s]in[2s]R/SEC
[11s]deg[2c10s]]);

write(30,f1,l1);write(30,f1,l2);write(30,f1,l3);write(30,f1,l4);
write(30,f2,omega2);
write(30,f5,x0);write(30,f5,y0);write(30,f5,z0);write(30,f2, h);
write(30,f6, m);
write(30,format([ssn.dd]),lamsq);
write(30,format([ssn.dd]),mu);
newline(30,2);

            h:=h×3.14159265/180;
            n:=0;
            x:=x0;
            p:=y0;
            q:=h×z0;
            r:=h↑2×f(x,p)/3;
            t:=p-q+3×r/2;
            s:=h↑2×f(-h,t)/3;

L1:         q:=q+r;
            p:=p+q;
            s:=p+r-s/2;
            x:=x+h;
            s:=h↑2×f(x,s)/3;
            q:=q+4×s;
            p:=p+q;
            x:=x+h;
            r:=h↑2×f(x,p)/3;
            q:=q+r;
            n:=n+1;
            write(30,format([snddddd.d]),x×180/3.14159265);
            write(30,format([s+d.ddddd+nd]),p);
            if n+5×5=n then newline(30,1);
            if p>1 then goto FAIL;
            goto L1;

 FAIL:      write text(30,[[c]UNSTABLE]);

end;
close(20);
close(30);
end→
```